

Fig. 11.4 Typical drained triaxial test results on loose Sacramento River sand: (a) principal stress ratio versus axial strain; (b) volumetric strain versus axial strain (after Lee, 1965).

example, 0.1 and 0.2 MPa), the volumetric strain is positive or *dilation* is taking place! Thus even an initially loose sand behaves like a dense sand; that is, it dilates if  $\sigma_{3c}'$  is low enough!

Now, let's look at the behavior of dense sand. The result of several drained triaxial tests on dense Sacramento River sand are presented in Fig. 11.5. Although the results are similar in appearance to Fig. 11.4, there are some significant differences. First, definite peaks are seen in the  $(\sigma_1'/\sigma_3')$ -strain curves, which are typical of dense sands (compare with Fig. 11.3a). Second, large *increases* of volumetric strain (dilation) are observed. However, at higher confining pressures, dense sand exhibits the behavior of loose sand by showing a *decrease* in volume or compression with strain.

By testing samples of the same sand at the same void ratios or densities but with different effective consolidation pressures, we can de-

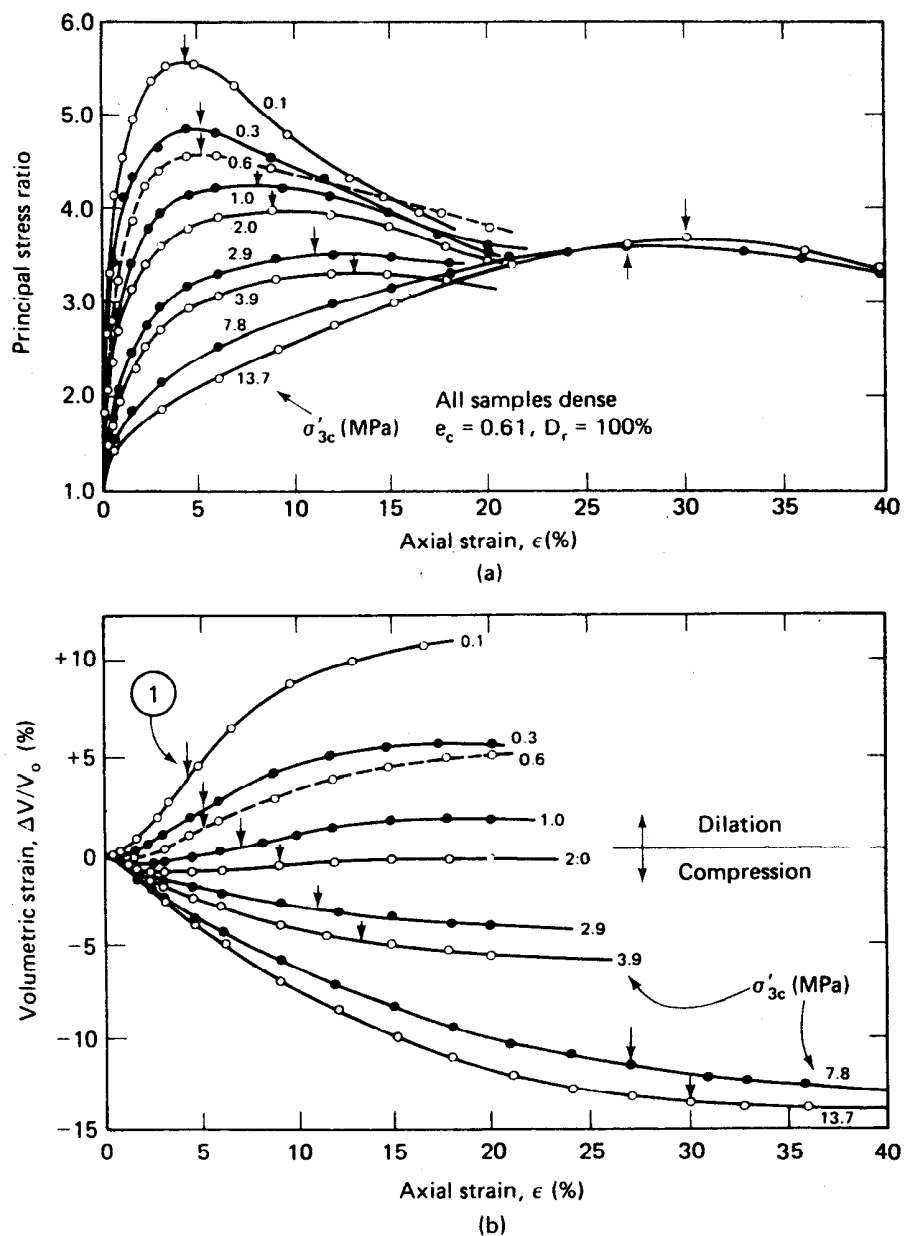


Fig. 11.5 Typical drained triaxial test results on dense Sacramento River sand: (a) principal stress ratio versus axial strain; (b) volumetric strain versus axial strain (after Lee, 1965).

termine the relationship between volumetric strain at failure and void ratio or relative density. We could define failure as either the maximum ( $\sigma_1 - \sigma_3$ ) or maximum  $\sigma'_1/\sigma'_3$ . For drained tests, failure occurs at the same strain according to both criteria. Points at failure are shown as small arrows in Fig. 11.5. Volumetric strain at failure versus void ratio at the end of consolidation, from the data in Figs. 11.4b and 11.5b for various confining pressures (other data have been added as well), are shown in Fig. 11.6. For example, point 1 in Fig. 11.5b is plotted as point 1 in Fig. 11.6. It can be seen that for a given confining pressure the volumetric strain decreases (becomes more negative) as the density decreases (void ratio increases). By definition, the critical void ratio is the void ratio *at failure* when the volumetric strain is zero. Thus for the various values of  $\sigma'_{3c}$  in Fig. 11.6,  $e_{crit}$  is the void ratio when  $\Delta V/V_o = 0$ . For example,  $e_{crit}$  for  $\sigma'_{3c} = 2.0$  MPa is 0.555.

We can see how  $e_{crit}$  varies with confining pressure by taking the critical void ratios of Fig. 11.6 and plotting them versus  $\sigma'_{3c}$ , as is done in Fig. 11.7. Here we have called  $\sigma'_{3c}$  the *critical* confining pressure  $\sigma'_{3c\ crit}$

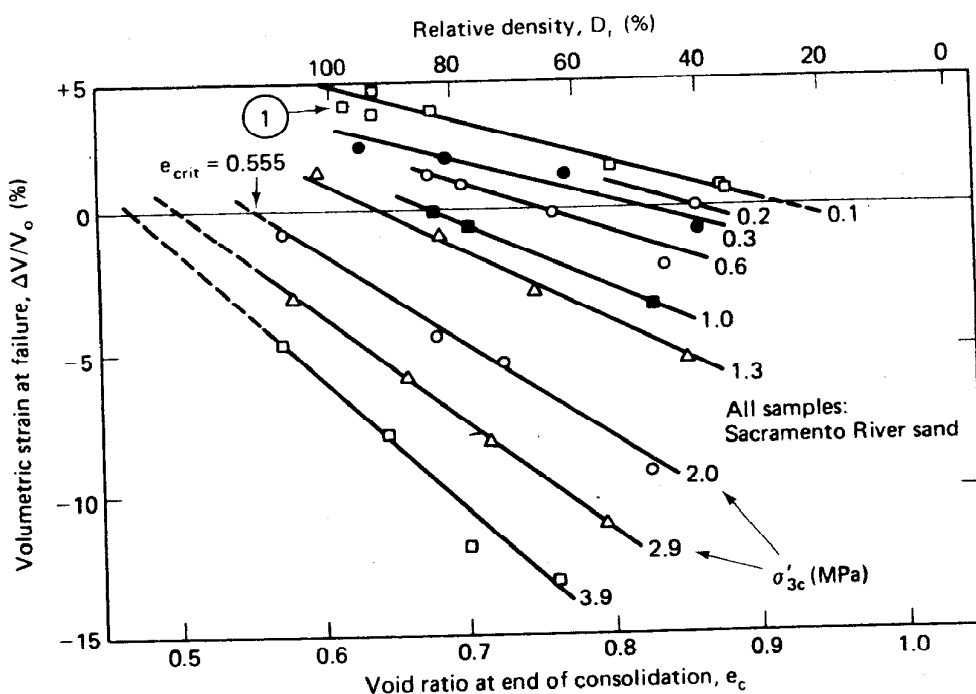


Fig. 11.6 Volumetric strain at failure versus void ratio at end of consolidation for drained triaxial tests at various confining pressures (after Lee, 1965).

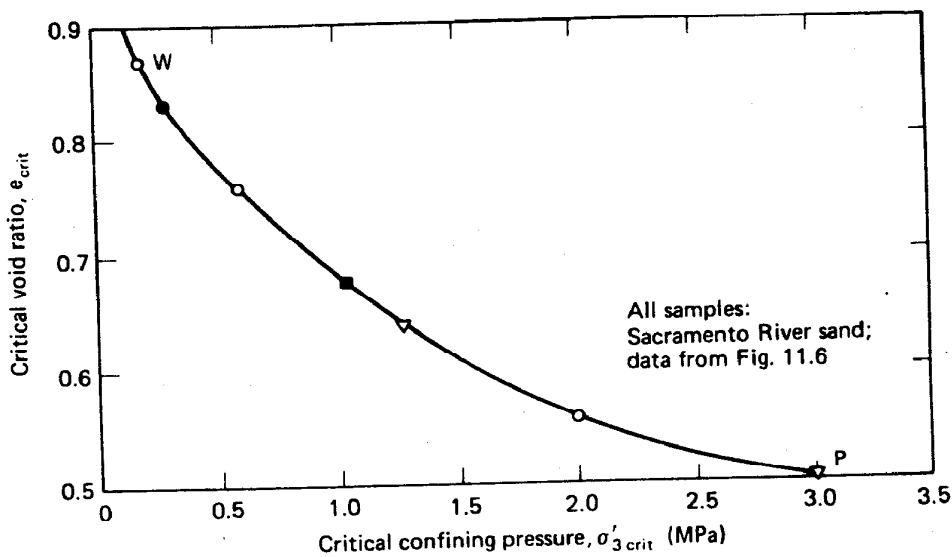


Fig. 11.7 Critical void ratio versus pressure conditions from drained triaxial tests. Data from Fig. 11.6 (after Lee, 1965).

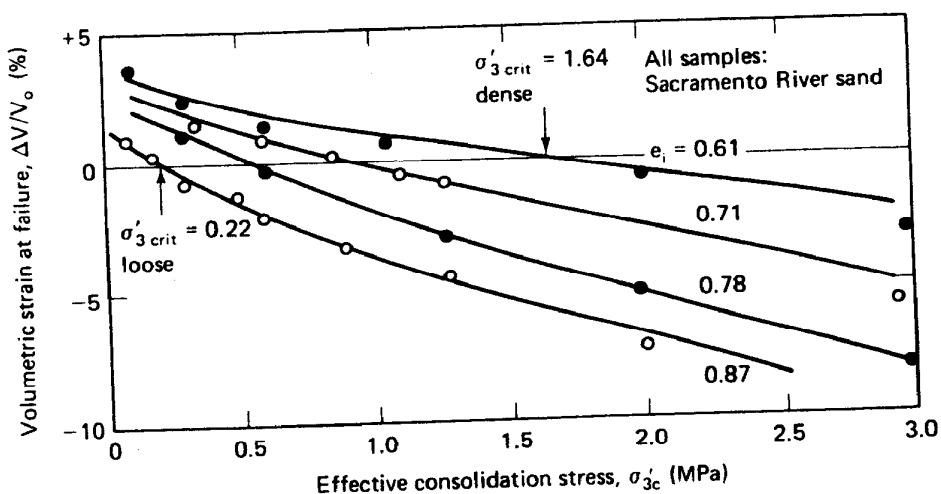
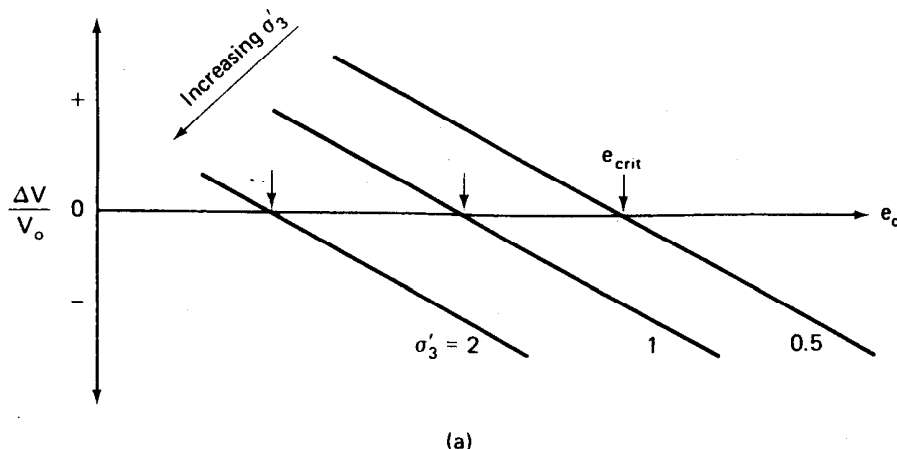


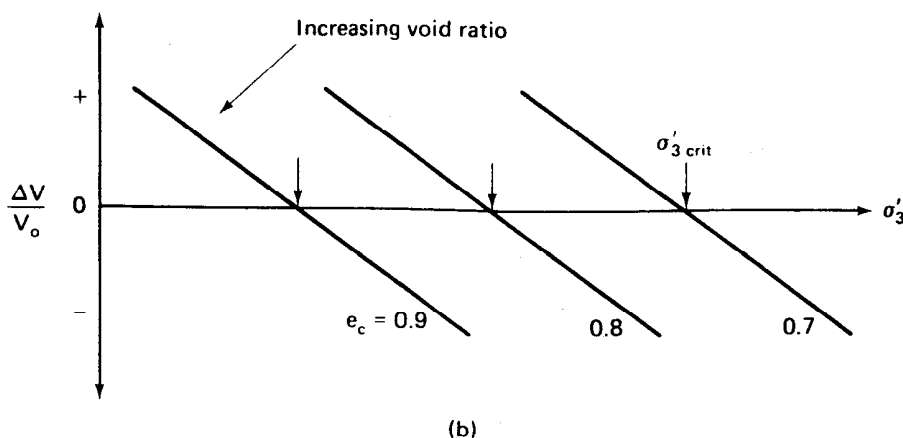
Fig. 11.8 Volumetric strain at failure versus effective consolidation stress for different initial void ratios (after Lee, 1965).

because this is the effective confining pressure at which zero volumetric strain occurs at failure for a given void ratio.

A second and just as interesting approach is to use the data shown in Figs. 11.4b and 11.5b (plus other data at intermediate void ratios) and plot the relationship between volumetric strain at failure and confining pressure for various values of void ratio after consolidation. Such a graph is shown in Fig. 11.8, although the void ratios indicated are initial void ratios and not the void ratios after consolidation. Note that the value of  $\sigma'_{3c}$  at  $\Delta V/V_o = 0$  is the critical confining pressure,  $\sigma'_{3\text{crit}}$ . Since they are drained tests,  $\sigma'_{3c} = \sigma'_{3f}$ . This relationship could also be obtained from Fig. 11.6 by noting the values of volumetric strain at constant void ratios and plotting  $\Delta V/V_o$  versus  $\sigma'_{3c}$ .



(a)



(b)

Fig. 11.9 Idealized volumetric strain data from drained triaxial tests: (a)  $\Delta V/V_o$  versus  $e_c$ ; (b)  $\Delta V/V_o$  versus  $\sigma'_3$ .

We can show the relationships of Figs. 11.6 and 11.8 in Fig. 11.9 (idealized). Since both Figs. 11.6 and 11.8 have a common axis, it is possible to combine them in a single three-dimensional graph known as the *Peacock diagram* (after William Hubert Peacock who first constructed such a diagram in 1967), as shown in Fig. 11.10.

With the Peacock diagram, we are able to predict the behavior of sand at any void ratio after consolidation  $e_c$  and at any confining pressure  $\sigma'_3$ . For example, if the effective confining pressure is given at point  $C$  in Fig. 11.10, which is higher than  $\sigma'_{3\text{ crit}}$  for this given void ratio  $e_c$ , then we would expect a decrease in the volume or a minus  $\Delta V/V_o$ , which is equal to the ordinate  $BS$ . On the other hand, if  $\sigma'_3$  is less than  $\sigma'_{3\text{ crit}}$ , such as point  $A$  for the given value of  $e_c$ , then a dilation or positive volume change will take place equal to the ordinate  $RD$ . As the void ratio after consolidation varies to-and-fro along the void ratio axis,  $\sigma'_{3\text{ crit}}$  varies, and so will the volume changes at failure. For a real sand, the Peacock diagram has curved surfaces. For example, the line  $KP$  in Fig. 11.10 should look like one of the curves in Fig. 11.8. The line  $PW$  in Fig. 11.10 is also curved. See line  $PW$  in Fig. 11.7; here you are looking at a plane on the Peacock diagram where  $\Delta V/V_o = 0$ .

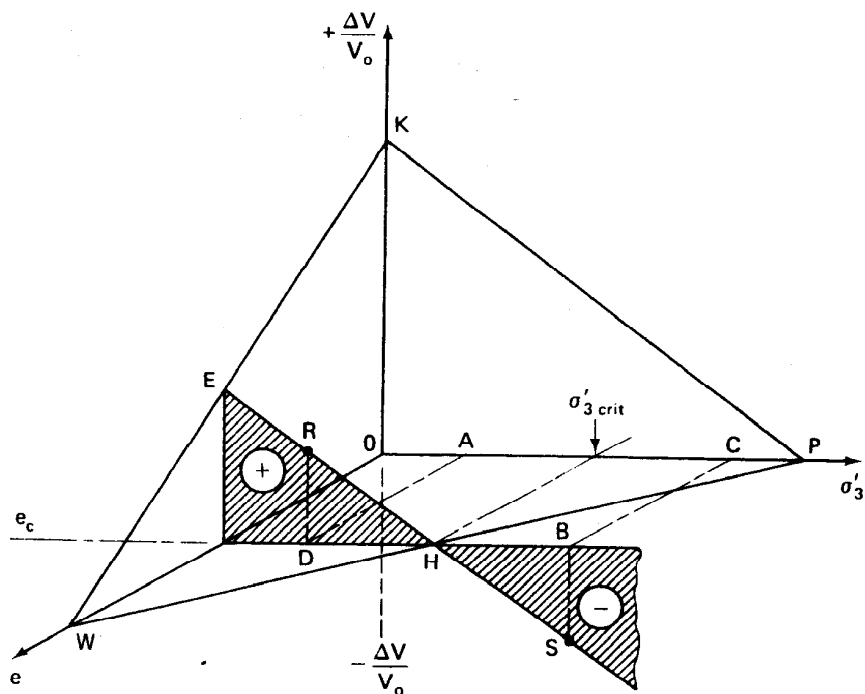


Fig. 11.10 Peacock diagram, which combines Figs. 11.9a and b in an idealized graph to show the behavior of drained triaxial tests on sand.

## 11.5 BEHAVIOR OF SATURATED SANDS DURING UNDRAINED SHEAR

The main difference between drained and undrained triaxial shear is that in an undrained test no volume change is allowed during axial loading. However, unless the confining pressure just happens to be at  $\sigma'_3 \text{ crit}$ , the soil will *tend to change volume* during loading. For example, referring to the Peacock diagram, Fig. 11.10, again, if a soil at  $e_c$  is tested *undrained* at a  $\sigma'_3$  at point C, then the sand sample would *tend* to decrease in volume, but it can't. As a result, a *positive* pore pressure is induced, which causes a *reduction* in the effective stress. The limiting or minimum effective pressure at failure is  $\sigma'_{3\text{crit}}$  because at this pressure  $\Delta V/V_0$  is zero. If no tendency towards volume change takes place, then no excess pore pressure is induced. So the maximum possible pore pressure in this example is equal to  $\sigma'_c - \sigma'_{3\text{crit}}$ , or the distance BH in Fig. 11.10. The Mohr circles at failure for this case are shown in Fig. 11.11a. The dashed circles E represent the effective stress conditions, whereas the solid circle T is in terms of total stresses. Since Eq. 7-13 always holds, the two circles are separated by the value of  $\Delta u$  induced at any time during the test. Since the volume change *tendency* is to reduce, a positive change (increase) in pore pressure is caused, which in turn results in a *reduction* in the effective stress. Thus, for this example,  $\Delta u = B - H = \sigma'_c - \sigma'_{3f} = \sigma'_c - \sigma'_{3\text{crit}}$ . The  $(\sigma_1 - \sigma_3)_f$  is given by Eq. 11-3 when the confining pressure at failure is  $\sigma'_{3\text{crit}}$ .

$$(\sigma_1 - \sigma_3)_f = \sigma'_{3\text{crit}} \left[ \left( \frac{\sigma_1}{\sigma'_3} \right)_f - 1 \right]$$

Also, if we were to run a *drained* test with the confining pressure equal to  $\sigma'_3c$  at point C, the drained strength would be much larger than the undrained strength since its Mohr circle must be tangent to the effective Mohr failure envelope. Just look at the relative sizes of the two effective Mohr circles in Fig. 11.11a.

A different response occurs when we run a test with the effective confining pressure less than  $\sigma'_{3\text{crit}}$  such as point A in Fig. 11.10. From the Peacock diagram, we would expect the sample to *tend* to dilate (ordinate RD). Since the specimen is prevented from actually expanding, a *negative* pore pressure is developed which *increases* the effective stress from D (A) towards H ( $\sigma'_{3\text{crit}}$ ). Thus, as in the previous example, the limiting effective stress is the critical confining pressure  $\sigma'_{3\text{crit}}$ . (The situation may arise where the negative pore water pressure approaches -100 kPa or -1 atmosphere, and cavitation takes place, but we will ignore this possibility in this chapter.) The whole point of this exercise is that we may predict the

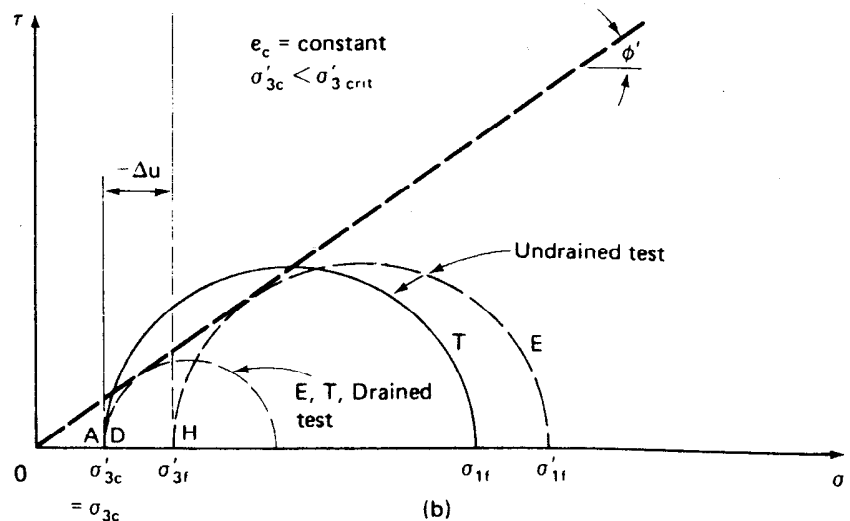
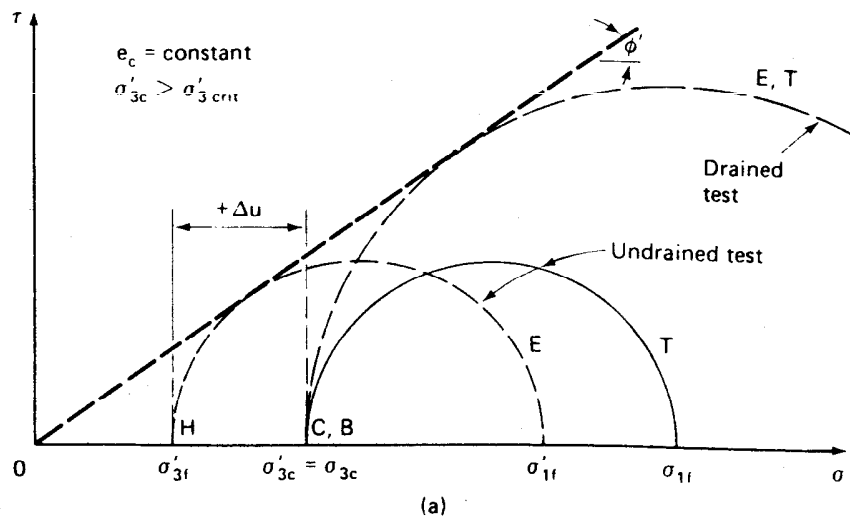


Fig. 11.11 The Mohr circles for undrained and drained triaxial compression tests: (a) case where  $\sigma'_3c > \sigma'_3\text{crit}$ ; (b) case where  $\sigma'_3c < \sigma'_3\text{crit}$ .

*undrained* behavior of sands from the *drained* behavior when we know the volume change *tendencies* as idealized in the Peacock diagram.

The Mohr circle representation for the case where  $\sigma'_3c < \sigma'_3\text{crit}$  is presented in Fig. 11.11b. The undrained test starts out at  $\sigma'_3c$ , point A, and since the induced pore water pressure is negative, the effective confining pressure increases until failure is reached at point H. Note that the effective stress Mohr circles E at failure in Figs. 11.11a and b are the same

**TABLE 11-1** A Summary of Concepts Shown in Fig. 11.11

Effective Consolidation Pressure	Mohr Circles		
	Drained, Effective = Total	Undrained, Effective	Undrained, Total
$\sigma'_c > \sigma'_{3\text{ crit}}$	Larger than undrained	Smaller than drained: Left of total stress circle $\sigma'_{3f} < \sigma'_c$	Smaller than drained: Right of effective stress circle
$\sigma'_c < \sigma'_{3\text{ crit}}$	Smaller than undrained	Larger than drained: Right of total stress circle $\sigma'_{3f} > \sigma'_c$	Larger than drained: Left of effective stress circle
$\sigma'_c \equiv \sigma'_{3\text{ crit}}$	All circles would be the same; because no volume change tendencies exist, $\Delta u = 0$ during the test.		

size because, for this void ratio  $e_c$ , the effective stress at failure is the same,  $\sigma'_{3\text{ crit}}$ . If the effective stress and void ratio are the same, then the samples would have the same compressive strength,  $\sigma'_{1f} - \sigma'_{3f}$ ; thus the circles have the same diameter. Note that the total stress circle  $T$ , at failure, is also the same size as the effective stress circle because  $(\sigma_1 - \sigma_3)_f$  is the same for both  $T$  and  $E$ ; also  $T$  lies to the *left* of  $E$ . This case is the opposite of Fig. 11.11a. (The total stress Mohr failure envelopes have been omitted from the figure to simplify things.) Note also that the *drained* Mohr circle for this second case is substantially *smaller* than the effective stress circle for the undrained case. As before, the circle starts at  $\sigma'_c$ , and it must be tangent to the effective Mohr failure envelope. Since the void ratio after consolidation  $e_c$  is a constant for all the tests shown in Fig. 11.11, all the effective Mohr circles must be tangent to the effective stress failure envelope.

A summary of the main points just discussed and shown in Fig. 11.11 is presented in Table 11-1. For a more comprehensive treatment of the undrained strength characteristics of sands see Seed and Lee (1967).

### EXAMPLE 11.1

**Given:**

A battery filler (rubber squeeze bulb plus glass tube) contains *dense* sand. The battery filler bulb and sand are completely saturated with water.

**Required:**

If the bulb is squeezed, describe what happens to the water level in the glass tube. Will it go up, down, or remain the same?

**Solution:**

Because the sand is dense, it will tend to dilate or expand when sheared. This action will create a slightly negative pressure in the water, which will draw water into the voids and cause the level in the glass tube to move downward.

---

**EXAMPLE 11.2****Given:**

The same apparatus as for Example 11.1, only now the bulb is filled with loose sand.

**Required:**

Predict the behavior of the water level in the glass tube when the bulb is squeezed.

**Solution:**

When loose sand is sheared, the soil will tend to decrease in volume. This action will create a positive pressure in the water, which will squeeze water out of the voids. Thus the water level in the tube will move upward. It follows that if the sand in the battery filler bulb is at its critical void ratio, then upon squeezing (shearing) the bulb, the water level may at first decrease slightly, but with continued squeezing it will return to its original level; that is, no net volume change will occur when the sand is at  $e_{crit}$ .

---

**EXAMPLE 11.3****Given:**

A CD triaxial test is conducted on a granular soil. At failure,  $\sigma'_1/\sigma'_3 = 4.0$ . The effective minor principal stress at failure was 100 kPa.

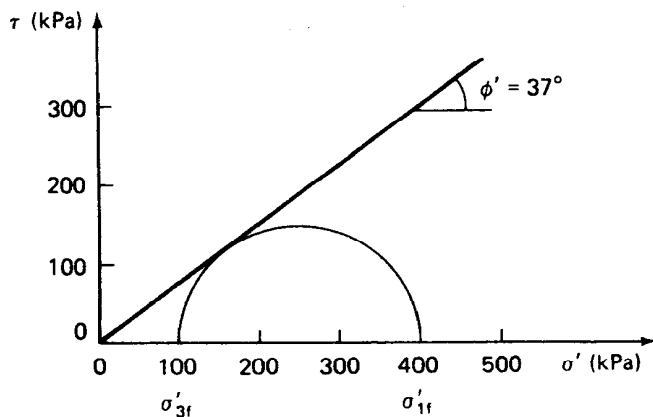


Fig. Ex. 11.3

**Required:**

- Compute  $\phi'$ .
- What is the principal stress difference at failure?
- Plot the Mohr circle and the Mohr failure envelope.

**Solution:**

- From Eqs. 10-14, 10-16, or 11-1, we know that

$$\frac{\sigma'_{1f}}{\sigma'_{3f}} = \frac{1 + \sin \phi'}{1 - \sin \phi'} = \tan^2\left(45^\circ + \frac{\phi'}{2}\right) = 4.0$$

Solving for  $\phi'$ , we obtain  $\phi' = 37^\circ$ .

- From Eq. 11-3,

$$(\sigma_1 - \sigma_3)_f = \sigma_3 \left( \frac{\sigma'_{1f}}{\sigma'_{3f}} - 1 \right) = 100 \text{ kPa} (4 - 1) = 300 \text{ kPa}$$

- See Fig. Ex. 11.3.

#### EXAMPLE 11.4

**Given:**

Figure 11.6.

**Required:**

What is the critical void ratio for Sacramento River sand when the confining pressure is 1.5 MPa?

**Solution:**

From Fig. 11.6, interpolating between the curves for  $\sigma'_3 = 1.3$  and  $2.0 \text{ MPa}$ , we find that  $e_c$  (for  $\sigma'_3 = 1.5$ ) is about 0.61 for Sacramento River sand.

---

### EXAMPLE 11.5

**Given:**

Figure 11.8.

**Required:**

What is the critical confining pressure for Sacramento River sand if the void ratio equals 0.75?

**Solution:**

From Fig. 11.8, we can interpolate between the curves for  $e_i = 0.71$  and 0.78 for the value of  $\sigma'_3$  when  $\Delta V/V_o$  is zero. We obtain a  $\sigma'_3$  of about 0.7 MPa.

---

### EXAMPLE 11.6

**Given:**

Figure 11.10, but scaled to the idealized behavior of Sacramento River sand (a combination of Figs. 11.6 and 11.8);  $\sigma'_{3\text{ crit}} = 0.4 \text{ MPa}$  and  $e_c = e_{\text{crit}} = 0.8$ .

**Required:**

Describe both the drained and undrained behavior of this sand if the test void ratios after consolidation at  $\sigma'_{3c} = 0.4 \text{ MPa}$  are (a) 0.85 and (b) 0.75.

**Solution:**

Since  $\sigma'_{3c}$  and  $e_c$  are at critical, there is by definition no volume change during shear. Thus our test plots at point H in Fig. 11.10, with the values of  $\sigma'_{3\text{ crit}}$  and  $e_c$  as given. (You can verify these values in Figs. 11.6 and 11.8.)

a. When  $e_c > e_{crit}$  ( $0.85 > 0.8$ ), then at  $\sigma'_{3c} = 0.4$  MPa the coordinates of our test would have to plot *below* the  $WOP$  plane, which means  $\Delta V/V_o$  is negative. During *drained* shear,  $\sigma'_3$  is constant (no excess pore pressure develops), and the specimen would consolidate and decrease in volume during shear. Its coordinates would be on the extension of plane  $WKP$ .

In *undrained* shear the specimen would *tend* to decrease in volume, but since it is undrained it cannot. Therefore the specimen would develop positive pore water pressure along with a concurrent decrease in  $\sigma'_3$ . In Fig. 11.10, the test coordinates must remain on the  $e = 0.85$  line *and* in the plane  $WOP$ . The only way this can happen is for  $\sigma'_3$  to decrease, which makes sense in view of the increase in pore water pressure.

b. When  $e_c < e_{crit}$  ( $0.75 < 0.80$ ) the opposite of (a) will happen: in drained shear,  $\sigma'_3$  is again constant and equal to 0.4 MPa, so for the coordinates of our test to remain on plane  $WKP$ , the  $\Delta V/V_o$  must increase. In undrained shear, the *tendency* towards volume increase would cause the pore water pressure to decrease and the  $\sigma'_3$  to increase. This is what happens when our test coordinates remain on plane  $WOP$ ; that is,  $\sigma'_3$  increases.

### EXAMPLE 11.7

**Given:**

Figure 11.10 is scaled to the behavior of Sacramento River sand (Figs. 11.6 and 11.8), with  $e_{crit} = 0.6$  and  $\sigma'_{3crit} = 1.6$  MPa.

**Required:**

Describe the behavior, both in drained and undrained shear, if we maintain this void ratio of 0.6 but test the specimen with  $\sigma'_{3c}$  of (a) 1.5 MPa and (b) 1.7 MPa.

**Solution:**

a. When  $\sigma'_{3c} < \sigma'_{3crit}$ , then the specimen will dilate and a positive  $\Delta V/V_o$  will occur. This behavior is similar to what happens to point A in Fig. 11.10. The dilation is measured by the ordinate *RD* so that the coordinates of our test remain on plane  $WKP$ .

In undrained shear, the *tendency* will be for dilation which is prevented; we must remain at  $e_c = 0.6$  and on plane  $WOP$ . Therefore  $\sigma'_3$  must increase, which makes sense physically since the induced pore water pressure tends to decrease.

b. When  $\sigma'_{3c} > \sigma'_{3\text{ crit}}$ , the behavior would be similar to path *BS* in Fig. 11.10 in drained shear. In undrained shear, the tendency towards compression would result in positive excess pore pressure and a decrease in  $\sigma'_3$ .

### EXAMPLE 11.8

**Given:**

A drained triaxial test on sand with  $\sigma'_3 = 150$  kPa and  $(\sigma'_1/\sigma'_3)_{\max} = 3.7$ .

**Required:**

- a.  $\sigma'_{1f}$ ,
- b.  $(\sigma_1 - \sigma_3)_f$ , and
- c.  $\phi'$ .

**Solution:**

- a.  $(\sigma'_1/\sigma'_3)_f = 3.7$ . Solve for  $\sigma'_{1f}$ .  $\sigma'_{1f} = 3.7(150) = 555$  kPa.
- b.  $(\sigma_1 - \sigma_3)_f = (\sigma'_1 - \sigma'_3)_f = 555 - 150 = 405$  kPa.
- c. Assume for sand that  $c' = 0$ . So, from Eq. 10-13,

$$\phi' = \arcsin \left( \frac{\sigma'_{1f} - \sigma'_{3f}}{\sigma'_{1f} + \sigma'_{3f}} \right) = \arcsin \frac{405}{705} = 35^\circ$$

Note: We could also determine  $\phi'$  graphically from the Mohr circle plotted for failure conditions, as shown in Fig. Ex. 11.8.

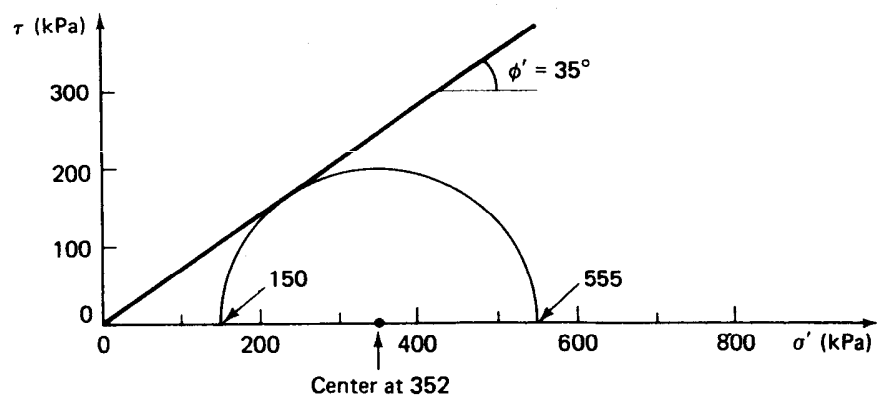


Fig. Ex. 11.8

---

### EXAMPLE 11.9

Given:

Assume the test specimen of Example 11.8 was sheared *undrained* at the same total cell pressure (150 kPa). The induced excess pore water pressure at failure  $\Delta u_f$  is equal to 70 kPa.

Required:

- a.  $\sigma'_{1f}$ ,
- b.  $(\sigma_1 - \sigma_3)_f$ ,
- c.  $\phi'$  in terms of *total* stress, and
- d. the angle of the failure plane  $\alpha_f$ .

Solution:

a., b. Since the void ratio after consolidation would be the same for this test as for Example 11.8, assume  $\phi'$  is the same. You can do this problem either (1) analytically or (2) graphically.

1. *Analytically*: We know that

$$(\sigma_1 - \sigma_3)_f = \sigma'_{3f} \left[ \left( \frac{\sigma'_1}{\sigma'_3} \right)_{\max} - 1 \right]$$

from Eq. 11-3.

$$\sigma'_{3f} = \sigma_{3f} - \Delta u_f = 150 - 70 = 80 \text{ kPa}$$

So

$$(\sigma_1 - \sigma_3)_f = 80(3.7 - 1) = 216 \text{ kPa}$$

$$\sigma'_{1f} = (\sigma_1 - \sigma_3)_f + \sigma'_{3f} = 216 + 80 = 296 \text{ kPa}$$

These are the answers to parts (a) and (b).

c. We can write Eqs. 10-13 and 11-1 in terms of total stresses. Using Eq. 10-13,

$$\sin \phi_{\text{total}} = \frac{\sigma_1 - \sigma_3}{\sigma_1 + \sigma_3} = \frac{216}{(296 + 70) + 150} = 0.42$$

$$\phi_{\text{total}} = 24.8^\circ$$

Using Eq. 11-1,

$$\frac{\sigma_{1f}}{\sigma_{3f}} (\text{no primes}) = \frac{(296 + 70)}{150} = 2.44 = \tan^2 \left( 45^\circ + \frac{\phi}{2} \right)$$

Solving for  $\phi_{\text{total}}$ , we obtain  $\phi_{\text{total}} = 24.8^\circ$ .

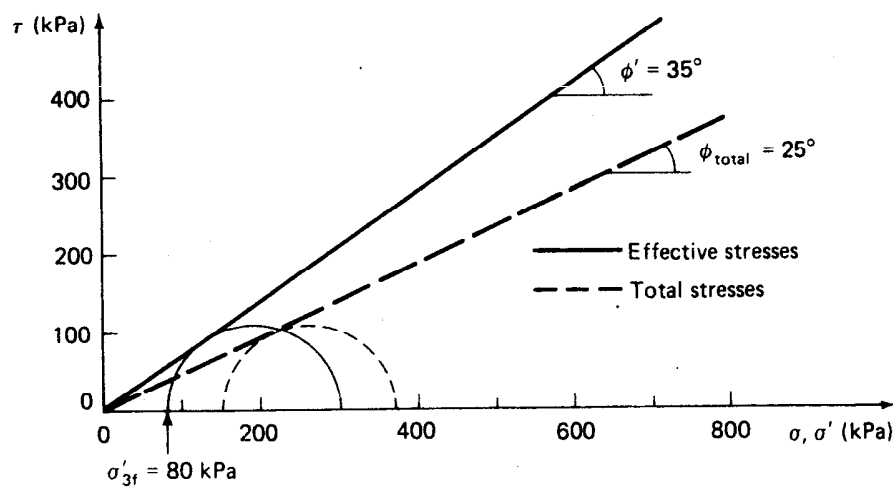


Fig. Ex. 11.9

2. *Graphically:* Plot the Mohr failure envelope with  $\phi' = 35^\circ$  on a Mohr diagram (Fig. Ex. 11.9). There is only *one* circle that is tangent to the envelope and with  $\sigma'_{3f} = 80 \text{ kPa}$  ( $150 - 70$ ). Once the circle is drawn (trial and error),  $\sigma'_{1f}$  is automatically determined ( $\sigma'_{1f} = 296 \text{ kPa}$ ) as is  $(\sigma_1 - \sigma_3)_f$ , the diameter of the failure circle ( $= 216 \text{ kPa}$ ).

The Mohr circle at failure in terms of total stresses has the same diameter since  $(\sigma_1 - \sigma_3) = (\sigma'_1 - \sigma'_3)$ . You can plot the total stress circle starting at  $\sigma_{3f} = 150$ , the total cell pressure, and determine  $\phi_{\text{total}}$ . Compare Figs. Ex. 11.8 and 11.9 with Fig. 11.11a.

d. From Eq. 10-10,  $\alpha_f = 45^\circ + \phi'/2 = 62.5^\circ$ .

### EXAMPLE 11.10

**Given:**

The same sand as for Example 11.9 except, that the cell pressure is 300 kPa.

**Required:**

$\Delta u_f$ .

**Solution:**

There are several approaches to this problem. Graphically, we could construct a total stress circle tangent to the total failure envelope shown in

Fig. Ex. 11.9 but starting at  $\sigma'_{3c} = \sigma'_{3f} = 300$  kPa. Then shift your compass or circle maker to the left until the circle is just tangent to the effective Mohr failure envelope.

$$\Delta u_f = \sigma_{3f} - \sigma'_{3f} = 300 \text{ kPa} - 160 = 140 \text{ kPa}$$

Analytically, use Eq. 11-1 and  $(\sigma_1/\sigma_3)_{\text{total}}$  from Ex. 11.9.

$$\sigma_{1f} = \sigma_{3f} \left( \frac{\sigma_1}{\sigma_3} \right)_{\text{total}} = 300(2.44) = 732 \text{ kPa}$$

$$\sigma_{1f} - \sigma_{3f} = 732 - 300 = 432 \text{ kPa}$$

From Eq. 11-3 and  $(\sigma'_1/\sigma'_3)_f = 3.7$  (Example 11.8),

$$\sigma'_{3f} = \frac{(\sigma_1 - \sigma_3)_f}{(\sigma'_1/\sigma'_3)_f - 1} = \frac{423}{3.7 - 1} = 160 \text{ kPa}$$

$$\Delta u_f = \sigma_{3f} - \sigma'_{3f} = 300 - 160 = 140 \text{ kPa}$$

Check:  $\Delta u_f = \sigma_{1f} - \sigma'_{1f} = 732 - 3.7(160) = 140 \text{ kPa}$

## 11.6 FACTORS THAT AFFECT THE SHEAR STRENGTH OF SANDS

Since sand is a "frictional" material we would expect those factors that increase the frictional resistance of sand to lead to increases in the angle of internal friction. First, let us summarize the factors that influence  $\phi$ .

1. Void ratio or relative density
2. Particle shape
3. Grain size distribution
4. Particle surface roughness
5. Water
6. Intermediate principal stress
7. Particle size
8. Overconsolidation or prestress

Void ratio, related to the density of the sand, is perhaps the most important single parameter that affects the strength of sands. Generally speaking, for drained tests either in the direct shear or triaxial test apparatus, the lower the void ratio (higher density or higher relative density), the higher the shear strength. The Mohr circles for the triaxial test data presented earlier are shown in Fig. 11.12 for various confining

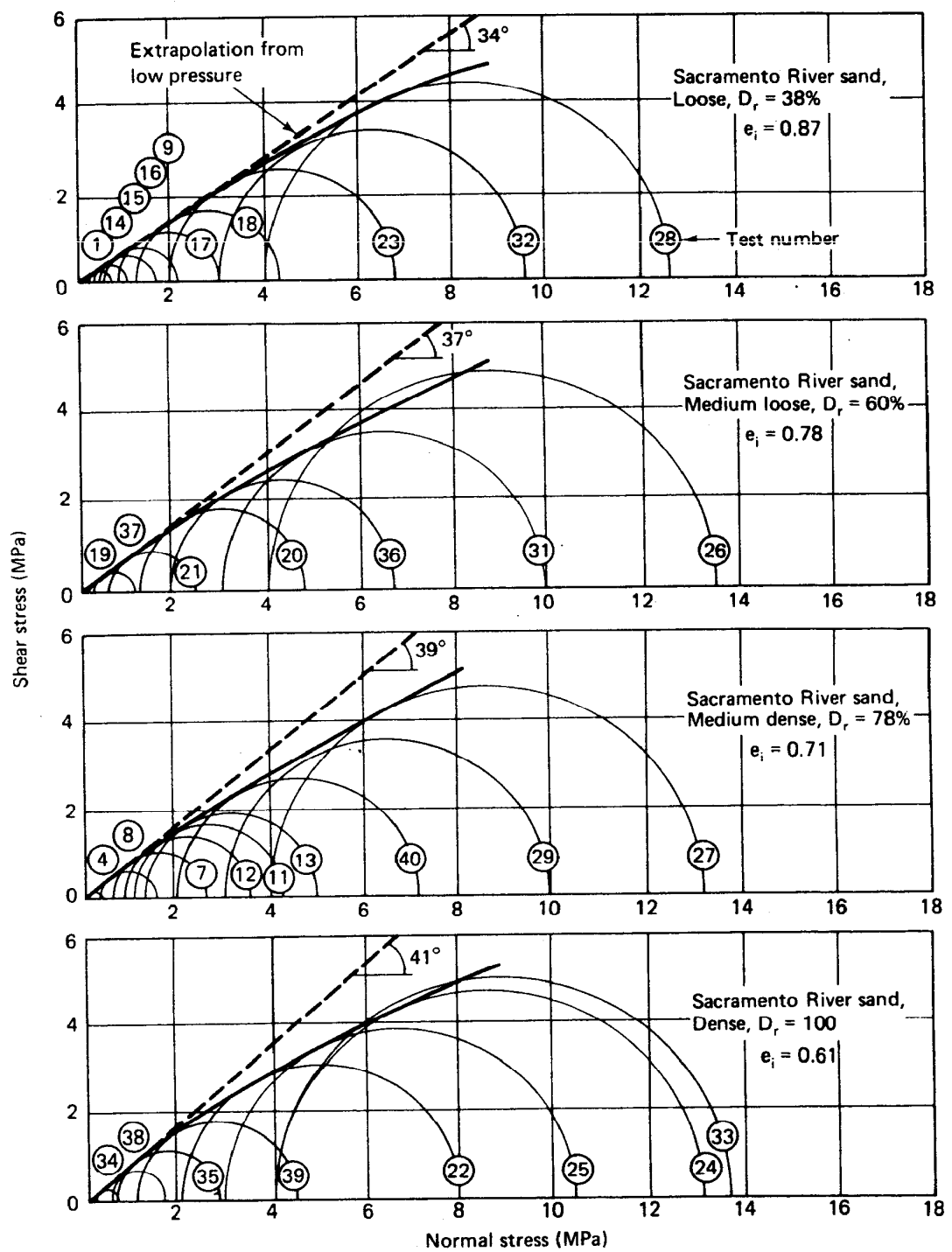


Fig. 11.12 Mohr circles and failure envelopes from drained triaxial tests, illustrating the effects of void ratio or relative density on shear strength (after Lee, 1965; also after Lee and Seed, 1967).

pressures and four initial void ratios. You can see that as the void ratio decreases, or the density increases, the angle of internal friction or angle of shearing resistance  $\phi$  increases.

Another thing you should notice is that the Mohr failure envelopes in Fig. 11.12 are curved; that is,  $\phi'$  is not a constant if the range in confining pressures is large. We usually speak of  $\phi'$  as if it were a constant, but we understand that the Mohr failure envelope really is curved.

The effects of relative density or void ratio, grain shape, grain size distribution, and particle size on  $\phi$  are summarized by Casagrande in Table 11-2. Values were determined by triaxial tests on saturated samples at moderate confining pressures. Generally speaking, with all else constant,  $\phi$  increases with increasing angularity (Fig. 2.5). If two sands have the same

**TABLE 11-2 Angle of Internal Friction of Cohesionless Soils\***

No.	General Description	Grain Shape	$D_{10}$ (mm)	$C_u$	Loose		Dense	
					$e$	$\phi$ (deg)	$e$	$\phi$ (deg)
1	Ottawa standard sand	Well rounded	0.56	1.2	0.70	28	0.53	35
2	Sand from St. Peter sandstone	Rounded	0.16	1.7	0.69	31	0.47	37†
3	Beach sand from Plymouth, MA	Rounded	0.18	1.5	0.89	29	—	—
4	Silty sand from Franklin Falls Dam site, NH	Subrounded	0.03	2.1	0.85	33	0.65	37
5	Silty sand from vicinity of John Martin Dam, CO	Subangular to subrounded	0.04	4.1	0.65	36	0.45	40
6	Slightly silty sand from the shoulders of Ft. Peck Dam, MT	Subangular to subrounded	0.13	1.8	0.84	34	0.54	42
7	Screened glacial sand, Manchester, NH	Subangular	0.22	1.4	0.85	33	0.60	43
8‡	Sand from beach of hydraulic fill dam, Quabbin Project, MA	Subangular	0.07	2.7	0.81	35	0.54	46
9	Artificial, well-graded mixture of gravel with sands No. 7 and No. 3	Subrounded to subangular	0.16	68	0.41	42	0.12	57
10	Sand for Great Salt Lake fill (dust gritty)	Angular	0.07	4.5	0.82	38	0.53	47
11	Well-graded, compacted crushed rock	Angular	—	—	—	—	0.18	60

\*By A. Casagrande.

†The angle of internal friction of the undisturbed St. Peter sandstone is larger than 60° and its cohesion so small that slight finger pressure or rubbing, or even stiff blowing at a specimen by mouth, will destroy it.

‡Angle of internal friction measured by direct shear test for No. 8, by triaxial tests for all others.

relative density, the soil that is better graded (for example, an SW soil as opposed to an SP soil) has a larger  $\phi$ . (As a reminder, two sands at the same void ratio may not necessarily have the same relative density.) Particle size, at constant void ratio, does *not* seem to influence  $\phi$  significantly. Thus a fine sand and a coarse sand at the same void ratio will probably have about the same  $\phi$ .

Another parameter, not included in Table 11-2, is surface roughness, which is very difficult to measure. It will, however, have an effect on  $\phi$ . Generally, the greater the surface roughness, the greater will be  $\phi$ . It has also been found that wet soils show a  $1^\circ$  to  $2^\circ$  lower  $\phi$  than if the sands were dry.

So far we have only discussed results from direct shear or triaxial tests in which  $\sigma_2 = \sigma_3$  or  $\sigma_1$ . To investigate the influence of the intermediate principal stress, other types of tests like plane strain or cuboidal shear tests must be used (Fig. 10.14). Research summarized by Ladd, et al. (1977) indicates that  $\phi$  in plane strain is larger than  $\phi$  in triaxial shear by  $4^\circ$  to  $9^\circ$  in dense sands and  $2^\circ$  to  $4^\circ$  for loose sands. A conservative estimate of the plane strain angle of internal friction  $\phi_{ps}$  may be found from triaxial test results  $\phi_{tx}$ , using the following equations (after Lade and Lee, 1976):

$$\phi_{ps} = 1.5\phi_{tx} - 17^\circ \quad (\phi_{tx} > 34^\circ) \quad (11-5a)$$

$$\phi_{ps} = \phi_{tx} \quad (\phi_{tx} \leq 34^\circ) \quad (11-5b)$$

The final factor on our list, overconsolidation or prestress of sands, has been found to not significantly affect  $\phi$ , but it strongly affects the compression modulus of granular materials (Lambrechts and Leonards, 1978). Ladd, et al. (1977) discuss the various effects of prestress on the behavior of granular materials.

All the factors mentioned above are summarized in Table 11-3. Some correlations between  $\phi'$  and dry density, relative density, and soil classification are shown in Fig. 11.13. This figure and Table 11-2 are very useful for estimating the frictional characteristics of granular materials. If you

TABLE 11-3 Summary of Factors Affecting  $\phi$

Factor	Effect
Void ratio $e$	$e \uparrow, \phi \downarrow$
Angularity $A$	$A \uparrow, \phi \uparrow$
Grain size distribution	$C_u \uparrow, \phi \uparrow$
Surface roughness $R$	$R \uparrow, \phi \uparrow$
Water $W$	$W \uparrow, \phi \downarrow$ slightly
Particle size $S$	No effect (with constant $e$ )
Intermediate principal stress	$\phi_{pr} \geq \phi_{tx}$ (see Eqs. 11-5a, b)
Overconsolidation or prestress	Little effect

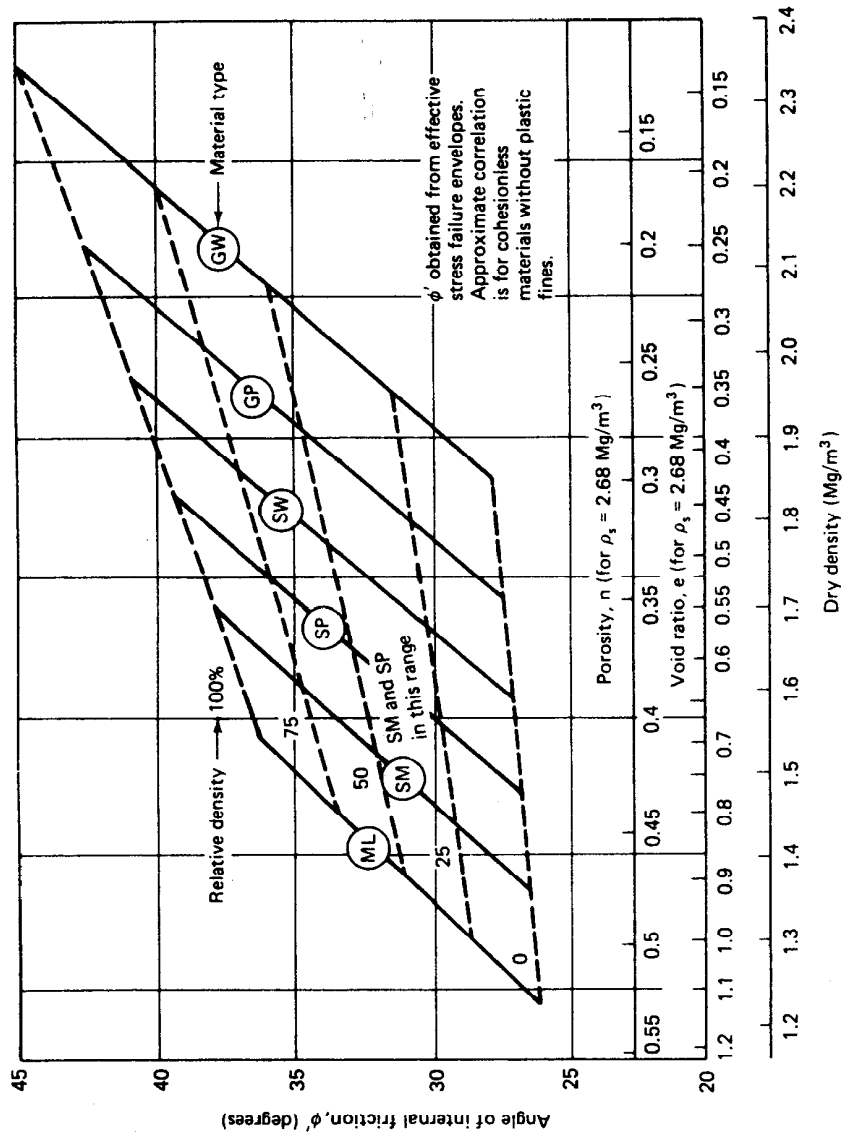


Fig. 11.13 Correlations between the effective friction angle in triaxial compression and the dry density, relative density, and soil classification (after U.S. Navy, 1971).

have a complete visual classification of the materials at your site, together with some idea of the in situ relative density, you already have a pretty good idea about the shear strength behavior of the soils in advance of a laboratory testing program. For small projects, such estimates may be all you need for design.

## 11.7 THE COEFFICIENT OF EARTH PRESSURE AT REST FOR SANDS

In Sec. 7.6 we defined the coefficient of earth pressure at rest as

$$K_o = \frac{\sigma'_{ho}}{\sigma'_{vo}} \quad (7-19)$$

where  $\sigma'_{ho}$  = the horizontal effective stress in situ, and

$\sigma'_{vo}$  = the vertical effective stress in situ.

We mentioned that a knowledge of  $K_o$  is very important for the design of earth-retaining structures and many foundations; it also influences liquefaction potential, as we shall soon see. Thus, if your assessment of the initial in situ stresses in the soil is inaccurate, you can be way off in your prediction of the performance of such structures.

You already know from Chapter 7 (Sec. 7.5) how to estimate  $\sigma'_{vo}$  from the densities of the overlying materials, the thicknesses of the various layers, and the location of the ground water table. Accurate measurements of  $\sigma'_{ho}$  are not easy, especially in sands. It is virtually impossible to install an earth pressure cell in situ, for example, without causing some disturbance and densification of the sands around the cell, and this changes the stress field at the very point of measurement. Consequently, the approach usually taken is to estimate  $K_o$  from theory or laboratory tests, and then calculate  $\sigma_{ho}$  and  $\sigma'_{ho}$  from Eq. 7-19.

The best known equation for estimating  $K_o$  was derived by Jaky (1944, 1948), which is a theoretical relationship between  $K_o$  and the angle of internal friction  $\phi'$ , or

$$K_o = 1 - \sin \phi' \quad (11-6)$$

This relationship, as shown in Fig. 11.14, seems to be an adequate predictor of  $K_o$  for normally consolidated sands. Since most of the points lie between 0.35 and 0.5 for these sands,  $K_o$  of 0.4 to 0.45 would be a reasonable average value to use for preliminary design purposes.

If the sand has been preloaded, then  $K_o$  is somewhat greater. Schmidt (1966, 1967) and Alpan (1967) suggested that the increase in  $K_o$  could be

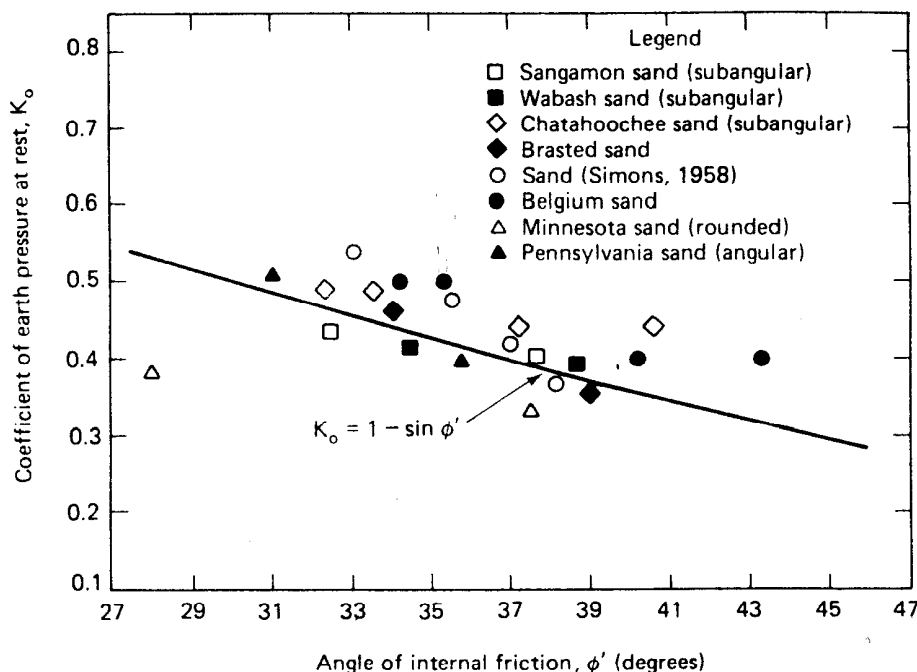


Fig. 11.14 Relationship between  $K_o$  and  $\phi'$  for normally consolidated sands (after Al-Hussaini and Townsend, 1975).

related to the overconsolidation ratio (OCR) by

$$K_{o-oc} = K_{o-nc} (\text{OCR})^h \quad (11-7)$$

where  $K_{o-oc} = K_o$  for the overconsolidated soil,

$K_{o-nc} = K_o$  for the normally consolidated soil, and

$h$  = an empirical exponent.

Values of  $h$  range between 0.4 and 0.5 (Alpan, 1967; Schmertmann, 1975) and even as high as 0.6 for very dense sands (Al-Hussaini and Townsend, 1975). Ladd, et al. (1977) pointed out that this exponent itself varies with OCR, and it seems to depend on the direction of the applied stresses. For example, Al-Hussaini and Townsend (1975) found a significantly lower  $K_o$  during reloading than during unloading in laboratory tests on a uniform medium sand. Thus  $K_o$  appears to be very sensitive to the precise stress history of the deposit.

We shall have more to say about this subject when we discuss  $K_o$  for clays.

## 11.8 LIQUEFACTION AND CYCLIC MOBILITY BEHAVIOR OF SATURATED SANDS

You may recall that we mentioned the phenomenon of liquefaction during our description of the quicksand tank (Sec. 7.8). We described the behavior of the very loose sands in the tank during the upward flow of water (Fig. 7.12a) or when a shock load was applied to the side of the tank (Fig. 7.12c). We also gave a physical explanation for this phenomenon. We said that when loose saturated sands are subjected to strains or shocks, there is a tendency for the sand to decrease in volume. This tendency causes a positive increase in pore pressure which results in a decrease in effective stress within the soil mass. Once the pore pressure becomes equal to the effective stress, the sand loses all its strength, and it is said to be in a state of *liquefaction*.

Examples of liquefaction briefly mentioned in Sec. 7.8 included the failure of Ft. Peck Dam, Montana, and the flow slides that have occurred along the banks of the lower Mississippi River. Here, liquefaction takes place under conditions of large statically induced strains (Casagrande, 1936a, 1950). We will call this statically (monotonic loading) induced condition *liquefaction*. River banks composed of loose uniform fine sands can liquefy when subjected to large strains, such as might be caused by steepening of the banks due to erosion, and the strains produce increased pore pressures. Such a situation is shown in Fig. 11.15. Initially a soil element at *A*, some distance from the slope, is under a much safer state of initial stress ( $K_0$  conditions—discussed in the previous section) than the element at *B*. As erosion starts at the base of the slope, the soil stresses are increased, the pore water pressure rises, and a limited zone (shown in Fig. 11.15a) can liquefy. As this material flows out into the river, additional stresses are applied to the adjacent soils, and they also can liquefy (Fig. 11.15b). In this way, liquefaction *progresses* inland until the material comes to equilibrium on a very flat slope angle (Fig. 11.15c). Some important characteristics of different types of flow slides are listed in Table 11-4. Other types of soils which may be afflicted by flow slides should be added to column 2: hydraulically placed fills of sands and silty sands such as mine waste or tailings dams. As mentioned in Sec. 7.8, these structures are built with very little engineering design or construction supervision, and liquefaction-type failures are relatively common. Notice also in Table 11-4 the character of the strains necessary to start flow (column 3). These strains can be caused by a static increase in stress, like the case of the riverbank erosion leading to progressive liquefaction, or they can be caused by dynamic or vibratory loads. Examples of this second type of

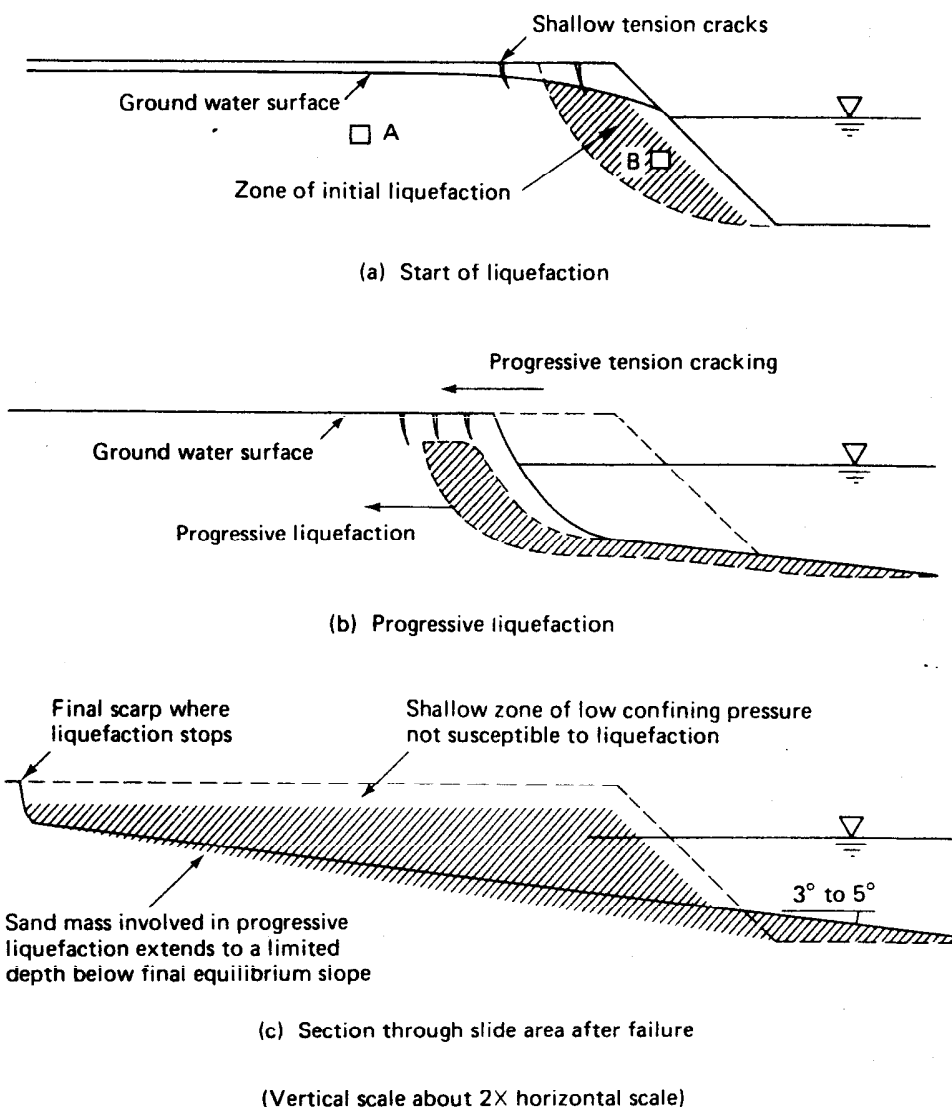


Fig. 11.15 Liquefaction in loose sand adjacent to a waterfront (after Casagrande, 1975).

loading are pile driving, blasting, traffic, rotating machinery, storm waves, and earthquakes. Because major earthquakes affect large areas, they can and have caused large deposits of loose saturated sand to liquefy (for example, Seed and Idriss, 1967; Seed and Wilson, 1967).

A different kind of liquefaction than that which occurs due to static stresses is called *cyclic mobility*. Here cyclic loads, like those from an earthquake, cause a buildup of pore pressures in medium to high density

**TABLE 11-4 Flow Slides in Soils\***

Sensitivity of Soil to Liquefaction ("type A")	Soils Which May Be Affected by Indicated Types of Flow Slides (2)	Character of Strain Necessary to Start Flow (3)	Character and Speed of Flow Failure (4)	Examples of Flow Failures (5)
High sensitivity, "type A"	Sand in bulked condition; rock flour	Small strains such as earthquake shocks, explosions, or vibrations simultaneously affecting a large mass	Rapid flow (a few minutes)	Flow failure of railroad embankment in Holland (1918); silt flows in Laurentian Mts.
Low sensitivity, "type B"	River sands; rock flour	Large strains <sup>†</sup> created simultaneously in a large volume; e.g., shear failure in clay or shale transmitted into overlying sand	Rapid flow (a few minutes)	Ft. Peck Dam (river sands in foundation and hydraulic fill sand in dam)
Low sensitivity, "type C"	River sands; rock flour; varved silts and clays; clays having very great sensitivity to remolding	Large strains created progressively	Progressive liquefaction; up to several hours' duration, depending on mass involved	Mississippi River bank slides; flow slides in Holland; flow slides in "bull's liver" and in varved clays in excavations

\*After A. Casagrande (1950).

<sup>†</sup>Large strains may be invited by intrusive pore pressures created, for example, in a varved clay. However, these intrusive pressures are only indirectly responsible for subsequent liquefaction in silt layers, or layers of super-sensitive clays.

saturated sands and induce measurable strains in samples that ordinarily exhibit a dilative response under static loads; this phenomenon is opposite to the behavior predicted by the Peacock diagram of Fig. 11.10. Thus *cyclic* stresses, if they are large enough and for a sufficient duration (that is, number of cycles), can cause medium dense to very dense saturated sands to liquefy under the right conditions of density and confining pressure. Loose sands, of course, fail at the least number of cycles.

Let's begin our discussion of the behavior of sands under cyclic loading by first studying some test results which showed liquefaction under static stresses. These tests, from Castro (1969), presented in Fig. 11.16, show the results of three CU tests and one CD test, all hydrostatically consolidated to 400 kPa. The relative densities  $D_r$  of each specimen after consolidation are also indicated on the figure next to the stress-strain curve for each specimen. The specimens were loaded axially (monotonically) by small dead-load increments of weight applied about every minute to the soil sample.

In test *A*, the one with the lowest  $D_r$ , the peak stress difference of 200 kPa was reached in 15 min, which corresponded to an axial strain of about 1%. Then, when the next small increment of load was applied, the specimen suddenly collapsed—liquefied—and in about 0.2 s the stress decreased from 200 to 30 kPa at 5% strain, where it remained as the specimen continued to flow. Notice how the pore pressure for specimen *A* remained the same during flow. At this maximum value of pore pressure, the effective minor principal stress was only about 15 kPa, and if you calculate the  $\phi'$  from these stresses (use Eq. 10-13 or 11-1), you get  $\phi' = 30^\circ$ .

The total and effective Mohr circles at the peak and during flow after liquefaction are shown in Fig. 11.17. Also shown for comparison are the results of the CD test on the same sand at the same  $D_r$ . Both tests indicate that  $\phi' = 30^\circ$  for this loose sand, although as pointed out by Casagrande (1975), the agreement may be only a coincidence. In any event, the effective stress circle at the peak on maximum stress difference lies below the effective failure envelope.

Figure 11.17 is another good illustration of the very large differences in the strength of sands, depending on the drainage conditions we discussed in the previous sections of this chapter. Here you see the results of CD versus CU tests on the same sand at the same relative density and at the same effective consolidation stress. The differences are even greater when you consider the strength of the sand after liquefaction. In a flow slide, this sand would simply flow out like a very dense liquid, and its equilibrium slope angle might be only a very few degrees.

Now let's look at the results of tests on specimens *B* and *C* in Fig. 11.15. Specimen *B* (Fig. 11.16) at  $D_r = 44\%$  also liquefied after a peak stress difference of 250 kPa was reached at about 2% strain—then the

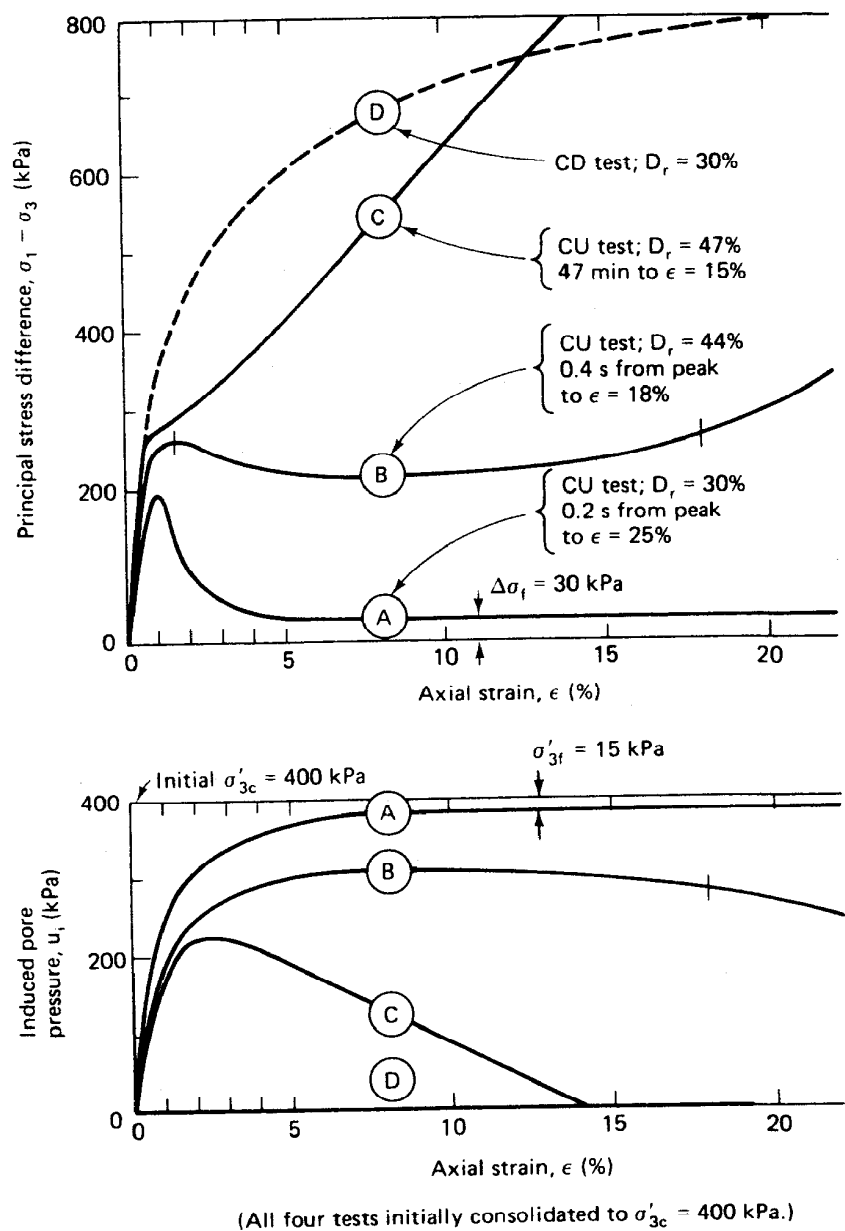


Fig. 11.16 Comparison of three hydrostatically consolidated CU tests and one CD test on banding sand loaded incrementally to failure (after Casagrande, 1975, from Castro, 1969).

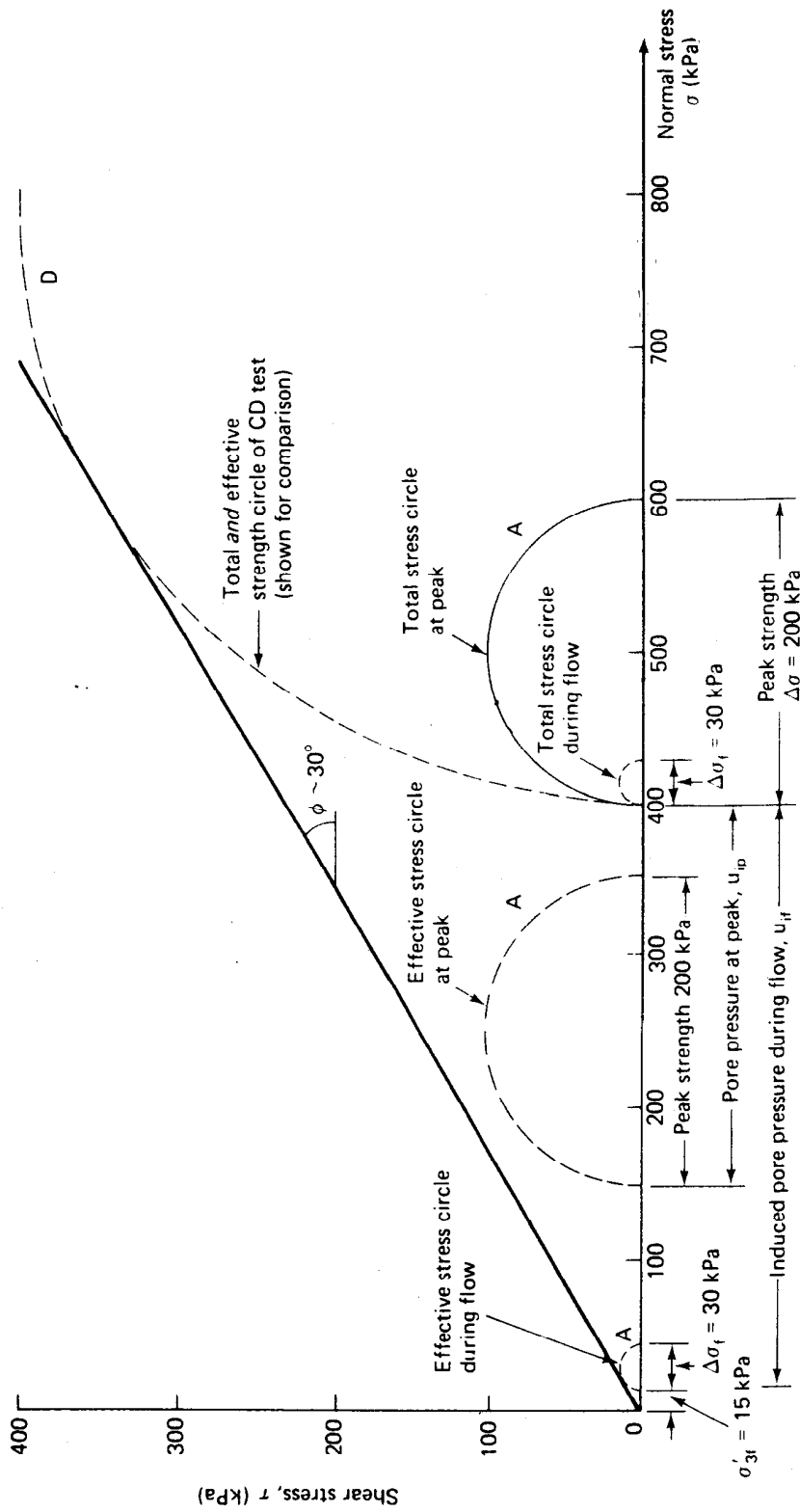


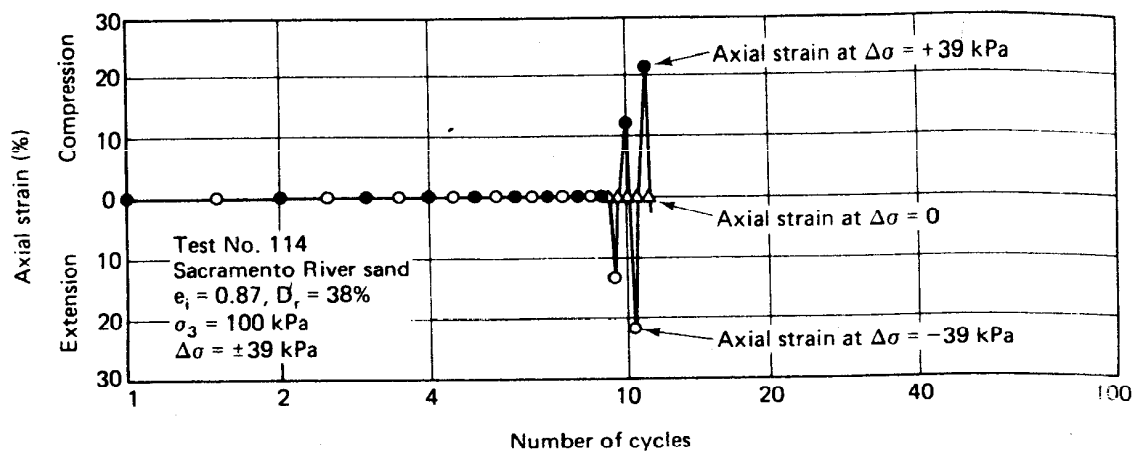
Fig. 11.17 Mohr circles in terms of total and effective stresses for the CU test (specimen A) and the CD test of Fig. 11.16. Condition at both maximum stress difference and during flow are shown (after Casagrande, 1975).

specimen flowed rapidly to a strain of 18% and stopped flowing. To get it moving again, additional small weights had to be added to the piston. Notice that the pore pressure induced in this sample during liquefaction was more than 300 kPa, and if you calculate  $\phi'$ , you get a value of about 32°. Since it was denser than specimen A, a higher friction angle is reasonable. Specimen C was slightly denser than B, and it never experienced liquefaction. The specimen obviously tried to dilate as the axial stress was increased since the pore pressure *decreased* after the maximum. These tests show how liquefaction occurs under static or monotonic loading. Their liquefaction behavior can be explained by the critical void ratio concept, and the Peacock diagram can be used to predict their behavior.

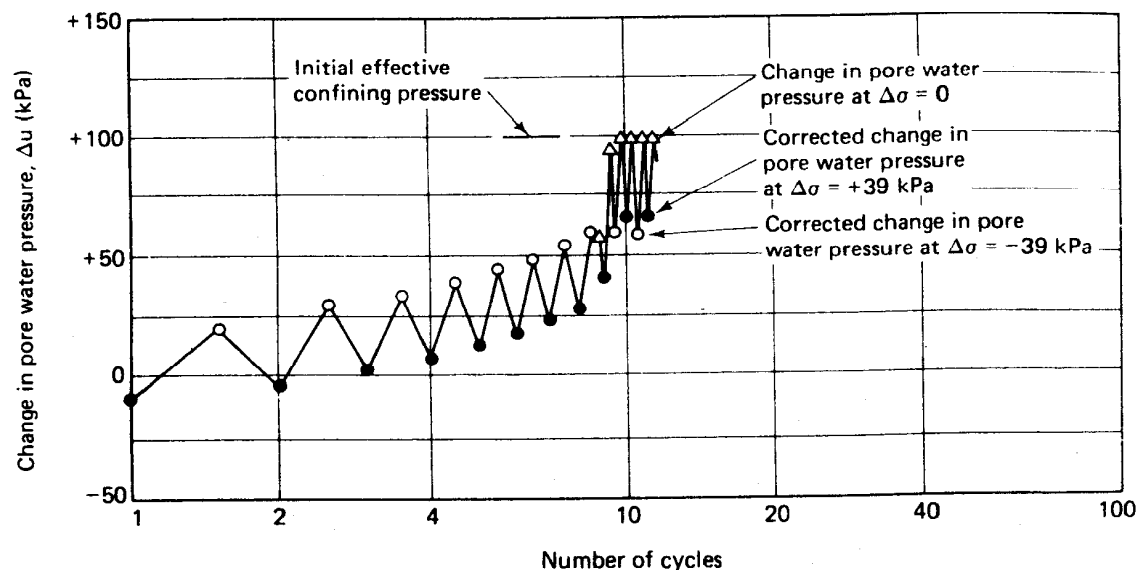
The occurrences of the 1964 Niigata, Japan, and the Anchorage, Alaska, earthquakes stimulated much research into the problems of ground subsidence and failure due to earthquake (dynamic) loading of saturated sands. Prof. H. B. Seed and his students at the University of California at Berkeley began to study this problem, using both hydrostatically and non-hydrostatically consolidated undrained cyclic triaxial tests to simulate earthquake loadings. Insight may be gained from a series of tests where the variables thought to govern the cyclic behavior of sands are tested in a systematic manner. From the Peacock diagram, it is evident that initial relative density and effective confining pressure are two key parameters. In addition, the magnitude of the cyclic stress and number of cycles to cause failure were studied. Several definitions of failure were used, such as various percent cyclic strains and when the pore pressure ratio ( $\Delta u/\sigma'_c$ ) equaled one.

Typical results from a hydrostatically consolidated cyclic undrained triaxial test on loose sand are shown in Fig. 11.18 (Seed and Lee, 1966). Very little strain developed during the first nine cycles of cyclic stress application, even though the pore pressures gradually increased. Then between the ninth and tenth cycles the pore pressure suddenly increased to a value equal to the confining pressure, and the specimen developed very large strains in the next couple of cycles. It was observed that the specimen was in a fluid condition over a wide range of strains. The suddenness of the collapse or *liquefaction* was also of interest. In several tests, the specimens showed very little strain, after even a relatively large number of cycles—then they would suddenly liquefy after only one or two more cycles were applied. All in all, it was found that loose sands behaved about as expected.

When dense sands were tested, however, the resulting behavior was quite surprising. Typical results of cyclic triaxial tests on the same sand as used in Fig. 11.18 and at the same effective consolidation pressure are shown in Fig. 11.19. Only the relative density is 78% now instead of the

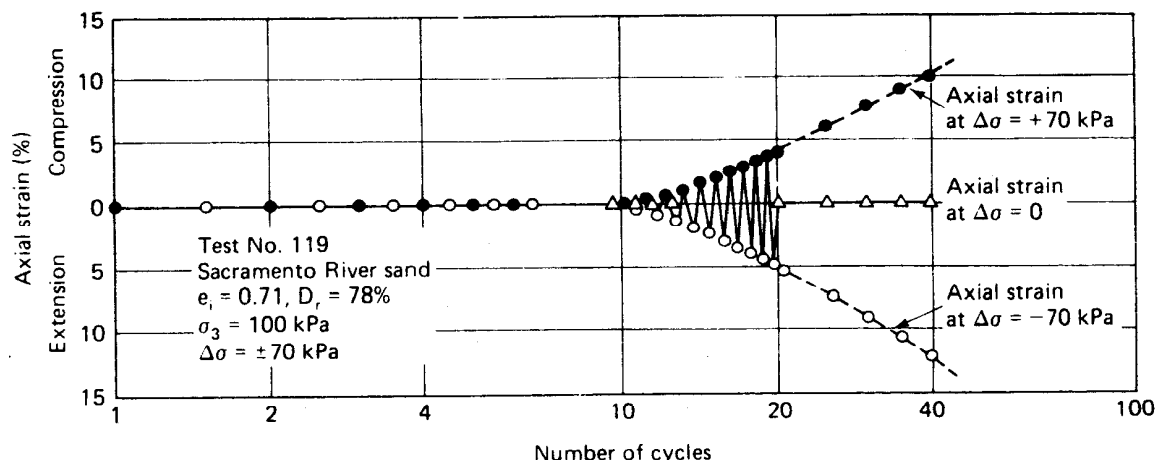


(a) Axial strain vs. number of cycles

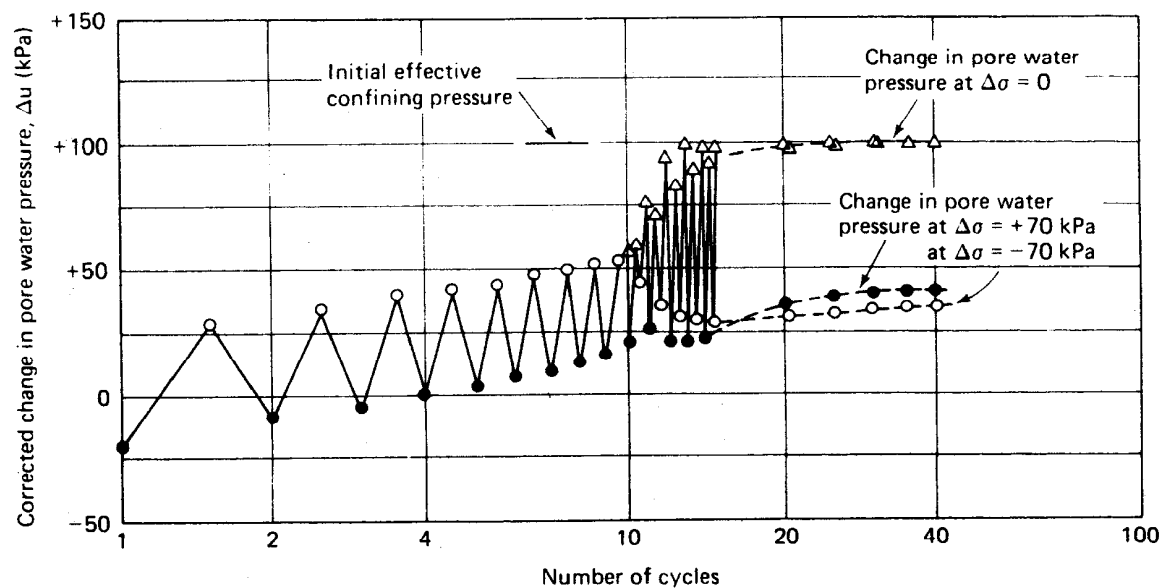


(b) Change in pore water pressure vs. number of cycles  
(corrected to mean extreme principal stress conditions)

Fig. 11.18 Typical cyclic triaxial test on loose sand (after Seed and Lee, 1966).



(a) Axial strain vs. number of cycles



(b) Corrected change in pore water pressure vs. number of cycles

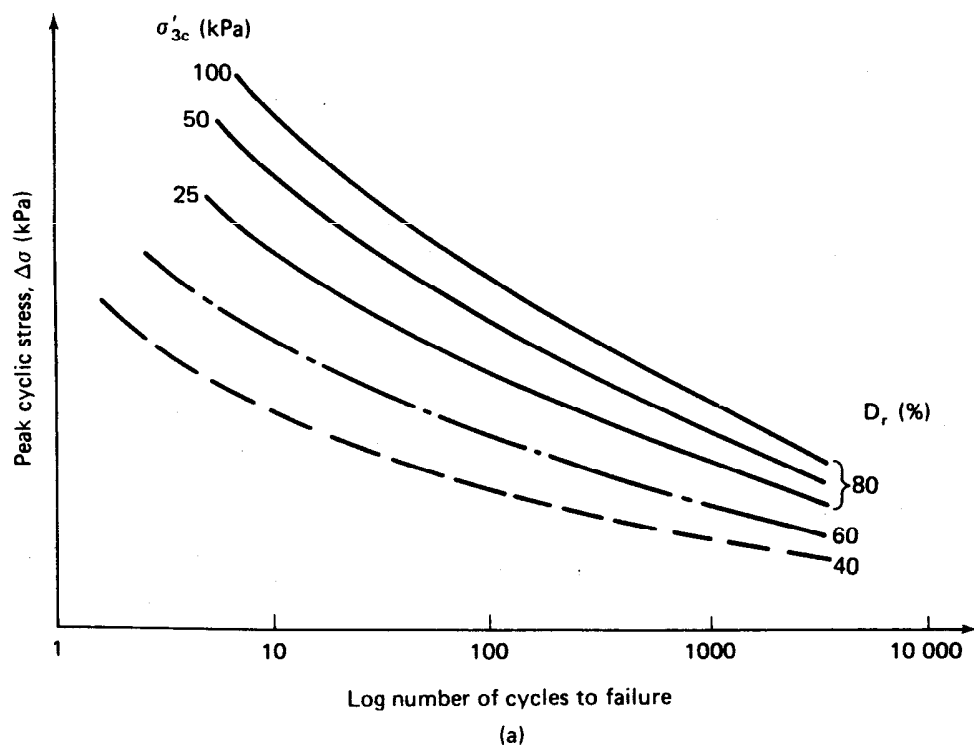
Fig. 11.19 Typical cyclic triaxial test on dense sand (after Seed and Lee, 1966).

previous 38%. During the first 10 or so cycles, very little axial strain occurred, but the induced pore water pressures gradually increased. At cycle 13, the pore pressure momentarily became equal to the total cell pressure when the principal stress difference was zero during the cycle; that is, the effective confining pressure was momentarily zero. Even though the effective stress was zero during part of the cycle, the specimen was still able to withstand additional cyclic stress. As can be seen in Fig. 11.19, the strain amplitude was less than 10% even after 20 cycles, and the sample did not collapse as was the case for the loose sand. Based on other tests, Seed and Lee (1966) also found that the lower the confining pressure, the more easily liquefaction, or *cyclic mobility* as it is now called, would develop. In other words, increasing the effective confining pressure would decrease the potential for cyclic mobility.

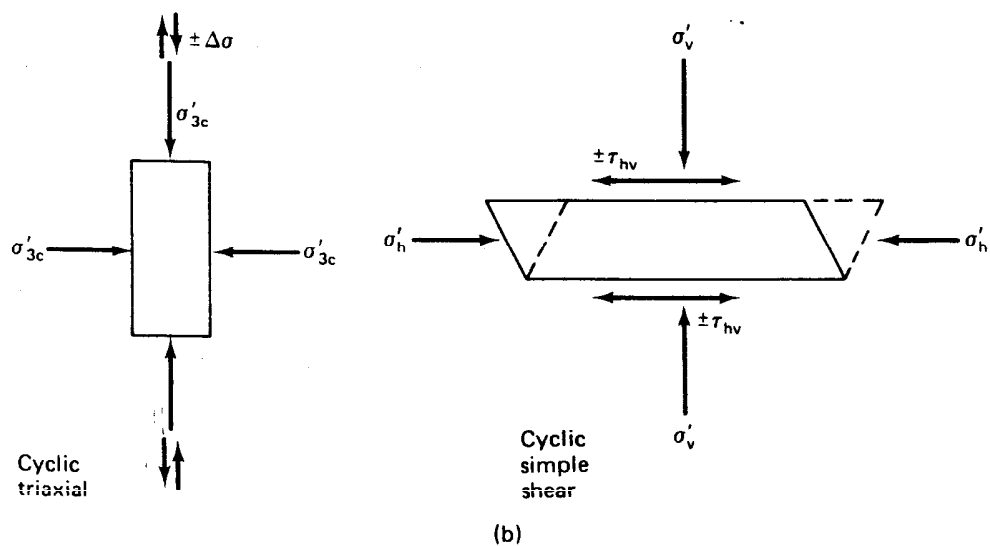
The variables that affect the cyclic mobility of saturated sands are shown in Fig. 11.20a, where peak cyclic stress versus log number of cycles is shown. It can be seen that as the peak stress is lowered, more cycles are required to fail the sample. If the relative density and/or the effective confining pressure is increased, it takes a higher cyclic stress to fail the sample for a given number of cycles to failure. Said in another way, it will take a larger number of cycles to cause failure for the same cyclic stress. The definition of cyclic stress is illustrated in Fig. 11.20b for both cyclic triaxial tests and cyclic simple shear tests. Cyclic simple shear tests seem to more closely represent actual field stress conditions. The differences in stress conditions between these two kinds of tests have been the subject of much research (for example, Seed and Peacock, 1971; Finn, et al., 1971; Park and Silver, 1975; and Castro, 1975).

Other factors have been found to influence the results of cyclic testing of saturated sands. The most significant factor is perhaps the method of sample preparation and the resulting soil structure (Mulilis, et al., 1975; Ladd, 1977). Other factors include previous cyclic strain history (from prior earthquakes, for example), the coefficient of earth pressure at rest,  $K_o$ , and the overconsolidation ratio of the soil deposit (Seed, 1979). As the value of  $K_o$  or OCR increases, a larger number of cycles to cause failure is required for a given cyclic stress. Prior cycling or prestraining causes the same result.

It is difficult to perceive that an initially dense sand could liquefy during cyclic loading. From our previous discussion in this chapter, dense sands *tend* to increase in volume (dilate), which means the pore pressure should decrease and the effective stresses should increase. Is it really possible that the opposite reaction can occur? Further, as was shown in the Peacock diagram (Fig. 11.10), increasing the effective confining stress on an initially dense sand tends to cause "loose"-type behavior; that is, it would increase (rather than decrease) the potential for liquefaction.



(a)



(b)

Fig. 11.20 (a) Generalized relationship between peak cyclic stress and number of cycles to cause cyclic mobility failure; effects of initial density and confining pressure are indicated; (b) definition of cyclic stress  $\Delta\sigma$  in the triaxial test or  $\tau_{hv}$  in the cyclic simple shear test.

Additional work by Castro (1969 and 1975) seemed to answer these anomalies. By very careful measurements of the failed cyclic triaxial specimens, he found a radical water content and void ratio redistribution in the samples at failure. They were alternately necking down and bulging out at the top, and he found the relative densities varied significantly throughout the specimen. The reasons for this behavior are complex and are discussed at some length by Casagrande (1975) and Castro (1969 and 1975). In any event, Castro's work seemed to explain that we were seeing two basically different phenomena: (1) classical liquefaction of loose sands, which we described earlier and which we all understand, and (2) the phenomenon called *cyclic mobility* which occurs in the laboratory during cyclic triaxial or simple shear tests.

These two phenomena are illustrated in Fig. 11.21, which is similar to Fig. 11.7. This figure is like looking upward from beneath the Peacock diagram on the *WOP* plane. The "steady-state line" represents the critical void ratio and effective stress relationship after liquefaction. Soils with void ratios and effective stresses lying above and to the right of the steady-state line are contractive or loose and thus are subject to liquefaction. For example, a sample starting at point *C* when stressed or vibrated

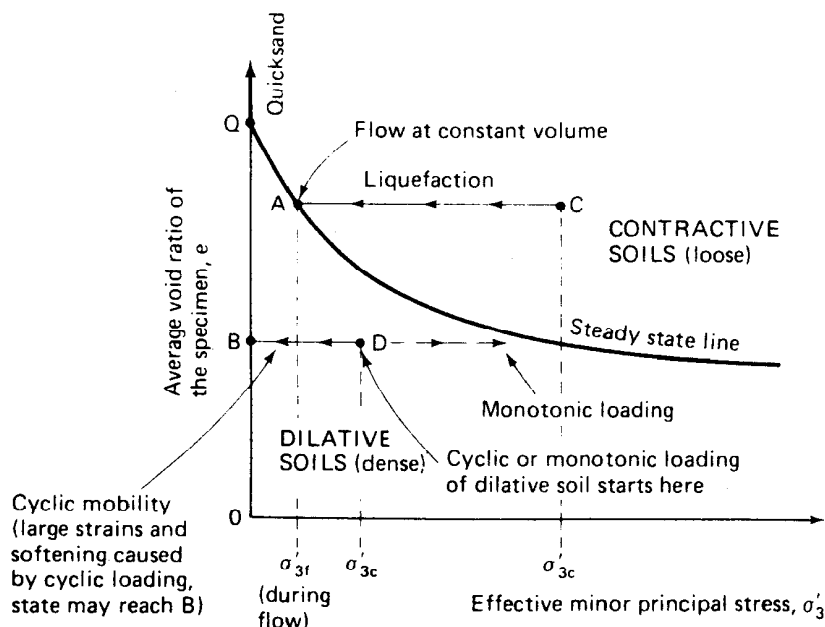


Fig. 11.21 State diagram showing liquefaction potential based on un-drained tests of saturated sands (after Castro and Poulos, 1977).

develops a large amount of positive excess pore pressure and ends up at point *A* on the steady-state line, where the sample has no further tendency to change volume. On the other hand, a dense dilative specimen originally at point *D* below the steady-state line, if subjected to cyclic shear, will move towards point *B*, a condition of zero effective stress. This is the condition of cyclic mobility defined above. If the same sample were loaded monotonically or statically in an ordinary triaxial test, then it would go in the opposite direction towards the steady-state line. This sample would behave just as we described in Sec. 11.5 for dense saturated sands under undrained loading. Note that there is nothing contradictory about this behavior. A state diagram showing the steady-state lines for several typical sands is shown in Fig. 11.22. The differences between liquefaction and cyclic mobility have been summarized by Castro and Poulos (1977) in Table 11-5.

However, the case is not closed on this subject. We can still use the results of the cyclic triaxial test and all our experience with it. Mulinis, et al. (1975) conducted cyclic triaxial tests where relative densities varied from 50% to 90% and the cyclic stress ratios ( $\tau/\sigma'_{eo}$ ) from 0.2 to 0.5. (These values of density and stress ratios adequately cover most conditions to be expected in the field.) They found that "...there was no apparent effect on nonuniform strains or water content redistribution in the samples prior to the development" of failure (Seed, 1979). After failure, the same nonuniform conditions (necking, bulging) as Castro observed were noticed. These results suggest that the cyclic triaxial test (carefully performed) can in fact be used to evaluate the behavior of field conditions by making appropriate corrections for  $K_o$  or by using the cyclic simple shear test with corrections (Seed, 1979).

What can you do to avoid a liquefaction failure? For the static case of natural slopes, monitoring of the field pore water pressures with piezometers may give some indication of impending instability. Observations of erosion and small slides along rivers may also help. If the problem involves earthquakes, it is impossible to control the number of cycles or the applied cyclic stresses. However it may be possible to increase the in situ density by removal and replacement of the loose soil or by compaction of the loose soils by techniques described in Chapter 5. Likewise, the addition of a surcharge fill or berm over a saturated sand layer will increase the effective stresses which should reduce the liquefaction potential (or at least the cyclic mobility!). Finally, it may be possible to permanently lower the ground water table by means of drains and/or pumping, which would reduce the possibility of liquefaction.

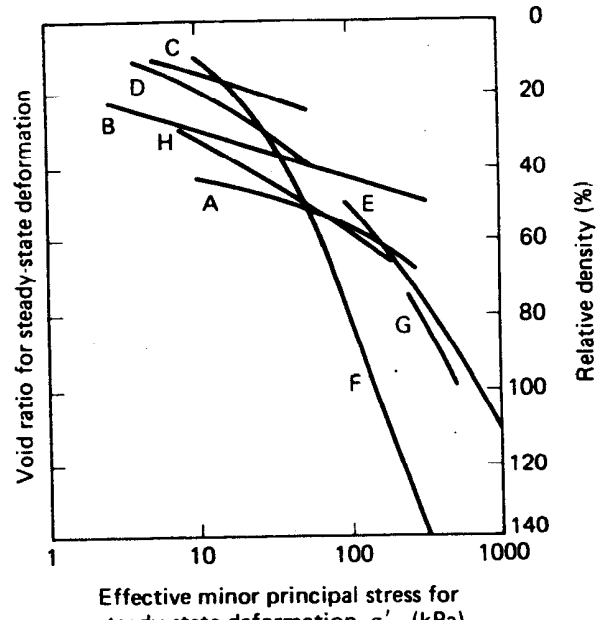
Clearly, the problem of a liquefaction failure in a deposit of loose saturated sands is real and should not be overlooked, especially for important structures such as dams and power plants. We don't have all the

**TABLE 11-5 Differences Between Liquefaction and Cyclic Mobility\***

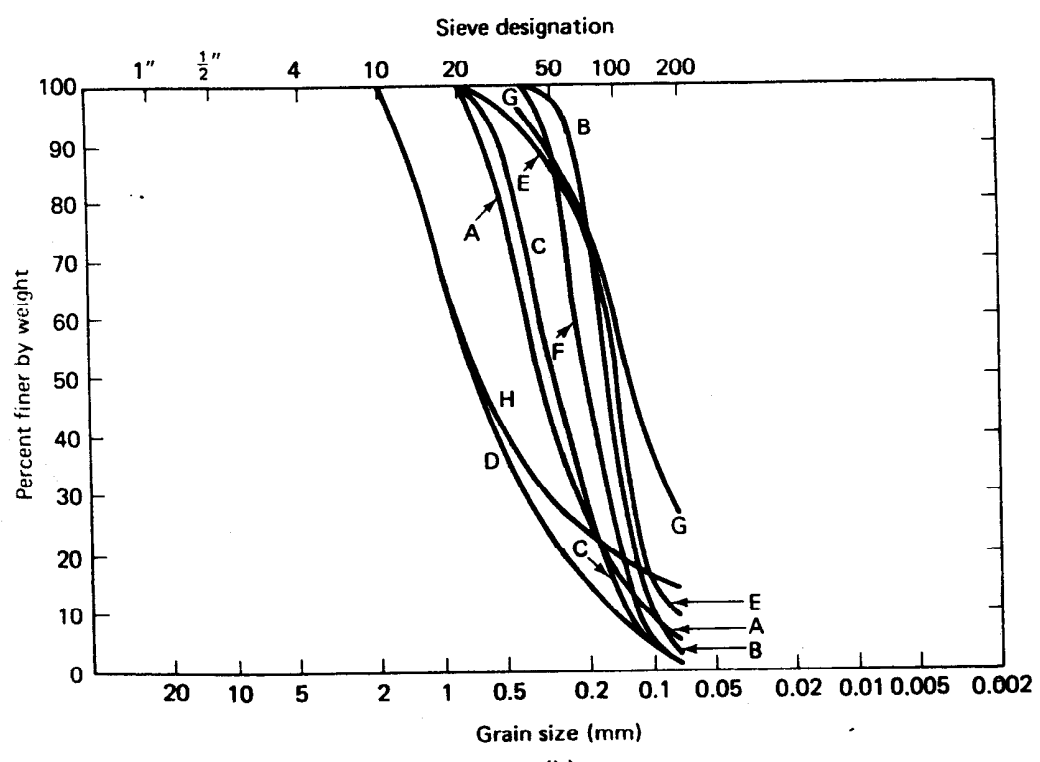
	Liquefaction	Cyclic Mobility
<b>General</b>	Most likely in uniform, fine, clean, loose sand. Static load can cause liquefaction. Cyclic loads causing shear stresses larger than the steady-state strength also can cause liquefaction.	Any soil in any state can develop cyclic mobility in the laboratory if the cyclic stresses are large enough.
<b>Effect of <math>\sigma'_{3c}</math> at constant void ratio for <math>\sigma'_{1c}/\sigma'_{3c}</math></b>	Increased $\sigma'_{3c}$ means larger deformations if liquefaction is induced. The magnitude and/or number of cyclic loads needed to cause liquefaction increases with $\sigma'_{3c}$ . Cyclic loads smaller than the steady-state strength cannot cause liquefaction but may cause cyclic mobility.	Increased $\sigma'_{3c}$ means increased cyclic load to cause cyclic mobility. But the cyclic mobility ratio <sup>†</sup> usually decreases with increasing $\sigma'_{3c}$ .
<b>Effect of <math>\sigma'_{1c}/\sigma'_{3c}</math> at constant void ratio and <math>\sigma'_{3c}</math></b>	Smaller additional loads are needed to cause liquefaction as $\sigma'_{1c}/\sigma'_{3c}$ increases. When $\sigma'_{1c}/\sigma'_{3c}$ is large, a soil is more unstable and may, in the extreme, be susceptible to "spontaneous" liquefaction."	In soils that have low permeability, increased $\sigma'_{1c}/\sigma'_{3c}$ seems to result in somewhat smaller cyclic mobility stresses, which is a reasonable trend. In clean sands, cyclic mobility stress increases with $\sigma'_{1c}/\sigma'_{3c}$ . This unusual result for clean sands is postulated to be due to the substantial test error due to redistribution of void ratio in the laboratory specimens.

\*After Castro and Poulos (1977).

<sup>†</sup>  $\frac{(\sigma_1 - \sigma_3)/2}{\sigma'_{3c}}$ , where  $(\sigma_1 - \sigma_3)$  is the dynamic principal stress difference, or the cyclic mobility stress.



(a)



(b)

Fig. 11.22 (a) State diagram showing steady-state lines for some typical sands; (b) grain size distributions. All specimens except G, which was undisturbed, were prepared by tamping the moist soil in layers (after Castro and Poulos, 1977).

Sand designation	Grain size distribution.			Grain shape	Maximum density (Mg/m <sup>3</sup> )	Minimum density (Mg/m <sup>3</sup> )
	D <sub>60</sub> (mm)	C <sub>u</sub>	% Finer than 0.074 mm (%)			
A	0.40	3.1	5	Subangular to angular	1.76	1.35
B	0.17	1.8	0	Subrounded	1.76	1.44
C	0.33	2.3	1	Angular	1.73	1.44
D	0.90	5.6	0	Subangular	1.83	1.54
E	0.17	2.1	8	Angular	1.62	1.27
F	0.23	2.0	0	Angular	1.17	0.90
G	0.15	—	26	Angular	—	—
H	0.85	~17	13	Subangular	1.99	1.57

(c)

Fig. 11.22 Continued (c) index properties for sands in (a) and (b).

answers, but fortunately research continues and practical design procedures are maturing (Seed, 1979). In most cases, however, the present designs await the ultimate test of their adequacy under field loading (earthquake) conditions.

### 11.9 STRESS-DEFORMATION AND STRENGTH CHARACTERISTICS OF SATURATED COHESIVE SOILS

What happens when shear stresses are applied to saturated cohesive soils? Most of the remainder of this chapter concerns this question. But first, let's briefly review what happens when saturated sands are sheared.

From our previous discussion, for example, you know that volume changes can take place in a drained test, and that the direction of the volume changes, whether dilation or compression, depends on the relative density as well as the confining pressure. If shear takes place undrained, then the volume change tendencies produce pore pressures in the sand.

Basically, the same things happen when clay soils are sheared. In drained shear, whether the volume changes are dilation or compression depends not only on the density and the confining pressure but also on the

stress history of the soil. Similarly, in undrained shear the pore pressures developed depend greatly on whether the soil is normally consolidated or overconsolidated.

Typically, engineering loads are applied much faster than the water can escape from the pores of a clay soil, and consequently excess hydrostatic or pore pressures are produced. If the loading is such that failure does not occur, then the pore pressures dissipate and volume changes develop by the process we call *consolidation* (Chapters 8 and 9). The primary difference in behavior between sands and clays, as mentioned when we discussed the compressibility of soils (Chapter 8), is in the *time* it takes for these volume changes to occur. The time aspect strictly depends on, or is a function of, the difference in permeability between sands and clays. Since cohesive soils have a much lower permeability than sands and gravels, it takes much longer for the water to flow in or out of a cohesive soil mass.

Now, what happens when the loading is such that a shear failure is imminent? Since (by definition) the pore water cannot carry any shear stress, all the applied shear stress must be resisted by the soil structure. Put another way, the shear strength of the soil depends *only on the effective stresses* and not on the pore water pressures. This does not mean that the pore pressures induced in the soil are unimportant. On the contrary, as the total stresses are changed because of some engineering loading, the pore water pressures also change, and until equilibrium of effective stresses occurs instability is possible. These observations lead to two fundamentally different approaches to the solution of stability problems in geotechnical engineering: (1) the *total stress approach* and (2) the *effective stress approach*. In the total stress approach, we allow no drainage to take place during the shear test, and we make the assumption, admittedly a big one, that the pore water pressure and therefore the effective stresses in the test specimen are identical to those in the field. The method of stability analysis is called the *total stress analysis*, and it utilizes the *total* or the *undrained shear strength*  $\tau_f$ , of the soil. The undrained strength can be determined by either laboratory or field tests. If field tests such as the vane shear, Dutch cone penetrometer, or pressuremeter test are used, then they must be conducted rapidly enough so that undrained conditions prevail *in situ*.

The second approach to calculate the stability of foundations, embankments, slopes, etc., uses the shear strength in terms of effective stresses. In this approach, we have to measure or estimate the excess hydrostatic pressure, both in the laboratory and in the field. Then, if we know or can estimate the initial and applied total stresses, we may calculate the effective stresses acting in the soil. Since we believe that shear strength and stress-deformation behavior of soils is really controlled or

determined by the effective stresses, this second approach is philosophically more satisfying. But, it does have its practical problems. For example, estimating or measuring the pore pressures, especially in the field, is not easy to do. The method of stability analysis is called the *effective stress analysis*, and it utilizes the *drained shear strength* or the shear strength in terms of effective stresses. The drained shear strength is ordinarily only determined by laboratory tests.

You probably recall, when we described triaxial tests in Sec. 10.5, that there are limiting conditions of drainage in the test which model real field situations. We mentioned that you could have consolidated-drained (CD) conditions, consolidated-undrained (CU) conditions, or unconsolidated-undrained (UU) conditions. It is also convenient to describe the behavior of cohesive soils at these limiting drainage conditions. It is not difficult to translate these test conditions into specific field situations with similar drainage conditions.

We mentioned in Sec. 10.5 that the unconsolidated-drained test (UD) is not a meaningful test. First, it models no real engineering design situation. Second, the test cannot be interpreted because drainage would occur during shear, and you could not separate the effects of the confining pressure and the shear stress.

As we did with sands, we shall discuss the shear behavior of cohesive soils with reference to their behavior during triaxial shear tests. You can think of the sample in the triaxial cell as representing a typical soil element in the field under different drainage conditions and undergoing different stress paths. In this manner, we hope you will gain some insight into how cohesive soils behave in shear, both in the laboratory and in the field. Keep in mind that the following discussion is somewhat simplified, and that real soil behavior is much more complicated. Towards the end of the chapter we shall indicate some of these complexities. Our primary references are Leonards (1962), Hirschfeld (1963), and Ladd (1964 and 1971b), as well as the lectures of Professor H. B. Seed and S. J. Poulos.

#### 11.9.1 Consolidated-Drained (CD) Test Behavior

We have already described this test when we discussed the strength of sands earlier in this chapter. Briefly, the procedure is to consolidate the test specimen under some state of stress appropriate to the field or design situation. The consolidation stresses can either be *hydrostatic* (equal in all directions, sometimes called *isotropic*) or *non-hydrostatic* (different in different directions, sometimes called *anisotropic*). Another way of looking at this second case is that a stress difference or (from the Mohr circles) a shear stress is applied to the soil. When consolidation is over, the "C" part of the CD test is complete.

During the "D" part, the drainage valves remain *open* and the stress difference is applied very slowly so that essentially *no* excess pore water pressure develops during the test. Professor A. Casagrande termed this test the S-test (for "slow" test).

In Fig. 11.23, the total, neutral, and effective stress conditions in an axial compression CD test at the end of consolidation, during application of axial load, and at failure are shown. The subscripts *v* and *h* refer to vertical and horizontal, respectively; *c* means consolidation. For conventional axial compression tests, the initial consolidation stresses are hydrostatic. Thus  $\sigma_v = \sigma_h = \sigma'_{3c}$  cell pressure, which is usually held constant during the application of the axial stress  $\Delta\sigma$ . In the axial compression test,  $\Delta\sigma = \sigma_1 - \sigma_3$ , and at failure  $\Delta\sigma_f = (\sigma_1 - \sigma_3)_f$ . The axial stress can be applied either by increasing the load on the piston incrementally (*stress-controlled* loading) or through a motor-jack system which deforms the sample at a constant rate (called a *constant rate of strain* test).

Note that at all the times during the CD test, the pore water pressure is essentially zero. This means that the total stresses in the drained test are

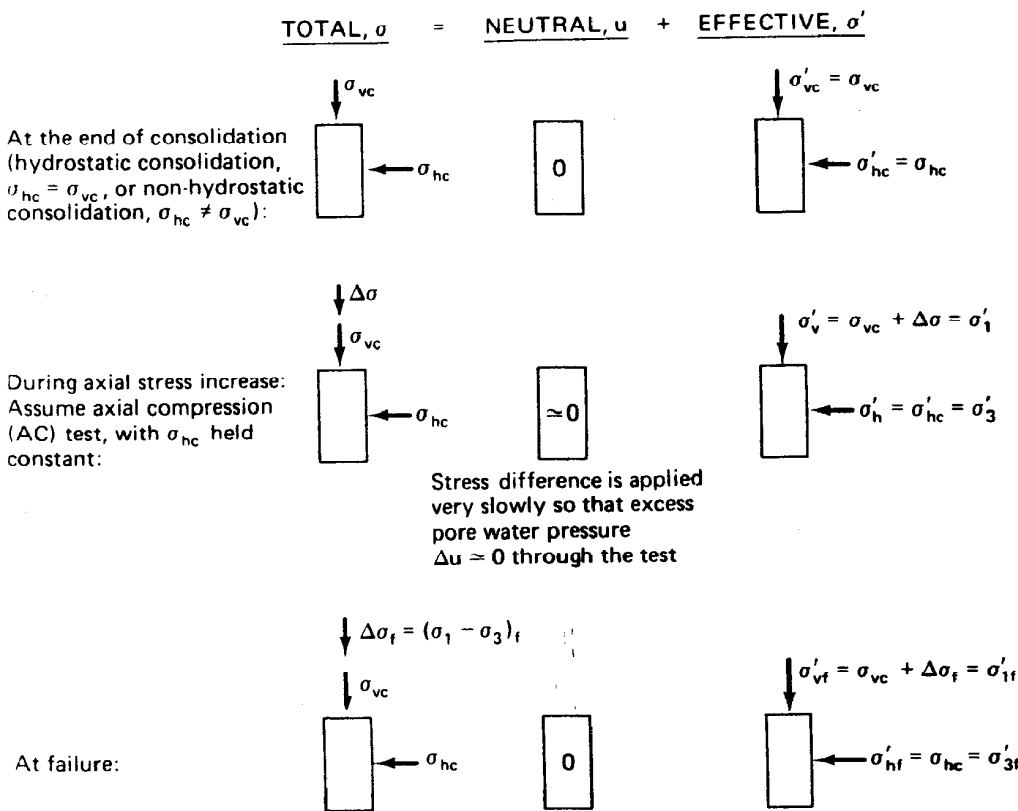


Fig. 11.23 Stress conditions in the consolidated-drained (CD) axial compression triaxial test.

always equal to the effective stresses. Thus  $\sigma_{3c} = \sigma'_{3c} = \sigma_{3f} = \sigma'_{3f}$ , and  $\sigma_{1f} = \sigma'_{1f} = \sigma'_{3c} + \Delta\sigma_f$ . If non-hydrostatic consolidation stresses were applied to the specimen, then  $\sigma_{1f} = \sigma'_{1f}$  would be equal to  $\sigma'_{1c} + \Delta\sigma_f$ .

Typical stress-strain curves and volume change versus strain curves for a remolded or compacted clay are shown in Fig. 11.24. Even though the two samples were tested at the same confining pressure, the overconsolidated specimen has a greater strength than the normally consolidated clay. Note also that it has a higher modulus and that failure [the maximum  $\Delta\sigma$ , which for the triaxial test is equal to  $(\sigma_1 - \sigma_3)_f$ ] occurs at a much lower strain than for the normally consolidated specimen. Note too the analogy to drained behavior of sands. The overconsolidated clay *expands* during shear while the normally consolidated clay *compresses* or consolidates during shear. This is analogous to the behavior described earlier for

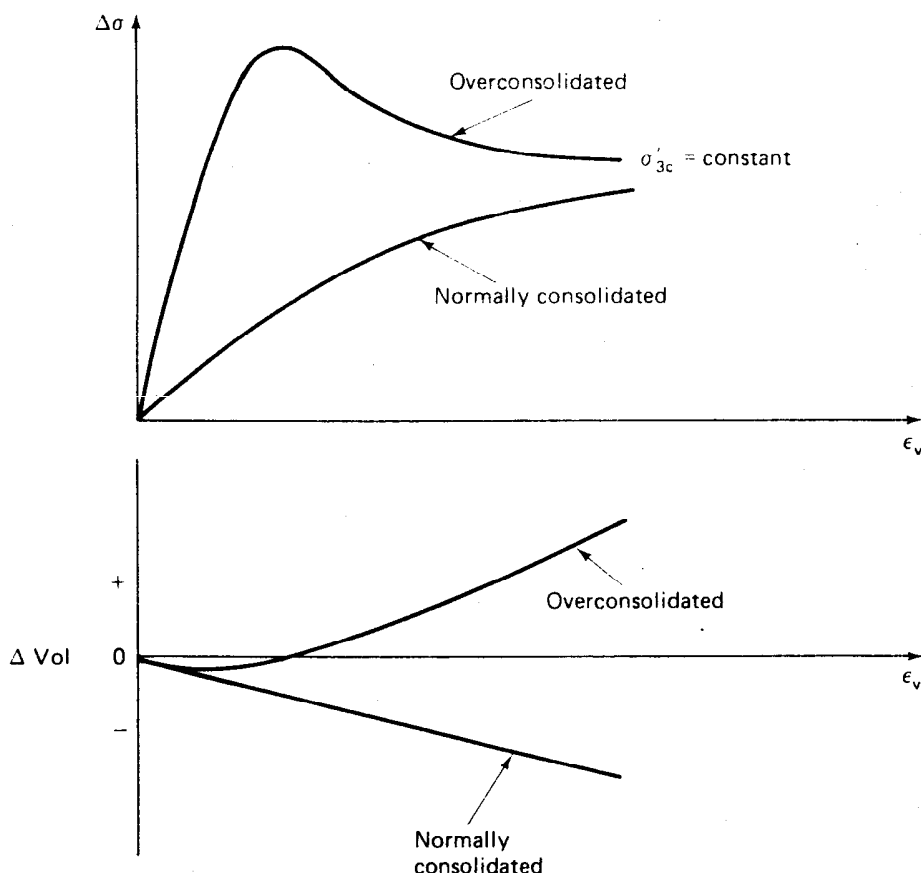


Fig. 11.24 Typical stress-strain and volume change versus strain curves for CD axial compression tests at the same effective confining stress.

sands: normally consolidated clays behave similarly to loose sands, whereas overconsolidated clays behave like dense sands.

In the CD triaxial test, the stress paths are straight lines since we usually keep one of the stresses constant and simply vary the other stress. Typical drained stress paths are shown in Fig. 10.22 for four common engineering situations which can be modeled in the triaxial test. The stress path for the axial compression test illustrated in Fig. 11.23 is the straight line  $AC$ .

The Mohr failure envelopes for CD tests of typical clay soils are shown in Figs. 11.25 and 11.26b. The envelope for a remolded clay as well as a normally consolidated undisturbed clay is shown in Fig. 11.25. Even though only one Mohr circle (representing the stress conditions at failure in Fig. 11.23) is shown, the results of three or more CD tests on identical specimens at different consolidation pressures would ordinarily be required to plot the complete Mohr failure envelope. If the consolidation stress range is large or the specimens do not have exactly the same initial water content, density, and stress history, then the three failure circles will not exactly define a straight line, and an average best-fit line by eye is drawn. The slope of the line determines the Mohr-Coulomb strength parameter  $\phi'$ , of course, in terms of effective stresses. When the failure envelope is extrapolated to the shear axis, it will show a surprisingly small intercept. Thus it is usually assumed that the  $c'$  parameter for normally consolidated non-cemented clays is essentially zero for all practical purposes.

For overconsolidated clays the  $c'$  parameter is greater than zero, as indicated by Fig. 11.26b. The overconsolidated portion of the strength envelope (DEC) lies above the normally consolidated envelope (ABCF). This portion (DEC) of the Mohr failure envelope is called the *preconsolidation hump*. The explanation for this behavior is shown in the  $e$  versus  $\sigma'$

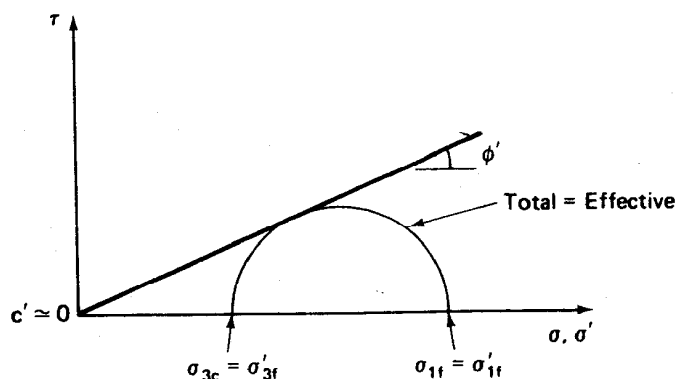


Fig. 11.25 Mohr failure envelope for a normally consolidated clay in drained shear.

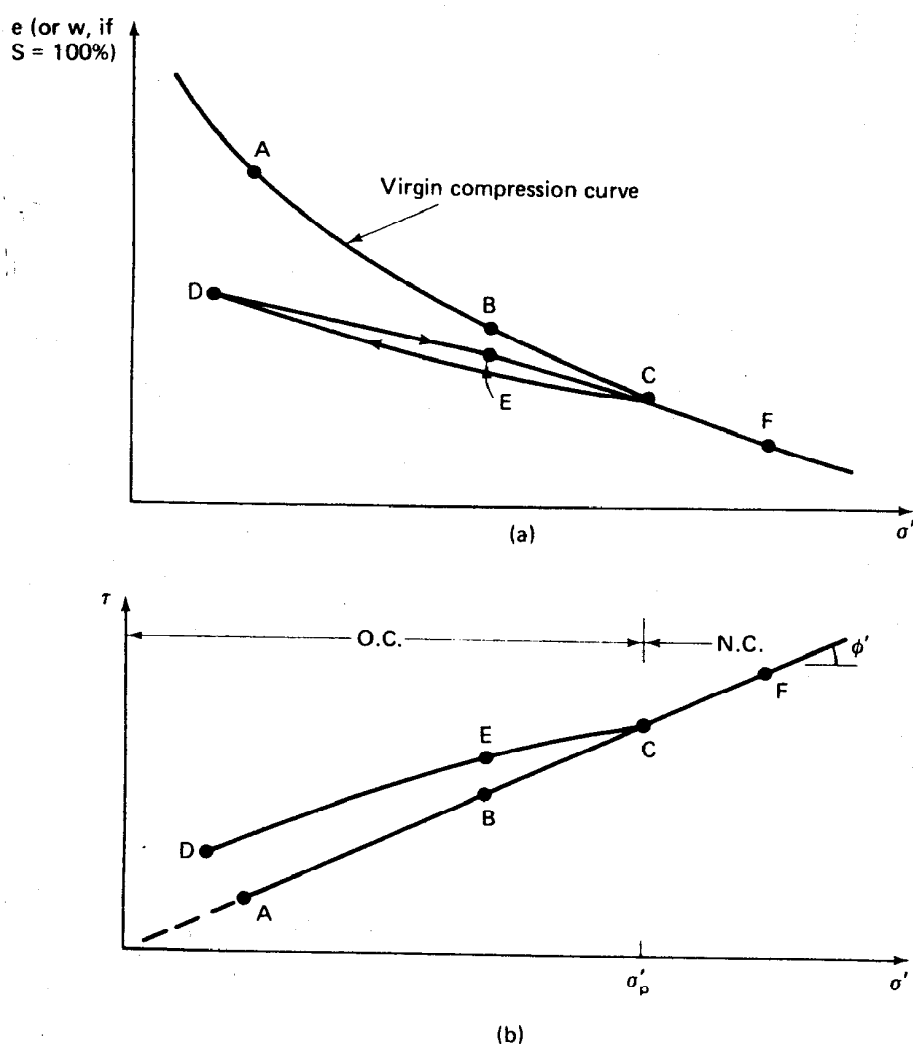


Fig. 11.26 (a) Compression curve; (b) Mohr failure envelope (DEC) for an overconsolidated clay.

curve of Fig. 11.26a. (Recall from Fig. 8.4 that the virgin compression curve when plotted arithmetically is concave upward.) Let us assume that we begin consolidation of a sedimentary clay at a very high water content and high void ratio. As we continue to increase the vertical stress we reach point  $A$  on the virgin compression curve and conduct a CD triaxial test. (We could, of course, do the same thing with a CD direct shear test.) The strength of the sample consolidated to point  $A$  on the virgin curve would correspond to point  $A$  on the normally consolidated Mohr failure envelope in Fig. 11.26b. If we consolidate and test another otherwise identical

specimen which is loaded to point *B*, then we would obtain the strength, again normally consolidated, at point *B* on the failure envelope in Fig. 11.26b. If we repeat the process to point *C* ( $\sigma'_p$ , the preconsolidation stress), then rebound the specimen to point *D*, then reload it to point *E* and shear, we would obtain the strength shown at point *E* in the lower figure. Note that the shear strength of specimen *E* is greater than specimen *B*, even though they are tested at exactly the same effective consolidation stresses. The reason for the greater strength of *E* than *B* is suggested by the fact that *E* is at a lower water content, has a lower void ratio, and thus is denser than *B*, as shown in Fig. 11.26a. If another specimen were loaded to *C*, rebounded to *D*, reloaded back past *E* and *C* and on to *F*, it would have the strength as shown in the figure at point *F*. Note that it is now back on the virgin compression curve and the normally consolidated failure envelope. The effects of the rebounding and reconsolidation have been in effect *erased* by the increased loading to point *F*. Once the soil has been loaded well past the preconsolidation pressure  $\sigma'_p$ , it no longer "remembers" its stress history.

#### 11.9.2 Typical Values of Drained Strength Parameters

For the Mohr failure envelopes of Figs. 11.25 and 11.26 we did not indicate any numerical values for the effective stress strength parameters  $\phi'$ . Average values of  $\phi'$  for undisturbed clays range from around  $20^\circ$  for normally consolidated highly plastic clays up to  $30^\circ$  or more for silty and sandy clays. The value of  $\phi'$  for compacted clays is typically  $25^\circ$  or  $30^\circ$  and occasionally as high as  $35^\circ$ . As mentioned earlier, the value of  $c'$  for normally consolidated non-cemented clays is very small and can be neglected for practical work. If the soil is overconsolidated, then  $\phi'$  would be less, and the  $c'$  intercept greater than for the normally consolidated part of the failure envelope (see Fig. 11.26b again). According to Ladd (1971b), for natural overconsolidated non-cemented clays with a preconsolidation stress of less than 500 to 1000 kPa,  $c'$  will probably be less than 5 to 10 kPa at low stresses. For compacted clays at low stresses,  $c'$  will be much greater due to the prestress caused by compaction. For stability analyses, the Mohr-Coulomb effective stress parameters  $\phi'$  and  $c'$  are determined over the range of effective normal stresses likely to be encountered in the field.

It has been observed (for example, Kenney, 1959) that there is not much difference between  $\phi'$  determined on undisturbed or remolded samples at the same water content. Apparently, the development of the maximum value of  $\phi'$  requires so much strain that the soil structure is broken down and almost remolded in the region of the failure plane.

Empirical correlations between  $\phi'$  and the plasticity index for normally consolidated clays are shown in Fig. 11.27. This correlation is based

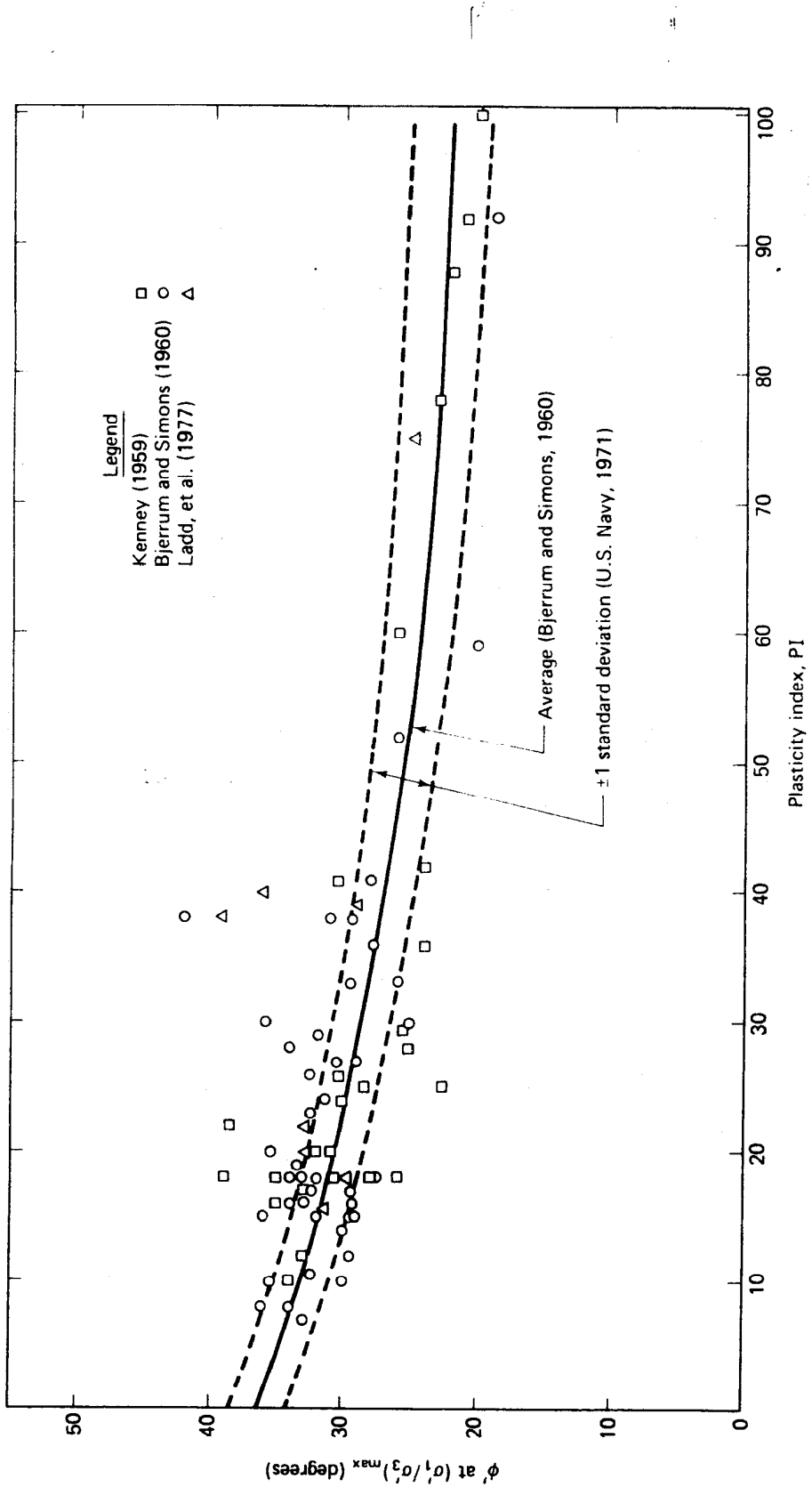


Fig. 11.27 Empirical correlation between  $\phi'$  and PI from triaxial compression tests on normally consolidated undisturbed clays (after U.S. Navy, 1971, and Ladd, et al., 1977).

on work by Kenney (1959), Bjerrum and Simons (1960), U.S. Navy (1971), and Ladd, et al. (1977). Since there is considerable scatter around the "average line," you should use this correlation with considerable caution. However Fig. 11.27 is useful for preliminary estimates and for checking laboratory results.

### 11.9.3 Use of CD Strength in Engineering Practice

Where do we use the strengths determined from the CD test? As mentioned previously, the limiting drainage conditions modeled in the triaxial test refer to real field situations. CD conditions are the most critical for the long-term steady seepage case for embankment dams and the long-term stability of excavations or slopes in both soft and stiff clays. Examples of CD analysis are shown in Fig. 11.28. How you actually go about making these analyses for stability can be found in textbooks on foundation and embankment dam engineering.

You should be aware that, practically speaking, it is not easy to actually conduct a CD test on a clay in the laboratory. To ensure that no pore pressure is really induced in the specimen during shear for materials with very low permeabilities, the rate of loading must be very slow. The time required to fail the specimen ranges from a day to several weeks (Bishop and Henkel, 1962). Such a long time leads to practical problems in the laboratory such as leakage of valves, seals, and the membrane that surrounds the sample. Consequently, since it is possible to measure the induced pore pressures in a consolidated-undrained (CU) test and thereby calculate the effective stresses in the specimen, CU tests are more practical for obtaining the effective stress strength parameters. Therefore CD triaxial tests are not very popular in most soils laboratories.

### 11.9.4 Consolidated-Undrained (CU) Test Behavior

As the name implies, the test specimen is first consolidated (drainage valves open, obviously) under the desired consolidation stresses. As before, these can either be hydrostatic or non-hydrostatic consolidation stresses. After consolidation is complete, the drainage valves are closed, and the specimen is loaded to failure in undrained shear. Often, the pore water pressures developed during shear are measured, and both the total and effective stresses may be calculated during shear and at failure. Thus this test can either be a total or an effective stress test. This test is sometimes called the *R-test*.

Total, neutral, and effective stress conditions in the specimen during the several phases of the CU test are shown in Fig. 11.29. The symbols are

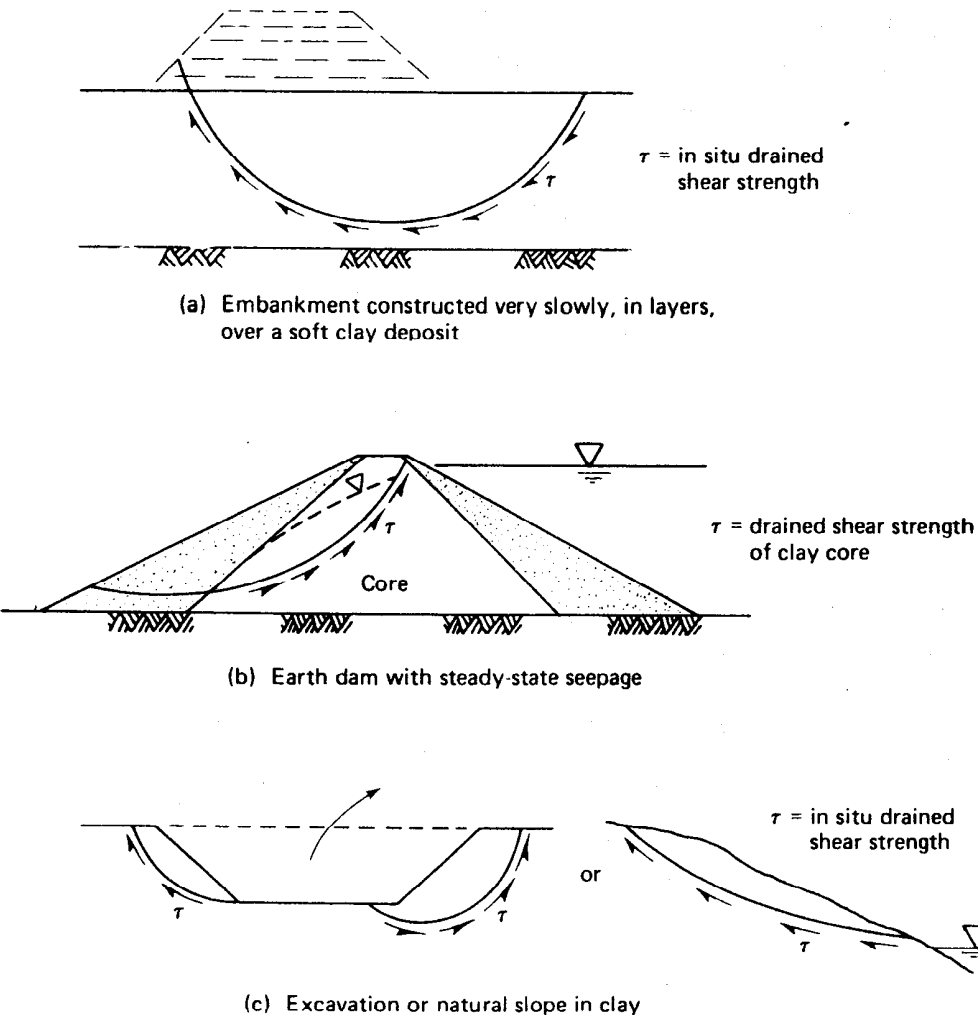


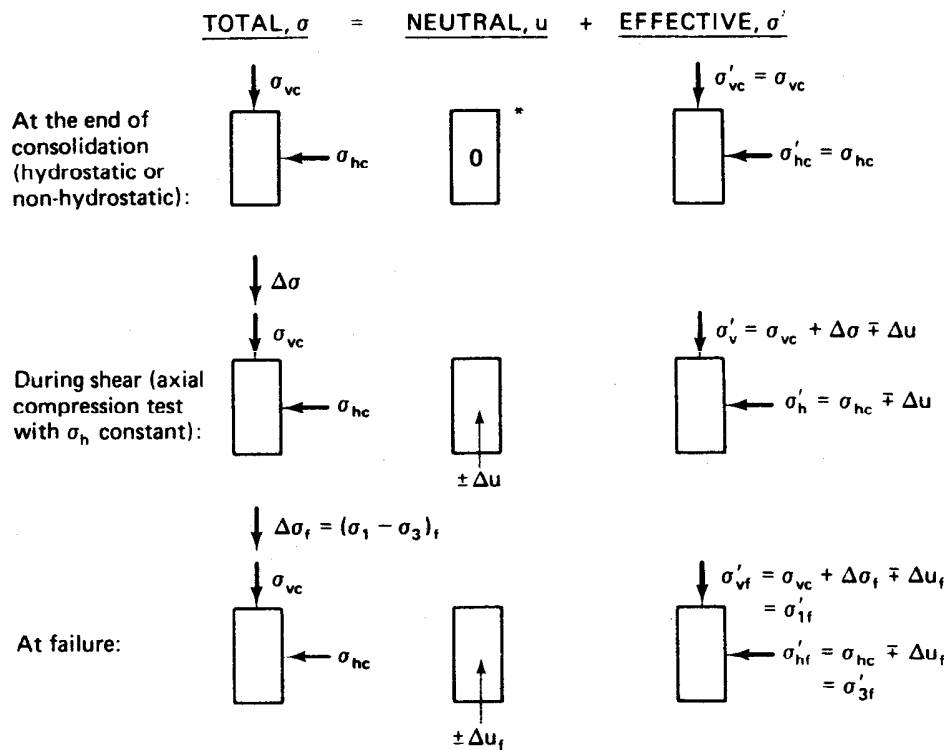
Fig. 11.28 Some examples of CD analyses for clays (after Ladd, 1971b).

the same as we used before in Fig. 11.23. The general case of unequal consolidation is shown, but typically for routine triaxial testing the specimen is consolidated hydrostatically under a cell pressure which remains constant during shear. Thus,

$$\sigma_{\text{cell}} = \sigma_{\text{oc}} = \sigma_{\text{hc}} = \sigma'_{\text{lc}} = \sigma'_{\text{3c}} = \sigma_{3f} \neq \sigma'_{3f}$$

$$\Delta\sigma_f = (\sigma_1 - \sigma_3)_f$$

Like the CD test, the axial stress can be increased incrementally or at a constant rate of strain. At failure, then, the test in Fig. 11.29 is rather conventional in that the axial stress is increased to failure (axial compres-



\*In practice, to ensure 100% saturation, which is necessary for good measurements of the pore water pressure, a *back pressure* is applied to the pore water. To keep the effective consolidation stresses constant, the total stresses during consolidation are accordingly increased by an amount exactly equal to the applied back pressure, which is the same as raising atmospheric pressure by a constant amount—the effective stresses on the clay do not change.

Example: Initial conditions with back pressure:

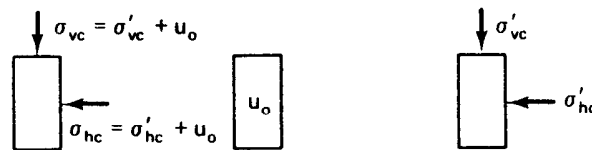
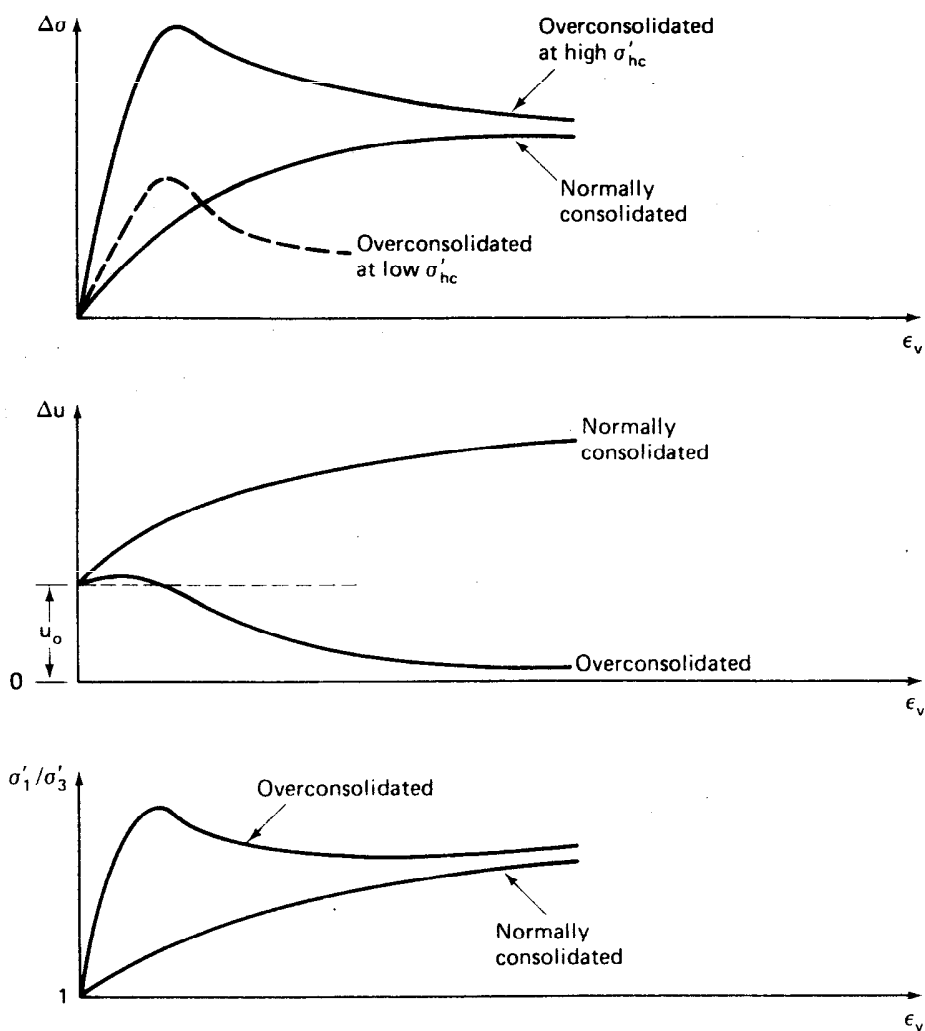


Fig. 11.29 Conditions in specimen during a consolidated-undrained axial compression (CU) test.

sion test). Note that the excess pore water pressure  $\Delta u$  developed during shear can either be positive (that is, increase) or negative (that is, decrease). This happens because the sample tries to either contract or expand during shear. Remember, we are not allowing any volume change (an undrained test) and therefore no water can flow in or out of the specimen during shear. Because volume changes are prevented, the *tendency* towards volume change induces a pressure in the pore water. If the specimen *tends* to contract or consolidate during shear, then the induced pore water pressure is *positive*. It wants to contract and squeeze water out of the pores, but cannot; thus the induced pore water pressure is positive. Positive pore pressures occur in normally consolidated clays. If the specimen *tends* to expand or swell during shear, the induced pore water pressure is *negative*. It wants to expand and draw water into the pores, but cannot; thus the pore water pressure decreases and may even go negative (that is, below zero gage pressure). Negative pore pressures occur in overconsolidated clays. Thus, as noted in Fig. 11.29, the *direction* of the induced pore water pressure  $\Delta u$  is important since it directly affects the magnitudes of the effective stresses.

Also you might note that in actual testing the initial pore water pressure typically is greater than zero. In order to ensure full saturation, a *back pressure*  $u_o$  is usually applied to the test specimen (Fig. 11.29). When a back pressure is applied to a sample, the cell pressure must also be increased by an amount equal to the back pressure so that the effective consolidation stresses will remain the same. Since the effective stress in the specimen does not change, the strength of the specimen is not supposed to be changed by the use of back pressure. In practice this may not be exactly true, but the advantage of having 100% saturation for accurate measurement of induced pore water pressures far outweighs any disadvantages of the use of back pressure.

Typical stress-strain,  $\Delta u$ , and  $\sigma'_1/\sigma'_3$  curves for CU tests are shown in Fig. 11.30, for both normally and overconsolidated clays. Also shown for comparison is a stress-strain curve for an overconsolidated clay at low effective consolidation stress. Note the peak, then the drop-off of stress as strain increases (work-softening material, Fig. 10.4). The pore pressure versus strain curves illustrate what happens to the pore pressures during shear. The normally consolidated specimen develops positive pore pressure. In the overconsolidated specimen, after a slight initial increase, the pore pressure goes "negative"—in this case, negative with respect to the back pressure  $u_o$ . Another quantity that is useful for analyzing test results is the principal (effective) stress ratio  $\sigma'_1/\sigma'_3$ . Note how this ratio peaks early, just like the stress difference curve, for the overconsolidated clay. Similar test specimens having similar behavior on an effective stress basis will have similarly shaped  $\sigma'_1/\sigma'_3$  curves. They are simply a way of normal-



Note: For hydrostatic consolidation,  $\sigma'_1/\sigma'_3 = 1$  at the start of the test; for non-hydrostatic consolidation,  $\sigma'_1/\sigma'_3 > 1$ .

Fig. 11.30 Typical  $\sigma$ - $\epsilon$ ,  $\Delta u$ , and  $\sigma'_1/\sigma'_3$  curves for normally and overconsolidated clays in undrained shear (CU test).

izing the stress behavior with respect to the effective minor principal stress during the test. Sometimes, too, the maximum of this ratio is used as a criterion of failure. However, in this text we will continue to assume failure occurs at the maximum principal stress difference (compressive strength).

What do the Mohr failure envelopes look like for CU tests? Since we can get both the total and effective stress circles at failure for a CU test when we measure the induced pore water pressures, it is possible to define

the Mohr failure envelopes in terms of both total and effective stresses from a series of triaxial tests conducted over a range of stresses, as illustrated in Fig. 11.31 for a normally consolidated clay. For clarity, only one set of Mohr circles is shown. These circles are simply plotted from the stress conditions at failure in Fig. 11.29. Note that the effective stress circle is displaced to the left, towards the origin, for the normally consolidated case, because the specimens develop positive pore pressure during shear and  $\sigma' = \sigma - \Delta u$ . Note that both circles have the *same diameter* because of our definition of failure at maximum  $(\sigma_1 - \sigma_3) = (\sigma'_1 - \sigma'_3)$ . You should verify that this equation is true. Once the two failure envelopes are drawn, the Mohr-Coulomb strength parameters are readily definable in terms of both total ( $c$ ,  $\phi$  or sometimes  $c_T$ ,  $\phi_T$ ) and effective stresses ( $c'$ ,  $\phi'$ ). Again, as with the CD test, the envelope for normally consolidated clay passes essentially through the origin, and thus for practical purposes  $c'$  can be taken to be zero, which is also true for the total stress  $c$  parameter. Note that  $\phi_T$  is less than  $\phi'$ , and often it is about one-half of  $\phi'$ .

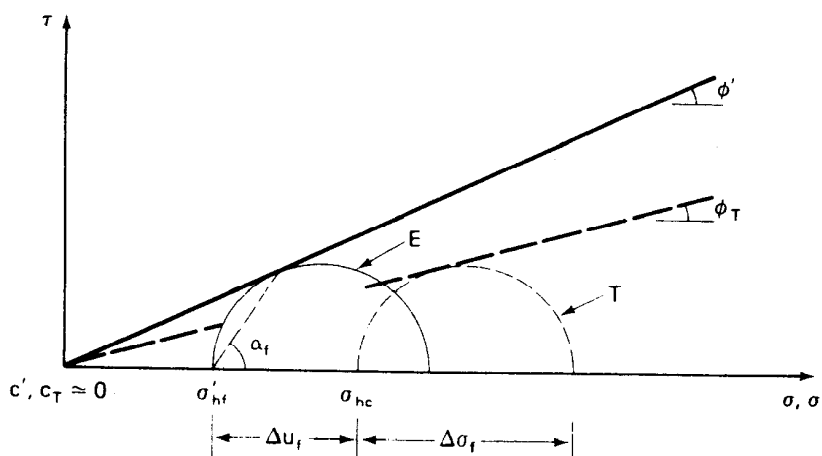


Fig. 11.31 Mohr circles at failure and Mohr failure envelopes for total ( $T$ ) and effective ( $E$ ) stresses for a normally consolidated clay.

Things are different if the clay is overconsolidated. Since an overconsolidated specimen tends to expand during shear, the pore water pressure decreases or even goes negative, as shown in Fig. 11.30. Because  $\sigma'_{3f} = \sigma_{3f} - (-\Delta u_f)$  or  $\sigma'_{1f} = \sigma_{1f} - (-\Delta u_f)$ , the effective stresses are *greater* than the total stresses, and the effective stress circle at failure is shifted to the *right* of the total stress circle, as shown in Fig. 11.32. The shift of the effective stress circle at failure to the right sometimes means that the  $\phi'$  is less than  $\phi_T$ . Typically, the complete Mohr failure envelopes are determined by tests on several specimens consolidated over the working

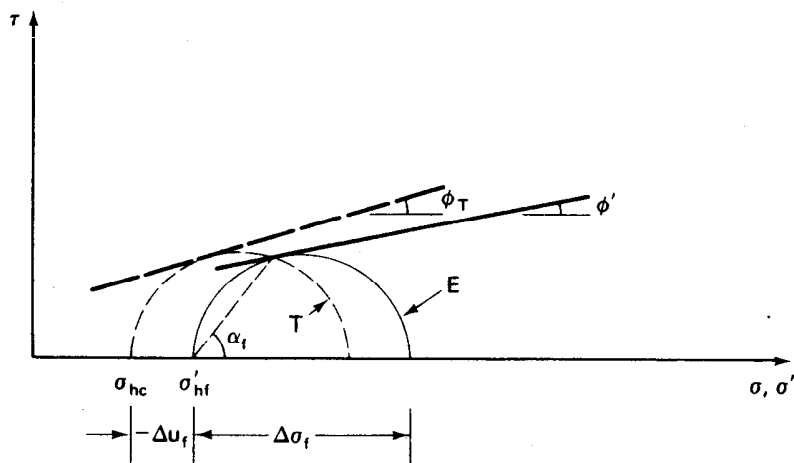


Fig. 11.32 Mohr circles at failure and Mohr failure envelopes for both total ( $T$ ) and effective ( $E$ ) stresses for an overconsolidated clay.

stress range of the field problem. Figure 11.33 shows the Mohr failure envelopes over a wide range of stresses spanning the preconsolidation stress. Thus some of the specimens are overconsolidated and others are normally consolidated. You should note that the "break" in the *total* stress envelope (point  $z$ ) occurs roughly about twice the  $\sigma'_p$  for typical clays (Hirschfeld, 1963). The two sets of Mohr circles at failure shown in Fig.

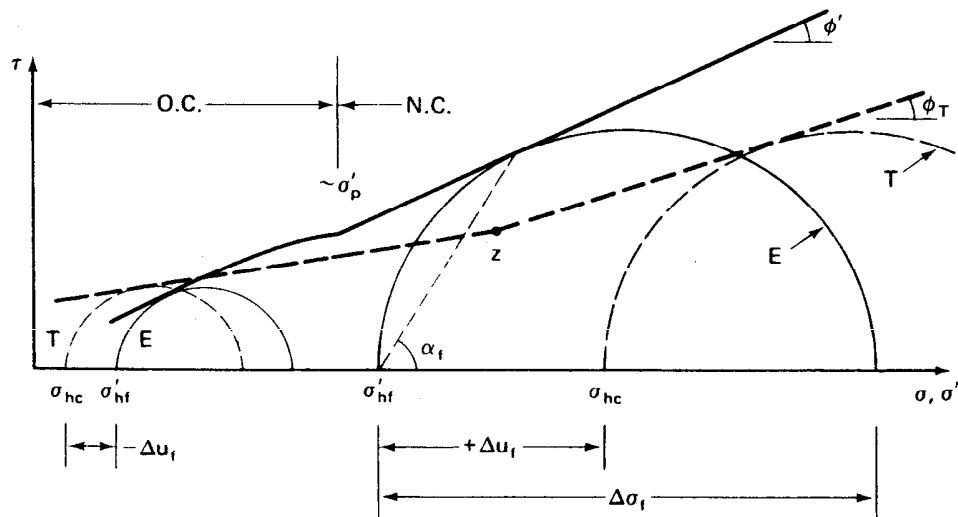


Fig. 11.33 Mohr failure envelopes over a range of stresses spanning the preconsolidation stress  $\sigma'_p$ .

11.33 correspond to the two tests shown in Fig. 11.30 for the "normally consolidated" specimen and the specimen "overconsolidated at low  $\sigma'_{hc}$ ."

You may have noticed that an angle  $\alpha_f$  was indicated on the effective stress Mohr circles of Figs. 11.31, 11.32, and 11.33. Do you recall the Mohr failure hypothesis wherein the point of tangency of the Mohr failure envelope with the Mohr circle at failure defined the angle of the failure plane in the specimen? If not, reread Sec. 10.4. Since we believe that the shear strength is controlled by the effective stresses in the specimen at failure, the Mohr failure hypothesis is valid in terms of *effective stresses only*.

Stress paths for the two tests of Fig. 11.33 are shown in Fig. 11.34. The tests are quite conventional, hydrostatically consolidated, axial compression tests. Let's look first at Fig. 11.34a, the stress paths for the test on normally consolidated clay. Three stress paths are shown, the effective stress path (ESP), the total stress path (TSP), and the total- $u_o$  stress paths,  $(T - u_o)$  SP. The paths begin on the hydrostatic axis at values of  $p$  equal to the total and effective consolidation pressures, respectively. Note that  $p = p' + u_o$ . The total stress path for axial compression and constant cell pressure is the straight line inclined at  $45^\circ$  as shown. Since positive pore pressures develop in the normally consolidated clay, the ESP lies to the *left* of the TSP because  $\sigma' = \sigma - \Delta u$ . The situation is directly analogous to that shown in Fig. 10.24. Note that  $q_f$  is the same for all three stress paths because we define the failure at the maximum  $(\sigma_1 - \sigma_3)$ . Figure 11.34a is similar to Fig. 10.24, except the initial consolidation in that case was non-hydrostatic ( $K_o < 1$ ).

Since the overconsolidated clay was tested in axial compression with a constant hydrostatic cell pressure, the two total stress paths of Fig. 11.34b are exactly like those of Fig. 11.34a—straight lines inclined at  $45^\circ$  to the hydrostatic axis. But the shape of the ESP is significantly different. Look back at the development of pore pressure with axial strain for this test in Fig. 11.30. See how it starts out slightly positive, then goes way negative (actually, less than  $u_o$ , as was explained previously). The same thing happens to the ESP in Fig. 11.34b. It goes slightly to the left ( $+\Delta u$ ) of the  $(T - u_o)$  SP at first, then as the pore pressure becomes increasingly negative, the ESP crosses the  $(T - u_o)$  SP until maximum  $q$  or  $q_f$  is reached. Again, because of the way we define failure,  $q_f$  is the same for all three stress paths. You may recall that the ESP in Fig. 11.34b for the overconsolidated clay has a shape similar to that shown in Fig. 10.25, except that the latter sample was consolidated with  $K_o > 1$ .

If you are still unclear about stress paths, it would be a good idea to reread Sec. 10.6.

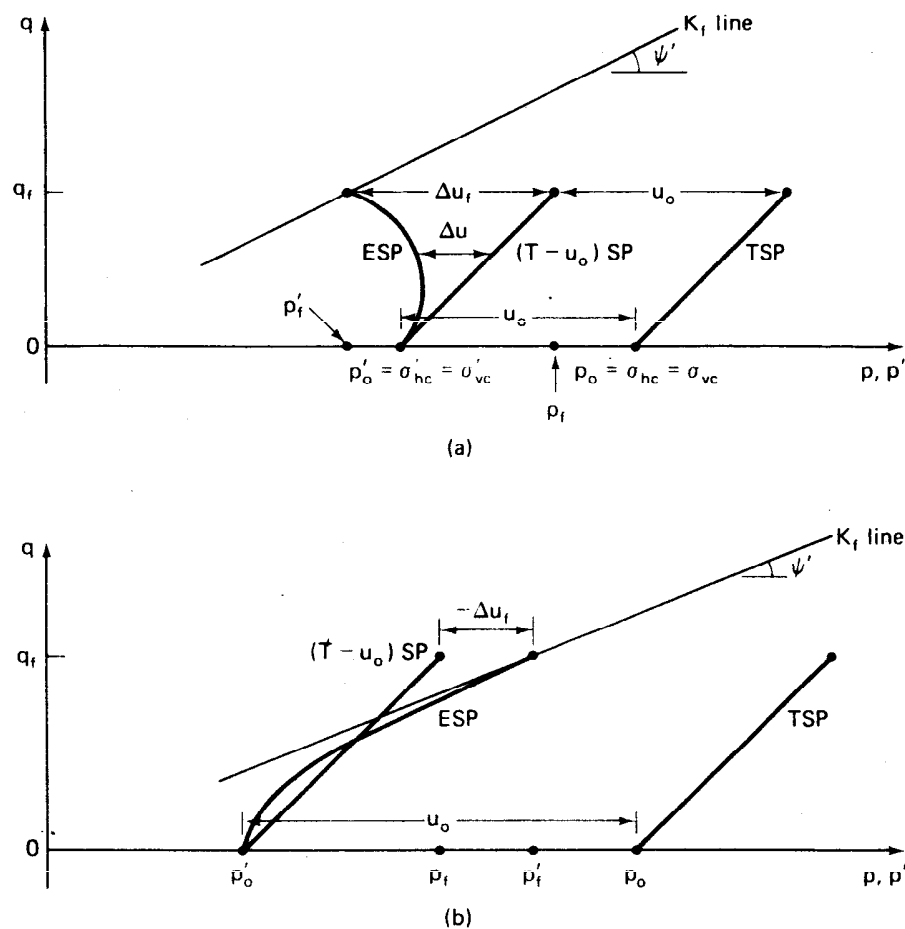


Fig. 11.34 Stress paths for the hydrostatically consolidated axial compression tests on (a) normally consolidated clays; (b) overconsolidated clays.

### 11.9.5 Typical Values of the Undrained Strength Parameters

Earlier in this section, we gave some typical values for  $c'$  and  $\phi'$  determined by CD triaxial tests. The range of values indicated is typical for effective stress strengths determined in CU tests with pore pressure measurements, with the following reservation. In our discussion so far, we have tacitly assumed that the Mohr-Coulomb strength parameters in terms of effective stresses determined by CU tests with pore pressure measurements would be the same as those determined by CD tests. We used the same

symbols,  $c'$  and  $\phi'$ , for the parameters determined both ways. This assumption is not strictly correct. The problem is complicated by alternative definitions of failure. We have used the maximum principal stress difference  $(\sigma_1 - \sigma_3)_{\max}$  to define failure throughout this chapter, but often in the literature and sometimes in practice you will find failure defined in terms of the maximum principal effective stress ratio  $(\sigma'_1/\sigma'_3)_{\max}$ , which is the same as the maximum obliquity (Eqs. 10-14 through 10-17). Depending on how the stress difference and the pore water pressures actually develop with strain, these two definitions may indicate different  $c$ 's and  $\phi$ 's. This is especially true for sensitive clays, as shown in Fig. 11.35.

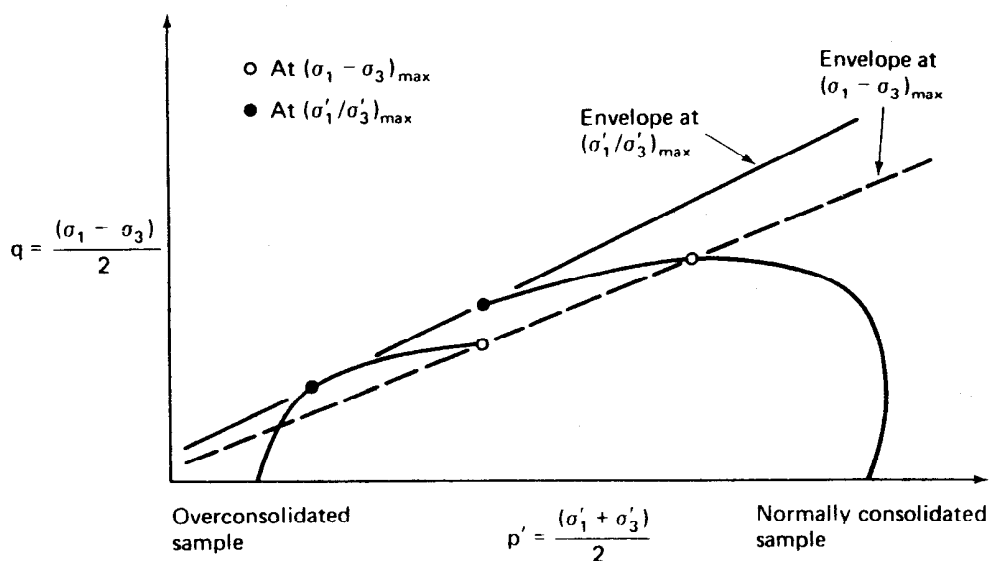
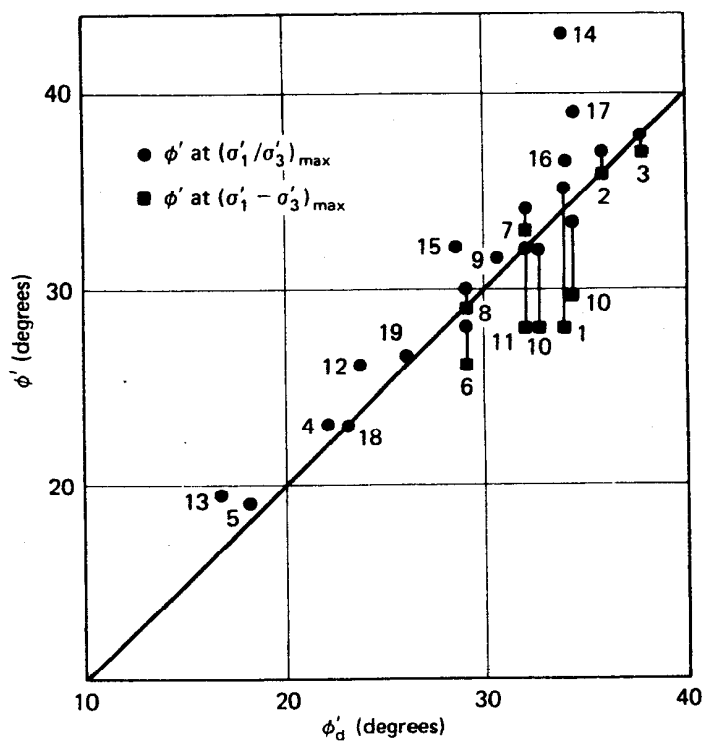


Fig. 11.35 Typical failure envelopes for CU tests on a sensitive clay, illustrating the effect of different failure criteria on the slope and intercept of the Mohr-Coulomb failure envelope (after Ladd, 1971b).

Bjerrum and Simons (1960) studied this problem in some detail, and their results are summarized in Fig. 11.36. Here,  $\phi'$  as defined at  $(\sigma'_1/\sigma'_3)_{\max}$  and  $(\sigma_1 - \sigma_3)_{\max}$  are plotted versus  $\phi'_d$ , the effective stress parameter determined in drained tests. Note that  $\phi'$  from the maximum principal effective stress ratio (the dots) is from  $0^\circ$  to  $3^\circ$  greater than  $\phi'_d$ . Also note that  $\phi'$  at maximum principal stress difference (the squares) is less than both  $\phi'_d$  and  $\phi'$  at the maximum principal effective stress ratio. In one case the difference is about  $7^\circ$ .

The point is that you should be careful when studying published data or engineering test reports to determine exactly how the strength tests were conducted, how failure was defined, and how any reported Mohr-Coulomb parameters were determined.



Clay	State	Reference
1 Cornwall	U	Kenney
2 Cornwall	R	"
3 Bersimis	R	"
4 Weald	R	Henkel
5 London	R	"
6 Oslo	U	N.G.I.
7 Fredrikstad	U	"
8 Lodalen	U	"
9 Fornebu	U	"
10 Drammen	U	"
11 Okernbråten	U	"
12 Seven Sisters	U	Casagrande and Rivard
13 North Ridge	U	" "
14 Organic	U	Casagrande
15 Boston blue	U	"
16 Weymouth	U	Hirschfeld
17 New Haven	U	"
18 Haslemere	R	Skempton and Bishop
19 Wiener Tegel	R	Hvorslev

U = undisturbed

R = remolded

Fig. 11.36 Relationship between  $\phi'_d$  determined from CD tests and  $\phi'$  determined from CU tests with pore pressures measured. Two failure criteria are indicated for the undrained tests (after Bjerrum and Simons, 1960).

For the Mohr-Coulomb strength parameters in terms of total stresses, the problem of definition of failure doesn't come up. Failure is defined at the maximum compressive strength  $(\sigma_1 - \sigma_3)_{\max}$ . For normally consolidated clays,  $\phi$  seems to be about half of  $\phi'$ ; thus values of  $10^\circ$  to  $15^\circ$  or more are typical. The total stress  $c$  is very close to zero. For overconsolidated and compacted clays,  $\phi$  may decrease and  $c$  will often be significant. When the failure envelope straddles the preconsolidation stress, proper interpretation of the strength parameters in terms of total stresses is difficult. This is especially true for undisturbed samples which may have some variation in water content and void ratio, even within the same geologic stratum.

In the section on typical values of drained strength parameters, we provided an empirical correlation for  $\phi'$  and PI (Fig. 11.27). These were for normally consolidated undisturbed clays tested in triaxial compression, and in fact most of the tests used to develop this figure were CU tests with pore pressures measured. Figure 11.27 still can be used for preliminary estimates and for checking laboratory test results because the differences in  $\phi'$ , depending on how failure is defined, etc., are less than the scatter in the figure.

#### 11.9.6 Use of CU Strength in Engineering Practice

Where do we use the CU strength in engineering practice? As mentioned before, this test, with pore pressures measured, is commonly used to determine the shear strength parameters in terms of both total and effective stresses. CU strengths are used for stability problems where the soils have first become fully consolidated and are at equilibrium with the existing stress system. Then, for some reason, *additional* stresses are applied quickly, with no drainage occurring. Practical examples include rapid drawdown of embankment dams and the slopes of reservoirs and canals. Also, in terms of effective stresses, CU test results are applied to the field situations mentioned in the earlier discussion of CD tests. Some of these practical examples are illustrated in Fig. 11.37.

Just as with CD tests, there are some problems with CU tests on clay. For proper measurement of the pore pressures induced during shear, special care must be taken to see that the sample is fully saturated, that no leaks occur during testing, and that the rate of loading (or rate of strain) is sufficiently slow so that the pore pressures measured at the ends of the specimen are the same as those occurring in the vicinity of the failure plane. As we mentioned, the use of back pressure is common to assure 100% saturation. The effects of the other two factors can be minimized by proper testing techniques, which are described at length by Bishop and Henkel (1962).

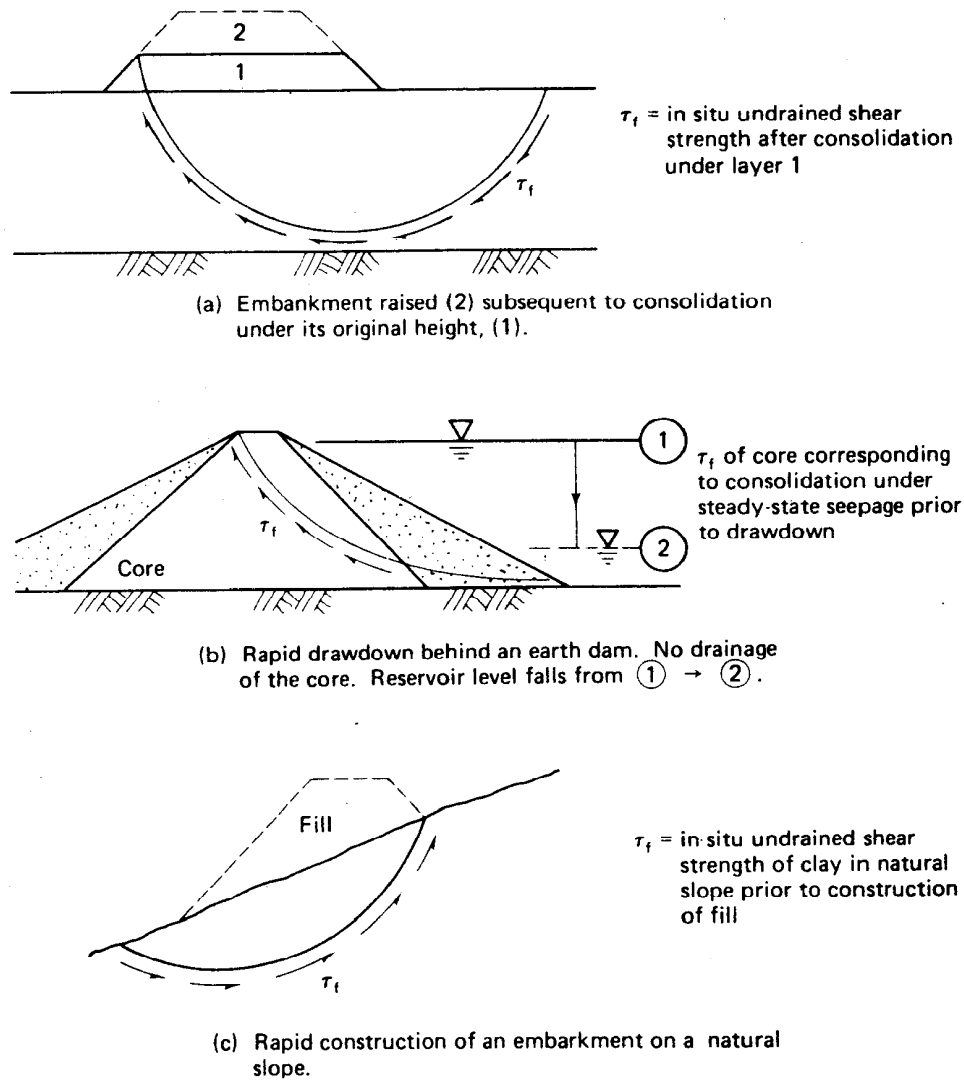


Fig. 11.37 Some examples of CU analyses for clays (after Ladd, 1971b).

Another problem, not often mentioned, results from trying to determine the long-term or effective stress strength parameters and the short-term or CU-total stress strength parameters from the same test series. The rates of loading or strain required for correct effective stress strength determination may not be appropriate for the short-term or undrained loading situation. The stress-deformation and strength response of clay soils is rate-dependent; that is, usually the faster you load a clay, the stronger it becomes. In the short-term case, the rate of loading in the field may be quite rapid, and therefore for correct modeling of the field

situation, the rates of loading in the laboratory sample should be comparable. Thus the two objectives of the CU-effective stress test are really incompatible. The best thing to do, though rarely done in practice, would be to have two sets of tests, one set tested CD modeling the long-term situation and the other CU set modeling the short-term undrained loading.

### EXAMPLE 11.11

**Given:**

A normally consolidated clay was consolidated under a stress of 150 kPa, then sheared undrained in axial compression. The principal stress difference at failure was 100 kPa, and the induced pore pressure at failure was 88 kPa.

**Required:**

Determine the Mohr-Coulomb strength parameters in terms of both total and effective stresses (a) analytically and (b) graphically. Plot the total and effective Mohr circles and failure envelopes. (c) Compute  $(\sigma'_1/\sigma'_3)_f$  and  $(\sigma_1/\sigma_3)_f$ . (d) Determine the theoretical angle of the failure plane in the specimen.

**Solution:**

To solve this problem we need to assume that both  $c'$  and  $c_T$  are negligible. Then we can use the obliquity relationships (Eqs. 10-14 through 10-17) to solve for  $\phi'$  and  $\phi_T$ .

a. To use these equations, we need  $\sigma_{1f}$ ,  $\sigma'_{1f}$ ,  $\sigma_{3f}$  and  $\sigma'_{3f}$ . We know  $\sigma_{3f} = 150$  kPa and  $(\sigma_1 - \sigma_3)_f = 100$  kPa. Therefore

$$\sigma_{1f} = (\sigma_1 - \sigma_3)_f + \sigma_{3f} = 100 + 150 = 250 \text{ kPa}$$

$$\sigma'_{1f} = \sigma_{1f} - u_f = 250 - 88 = 162 \text{ kPa}$$

$$\sigma'_{3f} = \sigma_{3f} - u_f = 150 - 88 = 62 \text{ kPa}$$

From Eq. 10-13,

$$\phi' = \arcsin \frac{100}{224} = 26.5^\circ$$

$$\phi_T = \arcsin \frac{100}{400} = 14.5^\circ$$

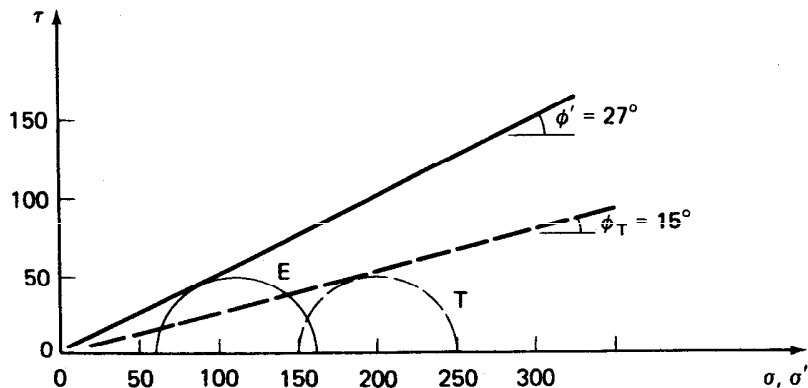


Fig. Ex. 11.11

b. The graphical solution including the failure envelopes is shown in Fig. Ex. 11.11. To plot the total and effective Mohr circles, we would still need to calculate  $\sigma_{1f}$ ,  $\sigma'_{1f}$  and  $\sigma'_{3f}$ . The centers of the circles are at (200, 0) for total stresses and at (112, 0) for effective stresses.

c. The stress ratios at failure are

$$\frac{\sigma'_1}{\sigma'_3} = \frac{162}{62} = 2.61$$

$$\frac{\sigma_1}{\sigma_3} = \frac{250}{150} = 1.67$$

Another way to get these values would be to use Eq. 10-14.

$$\frac{\sigma'_1}{\sigma'_3} = \frac{1 + \sin 26.5^\circ}{1 - \sin 26.5^\circ} = \frac{1.45}{0.55} = 2.61$$

$$\frac{\sigma_1}{\sigma_3} = \frac{1 + \sin 14.5^\circ}{1 - \sin 14.5^\circ} = \frac{1.25}{0.75} = 1.67$$

d. Use Eq. 10-10, in terms of *effective* stresses:

$$\alpha_f = 45^\circ + \frac{\phi'}{2} = 58^\circ \text{ from the horizontal}$$

#### 11.9.7 Unconsolidated-Undrained (UU) Test Behavior

In this test, the specimen is placed in the triaxial cell with the drainage valves closed from the beginning. Thus, even when a confining pressure is applied, no consolidation can occur if the sample is 100% saturated. Then,

as with the CU test, the specimen is sheared undrained. The sample is loaded to failure in about 10 to 20 min; usually pore water pressures are not measured in this test. This test is a *total stress test* and it yields the strength in terms of total stresses. A. Casagrande first called this test the *Q-test* (for "quick") since the sample was loaded to failure much more quickly than in the *S-test*.

Total, neutral, and effective stress conditions in the specimen during the several phases of the UU test are shown in Fig. 11.38. The symbols are as used before in Fig. 11.23 and 11.29. The test illustrated in Fig. 11.38 is

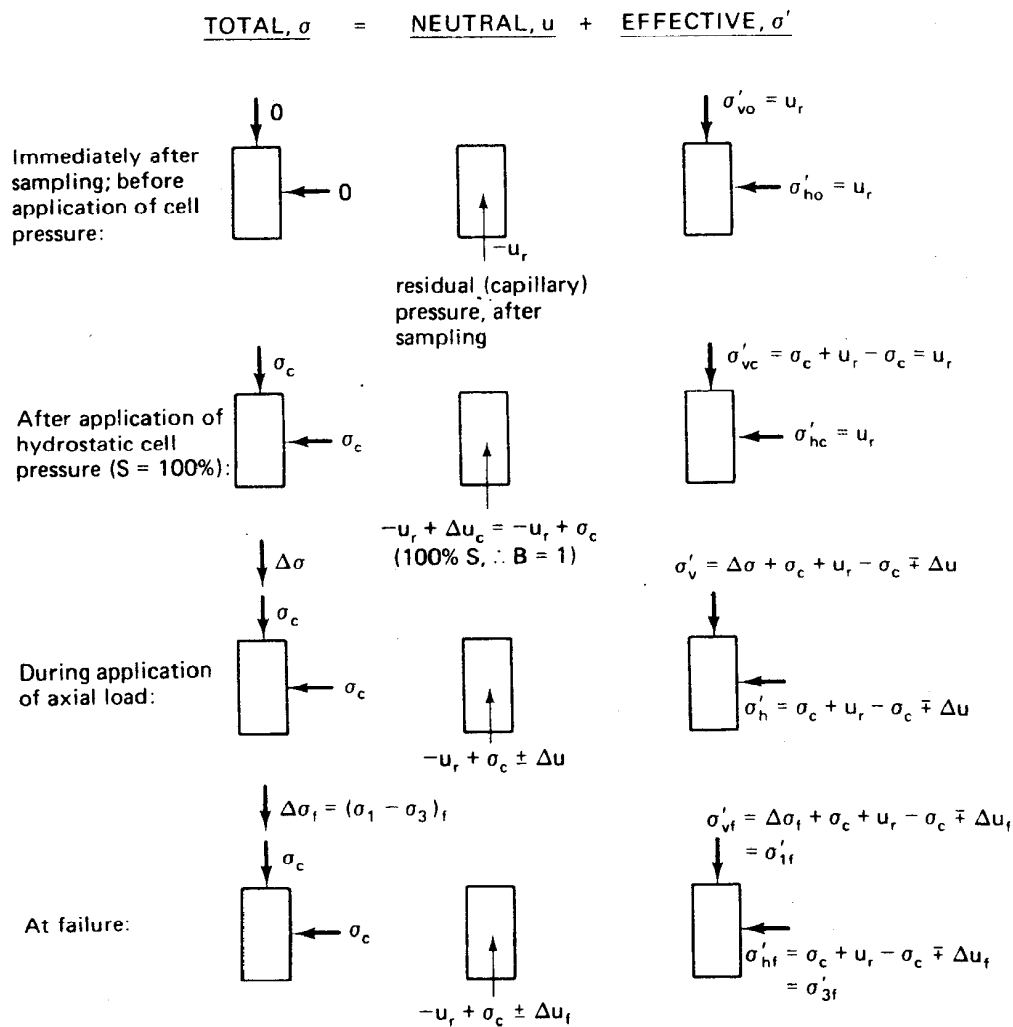


Fig. 11.38 Conditions in the specimen during the unconsolidated-undrained (UU) axial compression test.

quite conventional in that hydrostatic cell pressure is usually applied, and the specimen is failed by increasing the axial load, usually at a constant rate of strain. As with the other tests, the principal stress difference at failure is  $(\sigma_1 - \sigma_3)_{\max}$ .

Note that initially for undisturbed samples, the pore pressure is negative, and it is called the *residual pore pressure* —  $u_r$ , which results from stress release during sampling. Since the effective stresses initially must be greater than zero (otherwise the specimen would simply disintegrate) and the total stresses are zero (atmospheric pressure = zero gage pressure), the pore pressure must be negative. (See Fig. 10.21 for insight into the sampling process.) When the cell pressure is applied with the drainage valves closed, a positive pore pressure  $\Delta u_c$  is induced in the specimen, which is exactly equal to the applied cell pressure  $\sigma_c$ . All the increase in hydrostatic stress is carried by the pore water because (1) the soil is 100% saturated, (2) the compressibility of the water and individual soil grains is small compared to the compressibility of the soil structure, and (3) there is a unique relationship between the effective hydrostatic stress and the void ratio (Hirschfeld, 1963). Number 1 is obvious. Number 2 means that no volume change can occur unless water is allowed to flow out of (or into) the sample, and we are preventing that from occurring. Number 3 means basically that no secondary compression (volume change at constant effective stress) takes place. You may recall from the discussion of the assumptions of the Terzaghi theory of consolidation (Chapter 9) that the same assumption was required; that is, that the void ratio and effective stress were uniquely related. Thus there can be no change in void ratio without a change in effective stress. Since we prevent any change in water content, the void ratio and effective stress remain the same.

Stress conditions during axial loading and at failure are similar to those for the CU test (Fig. 11.29). They may appear to be complex, but if you study Fig. 11.38 you will see that the UU case is as readily understandable as the CU case.

Typically, stress-strain curves for UU tests are not particularly different from CU or CD stress-strain curves for the same soils. For undisturbed samples, especially the initial portions of the curve (initial tangent modulus), are strongly dependent on the *quality* of the undisturbed samples. Also, the sensitivity (Sec. 2.7) affects the shape of these curves; highly sensitive clays have sharply peaked stress-strain curves. The maximum stress difference often occurs at very low strains, usually less than 0.5%. Some typical UU stress-strain curves are shown in Fig. 11.39.

The Mohr failure envelopes for UU tests are shown in Fig. 11.40 for 100% saturated clays. All test specimens for fully saturated clays are presumably at the same water content (and void ratio), and consequently they will have the same shear strength since there is no consolidation

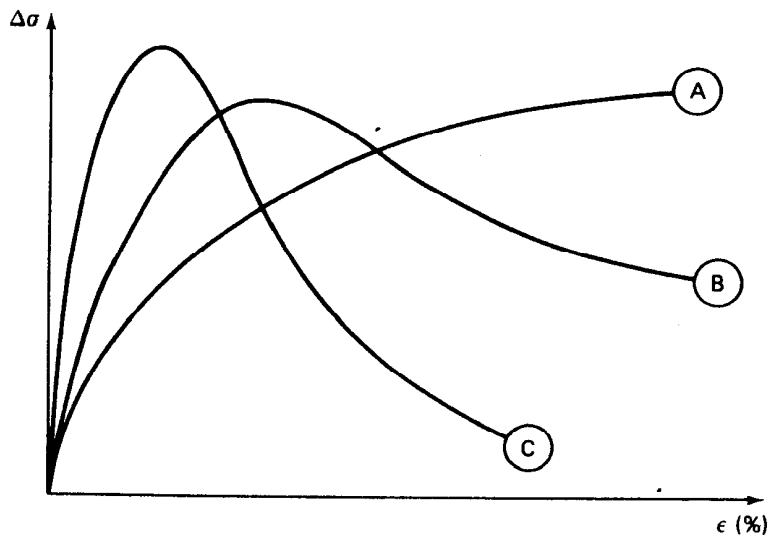


Fig. 11.39 Typical UU stress-strain curves for (A) remolded and some compacted clays, (B) medium sensitive undisturbed clay, and (C) highly sensitive undisturbed clay.

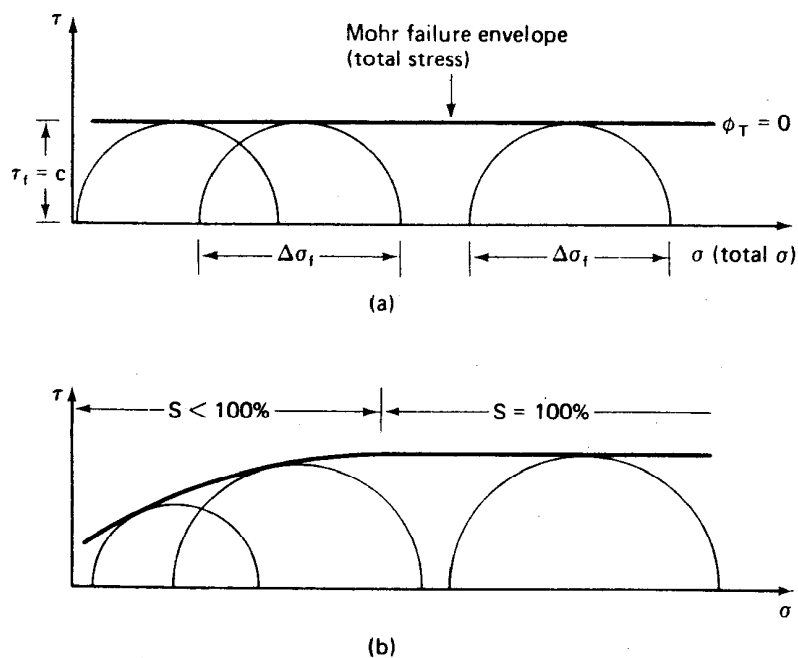


Fig. 11.40 Mohr failure envelopes for UU tests: (a) 100% saturated clay; (b) partially saturated clay.

allowed. Therefore all Mohr circles at failure will have the *same* diameter and the Mohr failure envelope will be a horizontal straight line (see Fig. 10.9c). This is a very important point. If you don't understand it, refer again to Fig. 11.38 to see that in the UU test the effective consolidation stress is the same throughout the test. If all the samples are at the same water content and density (void ratio), then they will have the same strength. The UU test, as previously mentioned, gives the shear strength in terms of total stresses, and the slope  $\phi_T$  of the UU Mohr failure envelope is *equal to zero*. The intercept of this envelope on the  $\tau$ -axis defines the total stress strength parameter  $c$ , or  $\tau_f = c$ , where  $\tau_f$  is undrained shear strength.

For partially saturated soils, a series of UU tests will define an initially curved failure envelope (Fig. 11.40b) until the clay becomes essentially 100% saturated due simply to the cell pressure alone. Even though the drainage valves are closed, the confining pressure will compress the air in the voids and decrease the void ratio. As the cell pressure is increased, more and more compression occurs and eventually, when sufficient pressure is applied, essentially 100% saturation is achieved. Then, as with the case for initially 100% saturated clays, the Mohr failure envelope becomes horizontal, as shown on the right side of Fig. 11.40b.

Another way of looking at the compression of partially saturated clays is shown in Fig. 11.41. As the cell pressure is increased incrementally,

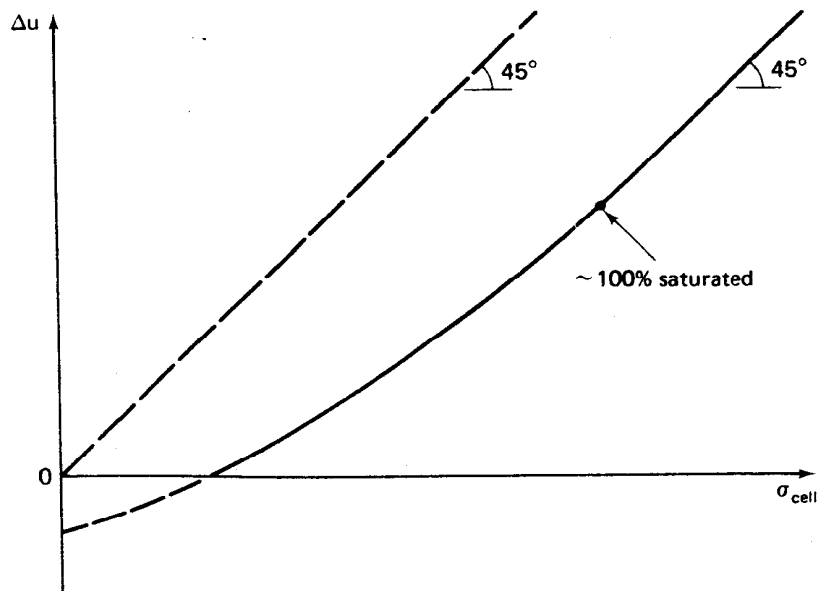
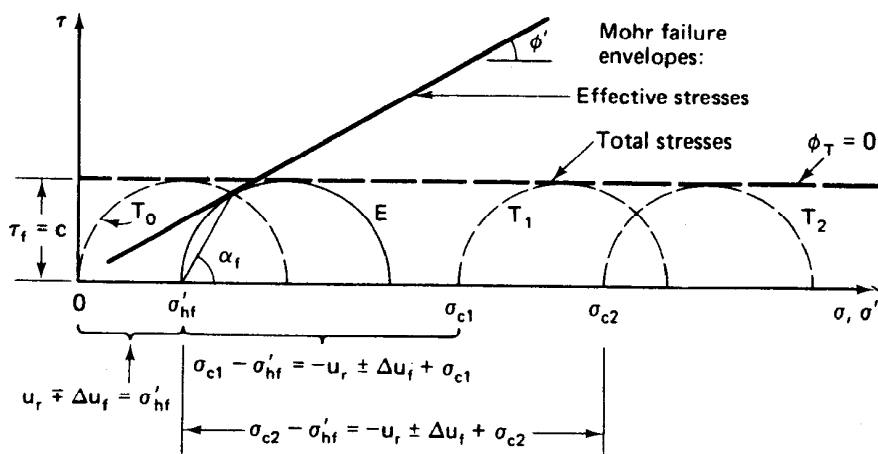


Fig. 11.41 Results obtained from a PH test on a partially saturated compacted clay (after Skempton, 1954, and Hirschfeld, 1963).

the measured increment of pore pressure increases gradually until at some point for every increment of cell pressure added, an equal increment of pore water pressure is observed. At this point, the soil is 100% saturated and the solid (experimental) curve becomes parallel to the  $45^\circ$  line shown in the figure.

In principle, it is possible to measure the induced pore water pressures in a series of UU tests although it is not commonly done. Since the effective stresses at failure are *independent* of the total cell pressures applied to the several specimens of a test series, there is only *one* UU effective stress Mohr circle at failure. This point is illustrated in Fig. 11.42. Note that no matter what the confining pressure (for example,  $\sigma_{c1}$ ,  $\sigma_{c2}$ , etc.), there is only one effective stress Mohr circle at failure. The minor effective principal stress at failure ( $\sigma'_{hf}$ ) is the same for *all* total stress circles shown in the figure. Since we have only one effective circle at failure, strictly speaking, we need to know both  $\phi'$  and  $c'$  in advance in order to draw the Mohr failure envelope in terms of effective stresses for the UU test. We could perhaps measure the angle of the failure plane in the failed UU specimens and invoke the Mohr failure hypothesis, but as was discussed in Sec. 10.4, there are practical problems with this approach. It should also be noted that the angle of inclination of the failure plane  $\alpha_f$  shown in Fig. 11.42 is defined by the effective stress envelope. Otherwise, as indicated in Fig. 10.9c and Eq. 10-10, theory would predict  $\alpha_f$  to be  $45^\circ$ .

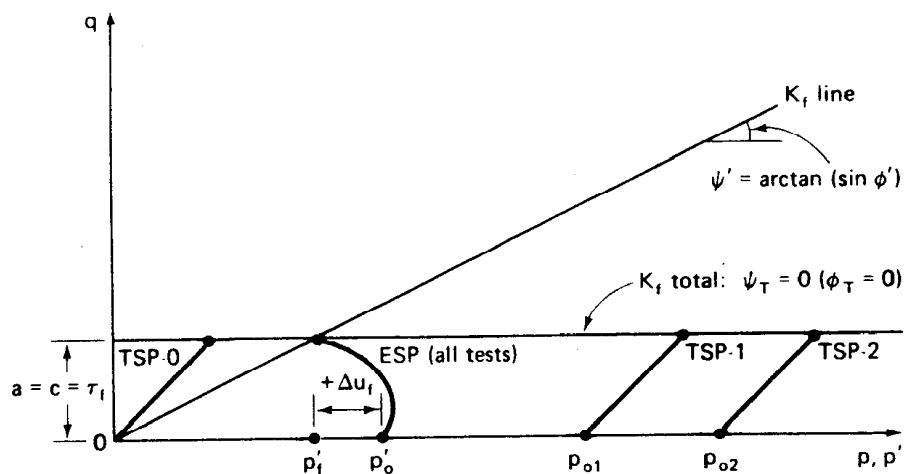


Note:  $\sigma'_{hf}$  is the same for all three total stress circles!

Fig. 11.42 UU test results, illustrating the unique effective stress Mohr circle at failure.

Since the strength ultimately is controlled or governed by the effective stresses, we believe that the physical conditions controlling the formation of a failure plane in the test specimen must in some fashion be controlled by the effective stresses acting in the specimen at failure. Thus Eq. 10-10 should be in terms of  $\phi'$  instead of  $\phi_T$ .

Stress paths for the UU tests of Fig. 11.42 are shown in Fig. 11.43. Behavior is for a normally consolidated clay, and the values of  $p$  and  $q$  for all three tests are listed in the table below the figure. Refer to Fig. 11.38 if necessary to verify these values. If the clay were overconsolidated, then from your knowledge of CU behavior you would expect the ESP to have a shape similar to those of Fig. 11.34b.



	Test	Initial Conditions		At Failure	
		$p_o$	$q_o$	$p_f$	$q_f$
Total stresses	0	0	0	$\frac{\Delta \sigma_f}{2}$	$\frac{\Delta \sigma_f}{2}$
	1	$\sigma_{c1}$	0	$\frac{\Delta \sigma_f + 2\sigma_{c1}}{2}$	$\frac{\Delta \sigma_f}{2}$
	2	$\sigma_{c2}$	0	$\frac{\Delta \sigma_f + 2\sigma_{c2}}{2}$	$\frac{\Delta \sigma_f}{2}$
Effective stresses	All	$p'_o$	$q_o$	$p'_f$	$q_f$
		$u_r$	0	$\frac{\Delta \sigma_f + 2u_r - 2\Delta u_f}{2}$	$\frac{\Delta \sigma_f}{2}$

Fig. 11.43 Stress paths for UU tests on a normally consolidated clay.  
Same tests as in Fig. 11.42.

### 11.9.8 Typical Values of UU Strengths

The undrained strength of clays varies widely. Of course,  $\phi_T$  is zero, but the magnitude of  $\tau_f$  can vary from almost zero for extremely soft sediments to several MPa for very stiff soils and soft rocks. Often, the undrained shear strength at a site is normalized with respect to the vertical effective overburden stress  $\sigma'_{vo}$  at each sampling point. Then the  $\tau_f/\sigma'_{vo}$  ratios are analyzed and compared with other data. This point is covered in more detail later in this chapter.

### 11.9.9 Unconfined Compression Test

We can, theoretically at least, conduct an *unconfined compression test* and obtain the UU-total stress strength. This test is a special case of the UU test with the confining or cell pressure equal to zero (atmospheric pressure). The stress conditions in the unconfined compression test specimen are similar to those of Fig. 11.38 for the UU test, except that  $\sigma_c$  is equal to zero, as shown in Fig. 11.44. If you compare these two figures, you will see that the effective stress conditions at failure are *identical* for both tests. And if the effective stress conditions are the same in both tests, then the strengths will be the same!

Practically speaking, for the unconfined compression test to yield the same strength as the UU test, several assumptions must be satisfied. These are as follows:

1. The specimen must be 100% saturated; otherwise compression of the air in the voids will occur and cause a decrease in void ratio and an *increase* in strength.
2. The specimen must not contain any fissures, silt seams, varves, or other defects; this means that the specimen must be *intact*, homogeneous clay. Rarely are overconsolidated clays intact, and often even normally consolidated clays have some fissures.
3. The soil must be very fine grained; the initial effective confining stress as indicated in Fig. 11.44 is the residual capillary stress which is a function of the residual pore pressure  $-u_r$ ; this usually means that *only clay soils* are suitable for testing in unconfined compression.
4. The specimen must be sheared rapidly to failure; it is a total stress test and the conditions must be undrained throughout the test. If the time to failure is too long, evaporation and surface drying will increase the confining pressure and too high a strength will result. Typical time to failure is 5 to 15 min.

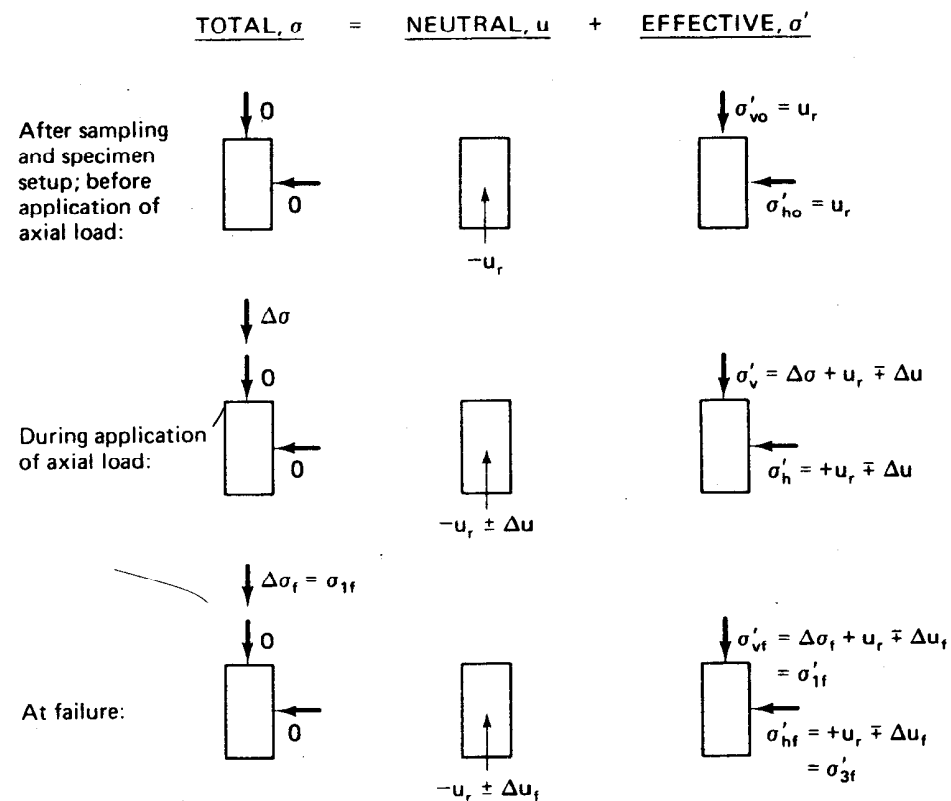


Fig. 11.44 Stress conditions for the unconfined compression test.

Be sure to distinguish between unconfined compressive strength ( $\sigma_1 - \sigma_3$ )<sub>f</sub> and the undrained shear strength, which is  $\tau_f = \frac{1}{2}(\sigma_1 - \sigma_3)_f$ .

### EXAMPLE 11.12

Given:

An unconfined compression test was conducted on a soft clay. The specimen was trimmed from the undisturbed tube sample and was 35 mm in diameter and 80 mm high. The load on the load ring at failure was 14.3 N, and the axial deformation was 11 mm.

Required:

Calculate the unconfined compressive strength and the shear strength of the soft clay sample.

**Solution:**

To calculate the stress at failure, we have to know the area of the specimen  $A_s$ . At failure it is *not* equal to the original area  $A_o$ , but is somewhat greater. (In compression, the specimen decreases in height and increases in diameter as long as Poisson's ratio (Eq. 8-33) is greater than zero.) So, first we need to determine the actual area of the specimen at failure. Since the specimen is tested in undrained shear, we can assume the volume is unchanged and that the specimen deforms as a right circular cylinder. Thus  $A_s$  at any strain  $\epsilon$  is

$$A_s = \frac{A_o}{1 - \epsilon} \quad (11-8)$$

Now we can calculate the area of the specimen. The strain at failure is  $\Delta L/L_o = 11 \text{ mm}/80 \text{ mm} = 0.1375$ , or 13.8%. Thus  $A_s = 1115 \text{ mm}^2$ . Now the compressive stress at failure is  $14.3 \text{ N}/1115 \text{ mm}^2 = 12.8 \text{ kN/m}^2 (\text{kPa})$ . If we had simply divided by the original area of the specimen, we would have obtained  $14.9 \text{ kN/m}^2$ , a significant error.

The shear strength for the unconfined compression test is one-half the compressive strength, or  $6.4 \text{ kPa}$ .

It should be noted that the actual shear stress on the failure plane at failure  $\tau_{ff}$  is somewhat less than the undrained shear strength  $\tau_f = c$  because  $\tau_{ff}$  occurs on a failure plane whose inclination is determined by the effective stresses, as explained previously for the UU test. The conditions and the approximate magnitude of associated error is indicated in Fig. 11.45a for the specimen at failure in Fig. 11.45b. The magnitude of the error depends on  $\phi'$ , as indicated by the calculations in Example 11.13.

---

### EXAMPLE 11.13

**Given:**

The stress conditions for the unconfined compression test shown in Figs. 11.45a and 11.45b.

**Required:**

Find the error in assuming the undrained shear strength  $\tau_f = c = \frac{1}{2} \Delta \sigma_f$ , rather than  $\tau_{ff}$  for a normally consolidated clay where  $\phi' = 30^\circ$ .

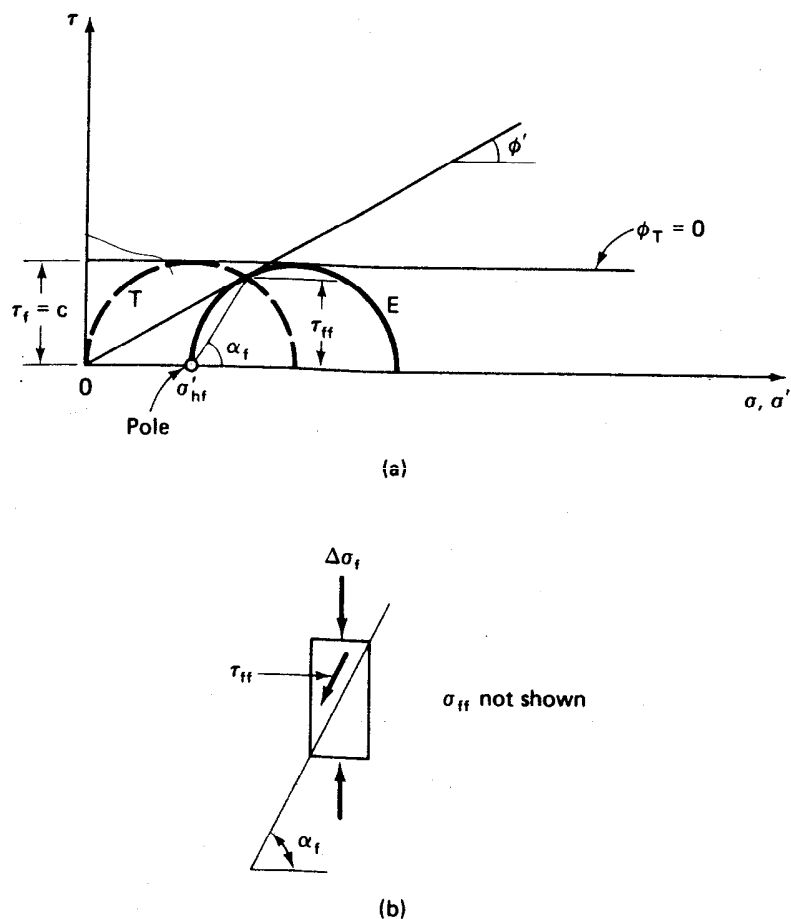


Fig. 11.45 (a) Difference between  $\tau_{ff}$  and  $\tau_f = c$  in an (b) unconfined compression test specimen (after Hirschfeld, 1963).

**Solution:**

From Eq. 10-6,

$$\begin{aligned}\tau_{ff} &= \frac{\sigma_1 - \sigma_3}{2} \sin 2\alpha_f \\ &= \frac{\Delta\sigma_f}{2} \sin 2\alpha_f\end{aligned}$$

From Eq. 10-10,  $\alpha_f = 45^\circ + \phi'/2$ . So  $\alpha_f = 60^\circ$ . Therefore

$$\tau_{ff} = \frac{\Delta\alpha_f}{2} \sin 120^\circ = 0.433\Delta\sigma_f$$

But  $\tau_f = c = 0.5\Delta\sigma_f$ .

Conclusion:  $\tau_f = c$  strength is about 15% greater than  $\tau_{ff}$  for  $\phi' = 30^\circ$ . Note that the error is less for smaller  $\phi'$  angles. Also note that

$$\tau_f = c = \frac{\Delta\sigma_f}{2} = \frac{(\sigma_1 - \sigma_3)_f}{2} = \tau_{\max}$$

The point illustrated by Example 11.13 is that the actual shear strength of the failure plane is *overestimated* by the one-half unconfined compressive strength. The magnitude of the error is probably about 15% at most.

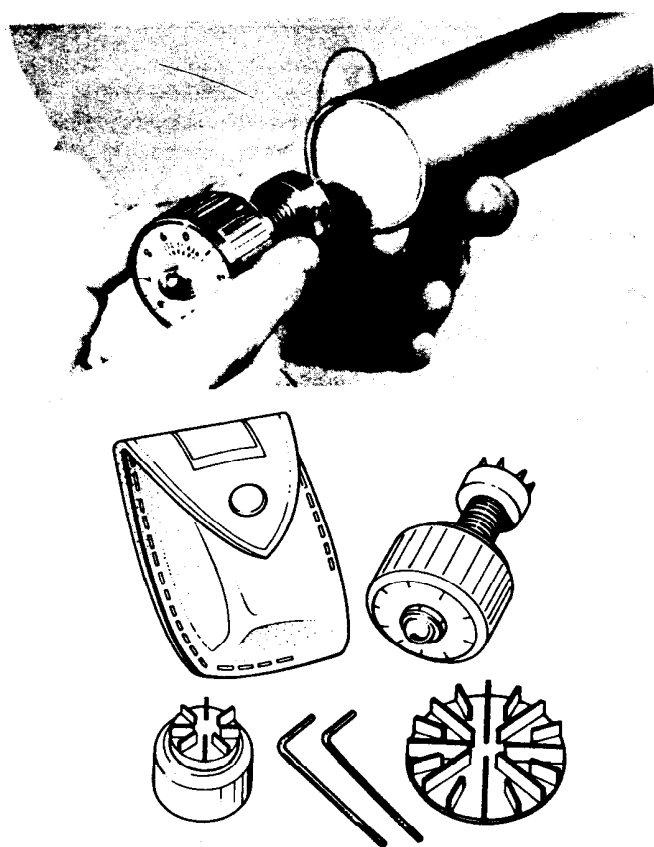
Why then does the unconfined compression test apparently work satisfactorily? It is far and away the most common laboratory strength test used today in the United States for the design of shallow and pile foundations in clay. Part of the answer lies in *compensating errors*. Sample disturbance especially tends to reduce the undrained shear strength. Anisotropy also is a factor, as is the assumption of plane strain conditions for most design analyses whereas the real stress conditions are more three dimensional. These factors tend to reduce the undrained shear strength so that the difference between  $\tau_f = c$  and  $\tau_{ff}$  becomes negligible in engineering practice. Several of these points are discussed by Ladd, et al. (1977).

#### 11.9.10 Other Ways to Determine the Undrained Shear Strength

There are other ways besides the unconfined compression test or the UU triaxial test to obtain the undrained shear strength of cohesive soils. Some of the field methods were mentioned briefly at the end of Sec. 10.5; other methods are used exclusively in the laboratory on undisturbed samples. In all the methods, loading to failure is assumed to take place so rapidly that undrained conditions exist. The result obtained from the test is then correlated with the undrained shear strength  $\tau_f$ .

Table 11-6 and Figs. 11.46 through 11.55 illustrate the methods commonly used for determining  $\tau_f$ . References are listed in the table if you need additional details about these tests or their interpretation.

Except for the SPT, all the field techniques listed in Table 11-6 were developed in Europe, but there has been increasing interest in them in recent years in North America (Ladd, et al., 1977). The conditions for a reliable unconfined compression test are not often met. More sophisticated laboratory testing techniques are attractive but increasingly expensive. Sampling of poor quality, unfortunately the rule rather than the exception in the United States, can significantly affect the measured shear strength. Some soils such as stiff fissured clays are difficult if not impossible to even



(a)

Diameter (mm)	Height of vanes (mm)	Maximum $\tau_f$ (kPa)
19	3	250
25	5	100 (standard)
48	5	20

(b)

Fig. 11.46 Torvane (TV): (a) Standard model shown on its side. The other two vanes, which can be attached to the standard Torvane, are for very soft or very stiff clays. (b) Specifications for the three vanes. (Photograph courtesy of Soiltest, Inc., Evanston, Illinois.)

**TABLE 11-6** Laboratory and Field Methods for Determining  $\tau_f$ 

No.	Test	Use	Fig. No.	Remarks
1	Torvane (TV)	Lab, field	11.46	Hand held; calibrated spring; quick; used on tube samples or the sides of exploratory trenches, etc. Sample tested is seen.
2	Pocket penetrometer (PP)	Lab, field	11.47	Same as above, except spring is cali- brated in unconfined compressive strength $(= 2\tau_f)$ .
3	Swedish fall- cone test (SFC)	Lab	11.48	Quick; sample tested is seen; used on tube samples. $\tau_f$ depends on cone angle and mass.
4	Vane shear test (VST)	Lab, field	11.49	Various sizes and configurations avail- able for both field and lab use. Height/ diameter ratio (H/D) = 2 for field vanes; H/D = 1 for lab vanes. Only lab vane sample is seen.
5	Standard penetration test (SPT)	Field	11.51	A standard "split-spoon" sampler is driven by a 63.5 kg hammer falling 0.76 m. The number of blows required to drive the sampler 0.3 m is called the <i>standard penetration resistance</i> , or <i>blow count</i> , $N$ . Disturbed sample obtained.
6	Dutch cone penetrometer (CPT)	Field	11.52	A 60° cone with a projected area of 10 cm <sup>2</sup> is pushed at 1 to 2 m/min. Point resistance $q_c$ and friction on the friction sleeve $f_s$ are measured either electrically or mechanically.
7	Pressuremeter (PMT)	Field	11.53	A cylindrical probe is inserted in a drill hole (may be self-boring). Lateral pressure is applied incrementally to side of hole.
8	Screw plate compresso- meter (SPC)	Field	11.54	The plate is screwed down to the desired testing depth; hydraulic pressure is applied incrementally and the settlement is observed; continue loading until the bearing capacity of the soil is reached.
9	Iowa borehole shear test (BST)	Field	11.55	Device is lowered into a borehole and ex- panded against the side walls ( $\sigma_n$ ). Then entire mechanism is pulled from ground sur- face and maximum load measured ( $\tau_f$ ). Stage test results are used to plot Mohr diagram for CD tests. Range of $\sigma_n$ is from about 30 to 100 kPa.

**TABLE 11-6** (cont.)

	Best For	Limitations	References
1	Very soft to stiff clays	Cohesive soils without pebbles, fissures, etc. Test only a small amount of soil near the surface. Only rough calibration with $\tau_f$ .	
2	Very soft to stiff clays	Same as above.	
3	Very soft to soft clays	Same as above, except good correlation with $\tau_f$ on soft, sensitive clays.	Hansbo (1957)
4	Soft to stiff clays	May overestimate $\tau_f$ ; see Fig. 11.50 for correction factor for very soft clays. Unreliable readings if vane encounters sand layers, varves, stones, etc., or if vane rotated too rapidly.	Cadling and Odenstad (1950) Bjerrum (1972) Schmertmann (1975) ASTM (1980) D 2573 Ladd, et al. (1977)
5	Granular soils	Very rough correlation with $\tau_f$ for cohesive soils. Boulders can cause problems. Results are sensitive to test details.	ASTM (1980) D 1586 de Mello (1971) Schmertmann (1975) Kovacs, et al. (1977)
6	All soil types except very coarse granular soils	Boulders cause problems. Requires local correlation for soft clays.	Sanglerat (1972) ESOPT (1974) Schmertmann (1975) Ladd, et al. (1977) ASTM (1980) D 3441
7	All soil types	Requires a correlation between $p_i$ and $\tau_f$ .	Ménard (1956, 1975) Schmertmann (1975) Ladd, et al. (1977) Baguelin, et al. (1978)
8	All soil types except very coarse granular soils	Mostly used to study the compressibility of granular soils. Schwab (1976) found good agreement with the screw plate and the vane shear test in plastic Swedish clays.	Janbu and Senneset (1973) Mitchell and Gardener (1975) Schwab (1976) Schmertmann (1970)
9	Loessial (silty) soils	Cannot be used with soils with 10% or more gravel or caving sands. Uncertain drainage conditions during shear makes the test difficult to interpret. (Is it CD or CU or somewhere in between?)	Wineland (1975) Schmertmann (1975)

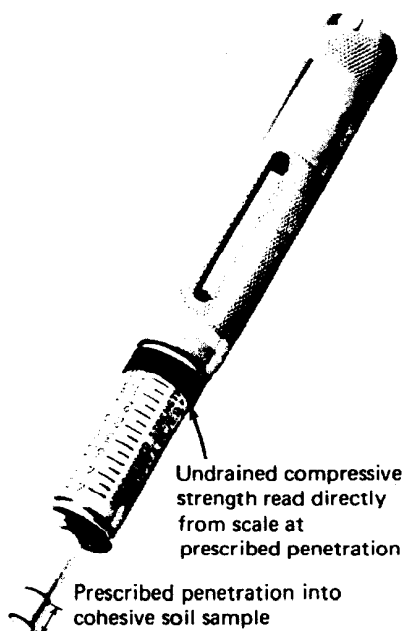
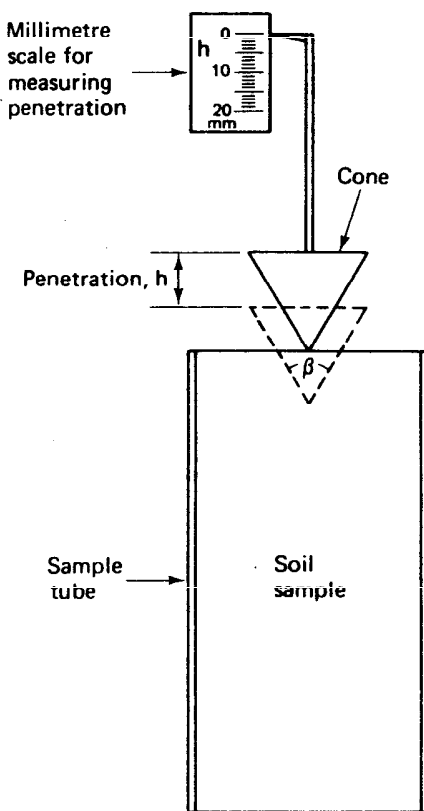


Fig. 11.47 Pocket penetrometer (PP), a hand-held device which indicates unconfined compressive strength (photograph courtesy of Soiltest, Inc., Evanston, Illinois).

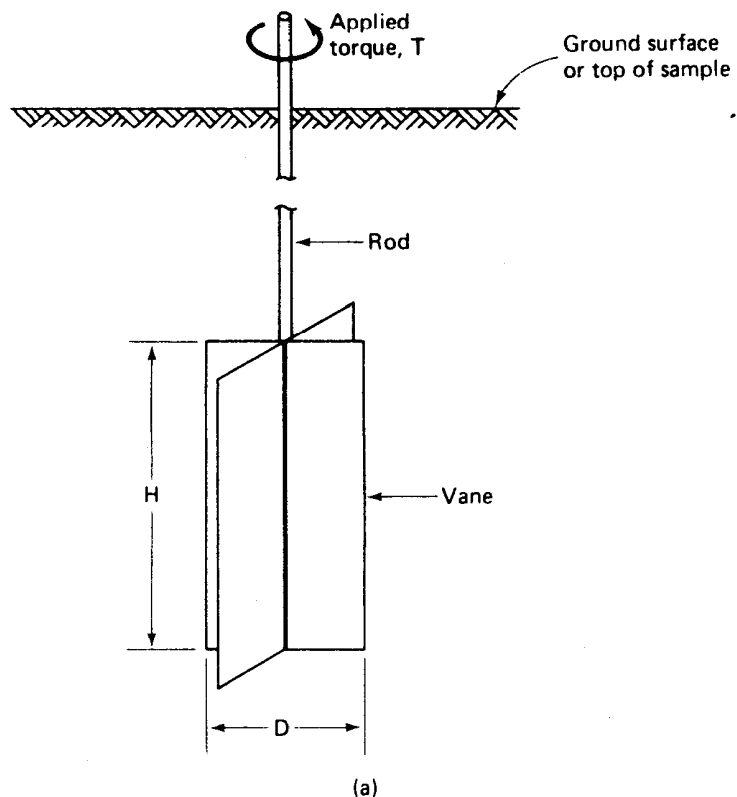
sample. There are statistical advantages, too, for having lots of indirect subsurface information obtained rapidly and at relatively low cost compared with a few, expensive laboratory tests on what may not even be the weakest or the most critical strata at the site. Finally, some soil properties ( $K_o$ , permeability, deformation modulus) can only be determined reliably in the field.

The major disadvantage of the in situ methods is that  $\tau_f$  is obtained only indirectly through correlations with laboratory tests or by backcalculation from theory or actual failures. Figure 11.50 is an example of the correction factor that must be applied to the field vane test to obtain the best estimate of the in situ  $\tau_f$ . Other correlations are provided in the references for each test listed in Table 11-6. Especially useful are the correlations presented by U.S. Navy (1971), de Mello (1971), and Schmertmann (1975) for the SPT and Dutch cone penetrometers. For the pressuremeter test, see Ménard (1975) and Baguelin, et al. (1978). In a real sense, then, these tests only give an *index* of the actual undrained shear strength of the soil.

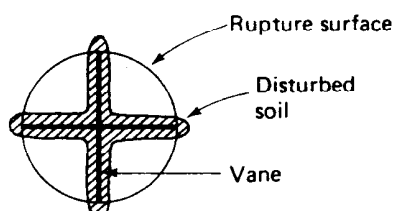


Mass (g)	Cone angle $\beta$ (degrees)	Range of $\tau_f$ (kPa)
400	30	10–250
100	30	25–63
60	60	0.5–11
10	60	0.08–2

Fig. 11.48 Principle of the Swedish fall-cone test (SFC). The undrained shear strength is proportional to the mass of the cone and inversely proportional to the penetration squared. The test must be calibrated (after Hansbo, 1957). Shear strength ranges are tabulated for the four standard cones.



(a)



(b)

(c) Typical sizes (H/D):

Lab: 12 X 12 mm  
16 X 16 mmField: 76 X 38 mm  
100 X 50  
130 X 65

(d) Theoretical formulas:

$$\frac{H}{D} = 1: \tau_f = \frac{3}{2} \frac{T_{\max}}{\pi D^3}$$

$$\frac{H}{D} = 2: \tau_f = \frac{6}{7} \frac{T_{\max}}{\pi D^3}$$

Fig. 11.49 (a) Principle of the vane shear test (VST); (b) end view of the vane, showing the probable zone of disturbance and the rupture surface (after Cadling and Odenstad, 1950); (c) typical vane sizes; (d) theoretical formulas for  $\tau_f$ , assuming a uniform stress distribution.

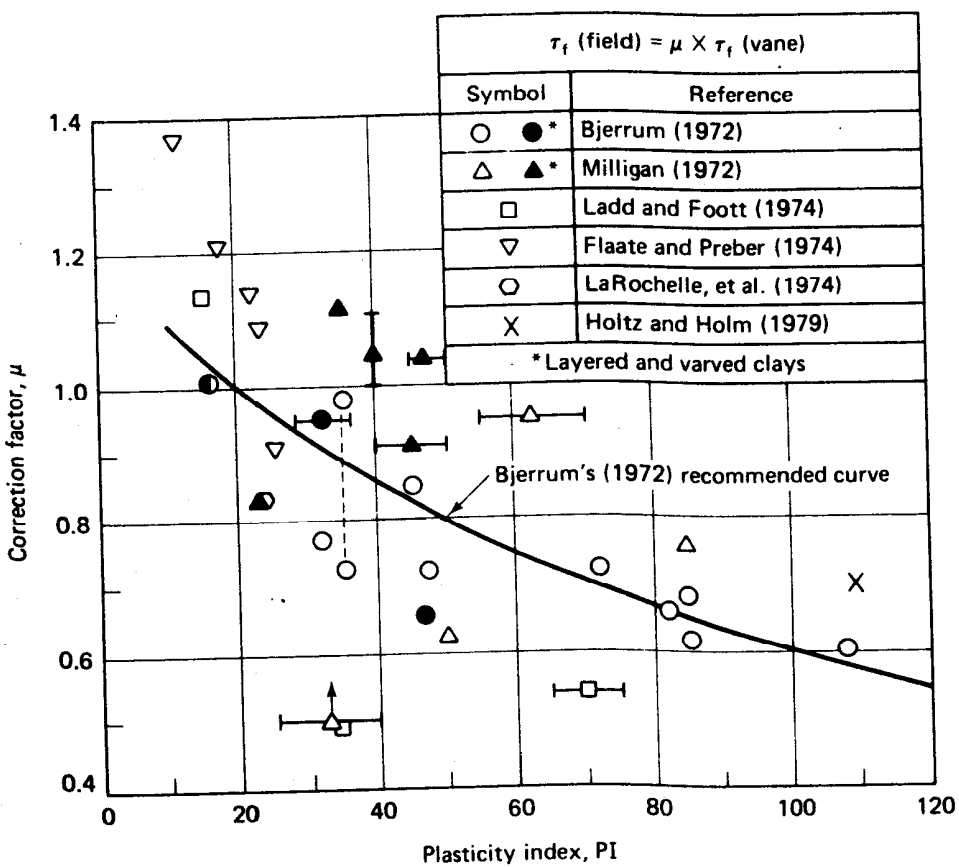
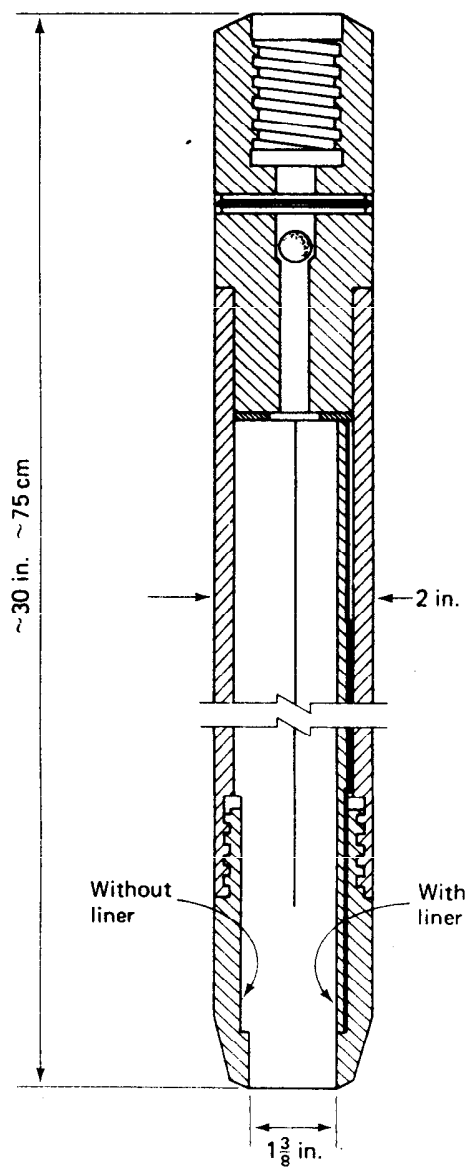


Fig. 11.50 Correction factor for the field vane test as a function of PI, based on embankment failures (after Ladd, 1975, and Ladd, et al., 1977).



(a)



(b)

**Fig. 11.51** Standard penetration test (SPT): (a) "split-spoon" sampler; (b) drill rig with sampler being inserted inside hollow stem auger at 1. The sleeve encloses the 63.5 kg hammer. Hammer in the raised position is shown at 2. (Drawing courtesy of Mobile Drilling Co., Indianapolis, Indiana. Photograph by W.D. Kovacs.)

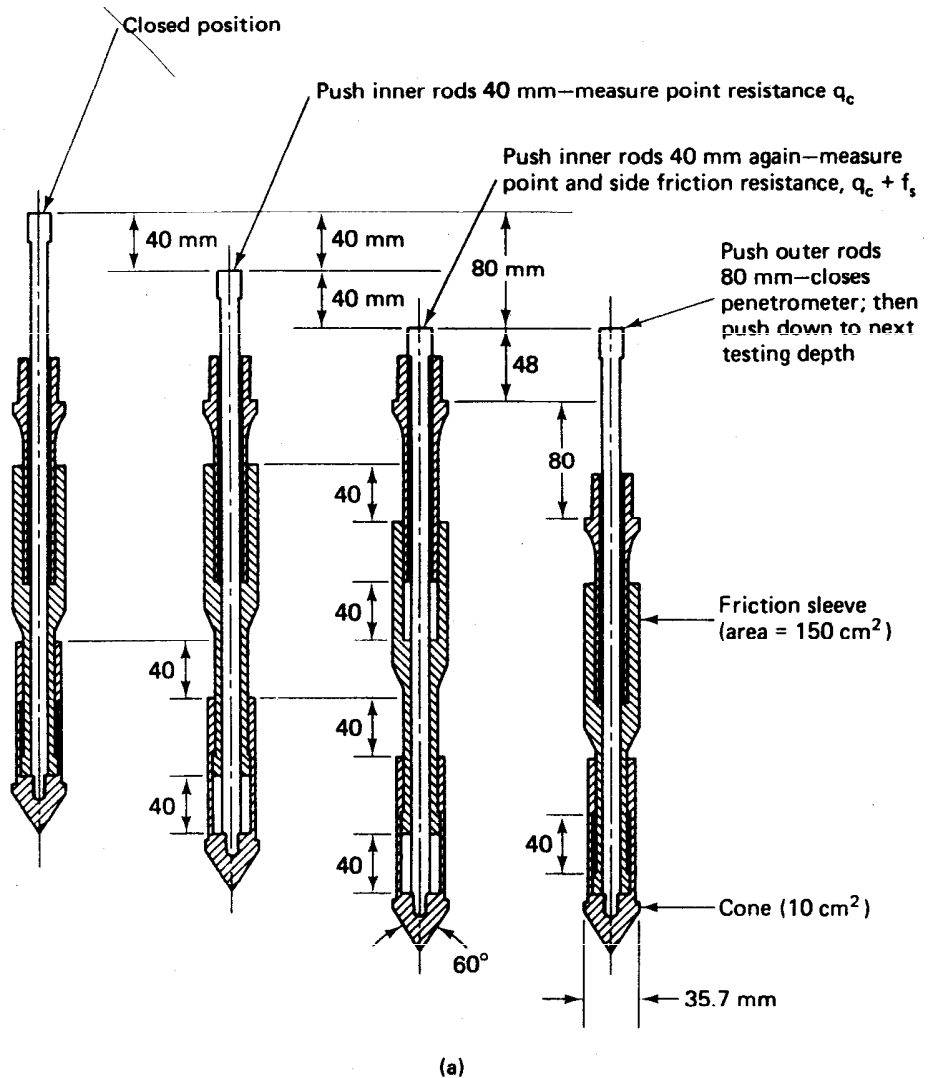
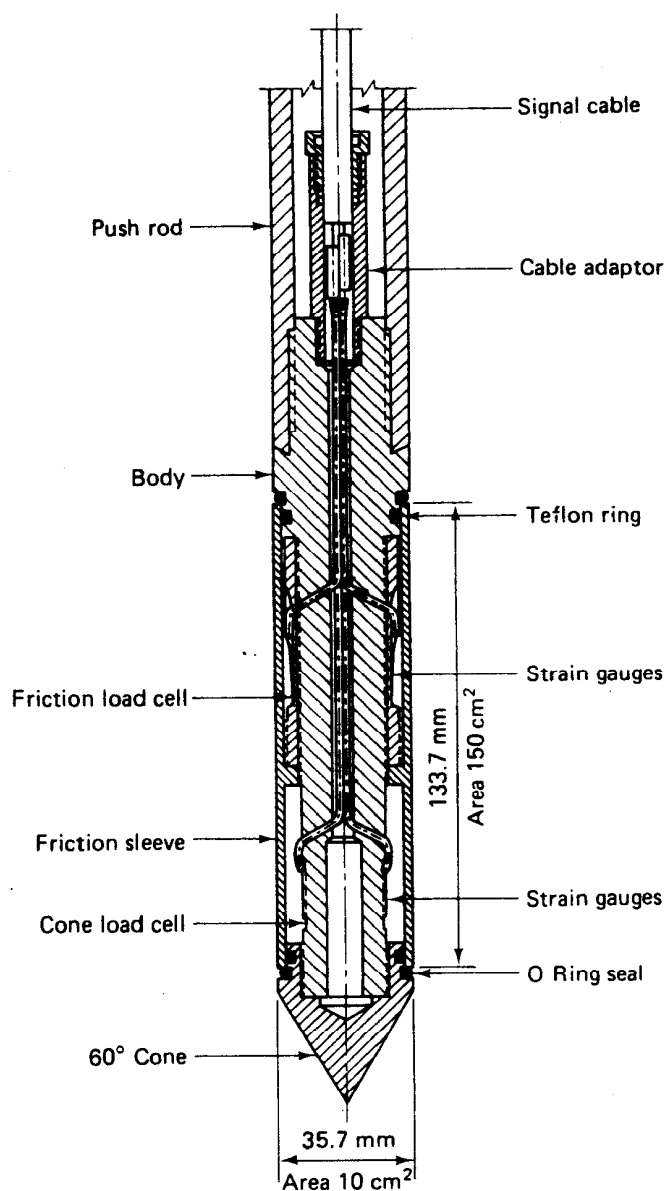
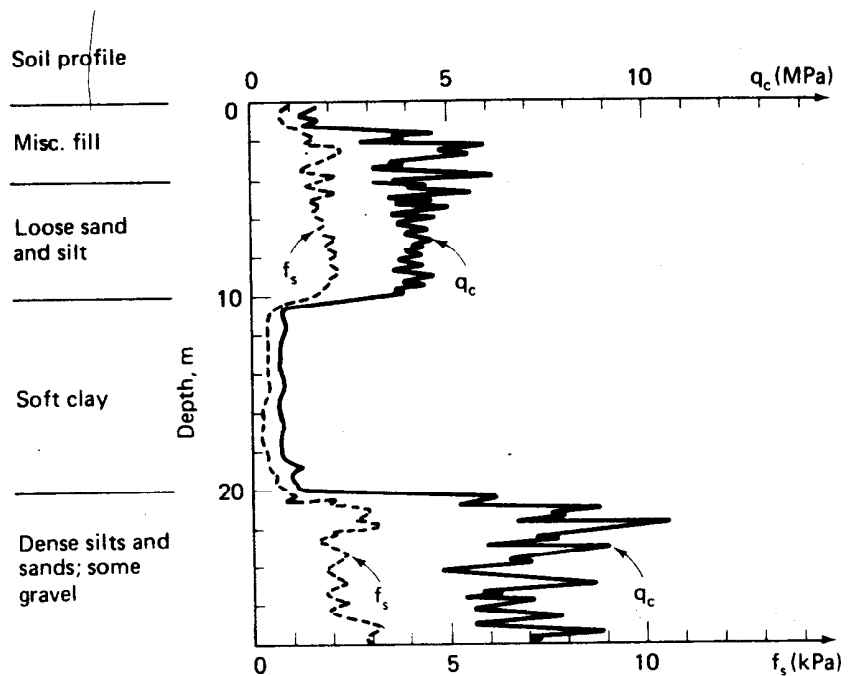


Fig. 11.52 Dutch cone penetrometer (CPT): (a) Begemann (1953) mechanical cone with friction sleeve.



(b)

Fig. 11.52 (cont.) Dutch cone penetrometer: (b) Cross section of a modern electrical penetrometer with strain-gage load cells to measure both the point resistance and the sleeve friction (after Holden, 1974).

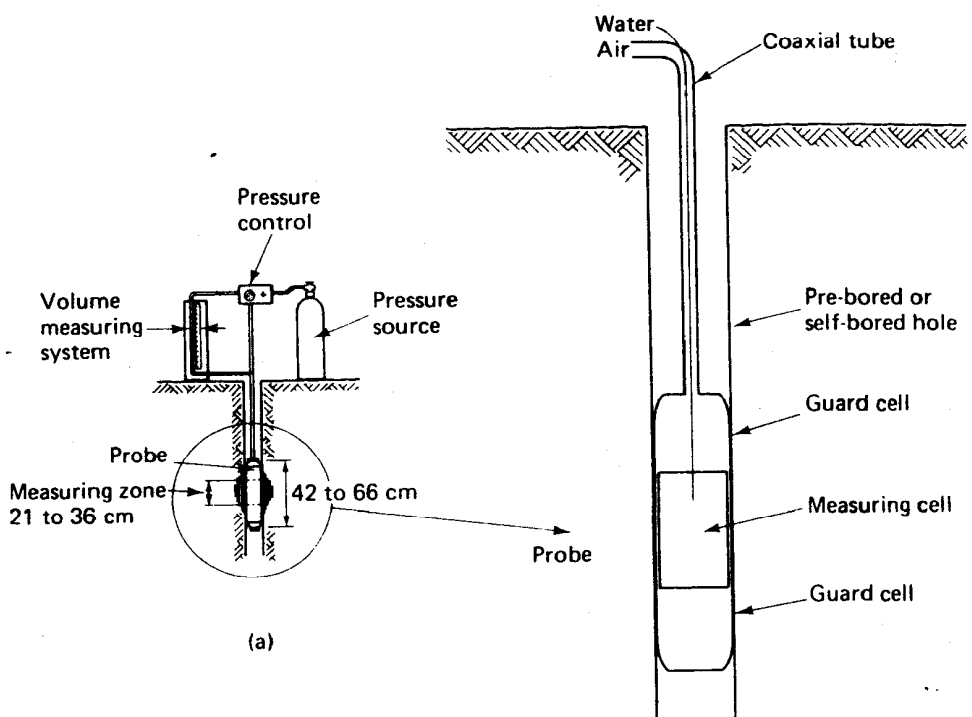


$$\tau_f = \frac{q_c - \rho g z}{N_c}$$

where  $\rho g z$  = total overburden pressure at depth  $z$   
 $N_c$  = correlation factor (bearing capacity factor); range from 5 to as high as 70, depending on the soil deposit

(c)

Fig. 11.52 (cont.) Dutch cone penetrometer: (c) Typical cone penetrometer test results correlated with the soil profile, and formula for calculating  $\tau_f$  from cone penetrometer results.



(b)

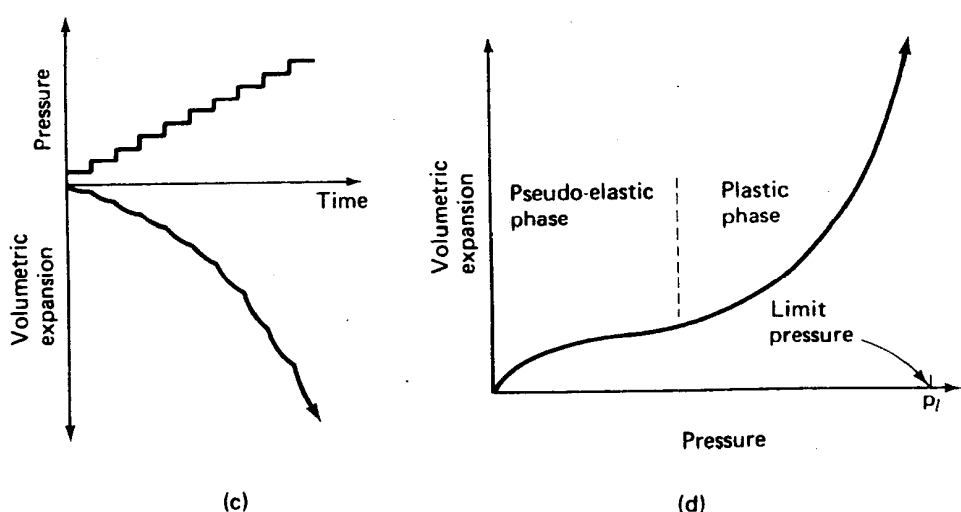
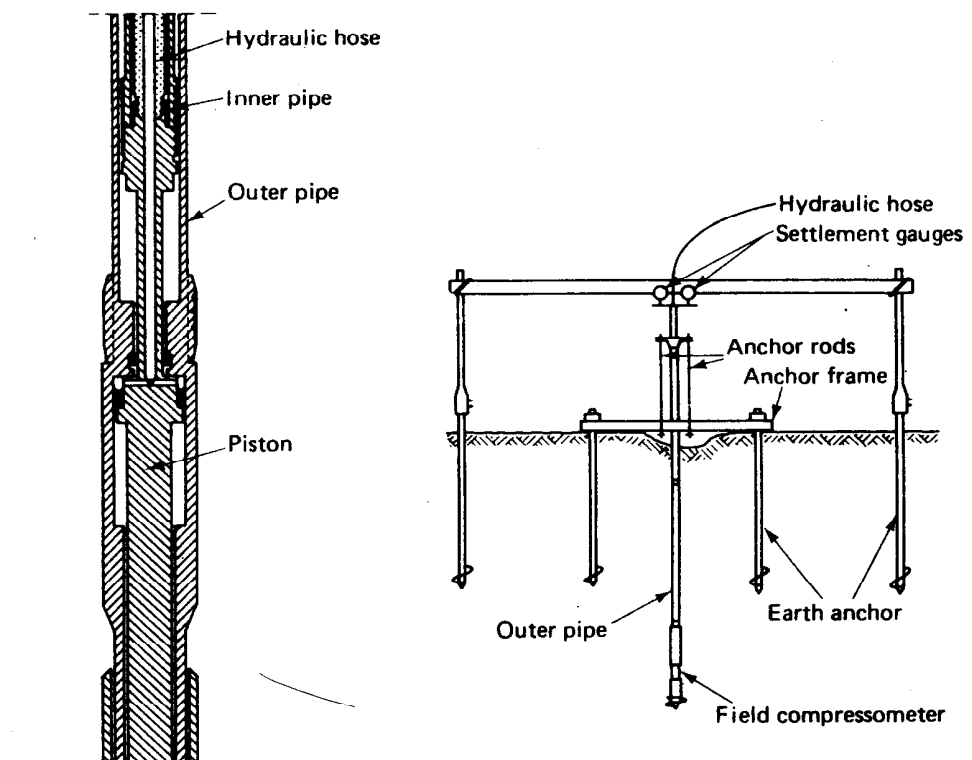
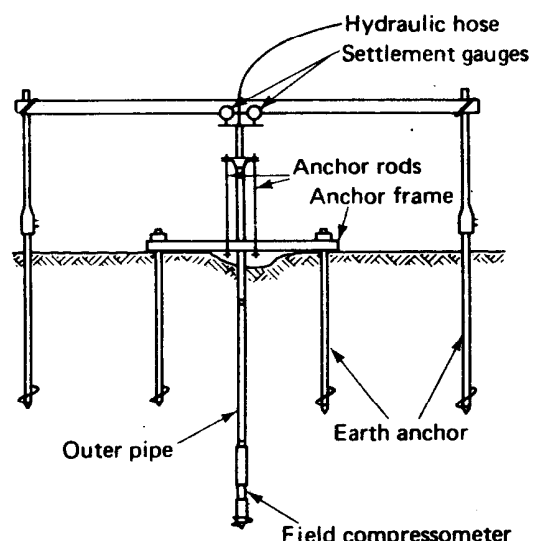


Fig. 11.53 Pressuremeter test (PMT): (a) Schematic diagram of probe and measuring system (after Mitchell and Gardner, 1975). (b) Detail of probe. Typical test results: (c) Pressure and volumetric expansion versus time, and (d) Volumetric expansion versus pressure (after Ménard, 1975).



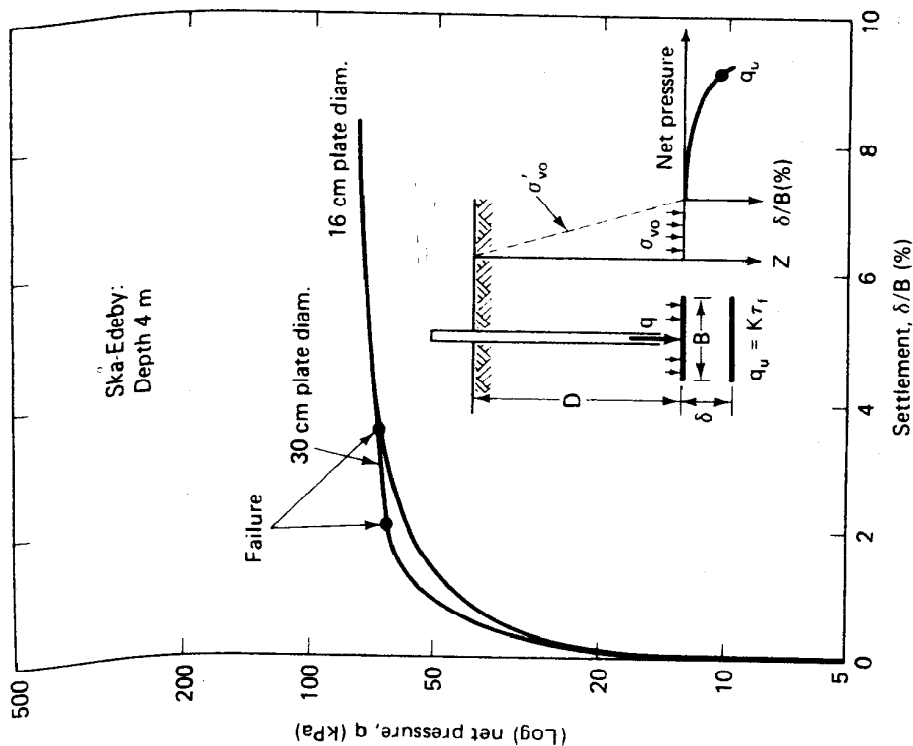
(a)

Two sizes:  
160 mm diameter  
300 mm diameter

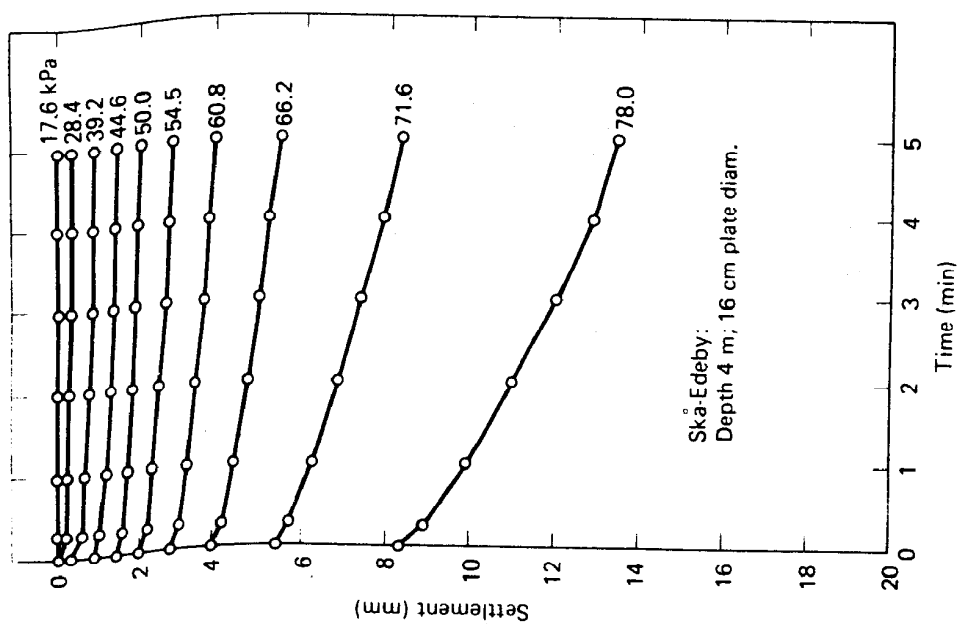


(b)

Fig. 11.54 Screw plate compressometer (SPC): (a) principle; (b) field setup (after Janbu and Senneset, 1973).



(c)



(d)

Fig. 11.54 (cont.) Screw plate compaction test: typical (c) settlement-time and (d) pressure-settlement data for Skå-Edeby clay, Sweden (after Schwab, 1976).

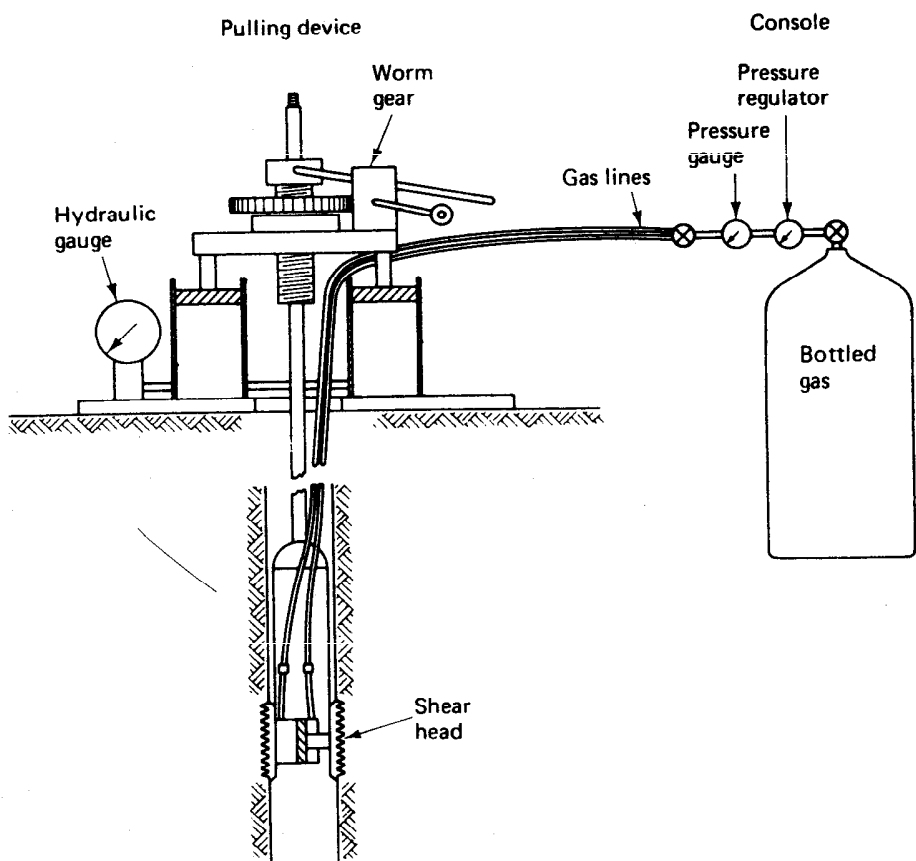


Fig. 11.55 The Iowa borehole shear (BST) device, showing the pressure source and instrumentation console, the pulling device, and the expanded shear head on the sides of a borehole (after Wineland, 1975).

### 11.9.11 Sensitivity

Earlier, in Sec. 2.7, we very generally defined *sensitivity* as the ratio of the undisturbed or natural strength of a clay to its remolded strength. *Strength* was left purposely vague. Now we can define sensitivity more precisely, at least within the precision limits of the strength measurements themselves. Usually, sensitivity is based on the unconfined compressive strength or the unconfined shear strength  $\tau_f = c$ , but the laboratory or field vane shear tests or the Swedish fall-cone test could also be used. *Sensitivity*  $S_t$  is therefore

$$S_t = \frac{\text{unconfined compressive strength (undisturbed)}}{\text{unconfined compressive strength (remolded)}} \\ = \frac{\tau_f(\text{undisturbed})}{\tau_f(\text{remolded})} \quad (11-9)$$

It should be noted that the remolded strength determination must be at the *same* water content—the natural water content  $w_n$ —as the water content of the undisturbed specimen. Table 11-7 indicates the range of sensitivity values commonly used in the United States, where highly sensitive clays are rare. Sensitive clays exist in other parts of the world, especially eastern Canada and Scandinavia. Other sensitivity scales are available besides those listed in Table 11-7 (for example, Skempton and Northe, 1952; Bjerrum, 1954).

**TABLE 11-7 Typical Values of Sensitivity**

Condition	Range of $S_i$	
	U.S.	Sweden
Low sensitive	2–4	< 10
Medium sensitive	4–8	10–30
Highly sensitive	8–16	> 30
Quick	16	> 50
Extra quick	—	> 100
Greased lightning	—	—

Figure 2.9 shows what happened to a sample of Leda clay from eastern Canada before and after remolding. Leda clays are often very stiff in their natural state. Their unconfined compressive strengths may be greater than 100 kPa, but their liquidity indices (Eq. 2-23), are often 2 or more. No wonder that their strengths are so low when they are thoroughly remolded! The sample shown in Fig. 2.9 had a sensitivity of about 1500 (Penner, 1963) which definitely qualifies it as extra quick (or even greased lightning!) according to Table 11-7. Note that with such clays, you have to use either a laboratory vane or fall-cone test to obtain the remolded  $\tau_f$  (Eden and Kubota, 1962).

Correlations between sensitivity and liquidity index have been made by several researchers, as shown in Fig. 11.56.

#### 11.9.12 Use of the Undrained (UU) Shear Strength in Engineering Practice

Like the CD and CU tests, the undrained or UU strength is applicable to certain critical design situations in engineering practice. These situations are where the engineering loading is assumed to take place so rapidly that there is no time for the induced excess pore water pressure to dissipate or for consolidation to occur during the loading period. We also assume that the change in total stress during construction does not affect the in situ undrained shear strength (Ladd, 1971b). Examples shown in Fig. 11.57 include the end of construction of embankment dams and foundations for

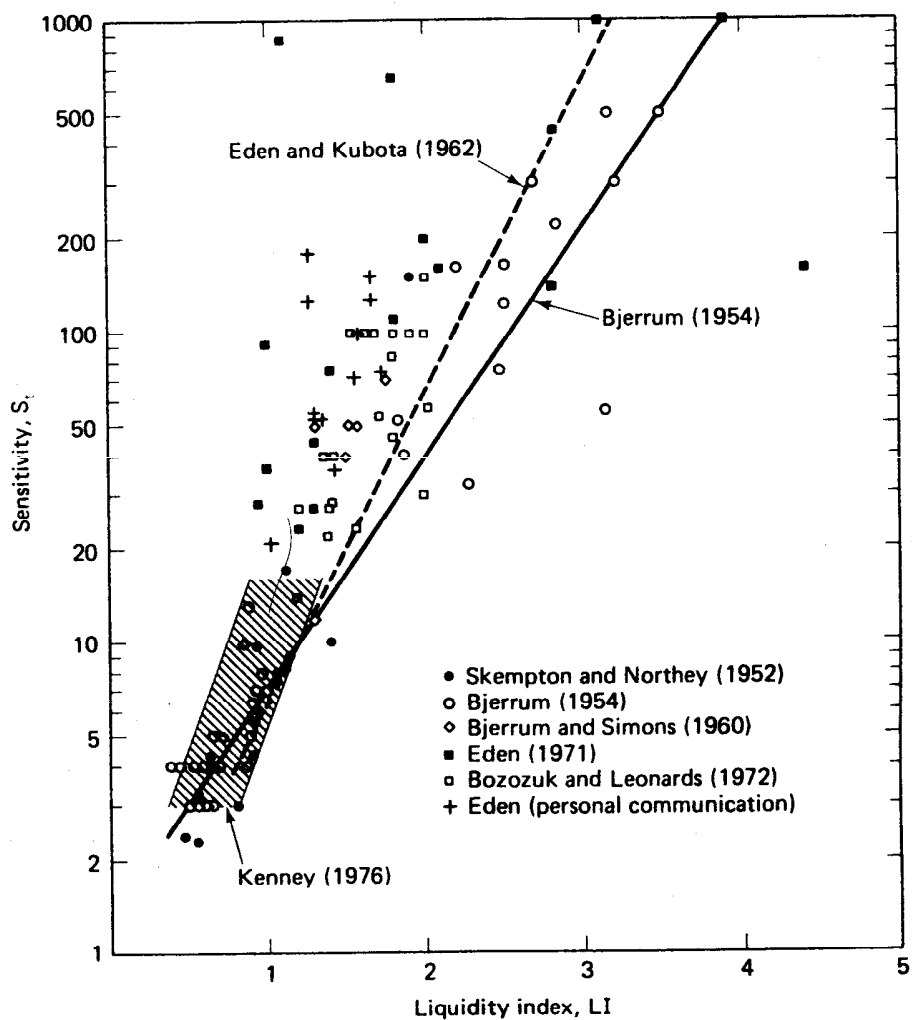


Fig. 11.56 The relationship between sensitivity and liquidity index for Scandinavian, British, Canadian, and some U.S. clays.

embankments, piles, and footings on normally consolidated clays. For these cases, often the most critical design condition is *immediately after* the application of the load (at the *end of construction*) when the induced pore pressure is the greatest but *before* consolidation has had time to take place. Once consolidation begins, the void ratio and the water content naturally decrease and the strength increases. So the embankment or foundation becomes increasingly *safier* with time.

One of the more useful ways to express the undrained shear strength is in terms of the  $\tau_f/\sigma'_{\text{oo}}$  ratio for normally consolidated clays. Sometimes this is called the *c/p ratio*. In natural deposits of sedimentary clays the

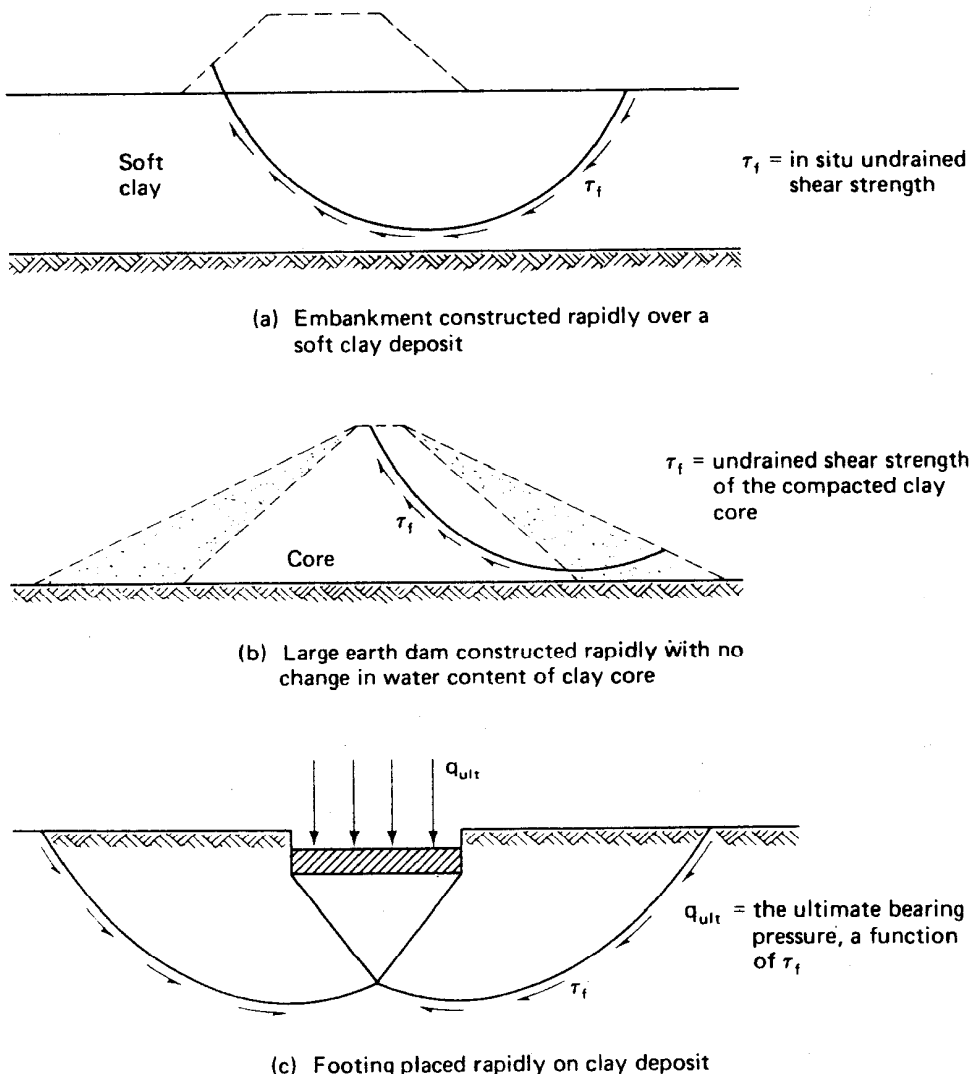


Fig. 11.57 Some examples of UU analyses for clay (after Ladd, 1971b).

undrained shear strength has been found to increase with depth, and thus it is proportional to the increase in effective overburden stress with depth. It was first observed by Skempton and Henkel (1953) and confirmed by Bjerrum (1954) that the  $\tau_f/\sigma'_v$  ratio seemed to increase with increasing plasticity index. Bjerrum's (1954) results are shown in Fig. 11.58 along with those of several other researchers; in addition, several best-fit correlations are also shown in the figure. There is a lot of scatter so Fig. 11.58 should only be used with caution. However, as with Fig. 11.27, such correlations are useful for preliminary estimates and for checking laboratory data.

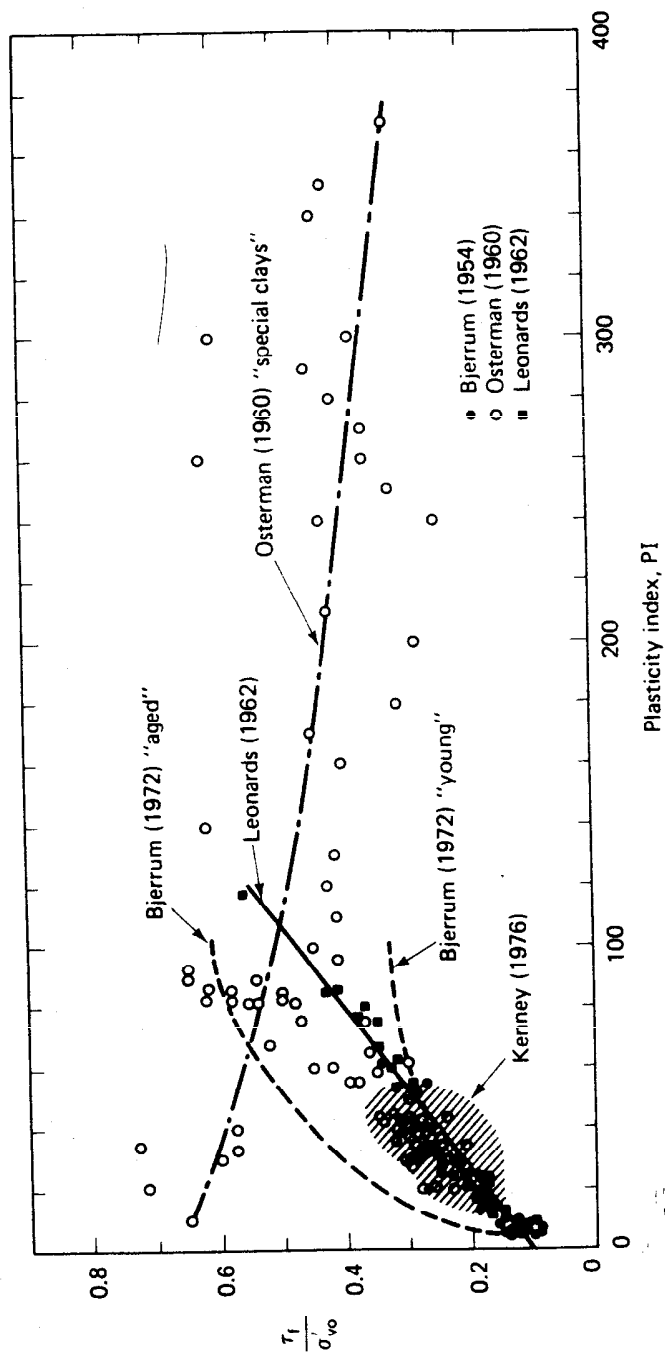


Fig. 11.58 Relationship between the ratio  $\tau_1/\sigma'_0$  and plasticity index for normally consolidated clays.

Kenney (1959) and Bjerrum and Simons (1960) presented some theoretical  $\tau_f/\sigma'_{vo}$  ratios versus PI based on the correlations of Fig. 11.27,  $K_o$ , and the Skempton pore pressure parameter  $A$  (to be discussed in Sec. 11.11). These theoretical relationships tended to decrease rather than increase with PI, but the agreement was satisfactory for  $PI > 30$ . Kenney (1959) concluded that  $\tau_f/\sigma'_{vo}$  was essentially independent of PI after all; rather, it probably depended on the geologic history of the clay.

Bjerrum and Simons (1960) also presented the relationship between  $\tau_f/\sigma'_{vo}$  and liquidity index (LI) for some Norwegian marine clays, as shown in Fig. 11.59. As you know from Fig. 11.56, the quick clays are those with very high LI's. Therefore it appears that Norwegian quick clays have a  $\tau_f/\sigma'_{vo}$  ratio of about 0.1 to 0.15.

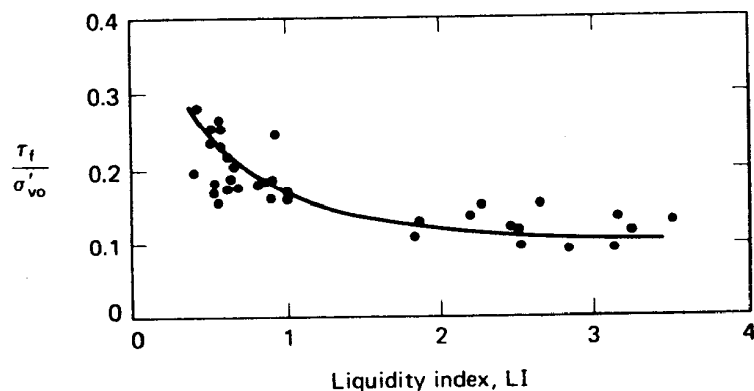


Fig. 11.59 Relationship between  $\tau_f/\sigma'_{vo}$  and liquidity index for Norwegian clays (after Bjerrum and Simons, 1960).

You should be aware of the fact that the  $\tau_f/\sigma'_{vo}$  ratio depends strongly on the total stress path. This point is discussed by Bjerrum (1972) and Ladd, et al. (1977), among others. In other words, you probably will obtain different values of  $\tau_f/\sigma'_{vo}$ , depending on whether you run field vane tests, axial compression or axial extension triaxial tests, or direct simple shear tests.

Sometimes it is better to normalize the undrained shear strength with respect to the effective *consolidation* pressure  $\sigma'_{vc}$  or the preconsolidation stress  $\sigma'_p$  if the clay is slightly overconsolidated. For these soils the undrained strength is really controlled by the effective consolidation pressure rather than the existing effective overburden stress. Bjerrum (1972) hypothesized that the ratio between  $\sigma'_p$  and  $\sigma'_{vo}$  would vary with PI, as shown in Fig. 11.60a. So-called "young" clays are normally consolidated recent sediments, thus they haven't had time to be overconsolidated by any of the factors listed in Table 8-1. On the other hand, "aged" clays are slightly overconsolidated, and Bjerrum found that the amount of overconsolidation increased somewhat with the PI (Fig. 11.60b). The resulting effect on

the strength was indicated by the dashed curves labeled "Bjerrum (1972)" in Fig. 11.58.

Recall from the discussion of the vane shear test that Bjerrum (1972) proposed a correction factor for the vane shear test based on a study of actual embankment failures (Fig. 11.50). For convenient reference, this figure is reproduced without all the data points as Fig. 11.60c.

Mesri (1975) discovered a very interesting relationship between all these observations. Combining Figs. 11.60a and 11.60b Mesri obtained Fig. 11.60d,  $\tau_f/\sigma'_p$  versus PI, which shows essentially the same behavior for "aged" and "young" clays. Now apply Bjerrum's correction factor  $\mu$  for the vane shear test to obtain the in situ strengths; the result is Fig. 11.60e. In other words,  $(\tau_f/\sigma'_{vc})_{field}$  is almost a constant equal to 0.22 and independent of PI! There is great uncertainty in such a conclusion because of the scatter in the empirical relationships upon which it is based, and the relationships shown in Figs. 11.60d and 11.60e may be only a coincidence.

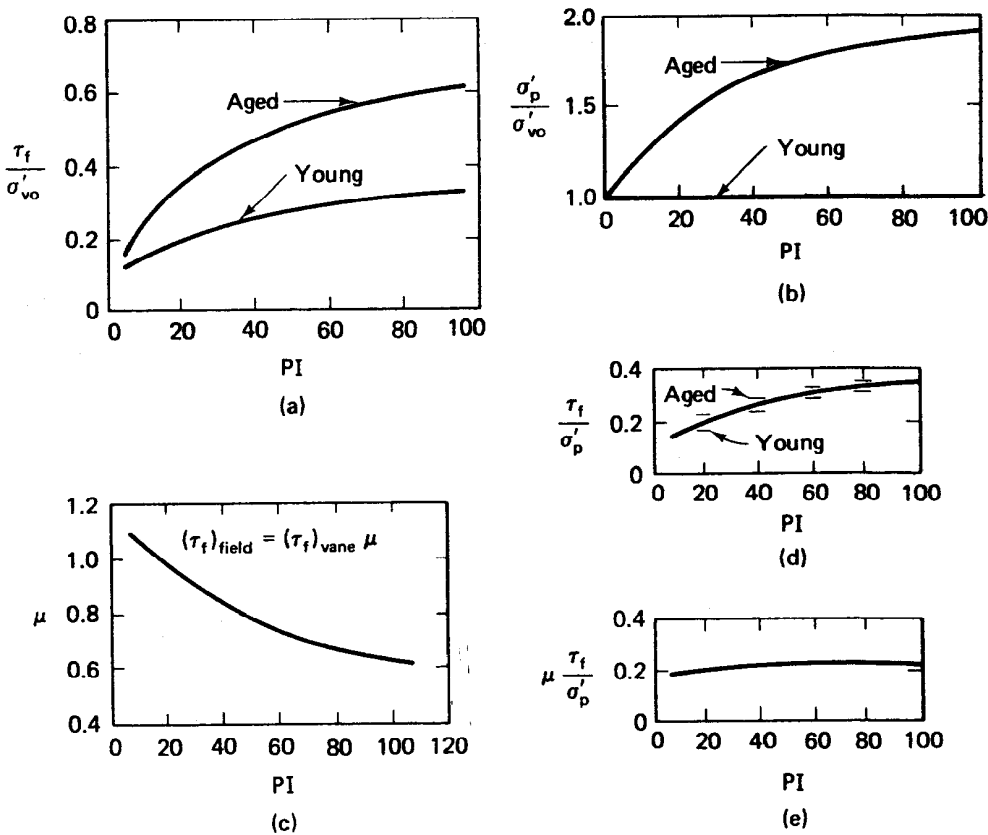


Fig. 11.60 (a)  $\tau_f/\sigma'_{vo}$  and (b)  $\sigma'_p/\sigma'_{vo}$  for normally consolidated late glacial clays (after Bjerrum, 1972); (c) Bjerrum's (1972) correction factor for the vane shear test; (d)  $\tau_f/\sigma'_p$  from (a) and (b); (e)  $\mu(\tau_f/\sigma'_p)$  (after Mesri, 1975).

Still the possibility that in situ  $\tau_f/\sigma'_p$  may well exist within a rather narrow range for soft sedimentary clays has tremendous practical implications (Ladd, et al., 1977).

In Chapter 8 we briefly mentioned that settlement analyses, to be complete, must also consider the *immediate* or *distortion settlement* of the structure. The procedures for calculating immediate settlement usually involve elastic theory, and one of the biggest problems is to determine or accurately estimate the elastic modulus for the soil. The obvious way would be to take the initial slope of the stress-strain curve, called the *tangent modulus*, as determined in the triaxial test. Or, because the stress-strain curves are so often curved, you could take the *secant modulus*, which is the slope of a straight line drawn from the origin to some predetermined stress level such as 50% of the maximum stress. These definitions are shown in Fig. 11.61. By the way, since the immediate settlement takes place before any consolidation can occur, the triaxial tests should be conducted *undrained*. Thus the modulus, however defined, is called the *undrained modulus*  $E_u$ .

However, as shown by many researchers, the undrained modulus is significantly affected by sample disturbance. Most of the time the disturbance tends to reduce the  $E_u$ , and thus you would tend to over-predict the immediate settlements in the field. Because of several other factors

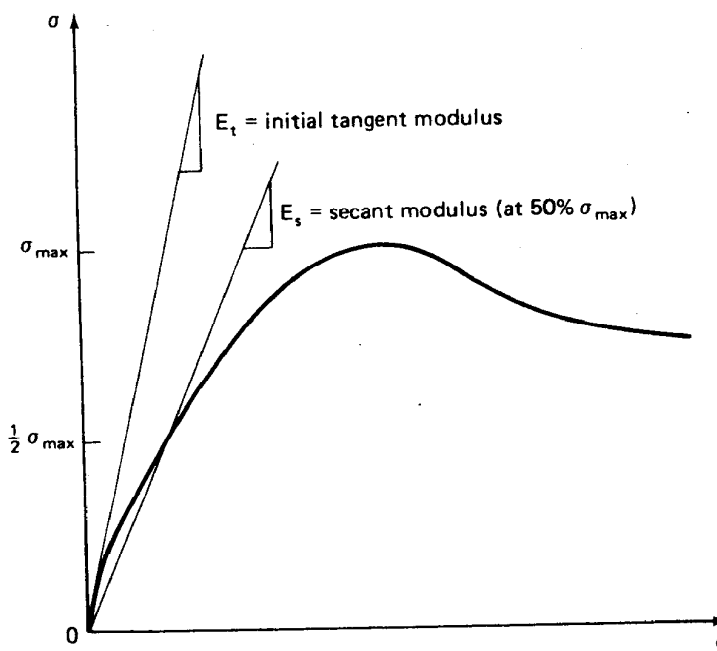


Fig. 11.61 Definitions of the initial tangent modulus and the secant modulus (usually defined at 50% of the maximum stress).

which affect the undrained modulus in laboratory tests (D'Appolonia, Poulos, and Ladd, 1971; Simons, 1974), field loading tests are sometimes used for important projects. Settlements are measured, and the modulus is backcalculated from elastic theory. Load tests have shown that stress level is one very important factor that strongly affects  $E_u$ . For example, large-scale loading tests carried out in Norway and Canada (Høeg, et al., 1969; Tavenas, et al., 1974) showed very little settlement since the load was applied rapidly until about one-half the failure load was reached. Then settlements started to accelerate as the load was increased. Thus the backcalculated  $E_u$  values were very dependent on the level of the shear stress applied by the surface load.

Because of all the problems with the laboratory determination of  $E_u$  and because large-scale field loading tests are expensive, it is common to assume that  $E_u$  is somehow related to the undrained shear strength. For example, Bjerrum (1972) said that the ratio  $E_u/\tau_f$  ranges from 500 to 1500, with  $\tau_f$  determined by the vane shear test. The lowest value is for highly plastic clays, where the applied load is large compared to the value of  $\sigma'_p - \sigma'_{vo}$  (that is, the added stress to the foundation is relatively large). The higher value is for clays of low plasticity, where the added load is relatively small. D'Appolonia, Poulos, and Ladd (1971) reported an average  $E_u/\tau_f$  of 1200 for load tests at 10 sites, but for the clays of higher plasticity the range was 80 to 400. Simons (1974) found published values ranged from 40 to 3000! These cases plus a few others we have taken from the literature are plotted versus PI in Fig. 11.62 for soft clays. Stiff fissured soils and glacial tills are not included. There is much scatter for  $PI < 50$  but not much data for  $PI > 50$ . It seems reasonable to simply use Bjerrum's recommendation ( $E_u/\tau_f$  of 500 to 1500) and the procedures developed by D'Appolonia, et al. (1971) for estimating immediate settlements of soft clays.

Another factor which strongly affects the undrained shear strength of clays is stress history. We mentioned this factor when we pointed out the difference in behavior between normally consolidated and overconsolidated clays (see, for example, Figs. 11.30 and 11.33). Let's first consider some data showing how the normalized undrained strength  $\tau_f/\sigma'_{vc}$  varies with the overconsolidation ratio (OCR). These data are shown for six clays in Fig. 11.63. If you take the ratio of the  $\tau_f/\sigma'_{vc}$  ratios, as shown in Fig. 11.64, all these soils fall into a rather narrow band, with only the varved clay somewhat lower. Ladd, et al. (1977) showed that this ratio of ratios is approximately equal to the OCR to the 0.8 power, or

$$\frac{(\tau_f/\sigma'_{vc})_{oc}}{(\tau_f/\sigma'_{vc})_{nc}} = (\text{OCR})^{0.8} \quad (11-10)$$

Relationships such as this can be useful for comparing strength data from different sites or even from the same site.

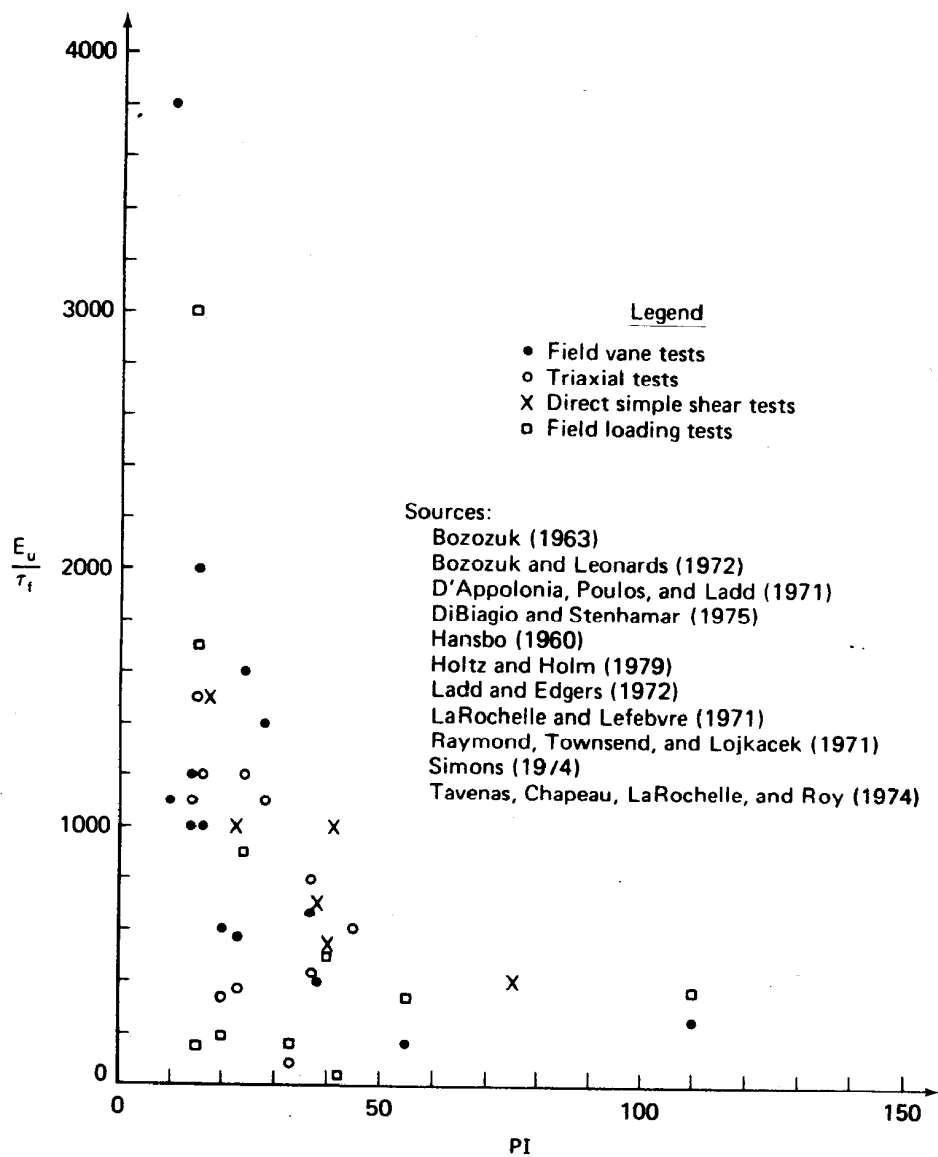


Fig. 11.62 The ratio  $E_u/\tau_f$ , versus plasticity index, as reported by several authors.

Ladd, et al. (1977) also showed how  $E_u/\tau_f$  varies with OCR, but the relationship is not so simple because, as we mentioned earlier,  $E_u/\tau_f$  depends so strongly on the level of shear stress. In general, however, it decreases with increasing OCR for a given stress level (Fig. 11.65).

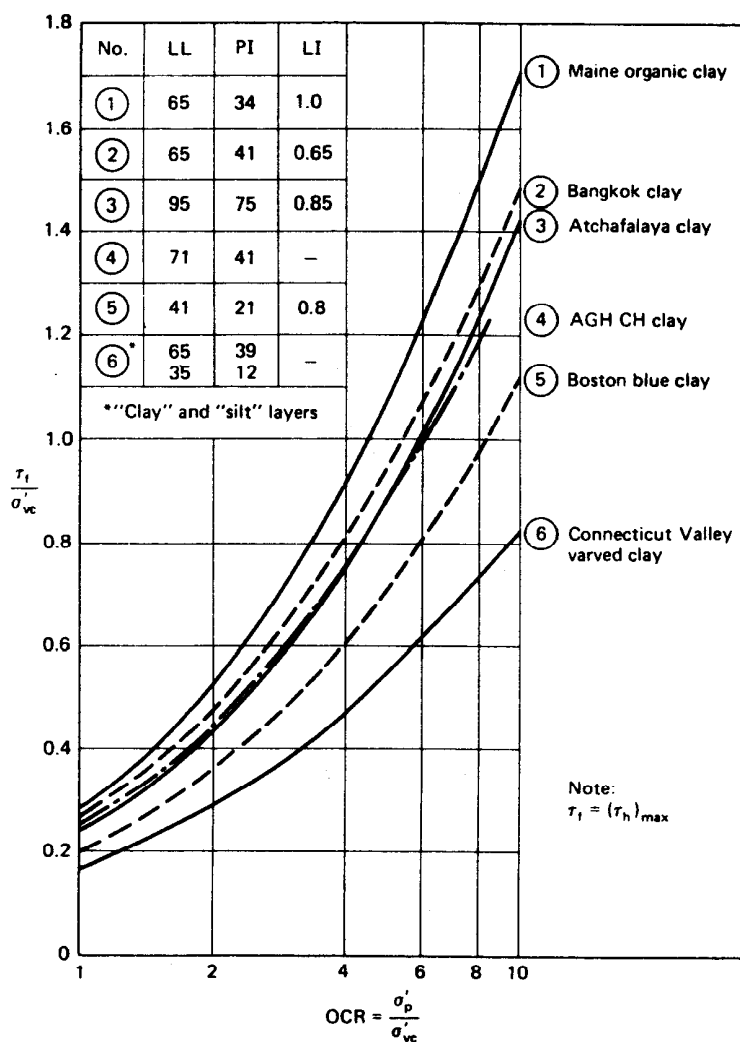


Fig. 11.63 Undrained strength ratio versus overconsolidation ratio from direct-shear tests on six clays (after Ladd and Edgers, 1972, and Ladd, et al., 1977).

#### 11.9.13 Special Problems of the Shear Strength of Cohesive Soils

All of the previous discussion has been limited to "well-behaved" cohesive soils. These are the relatively homogeneous marine and fresh water sedimentary clays of low to medium sensitivity which are normally consolidated or only slightly overconsolidated. As you might surmise, there are

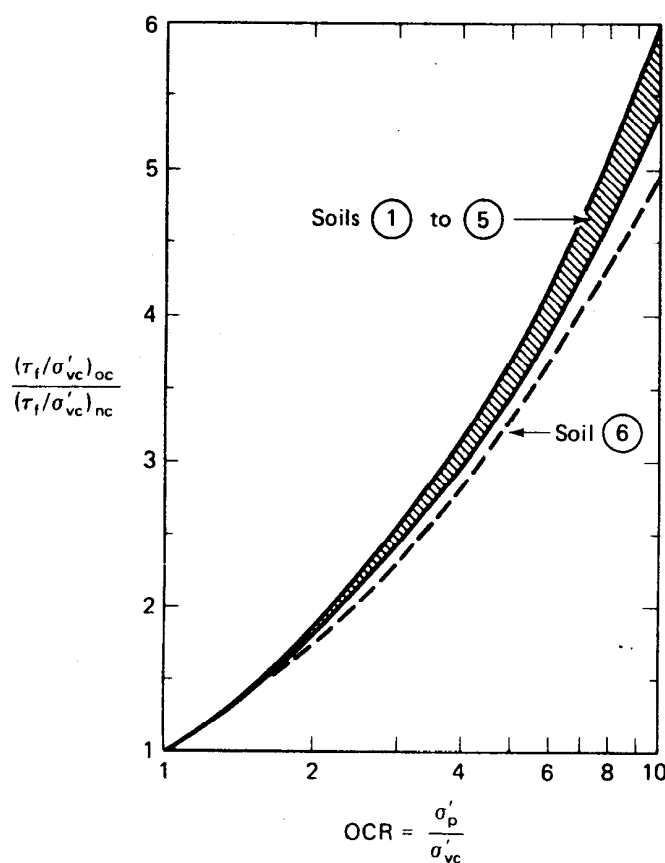


Fig. 11.64 Relative increase in undrained strength ratio with OCR from direct simple shear tests (soils 1 through 6 are identified in Fig. 11.63) (after Ladd, et al., 1977).

many cohesive soil deposits throughout the world that are not "well-behaved." In fact, such soils are probably the rule rather than the exception. In this list are included stiff fissured clays, peats and other organic soils, varved and layered soils, highly sensitive clays, and residual and tropical soils. Often these problem soils possess fissures and other defects that make them difficult to sample and test in the laboratory. They may be very heterogeneous and highly variable even within the confines of a small building site. In situ testing techniques described earlier are a good way to obtain some subsurface information as well as an idea of the statistical spread or variability of the material at the site. In addition to the usual geotechnical literature, two European conferences have been concerned with problem soils—the Geotechnical Conference (Oslo, 1967) and the Seventh European Conference on Soil Mechanics and Foundation Engineering held in Brighton, England, in 1979. The latter conference had as

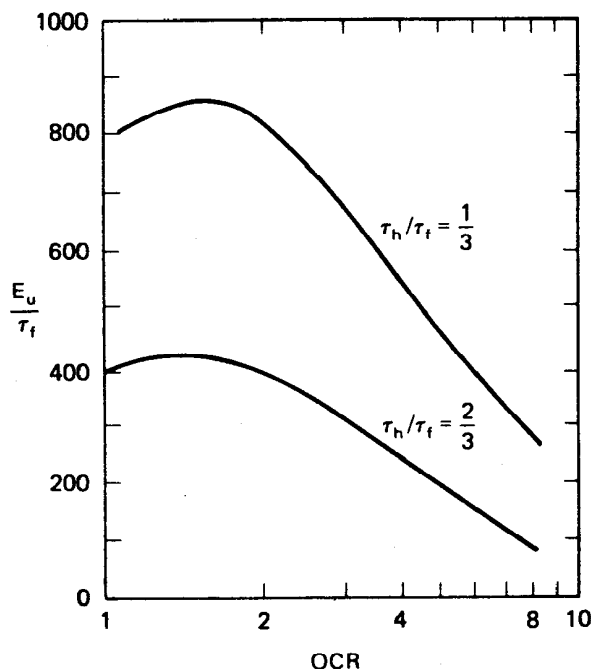
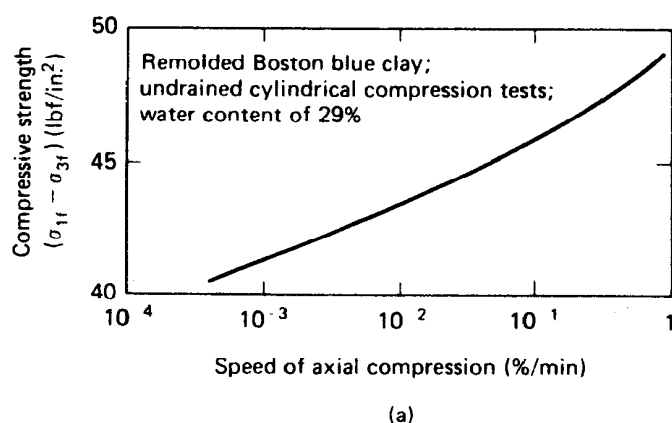


Fig. 11.65 Effect of OCR on  $E_u/\tau_f$ , from direct simple shear tests on Bangkok clay. (After Ladd and Edgers, 1972, and Ladd, et al., 1977).

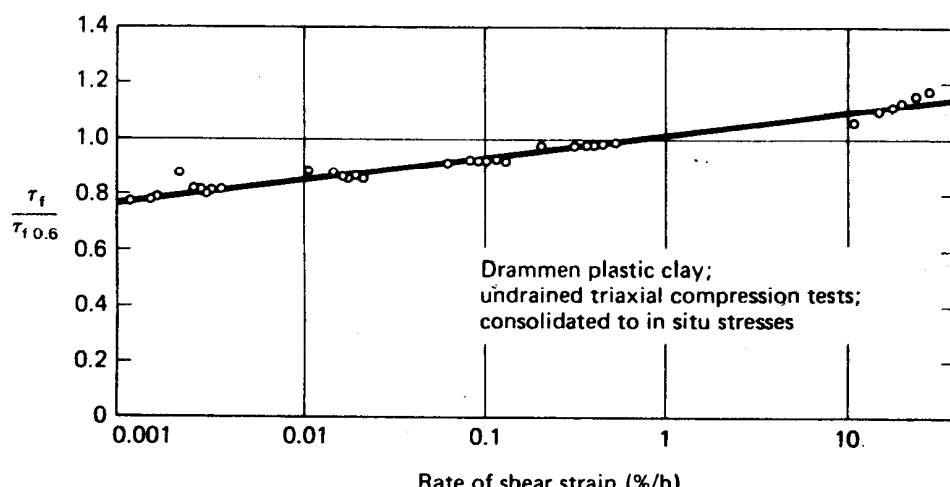
its main theme the determination of design parameters for a wide variety of soil conditions. Sometimes the Asian and African regional conferences have sessions on problems associated with residual and tropical soils.

There are some other factors that strongly affect the shear strength of clay soils that are not related to a specific geologic deposit or region of the world. We commonly assume that clays are isotropic—that is, their strength is the same in all directions. It has been known for many years that the undrained strength of many clays is directionally dependent (for example, Hvorslev, 1960). Recently, even  $c'$  and  $\phi'$  have been found to be *intrinsically anisotropic* (for example, Saada and Bianchini, 1965). There is also evidence of an *apparent anisotropy* due to the stress system, both during consolidation and during shear. Anisotropy is important because, for stability analyses, the variation of the shear strength with direction along a potential sliding surface significantly affects the calculated safety factor. This variation is shown by Bjerrum (1972), and it is one of the details included in the correction factor to the vane strength (Fig. 11.50).

Another factor included in Bjerrum's vane shear correction factor is the *strain rate effect*. Taylor (1948) showed that the undrained strength of a remolded Boston blue clay increased about 10% per log cycle of time increase in speed of shear (Fig. 11.66a). Bjerrum (1972) showed about the



(a)



(b)

Fig. 11.66 Effect of rate of loading on the undrained strength of (a) Boston blue clay (after Taylor, 1948); and (b) Drammen, Norway, plastic clay. The strength ratio in these latter tests is with respect to the strength at the NGI standard rate of 0.6% per h (after Bjerrum, 1972).

same increase in CU tests on a Norwegian plastic clay (Fig. 11.66b). Difference between the rate of loading in the laboratory and in the field can sharply affect the undrained shear strength. Ladd, et al. (1977) also discussed this point.

Finally, we mention briefly the problem of the *residual strength* of soils. When stiff overconsolidated clays have work-softening stress-strain curves like those shown in Fig. 11.24, the ultimate strength at large strains is called the *residual strength* of the soil (Skempton, 1964; 1977). A torsional or ring shear device such as shown in Fig. 10.15a is used to determine the residual strength.

## 11.10 PORE PRESSURE PARAMETERS

It should now be apparent that when saturated soils are loaded, pore water pressures will develop. In the case of one-dimensional loadings (Chapter 8), the induced pore water pressure is initially *equal* to the magnitude of the applied vertical stress. In three-dimensional or triaxial-type loadings, pore water pressures are also induced, but the actual magnitude will depend on the soil type and its stress history. Of course the rate of loading as well as the soil type determines whether we have drained or undrained loading.

It is often necessary in engineering practice to be able to estimate just how much excess pore water pressure develops in undrained loading due to a given set of stress changes. Note that these stress changes are in terms of *total stresses*, and they can be either hydrostatic (equal all-around) or non-hydrostatic (shear). Because we are interested in how the pore water pressure  $\Delta u$  responds to these changes in total stress,  $\Delta\sigma_1$ ,  $\Delta\sigma_2$ , and  $\Delta\sigma_3$ , it is convenient to express these changes in terms of *pore pressure coefficients* or *parameters*, which were first introduced in 1954 by Prof. A. W. Skempton of Imperial College in England.

In general, we can visualize the soil mass as a compressible soil skeleton with air and water in the voids. If we increase the principal stresses acting on a soil element, as in the triaxial test for example, then we will obtain a decrease in volume of the element and an increase in pore pressure. Refer again to Fig. 11.38, which represents the stress conditions in the UU test. Consider what happens when we apply the hydrostatic cell pressure  $\sigma_c$  and prevent any drainage from occurring. If the soil is 100% saturated, then we will obtain a change in pore pressure  $\Delta u (= \Delta u_c$  in Fig. 11.38), numerically equal to the change in cell pressure  $\Delta\sigma_c (= \sigma_c$  in Fig. 11.38) we just applied. In other words, the ratio  $\Delta u / \Delta\sigma_c$  equals 1. If the soil were less than 100% saturated, then the ratio of the induced  $\Delta u$  due to the increase in cell pressure  $\Delta\sigma_c$  would be less than 1. It can be shown (see Appendix B-3 for details) that this ratio for the ordinary triaxial test is

$$\frac{\Delta u}{\Delta\sigma_3} = \frac{1}{1 + \frac{nC_v}{C_{sk}}} = B \quad (11-11)$$

where  $n$  = porosity,

$C_v$  = compressibility of the voids, and

$C_{sk}$  = compressibility of the soil skeleton.

For convenience, Prof. Skempton called this ratio  $B$ . The pore pressure parameter  $B$  expresses the increase in pore pressure in undrained loading due to the increase in hydrostatic or cell pressure.

If the soil is completely saturated with water, then  $C_v = C_w$ , and for most soils  $C_w/C_{sk} \rightarrow 0$  since the compressibility of water  $C_w$  is so small compared with the compressibility of the soil skeleton. Therefore, for saturated soils,  $B = 1$ . If the soil is dry, then the ratio of  $C_v/C_{sk}$  approaches infinity since the compressibility of air is vastly greater than the soil structure; hence  $B = 0$  for dry soils. Partially saturated soils have values of  $B$  ranging between 0 and 1. Because in general both  $C_v$  and  $C_{sk}$  are nonlinear for soils, the relationship between  $B$  and the degree of saturation  $S$  is also nonlinear, as shown in Fig. 11.67. This relationship will depend on the soil type and stress level, and the exact relationship will have to be determined experimentally.

Equation 11-11 is very useful in the triaxial testing to determine if the test specimen is saturated. The pore pressure response to a small change in cell pressure is measured, and  $B$  is calculated. If  $B = 1$  or nearly so, then for soft clays the test specimen is saturated. However if the soil skeleton is relatively stiff, then it is possible to have  $B$  less than 1 and still have  $S = 100\%$  (see Table 11-8). This condition is possible because as  $C_{sk}$  gets smaller (a more rigid soil skeleton), the ratio  $C_w/C_{sk}$  becomes larger; thus  $B$  decreases. Wissa (1969) and Black and Lee (1973) suggest procedures to increase saturation and thereby increase the reliability of pore pressure measurements in undrained tests.

Now let's apply a stress difference or a shear stress to our soil sample (see Fig. 11.38 again for the UU test). In this case, a pore pressure  $\Delta u$  is induced in the specimen due to the change in stress difference  $\Delta\sigma = \Delta\sigma_1 - \Delta\sigma_3$ , or we can write, as Prof. Skempton did for triaxial compression

**TABLE 11-8** Theoretical  $B$ -Values for Different Soils at Complete or Nearly Complete Saturation\*

Soil Type	$S = 100\%$	$S = 99\%$
Soft, normally consolidated clays	0.9998	0.986
Compacted silts and clays; lightly over consolidated clays	0.9988	0.930
Overconsolidated stiff clays; sands at most densities	0.9877	0.51
Very dense sands; very stiff clays at high confining pressures	0.9130	0.10

\*After Black and Lee (1973).

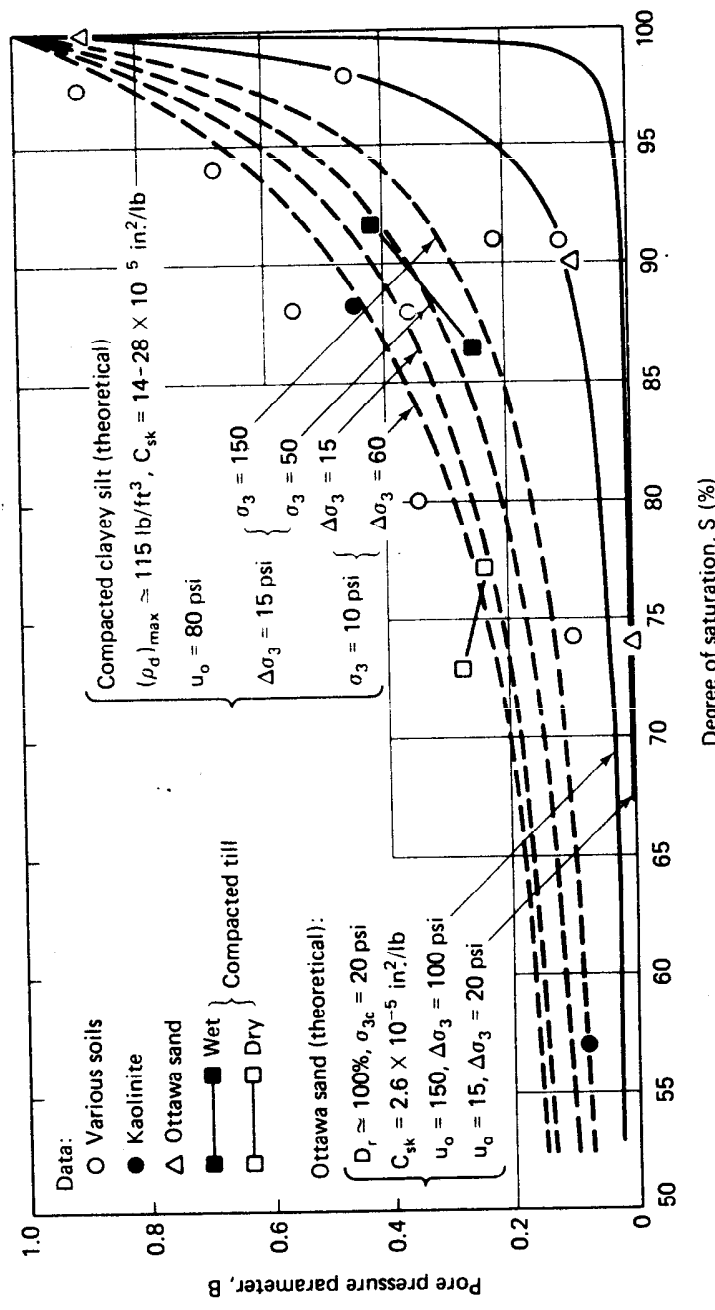


Fig. 11.67 The pore pressure parameter  $B$  as a function of the degree of saturation for several soils (after Black and Lee, 1973).

conditions ( $\Delta\sigma_2 = \Delta\sigma_3$ ),

$$\Delta u = B \frac{1}{3} (\Delta\sigma_1 - \Delta\sigma_3) \quad (11-12)$$

if the soil skeleton is *elastic*. Since soils in general are not elastic materials, the coefficient for the principal stress difference term is not 1/3. So Skempton used instead the symbol  $A$  for this coefficient. Now we can combine Eqs. 11-11 and 11-12 to take into account the two components of pore pressure: (1) that due to change in average or mean stress and (2) that due to change in shear stress, or

$$\Delta u = B [\Delta\sigma_3 + A(\Delta\sigma_1 - \Delta\sigma_3)] \quad (11-13)$$

Equation 11-13 is the well-known Skempton equation for relating the induced pore pressure to the changes in *total* stress in undrained loading. If  $B = 1$  and  $S = 100\%$ , then we normally write Eq. 11-13 as

$$\Delta u = \Delta\sigma_3 + A(\Delta\sigma_1 - \Delta\sigma_3) \quad (11-14)$$

Sometimes it is convenient to write Eq. 11-14 as

$$\Delta u = B \Delta\sigma_3 + \bar{A}(\Delta\sigma_1 - \Delta\sigma_3) \quad (11-15)$$

where  $\bar{A} = BA$ .

Equations 11-13 through 11-15 are derived in detail in Appendix B-3. There we show that these equations are true for both triaxial compression ( $\Delta\sigma_2 = \Delta\sigma_3$ ) and triaxial extension ( $\Delta\sigma_2 = \Delta\sigma_1$ ) conditions, although the specific value of  $A$  is dependent on the stress path, as discussed in Sec. 11.12.

Like the parameter  $B$ , the parameter  $A$  also is not a constant; it must be determined for each soil and stress path. The parameter  $A$  is very dependent on the strain, the magnitude of  $\sigma_2$ , the overconsolidation ratio, anisotropy, and for natural clays tested in the laboratory, on sample disturbance. Table 11-9 relates the type of clay to different values of the  $A$  parameter at failure,  $A_f$ , in triaxial compression. Of course  $A$  can be calculated for the stress conditions at any strain up to failure, as well as at failure.

The Skempton pore pressure coefficients are most useful in engineering practice since they enable us to predict the induced pore pressure if we know or can estimate the change in the total stresses. In the field, the Skempton equations are used, for example, when we want to estimate the pore pressure response during undrained loadings that might be applied by

**TABLE 11-9** Values of  $A_f$  for Various Soil Types\*

Type of Clay	$A_f$
Highly sensitive clays	+ $\frac{3}{4}$ to + $1\frac{1}{2}$
Normally consolidated clays	+ $\frac{1}{2}$ to + 1
Compacted sandy clays	+ $\frac{1}{4}$ to + $\frac{3}{4}$
Lightly overconsolidated clays	0 to + $\frac{1}{2}$
Compacted clay-gravels	- $\frac{1}{4}$ to + $\frac{1}{4}$
Heavily overconsolidated clays	- $\frac{1}{2}$ to 0

\*After Skempton (1954).

a highway embankment constructed on a very soft clay foundation. Typically, the embankment is constructed more rapidly than the excess pore water pressure can dissipate, and thus we assume that undrained conditions apply. The increase in excess pore pressure can result in instability if the pore pressure gets too high. Consequently, it is important to be able to estimate just how high the pore pressures are likely to get and thereby obtain some idea of how close to failure the embankment might be. If it is too high, stage construction might be utilized; then field monitoring of the pore pressures would be advisable. Skempton's parameters have also been used for the design and construction control of compacted earthfill dams.

---

#### EXAMPLE 11.14

Given:

The CU test of Example 11.11.

Required:

$A_f$ .

Solution:

Use Eq. 11-13. Since pore pressures were measured, the specimen must have been saturated. Thus assume  $B = 1$ . So  $A$  at failure is

$$A_f = \frac{\Delta u - \Delta \sigma_3}{\Delta \sigma_1 - \Delta \sigma_3}$$

In an ordinary triaxial compression test,  $\Delta\sigma_3 = 0$  since the cell pressure is held constant throughout the test (see Fig. 11.29). From Example 11.11,  $\Delta\sigma_{1f} = (\sigma_1 - \sigma_3)_f = 100$  kPa and  $\Delta u_f = 88$  kPa. Therefore

$$A_f = \frac{88}{100} = 0.88$$

From Table 11-9 you can see that the clay was probably somewhat sensitive.

As shown by Law and Holtz (1978) and in Appendix B-3, where rotation of principal stresses occurs, it is better to define the pore pressure parameter  $A$  in terms of principal stress increments which are independent of the initial stress system. If this is done, then the equations for  $A$  for each of the common triaxial stress paths (discussed in Sec. 11.12) are

$$A_{ac} = \frac{\Delta u}{\Delta \sigma_v} \quad (11-16)$$

$$A_{le} = 1 - \frac{\Delta u}{\Delta \sigma_h} \quad (11-17)$$

$$A_{ae} = 1 - \frac{\Delta u}{\Delta \sigma_v} \quad (11-18)$$

$$A_{lc} = \frac{\Delta u}{\Delta \sigma_h} \quad (11-19)$$

It is also shown in Appendix B-3 that

$$A_{ac} = A_{le} \quad (11-20)$$

and

$$A_{ae} = A_{lc} \quad (11-21)$$

You will find these equations useful in Sec. 11.12 (and for the problems at the end of this chapter).

A more general pore pressure equation was proposed by Henkel (1960) to take into account the effect of the intermediate principal stress. It is

$$\Delta u = B(\Delta \sigma_{oct} + \alpha \Delta \tau_{oct}) \quad (11-22)$$

where

$$\sigma_{\text{oct}} = \frac{1}{3}(\sigma_1 + \sigma_2 + \sigma_3) \quad (11-23)$$

$$\tau_{\text{oct}} = \frac{1}{3}\sqrt{(\sigma_1 - \sigma_2)^2 + (\sigma_2 - \sigma_3)^2 + (\sigma_3 - \sigma_1)^2} \quad (11-24)$$

and  $a$  is the *Henkel pore pressure parameter*. Sometimes the Henkel parameter is denoted by the symbol  $\alpha$ , and sometimes  $a = 3\alpha$ . Equation 11-22 is derived in Appendix B-3. Also in B-3, the equations for getting the equivalent Skempton  $A$  from Henkel's  $a$  parameter for triaxial compression and extension conditions are developed. These relationships are for triaxial compression (AC and LE) conditions

$$A = \frac{1}{3} + a \frac{\sqrt{2}}{3} \quad (11-25)$$

For triaxial extension (AE and LC) conditions

$$A = \frac{2}{3} + a \frac{\sqrt{2}}{3} \quad (11-26)$$

These equations mean, of course, that  $a = 0$  for elastic materials (since  $A = \frac{1}{3}$  in triaxial compression and  $A = \frac{2}{3}$  in triaxial extension).

If you have some idea of what the intermediate principal stress is in the field, then you probably should use Eqs. 11-22 through 11-24 to estimate the in situ pore pressures. It is not easy to predict the field pore pressures from laboratory test results, primarily because the pore pressure parameters are very sensitive to sample disturbance. Höeg, et al. (1969), D'Appolonia, et al. (1971), and Leroueil, et al. (1978a and b) provide methods for estimating pore pressures under embankments on soft clays.

## 11.11 THE COEFFICIENT OF EARTH PRESSURE AT REST FOR CLAYS

As is true for sands, a knowledge of the coefficient of earth pressure at rest,  $K_o$ , for a clay deposit is often very important for the design of earth-retaining structures, excavations, and some foundations. In Sec. 11.7, we indicated some typical values of  $K_o$  for sands. We said that  $K_o$  was empirically related to  $\phi'$  (Eq. 11-6 and Fig. 11.14), and we also mentioned that the coefficient for overconsolidated sand deposits is greater than for normally consolidated sands (Eq. 11-7).

Correlations between  $K_o$  and  $\phi'$  have been made for clays by Brooker and Ireland (1965) and others. Their data for normally consolidated clays

Remolded	Undisturbed	Reference
○		Brooker and Ireland (1965)
□		R. Ladd (1965)
◎	●	Bishop (1958)
	◆	Simons (1958)
	▲	Campanella and Vaid (1972)
◎		Compiled by Wroth (1972)
*		Abdelhamid and Krizek (1976)

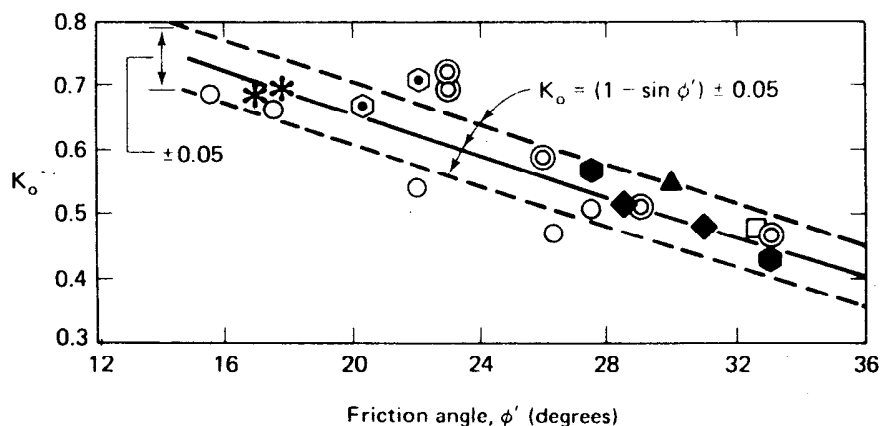


Fig. 11.68  $K_o$  versus  $\phi'$  for normally consolidated clays (after Ladd, et al., 1977).

are shown in Fig. 11.68. Brooker and Ireland (1965) also found a tendency for the normally consolidated  $K_o$  to increase with plasticity index. Massarsch (1979) has collected the results from 12 investigations, including the compilation by Ladd, et al. (1977), and they are shown in Fig. 11.69. The intercept of the best-fit line of Fig. 11.69 is very close to the average of  $K_o$  for sands shown in Fig. 11.14.

The effect of increasing the overburden stress and subsequent unloading on  $\sigma'_h$  and  $K_o$  is shown in Figs. 11.70a and b, respectively. During sedimentation, the effective horizontal stress  $\sigma'_h$  increases in proportion to the increase in effective vertical stress, so  $K_o$  is constant. If unloading occurs because of erosion, for example, then there is a hysteresis effect, and the value of  $K_o$  increases. Depending on how much unloading actually takes place, it is possible for the lateral stresses to approach a state of

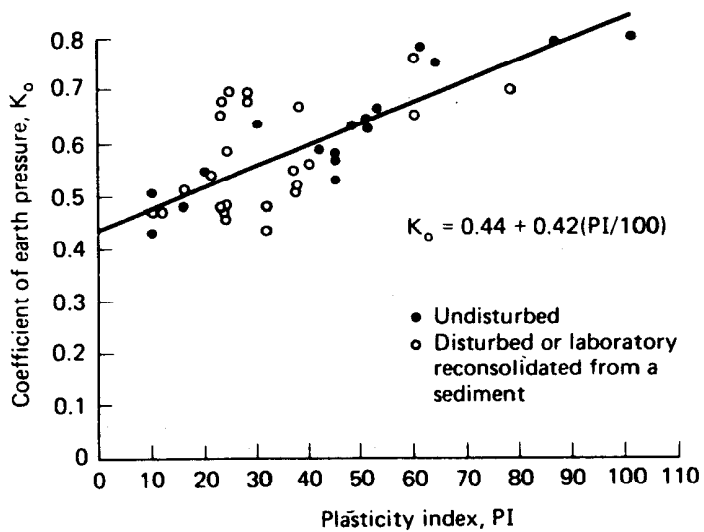


Fig. 11.69 Correlation between  $K_o$  from laboratory tests and plasticity index PI (after Massarsch, 1979).

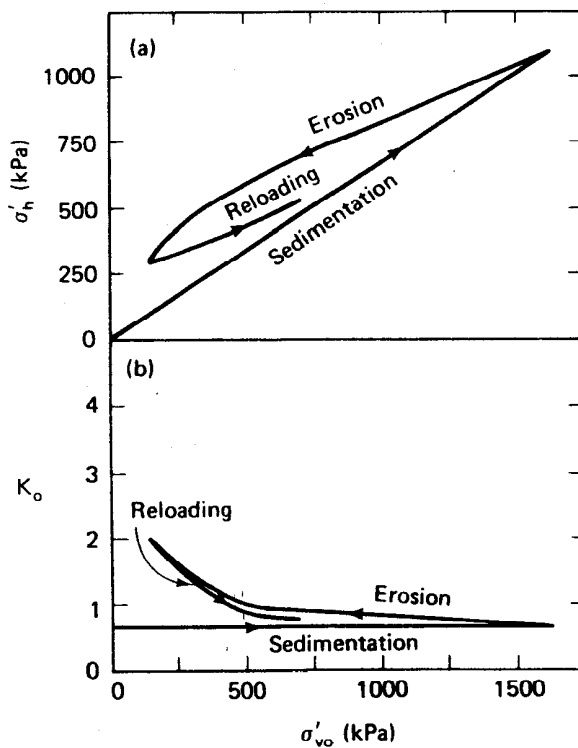


Fig. 11.70 Relationships showing the effect of a changing overburden stress during sedimentation, erosion, and reloading on (a) horizontal stress  $\sigma'_h$  and (b) coefficient of earth pressure at rest,  $K_o$  (after Morgenstern and Einstein, 1970).

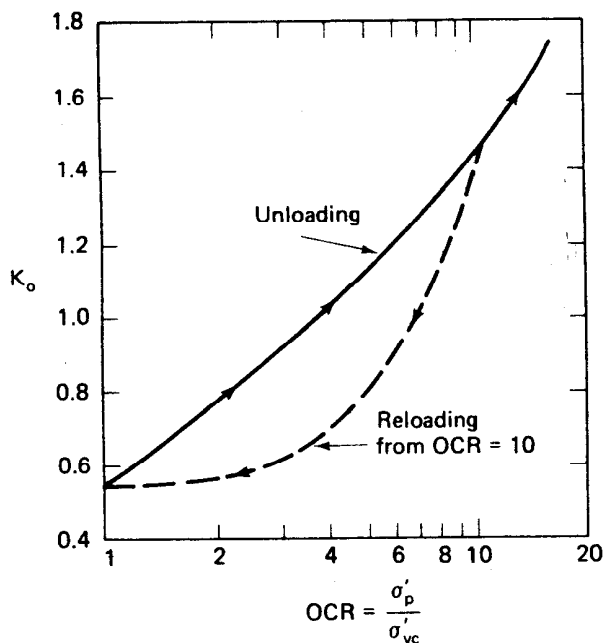


Fig. 11.71 Effect of overconsolidation on  $K_o$  of a sensitive clay during unloading and reloading. The data by Campanella and Vaid (1972) was replotted by Ladd, et al. (1977).

failure;\* that is, the ratio  $\sigma'_h/\sigma'_{vo}$  could be 3.0 or 3.5, which corresponds to  $\phi' = 30^\circ$  or  $35^\circ$  (Eq. 10-14). If there is subsequent reloading, then the  $K_o$  tends to decrease, as shown in Fig. 11.70b.

The effect of overconsolidation on the  $K_o$  of a sensitive clay is shown in Fig. 11.71. Again, there is some hysteresis when the clay is rebounded from a high OCR. There is limited evidence that the relationship between  $K_o$  and OCR depends to some extent on the plasticity of the clay (Fig. 11.72). Ladd, et al. (1977) also determined the exponent  $h$  in Eq. 11-7 for several clays during unloading and recompression. For clays with a PI of about 20, a value of  $h = 0.4$  is reasonable. Then  $h$  decreases slightly as PI increases, with the lowest value of  $h = 0.32$  at PI = 80. These values of  $h$  are somewhat lower than those for sands (Sec. 11.7). Keep in mind too that all these data are for laboratory consolidated samples. Field behavior is much more erratic, as shown by Massarsch, et al. (1975, Fig. 18). These authors as well as Tavenas, et al. (1975) and Wroth (1975) describe techniques for estimating the  $K_o$  in situ in deposits of soft clays. Wroth (1975) also discusses the effects of erosion and a fluctuating ground water

\*In terms of lateral earth pressures, this is called a *passive state of failure*, and the stress ratio  $K_p$  is called the *coefficient of passive earth pressure*.

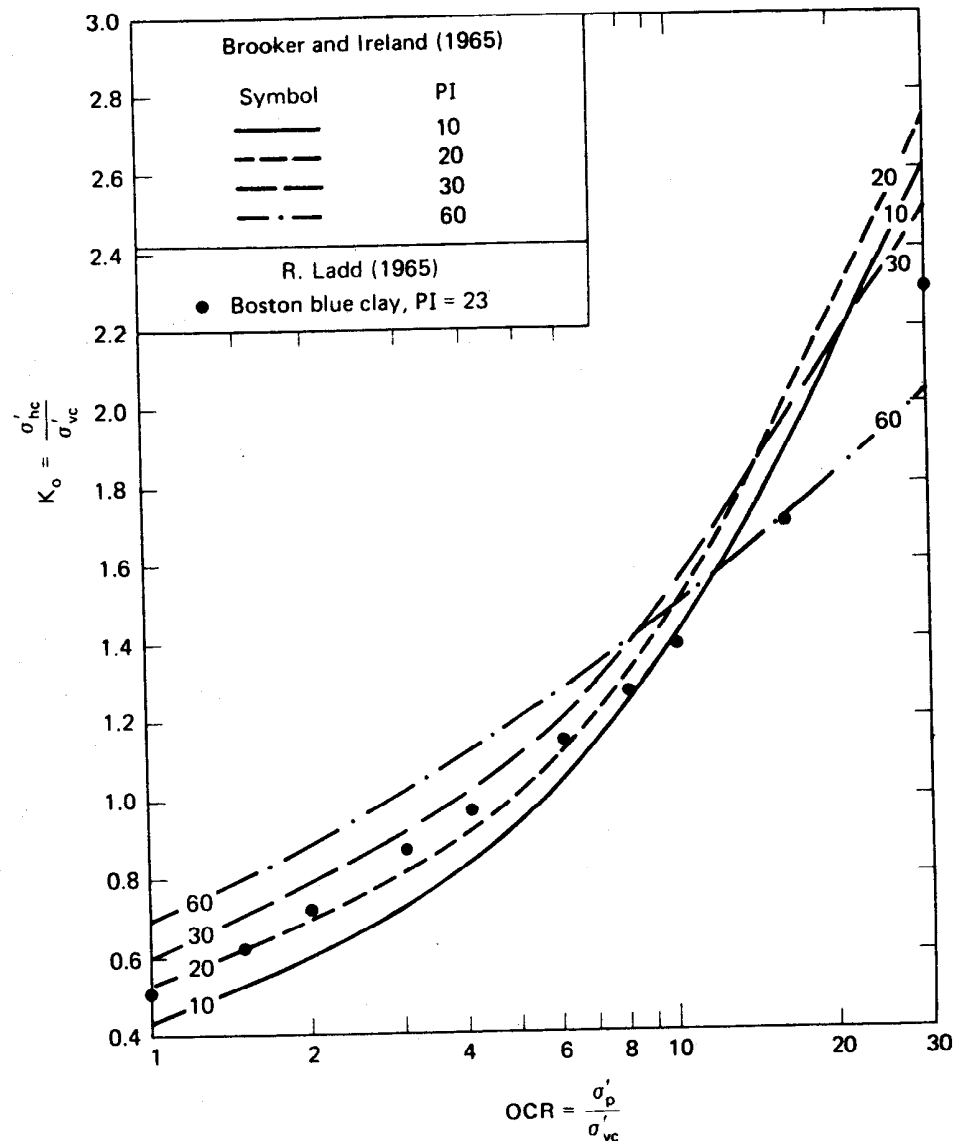


Fig. 11.72  $K_o$  versus OCR for soils of different plasticities.  
The data by Brooker and Ireland (1965, Fig. 11) was re-plotted by Ladd (1971a).

table on the variation of  $K_o$  with depth. Generally, the upper few metres of a soft clay deposit are overconsolidated (the *dry crust*) and  $K_o$  can be quite high. Then it will decrease with depth as the OCR decreases, until it is equal to the normally consolidated value when  $\text{OCR} = 1$ .

### 11.12 STRESS PATHS DURING UNDRAINED LOADING—NORMALLY CONSOLIDATED CLAYS

We show examples of stress paths for undrained loading of normally consolidated clays in Figs. 10.24, 10.26, 11.34a, and 11.43. Undrained stress paths for overconsolidated clays are shown in Figs. 10.25 and 11.34b. From our comments concerning those figures you should now understand why these stress paths have the shapes they do have. The stress paths we showed for undrained shear were for the most common type of triaxial test used in engineering practice, the axial compression (AC) test. Most of the time, the initial consolidation stresses are *hydrostatic* ( $K_o = 1$ ) because laboratory procedures are simpler. However, a better model for in situ stress conditions would be *non-hydrostatic* consolidation; that is, the axial stress would be different than the cell pressure ( $K_o \neq 1$ ). As we mentioned in Sec. 10.6, there are stress paths other than axial compression that model real engineering design situations. Some of these are shown in Fig. 11.73, along with their laboratory model. Axial compression (AC) models foundation loading such as from an embankment or footing. Lateral extension (LE) models the active earth pressure conditions behind retaining walls. Axial extension (AE) models unloading situations like excavations, and lateral compression (LC) models passive earth pressure conditions such as might occur around an earth anchor.

If you think about it, the ordinary triaxial test is not the best model for the design conditions illustrated in Fig. 11.73. It would be all right for cases (a) and (c) if the foundation or excavation were circular in shape (for example, an oil tank, missile silo, or reactor pit). The more usual case is where one dimension (perpendicular to the page in Fig. 11.73) is very long compared to the others. This is the case for *plane strain*. Examples are long embankments, strip footings, and long retaining walls. In these cases, strictly speaking, the shear strengths should be determined by using plane strain tests (Fig. 10.14b). The laboratory models of Fig. 11.73 can also apply to stress conditions in this test just as well as in the triaxial test. Since the plane strain test is more complicated in several respects than the triaxial test, it is not often used in engineering practice. Triaxial strengths are still commonly obtained for design problems that are obviously plane strain.

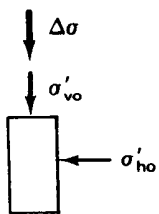
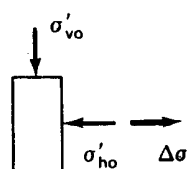
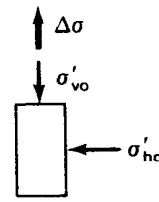
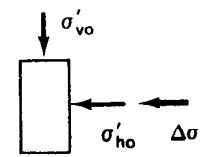
Field Situation	Laboratory Model
(a) Foundation loading	Axial compression (AC) 
(b) Active earth pressure	Lateral extension (LE) 
(c) Foundation unloading (excavation)	Axial extension (AE) 
(d) Passive earth pressure	Lateral compression (LC) 

Fig. 11.73 Some common field stability situations along with their laboratory model.

It is important that you know how to make the computations necessary to plot undrained stress paths; the procedures for doing so are illustrated by the following examples.

### EXAMPLE 11.15

**Given:**

The  $\sigma$ - $\epsilon$  and  $u$ - $\epsilon$  data of Fig. Ex. 11.15a were recorded when the normally consolidated clay of Ex. 11.11 was tested in axial compression.

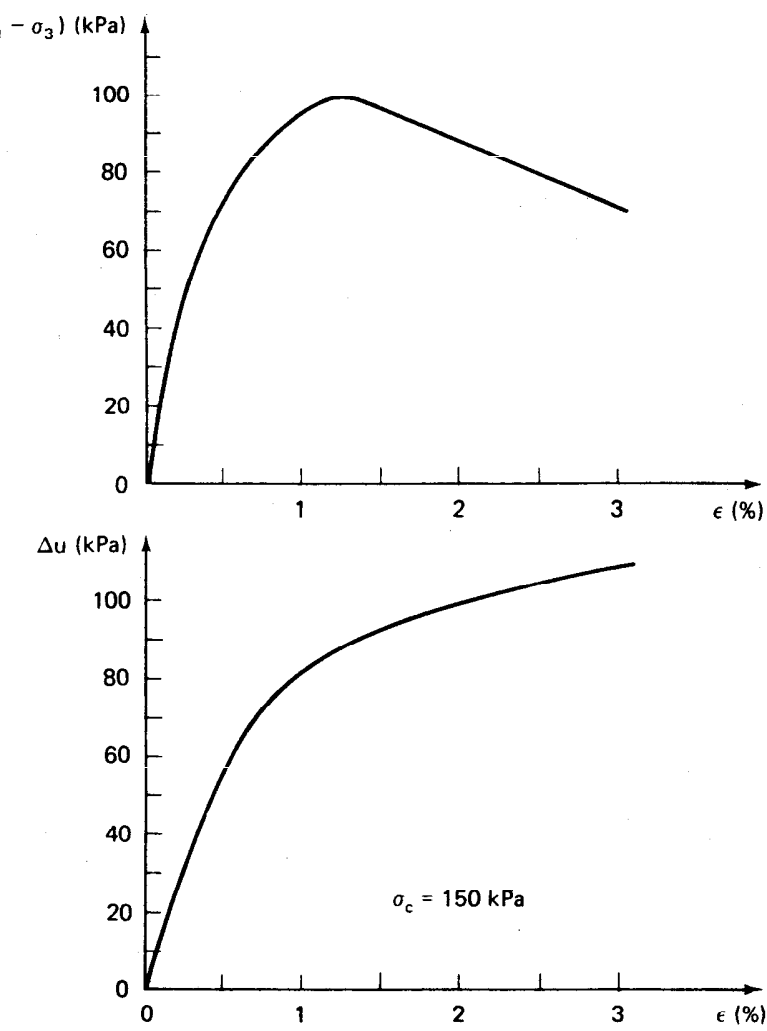


Fig. Ex. 11.15a

**Required:**

Draw the total and effective stress paths for this test. Determine the Mohr-Coulomb strength parameters.

**Solution:**

Using Eqs. 10-18 and 10-19, we have to determine  $p$ ,  $p'$ ,  $q$ , and  $q'$  for several strains in order to plot the stress paths. Usually five or six points are sufficient. Sometimes, to keep things in order, a table is helpful. Then just fill in the appropriate columns. It may also be helpful to know that

$$\sigma_1 + \sigma_3 = (\sigma_1 - \sigma_3) + 2\sigma_3 \quad (11-27)$$

and

$$\frac{\sigma_1 + \sigma_3}{2} = \frac{\sigma_1 - \sigma_3}{2} + \sigma_3 \quad (11-28)$$

Also, since  $\sigma' = \sigma - u$ ,  $p' = p - u$ . And finally,

$$\frac{\sigma'_1 + \sigma'_3}{2} = \frac{\sigma_1 - \sigma_3}{2} + \sigma'_3 \quad (11-29)$$

because  $(\sigma'_1 - \sigma'_3) = (\sigma_1 - \sigma_3)$ .

Now just choose the values of  $(\sigma_1 - \sigma_3)$  and  $\Delta u$  at several convenient strains, and fill in the table (Table Ex. 11.15) by using the above equations. Note that  $\sigma_3$  in Example 11.11 was 150 kPa.

TABLE EX. 11.15

$\epsilon$ (%)	$\sigma_1 - \sigma_3$ (kPa)	$\Delta u$ (kPa)	$\sigma'_3$ (kPa)	$\frac{q = \sigma_1 - \sigma_3}{2}$ (kPa)	$\frac{p = \sigma_1 + \sigma_3}{2}$ (kPa)	$\frac{p' = \sigma'_1 + \sigma'_3}{2}$ (kPa)
Failure	$\frac{1}{4}$	49	35	115	24.5	174.5
	$\frac{1}{2}$	73	57	93	36.5	186.5
	$\frac{3}{4}$	86	72	78	43.0	193.0
	1	94	79.5	68	47.0	197.0
	$1\frac{1}{4}$	100	88	62	50.0	200.0
	$1\frac{1}{2}$	96	92	58	48.0	198.0
	2	89	99	51	44.5	194.5
						95.5

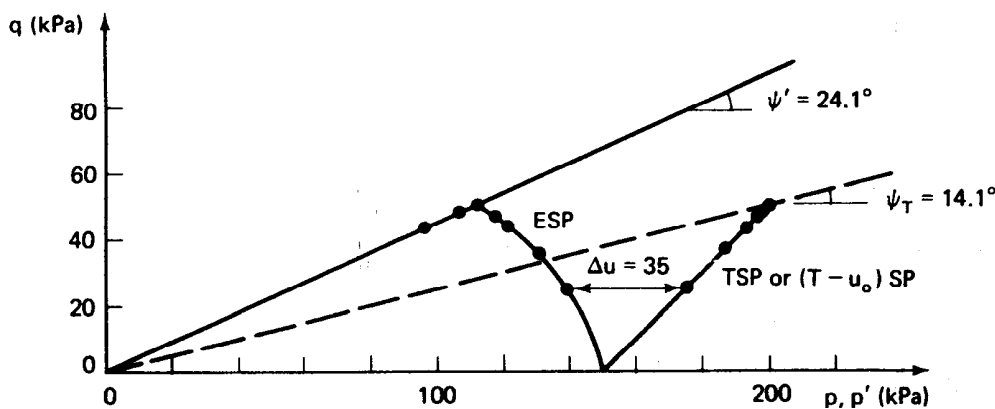


Fig. Ex. 11.15b

Total and effective stress paths are shown in Fig. Ex. 11.15b. The failure lines are also drawn, assuming  $a' = a = 0$ .

Since  $\psi' = 24.1^\circ$ ,  $\phi' = 26.6^\circ$

and

$\psi_T = 14.1^\circ$ ,  $\phi_T = 14.5^\circ$

Note that the problem could be solved graphically by plotting the TSP first, then scaling off the corresponding  $\Delta u$  values horizontally to the left of the TSP; one point done this way is shown in Fig. Ex. 11.15b.

### EXAMPLE 11.16

Given:

A long embankment shown in Fig. Ex. 11.16a is to be constructed rapidly on a deposit of soft organic silty clay in northern Sweden. The soil profile and properties are also shown in Fig. Ex. 11.16a. Assume  $K_o = 0.6$ . Also assume  $A$  before failure is about 0.35; at failure,  $A_f = 0.5$  (after Holtz and Holm, 1979).

Required:

Determine the TSP,  $(T - u_o)SP$ , and ESP for a typical element 5 m below the centerline of the embankment.

Solution:

First, calculate the initial stress conditions for the element. Use Eqs. 7-13,

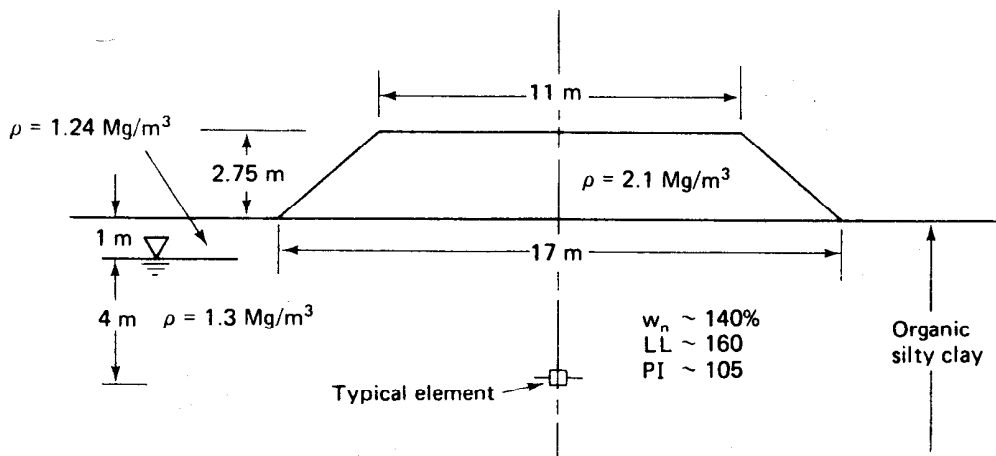


Fig. Ex. 11.16a

7-14, and 7-15.

$$\begin{aligned}
 \sigma_{v0} &= 1.24(9.81)(1) + 1.30(9.81)(4) = 63 \text{ kPa} \\
 u_o &= 1.0(9.81)(4) = 39 \text{ kPa} \\
 \sigma'_{v0} &= \sigma_{v0} - u_o = 24 \text{ kPa} \\
 \sigma'_{ho} &= 0.6\sigma'_{v0}(K_o = 0.6) = 14 \text{ kPa} \\
 \sigma_{ho} &= \sigma'_{ho} + u_o = 53 \text{ kPa}
 \end{aligned}$$

Second, calculate the  $\Delta\sigma$  due to the embankment.

$$\Delta\sigma \text{ at the surface} = 2.1(9.81)(2.75) = 57 \text{ kPa}$$

$\sigma_z$  at  $-5 \text{ m}$ ; use Fig. 8.23,

$$\begin{aligned}
 I &= 0.45 \times 2 = 0.9 \\
 \sigma_z &= 0.9 \times 57 = 51 \text{ kPa}
 \end{aligned}$$

This is  $\Delta\sigma_v$  on the typical element.

To determine the increase in horizontal stress  $\Delta\sigma_h$ , there are equations and some charts available for a limited number of geometries (see, for example, Poulos and Davis, 1974). In this case, assume the increase in horizontal stress is one-third of the increase in vertical stress.

$$\Delta\sigma_h = 0.33(51) = 17 \text{ kPa}$$

Next, use Eqs. 10-18 and 10-19 to determine  $q$ ,  $p$ , and  $p'$  for both initial and final conditions. Don't forget the conditions for the  $(T - u_o)$  SP. To get the final effective stresses, we need to estimate the induced pore pressures. Use the pore pressure parameter information given. Assume initially that the soil is not stressed to failure; so  $A = 0.35$ .  $B = 1$  below

the water table. Use Eq. 11-14.

$$\Delta u = \Delta \sigma_3 + A(\Delta \sigma_1 - \Delta \sigma_3) = 17 + 0.35(51 - 17) = 29 \text{ kPa}$$

If the embankment was overstressing the underlying soil, then the induced  $\Delta u$  would be 34 kPa (because  $A = 0.5$ ). If we used Henkel's pore pressure equations, Eqs. 11-22 and 11-25, we would predict  $\Delta u$  to be about 32 kPa. As we said in Sec. 11.10, predicting in situ pore pressures is not easy.

It is sometimes helpful when calculating stress paths to draw little elements with the appropriate total, total  $- u_o$ , neutral, and effective stresses indicated (similar to Fig. 11.29). This technique is shown in Fig. Ex. 11.16b both for initial conditions and after loading. Note that stresses on the elements for initial conditions are those we calculated at the beginning of this example. For final stresses, the vertical total stress increased by 51 kPa and the horizontal total stress increased by 17 kPa, as we determined previously from elastic theory. The induced pore pressures shown are those we found from the pore pressure equation. The calculations for  $p$ ,  $p'$ , and  $q$  for both initial and final conditions are shown below the elements.

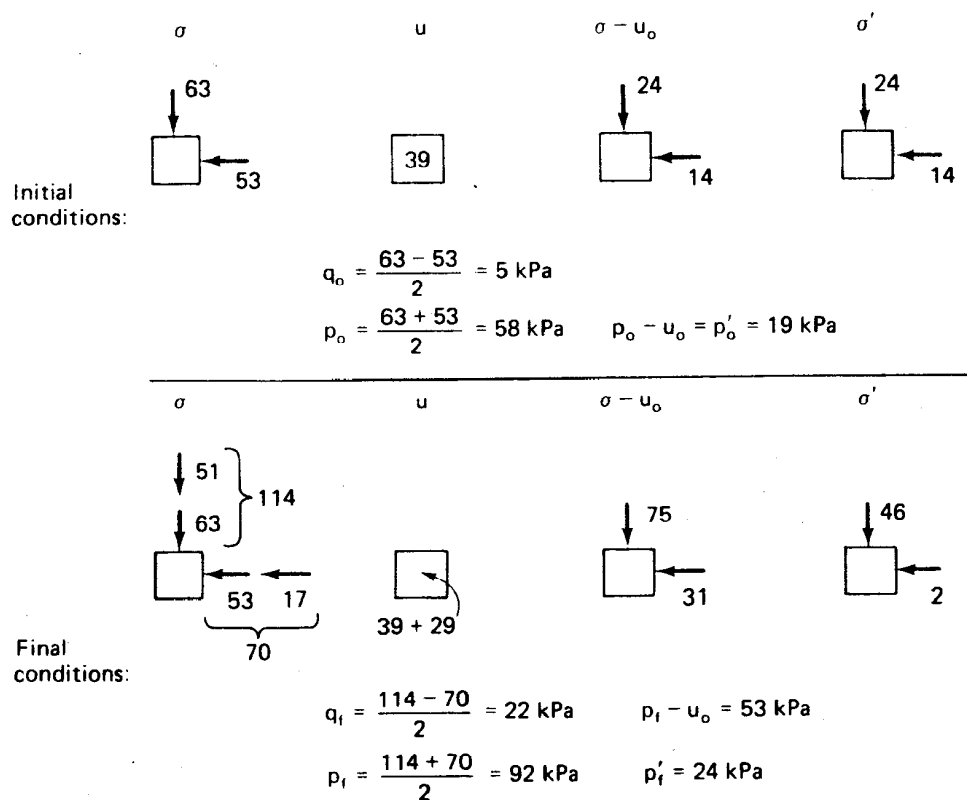


Fig. Ex. 11.16b

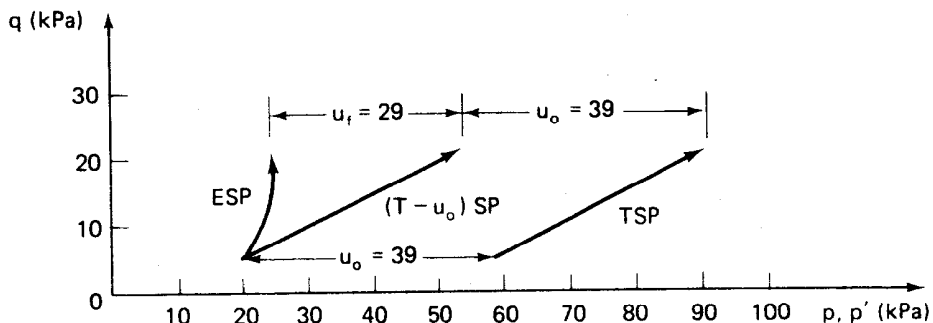


Fig. Ex. 11.16c

Finally, plot the stress paths on the  $p$ - $q$  diagram, as shown in Fig. Ex. 11.16c. Sketch the ESP so as to have a shape similar to those shown previously (for example, Figs. 11.34 and 11.43) for normally consolidated clays.

The next example is a little more complicated. First, we shall construct the stress paths and determine the strength parameters for an axial compression test; then we shall use the AC test and our knowledge of stress paths to determine the pore pressure response of a lateral extension test. We will see that the effective stress paths for both tests are identical, even though the total stress paths are very different.

### EXAMPLE 11.17

**Given:**

Two identical specimens (same  $w$ ,  $e$ , etc.) of a normally consolidated saturated clay were hydrostatically consolidated ( $K_o = 1$ ) and then sheared undrained. In test *A*, the axial compression (AC) test, the cell pressure was held constant while the axial stress was increased until failure. Specimen *B* was failed by lateral extension (LE) in which the vertical stress was held constant while the cell pressure was decreased until failure occurred. Stress-strain and pore pressure data for test *A* are shown in Table Ex. 11.17a.

**Required:**

- Compute and plot the stress-strain and pore pressure-strain curves for test *A*.
- Plot the TSP and ESP for both tests.

- c. Determine  $\phi'$  and  $\phi_T$  for both tests.
- d. Show that the stress-strain curve for the test A (AC) is identical to that for the test B (LE).
- e. Evaluate the pore pressure-strain data for test B from the LE stress paths.
- f. Compute the pore pressure parameter  $\bar{A}$  for both tests.

**TABLE EX. 11.17a Test A (AC test data)\***

$\epsilon$ (%)	$\Delta\sigma/\sigma'_c$	$\Delta u/\sigma'_c$
0	0	0
1	0.35	0.19
2	0.45	0.29
4	0.52	0.41
6	0.54	0.47
8	0.56	0.51
10	0.57	0.53
12	0.58	0.55

\*After Ladd (1964).

### Solution:

a. Plot  $\sigma$ - $\epsilon$  and  $\Delta u$ - $\epsilon$  curves for test A (AC), as shown in Fig. Ex. 11.17a. Note that the data in Table Ex. 11.17a is normalized with respect to the effective consolidation stress  $\sigma'_c$  in the test. We could assume a  $\sigma'_c$  (in whatever units the test was conducted), or we can work everything out in terms of the normalized stresses.

b. As for the previous example, it is helpful to sketch elements showing the total, neutral, and effective stresses for the initial consolidation conditions, during shear, and at failure, as is done in Fig. Ex. 11.17b. Use these stresses to compute the TSP for both tests and the ESP for the AC test. Since at this time we don't know anything about the pore pressures developed in the LE test, we cannot plot its ESP.

Calculations for  $p$ ,  $p'$ , and  $q$  for test A (AC):

Initial conditions:

$$p_o = p'_o = \frac{1+1}{2} = 1$$

$$q_o = \frac{1-1}{2} = 0$$

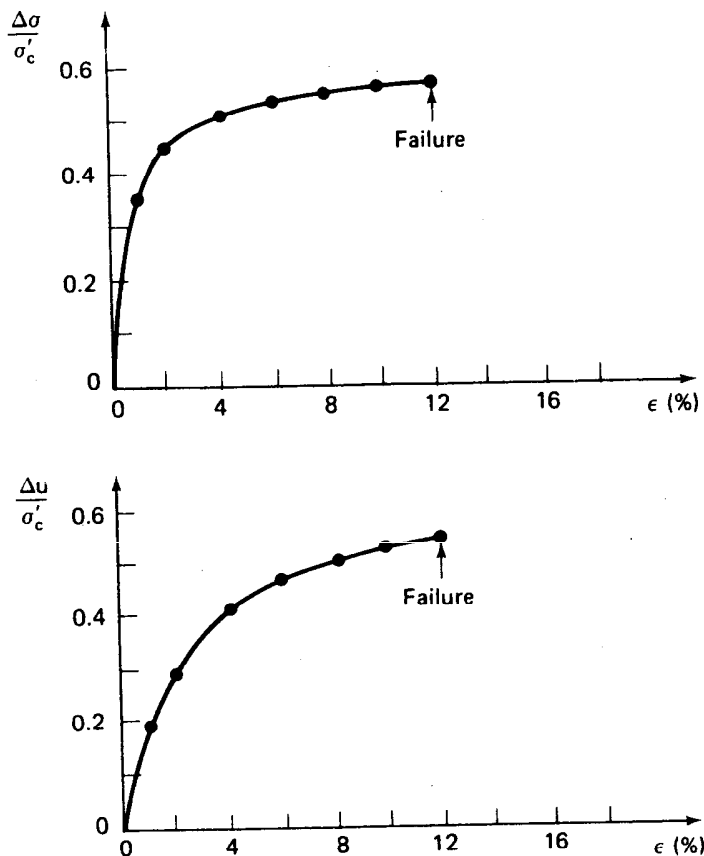


Fig. Ex. 11.17a Stress-strain and pore pressure-strain curves for the AC test.

At failure:

$$p_f = \frac{1.58 + 1}{2} = 1.29$$

$$p'_f = p_f - \Delta u = 0.74$$

$$\left( \text{Check: } p'_f = \frac{1.03 + 0.45}{2} = 0.74 \right)$$

$$q_f = \frac{1.58 - 1}{2} = 0.29$$

$$\left( \text{Check: } \frac{1.03 - 0.45}{2} = 0.29 \right)$$

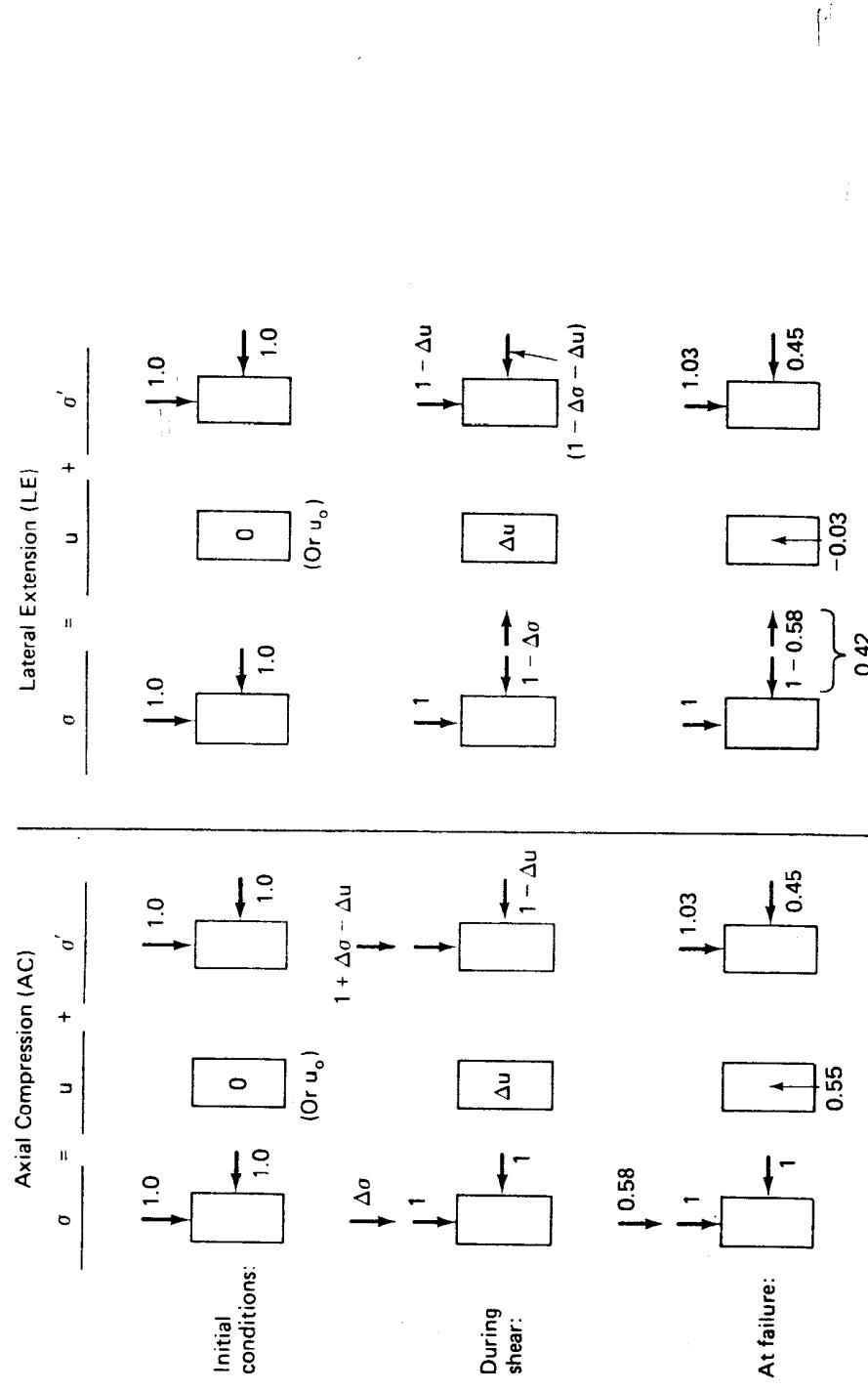


Fig. Ex. 11.17b Total, neutral, and effective stress conditions for the AC and LE tests.

For Test B (LE):

$$p_o = p'_o = \frac{1+1}{2} = 1$$

$$q_o = \frac{1-1}{2} = 0$$

$$p_f = \frac{1+0.42}{2} = 0.71$$

$$q_f = \frac{1-0.42}{2} = 0.29$$

Now plot the TSP's for both test A (AC) and test B (LE). We know that the TSP's will be straight lines inclined at  $45^\circ$  from the stress conditions in both tests since one of the principal stresses remains constant during the test. Therefore we need only calculate and plot the end points  $q_o$ ,  $p_o$ , and  $q_f$  on Fig. Ex. 11.17c, and connect these points with straight lines.

Intermediate points for both the TSP and ESP may be calculated from the stress-strain and pore pressure-strain information of Table 11.17a and Fig. Ex. 11.17a. This process is exactly like that shown in Example 11.15. Usually it is easier to do the problem graphically by simply plotting the intermediate  $q$  values on the TSP ( $q = \Delta\sigma/2$ ) at several conveniently spaced strains. This determines the intermediate  $p$  values. Then, scale off the  $\Delta u$  values horizontally to determine the intermediate  $p'$  values at these same strains. This process, shown in Fig. Ex. 11.15b and Fig. Ex. 11.17c, determines the corresponding ESP.

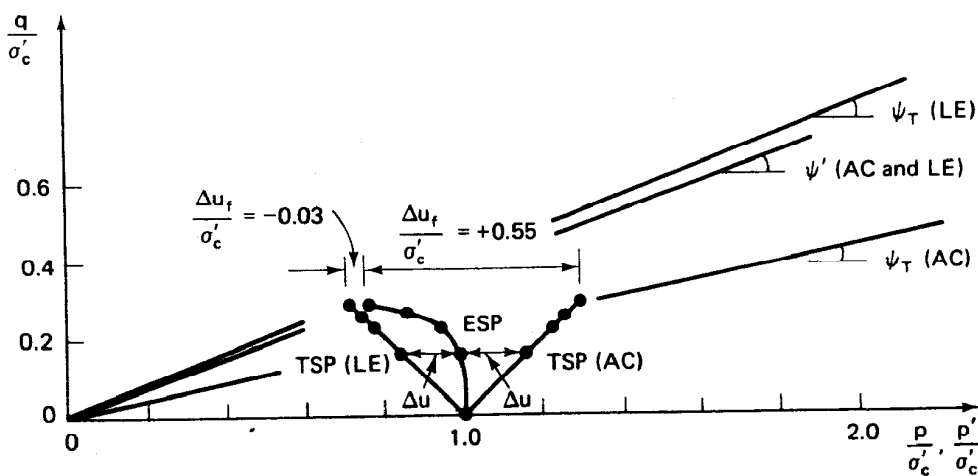


Fig. Ex. 11.17c Stress paths for the AC and LE tests.

Note that only one ESP is shown for *both* tests. This is so because the effective stress conditions in both tests are the same. Why? Note that during shear the stress difference  $\Delta\sigma$ , which is equal to  $(\sigma_1 - \sigma_3)$ , is the same for both tests. Looking at it another way:

For the AC test,

$$\Delta\sigma_{AC} = 1 + \Delta\sigma - 1 = \Delta\sigma$$

For the LE test,

$$\Delta\sigma_{LE} = 1 - 1 + \Delta\sigma = \Delta\sigma$$

Therefore at every strain (including at failure)  $\Delta\sigma_{AC} = \Delta\sigma_{LE}$ . Thus the stress-strain curves for both tests must be the *same*. So, if we plotted the LE stress-strain curve, it would look exactly like the AC curve shown in Fig. Ex. 11.17a. By the way, this is the answer to part d.

If the two specimens have exactly the same stress-strain curve and identical strengths, then the effective stress conditions in the specimens must be identical, both at failure and during loading. This means that the ESP's must also be the same.

Another way of looking at this is that in the LE test, the change in stress difference  $\Delta\sigma$  is produced by a change, a decrease, in cell or hydrostatic pressure. When the hydrostatic pressure changes, in an undrained test, only a change in pore pressure results, not a change in effective stresses. If there is no change in effective stresses, then the stress-strain and strength behavior must be the same (Hirschfeld, 1963). The only difference at failure between the tests must be in the amount of pore pressure  $\Delta u$  that develops. If this is true at failure, then it is true throughout the test. Therefore we can construct the pore pressure-strain curve [part e. of this example] for the test B (LE) from the stress path plots.

As with test A (AC) the amount of pore pressure developed in test B (LE) is simply the horizontal distance between the TSP and the ESP for that test. Note that for the LE test all values of  $\Delta u$  are *negative*. The

TABLE EX. 11.17b Test B (LE test data)

$\epsilon$ (%)	$\Delta\sigma/\sigma'_c$	$\Delta u/\sigma'_c$
0	0	0
1	0.35	- 0.16
2	0.45	- 0.16
4	0.52	- 0.11
6	0.54	- 0.07
8	0.56	- 0.05
10	0.57	- 0.04
12	0.58	- 0.03

constructed pore pressure-strain curve for the LE test is shown in Fig. Ex. 11.17d along with the stress-strain curve for both tests and the pore pressure-strain curve for the AC test. For easy comparison, numerical values of the pore pressure are listed in Table Ex. 11.17b. Fig. Ex. 11.17d and Table Ex. 11.17b are solutions to part e.

Now you can see where the effective stress values for the LE test in Fig. Ex. 11.17b came from. Another curious fact about the AC and LE test is that the numerical difference between the two pore pressure curves at a

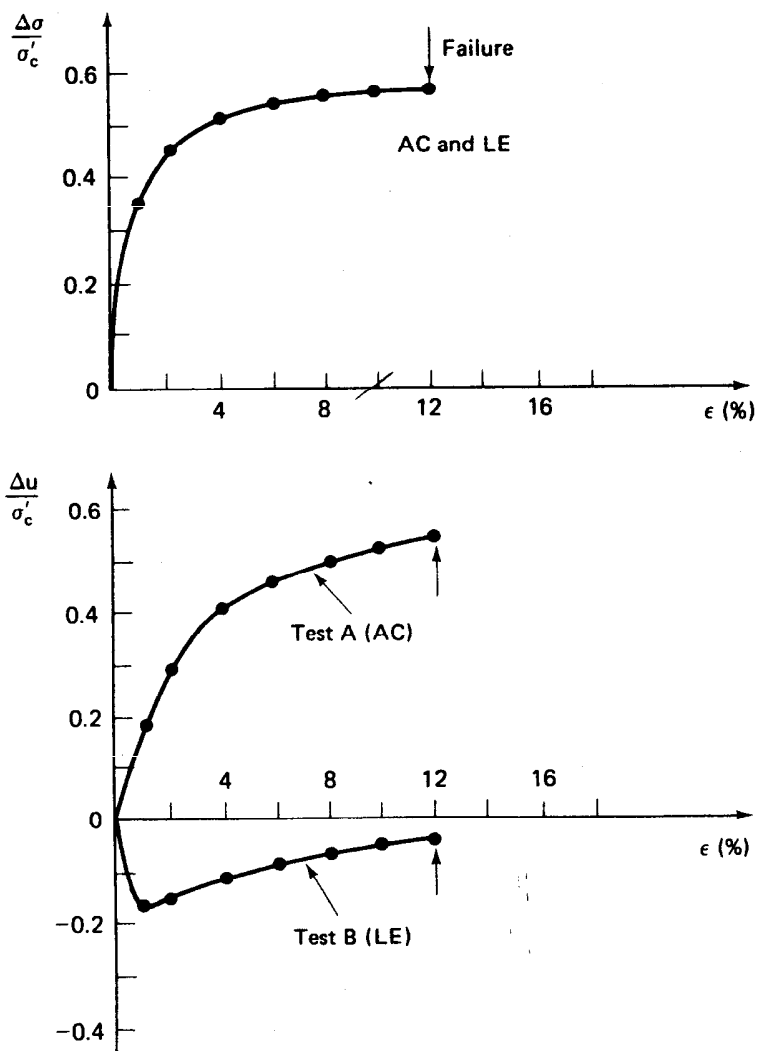


Fig. Ex. 11.17d Stress-strain and pore pressure-strain data for both tests.

given strain is exactly equal to the principal stress difference at that strain. You can check this statement by using the values of Tables Ex. 11.17a and b or scaling off  $\Delta\sigma$  values between the two  $\Delta u$  curves of Fig. Ex. 11.17d. Also the horizontal distance between the two TSP's in Fig. Ex. 11.17c is equal to  $\Delta\sigma$  at a given strain.

Now that we know the TSP's and ESP's for both tests, we can compute  $\phi'$  and  $\phi_T$  for the two tests [part c]. From Fig. Ex. 11.17c we can measure the angles  $\psi'$ ,  $\psi_{T(AC)}$ , and  $\psi_{T(LE)}$  with a protractor, or we can use Eq. 10-21. Since the clay is normally consolidated, we shall assume that  $c' \approx 0$  and this is why we drew the intercepts  $a$  and  $a'$  on the  $p-q$  diagram to be essentially zero. From Eqs. 10-24 and 10-25 we may readily compute  $\phi'$ ,  $\phi_{T(AC)}$ , and  $\phi_{T(LE)}$ . These values are shown in Table Ex. 11.17c.

**TABLE EX. 11.17c** Strength Parameters from Fig. Ex. 11.17c (in degrees)

Angle	Test A (AC)	Test B (LE)
$\psi_T$	12.5	22
$\phi_T$	12.8	23.8
$\psi'$	21	21
$\phi'$	22.6	22.6

f. Let us now compute the pore pressure parameter  $\bar{A}$  for both tests. By Eq. 11-15,

$$\bar{A}_f = \frac{\Delta u - \Delta\sigma_3}{\Delta\sigma_1 - \Delta\sigma_3}$$

To obtain the stress changes during the test, it is usually easier to refer to the elements of Fig. Ex. 11.17b, and select the changes in total stress from the initial conditions to the conditions at failure.

For the test A (AC),  $\Delta\sigma_3 = 0$  and  $\Delta\sigma_1 = \sigma_{1f} - \sigma_{1o} = 1.58 - 1.0 = 0.58$ ;  $\Delta u_f = 0.55$ . So,

$$\bar{A}_f = \frac{0.55 - 0}{0.58 - 0} = 0.95$$

For the test B (LE),  $\Delta\sigma_1 = 0$  and  $\Delta\sigma_3 = \sigma_{3f} - \sigma_{3o} = 0.42 - 1.0 = -0.58$ ;  $\Delta u_f = -0.03$ . So,

$$\bar{A}_f = \frac{-0.03 - (-0.58)}{0 - (-0.58)} = \frac{0.55}{0.58} = 0.95$$

If this is confusing, it might be easier to use Eq. 11-17 for the LE test,

$$\bar{A}_{le} = 1 - \frac{\Delta u}{\Delta\sigma_h} = 1 - \frac{\Delta u}{\Delta\sigma_3} = 1 - \frac{-0.03}{-0.58} = 0.95$$

(Of course we knew from Eq. 11-20 that  $\bar{A}_{le}$  should equal  $\bar{A}_{ac}$ .) The term

$\Delta\sigma_h$  is negative because it is decreased during the LE test (refer again to Fig. Ex. 11.17b).

What conclusions can we draw from this example? First, both the axial compression and lateral extension tests have identical stress-strain curves and their compressive strengths  $\Delta\sigma_f$  are the same. If the stress-strain curves are the same, then they have the same  $E$  modulus. They also have the same ESP. However they have markedly different TSP's and markedly different pore pressure responses, but  $A_f$  (and thus  $\bar{A}_f$ ) is the same for both tests. We can summarize these observations as follows:

- Same  $\Delta\sigma$  and  $\Delta\sigma_f$
- Same  $\sigma$ - $\epsilon$  curves and  $E$  modulus
- Same ESP
- Same  $\phi'$
- Same  $A_f$  (and  $\bar{A}_f$ )
- Different TSP
- Different  $\phi_T$
- Different  $\Delta u$

In Example 11.17 we showed the stress conditions and plotted the stress paths for the AC and LE tests, where you will note that the principal stresses at failure had the same orientation as they did at the beginning of the test. For the axial extension (AE) and lateral compression (LC) tests (see Figs. 10.22 and 11.73 for a review of these tests), the principal stresses *rotate* during shear, and the stress paths go *below* the horizontal axis. In this case,  $q$  becomes negative. If we went through a similar exercise as we did in Example 11.17, we would reach the same conclusions as for the AC and LE tests: they have the same strength, ESP,  $A_f$ , and  $\phi'$ , but different TSP and  $\Delta u$ . The stress conditions for the AE and LC tests are shown in Fig. 11.74; you might compare these stresses with those shown in Fig. Ex. 11.17b and see what is meant by the rotation of principal stresses. Figure 11.75 then shows typical test results from AE and LC tests. The stress paths for both tests are shown in Fig. 11.76.

The difference between the AC-LE and the AE-LC tests is really a function of the intermediate principal stress  $\sigma_2$ . Note that for the first two types of tests we assume that  $\sigma_2 = \sigma_3$ , and there is no rotation of principal stresses from the beginning of the test until failure. On the other hand, for the AE-LC tests  $\sigma_2 = \sigma_1$ , and a rotation of principal stresses occurs. This rotation would be even more dramatic if, for initial conditions, we had different vertical stresses than horizontal stresses: that is, if  $\sigma_{vo} \neq \sigma_{ho} = \sigma_{cell}$ . For this initial condition,  $\sigma_{vo} = \sigma_{lo}$  and  $\sigma_{ho} = \sigma_{3o} = \sigma_{cell}$ . For both the AE and LC tests, the horizontal stress at failure becomes the major principal stress, as shown in Fig. 11.74.

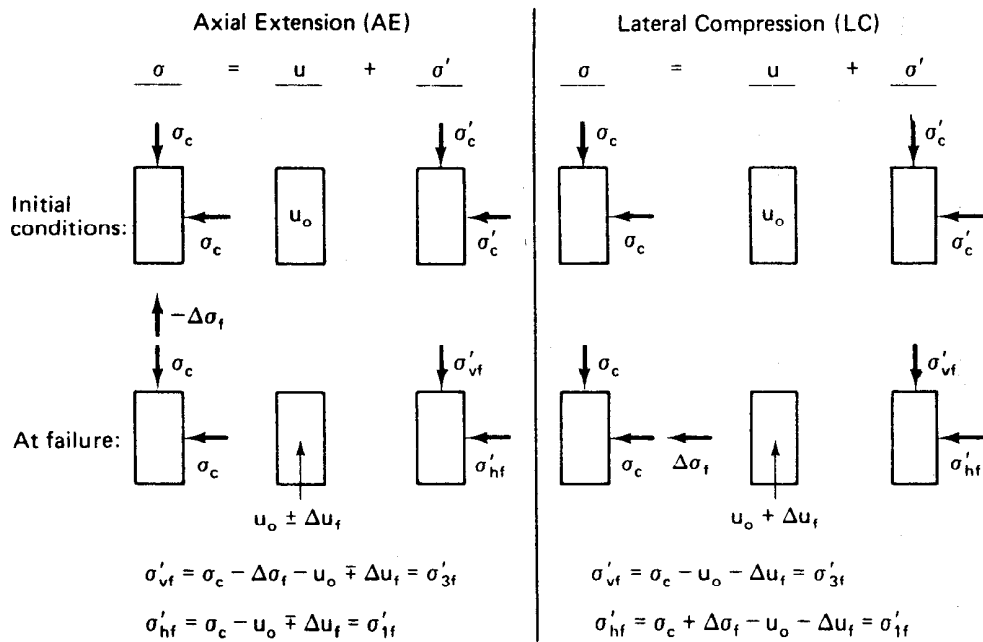


Fig. 11.74 Stress conditions for the axial extension (AE) and lateral compression (LC) tests. Note that the major principal stress is now horizontal for both these tests at failure.

Some actual test data on natural clays is shown in Figs. 11.77 and 11.78. These results verify the assertions made above that the ESP,  $\sigma-\epsilon$ , and  $A_f$  responses of AC and LE, and AE and LC tests are essentially the same for saturated soils. The effective stress and  $\sigma-\epsilon$  behavior is determined *only* by the sign and magnitude of the principal stress difference,  $\Delta\sigma = \sigma_v - \sigma_h$ , and is independent of the particular shape of the total stress path (Bishop and Wesley, 1975).

Note that the ESP for the AE and LC tests in Figs. 11.77 and 11.78 did not cross the AE-TSP as it did in Fig. 11.76. This means that the induced pore pressure in these tests did not go slightly negative, in contrast to the behavior of Fig. 11.76. The specific ESP characteristics for any given soil must be determined by laboratory tests.

The angle of inclination of the failure planes as determined according to the Mohr failure hypothesis (discussed in Sec. 10.4) is different for the AE and LC tests because of the rotation of principal stresses. We may determine this angle by using the pole method. This procedure is shown in Fig. 11.79 for the AC and AE tests; similar results would be found for the LE and LC tests. In summary, then, for:

For AC and LE, no rotation of  $\sigma_1$  and  $\sigma_3$ :  $\alpha_f = 45^\circ + \phi'/2$

For AE and LC, with rotation of  $\sigma_1$  and  $\sigma_3$ :  $\alpha_f = 45^\circ - \phi'/2$

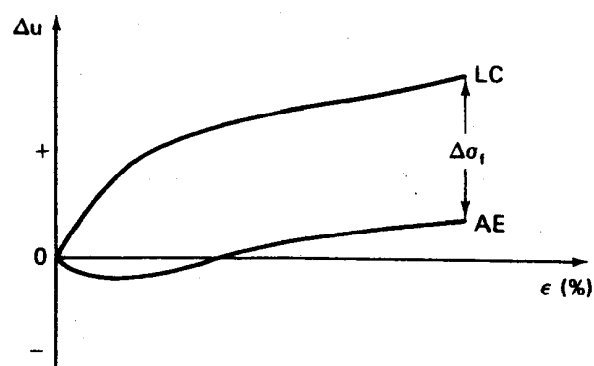
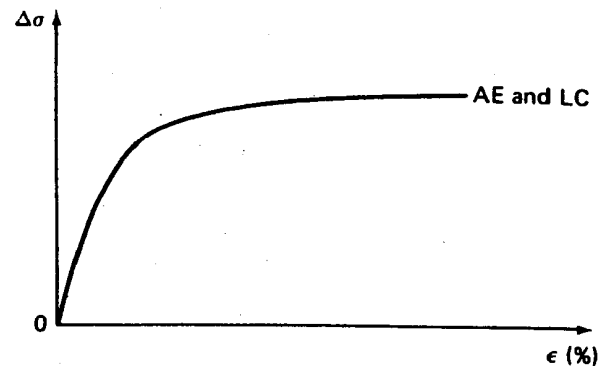


Fig. 11.75 Stress-strain and pore pressure-strain curves for AE and LC tests on a normally consolidated clay (after Hirschfeld, 1963).

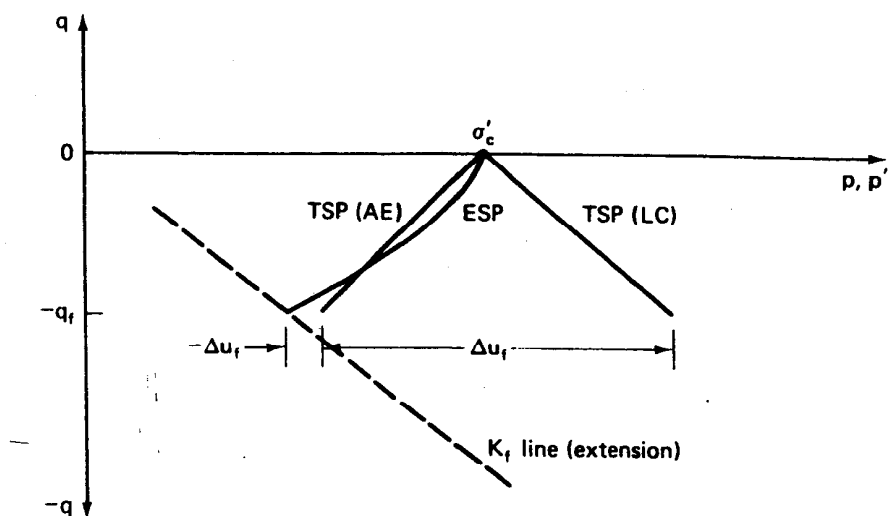


Fig. 11.76 Stress paths for the AE and LC tests—normally consolidated clay.

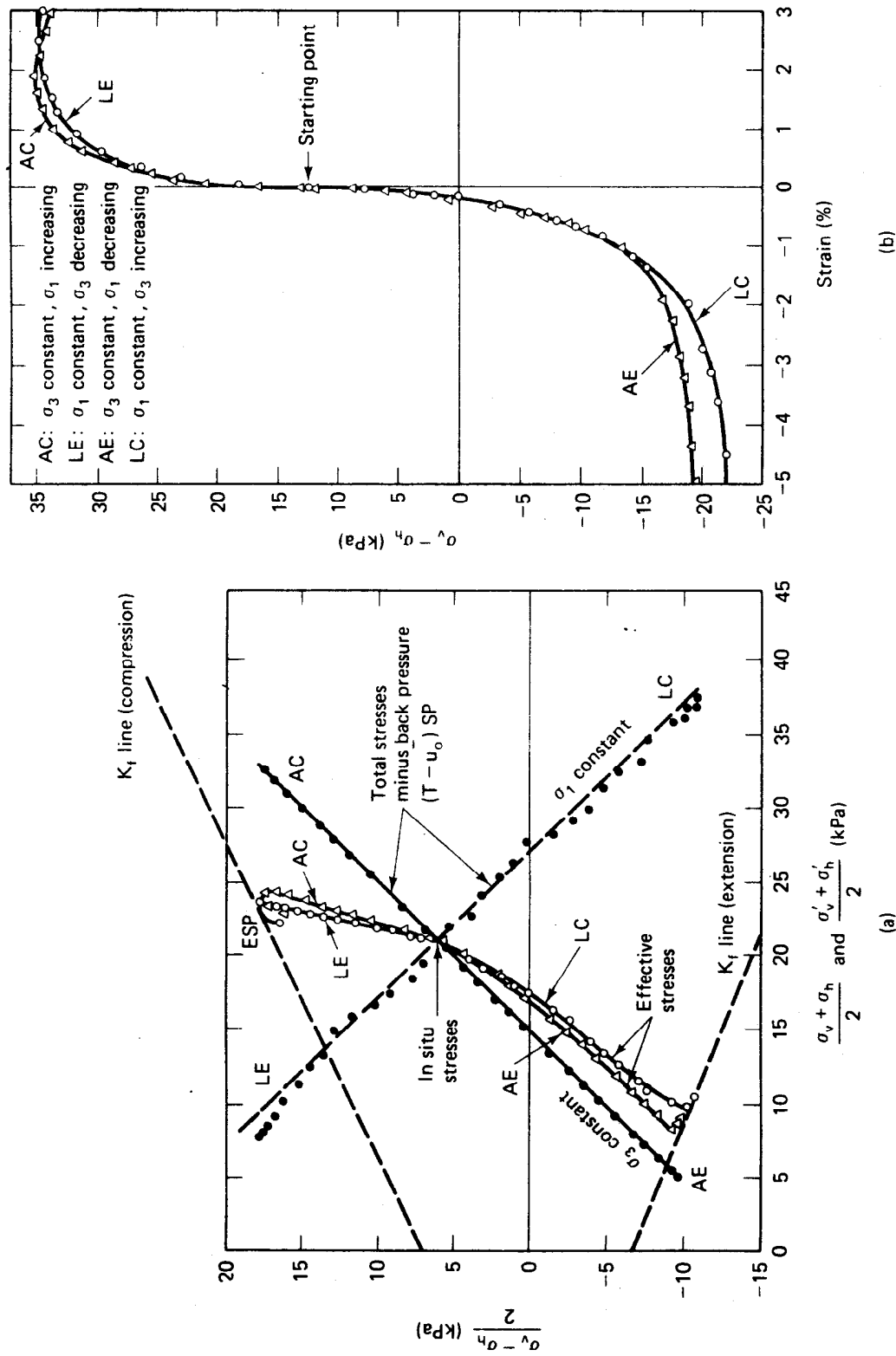
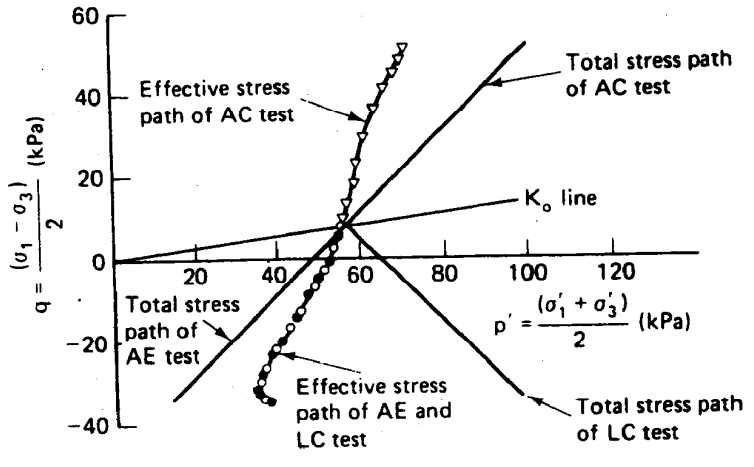
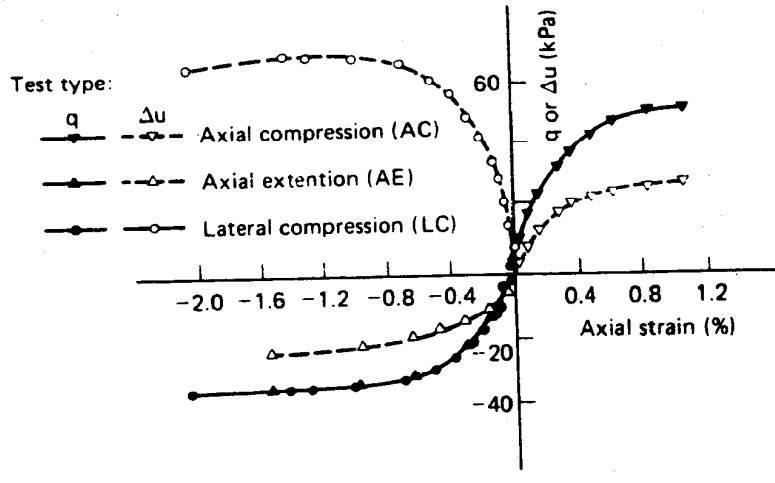


Fig. 11.77 (a) Total and effective stress paths and (b) stress-strain curves for  $K_0$ -consolidated undrained triaxial tests on a normally consolidated clay (after Bishop and Wesley, 1975).



(a)



(b)

Specimen	$K_0$	Test Type	$w_n$ (%)	$w_f$ (%)	$\left(\frac{\sigma_1 - \sigma_3}{2}\right)_{max}$ (kPa)	$A_f$
Kars clay:						
195-22-5	0.75	AC	71.5	70.4	51.2	0.39
195-22-7	0.75	LC	73.5	72.0	34.9	0.73
195-22-3	0.75	AE	71.5	70.3	34.5	0.73

\*  $A_f$  is the pore pressure parameter at failure based on expressions in Table B-3-2.

Fig. 11.78 (a) Total and effective stress paths and (b) stress-strain and pore pressure-strain response of  $K_0$ -consolidated undrained triaxial tests on undisturbed samples of Leda clay from Kars, Ontario (after Law and Holtz, 1978).

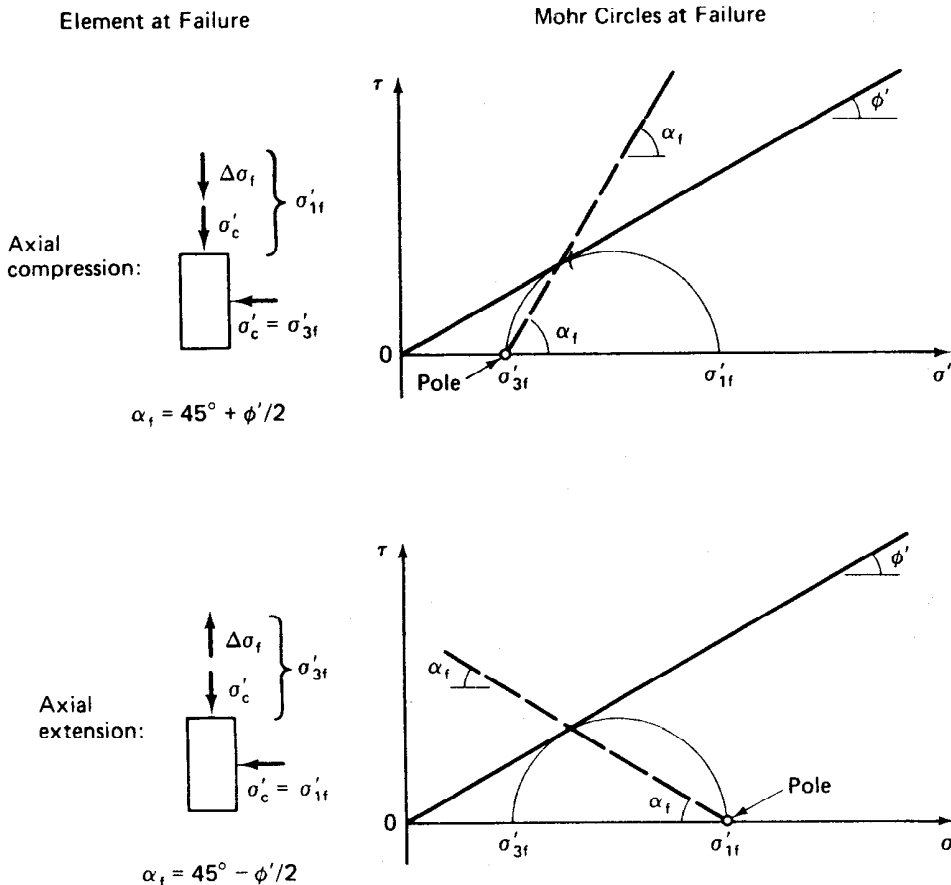


Fig. 11.79 Angle of inclination of the failure plane for AC and AE tests.

### 11.13 STRESS PATHS DURING UNDRAINED LOADING—OVERCONSOLIDATED CLAYS

All of the previous section on undrained stress paths concerned the behavior of normally consolidated clays. For overconsolidated clays, the principles are the same but the shapes of the stress paths are different because the developed pore pressures are different. Examples of stress paths for axial compression tests on overconsolidated clays are shown in Figs. 10.25 and 11.34b. Knowing how the excess pore water pressures develop along with the shapes of the total stress paths for the various types of tests, you can readily construct the ESP's for overconsolidated clays.

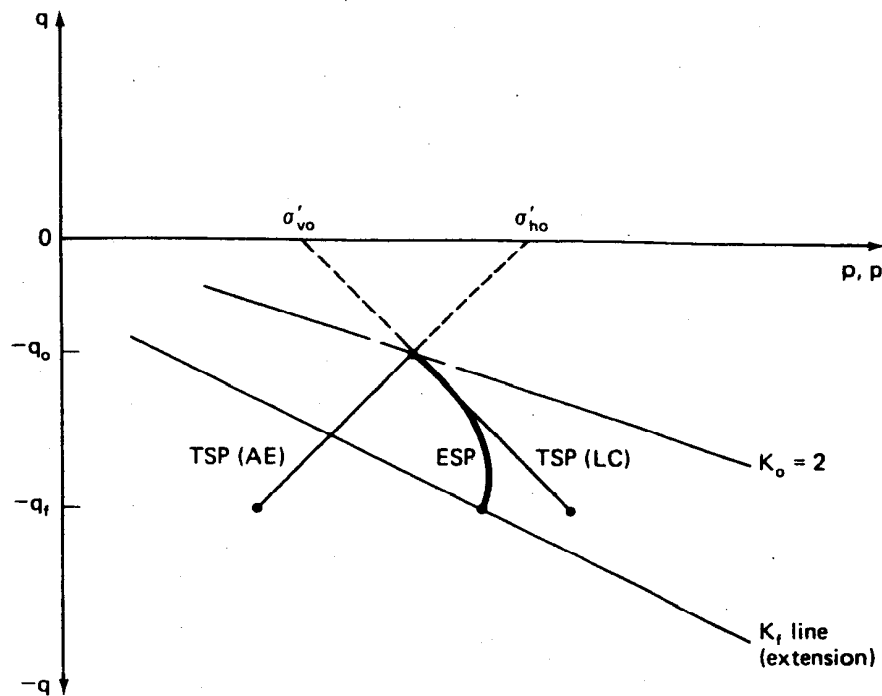


Fig. 11.80. AE and LC stress paths for an overconsolidated clay.

As discussed in Sec. 11.11, overconsolidated clays usually have a  $K_o$  much greater than one. Therefore the stress paths for overconsolidated clays in situ (or for samples reconsolidated to in situ stresses in the laboratory) will start from below the hydrostatic ( $K_o = 1$ ) axis, as shown in Fig. 10.25. Figure 11.80 shows how the stress paths for AE and LC tests on an overconsolidated clay might appear.

### EXAMPLE 11.18

**Given:**

Consolidated undrained triaxial compression tests are conducted on an overconsolidated clay with preconsolidation stress  $\sigma'_p$  of 800 kPa, which is equivalent to an OCR of 10. The results are shown in Fig. Ex. 11.18a. Another CU test is conducted on the same clay at the same OCR and thus the same  $\sigma'_p$ . In the latter test, the lateral stress is not held constant, but is increased at the same time as the axial stress is increased so that  $\Delta\sigma_3 = 0.2\Delta\sigma_1$ . (See Fig. Ex. 11.18b.) Assume that the test results on this clay

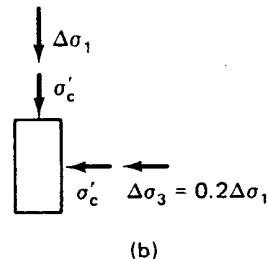
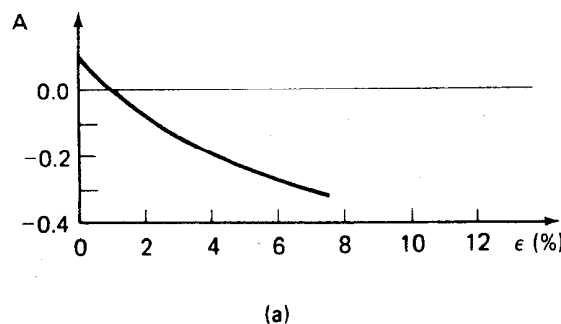
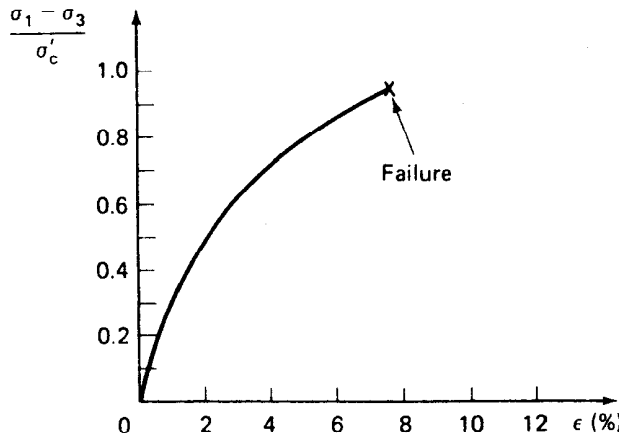


Fig. Ex. 11.18a

Fig. Ex. 11.18b

shown in Fig. Ex. 11.18a are valid for all ways of changing the boundary stresses in compression, that is, both  $\sigma_1$  and  $\sigma_3$  increasing during the test.

**Required:**

Predict the behavior of the second CU test.

- Calculate the quantities and fill in the columns of Table Ex. 11.18 for 0, 0.5, 2.5, 5, and 7.5% strain.
- Draw the TSP and the ESP for this test.

**Solution:**

a. Table Ex. 11.18, filled in.

TABLE EX. 11.18\*

$\epsilon$ (%)	$\Delta\sigma_1$	$\Delta\sigma_3$	$\sigma_1$	$\sigma_3$	$A$	$\Delta u$
0	0	0	80	80	+ 0.1	0
0.5	16	3.2	96	83.2	+ 0.05	+ 3.6
2.5	58	11.6	138	91.6	- 0.11	+ 6.5
5.0	80	16.0	160	96.0	- 0.23	+ 1.3
7.5	94	18.8	174	98.8	- 0.32	- 5.3

\*All stresses in kPa.

b. Fig. Ex. 11.18c. Note that  $\sigma'_c = \sigma'_p / (\text{OCR})$  from Eq. 8-2. Thus

$$\sigma'_c = \frac{800}{10} = 80 \text{ kPa}$$

Also

$$\sigma_1 = \sigma'_c + \Delta\sigma_1$$

$$\sigma_3 = \sigma'_c + \Delta\sigma_3 = \sigma'_c + 0.2\Delta\sigma_1$$

$$(\sigma_1 - \sigma_3) = \Delta\sigma_1 - 0.2\Delta\sigma_1 = 0.8\Delta\sigma_1$$

$$\frac{(\sigma_1 - \sigma_3)}{\sigma'_c} = \frac{0.8\Delta\sigma_1}{\sigma'_c}$$

But,  $\sigma'_c = 80 \text{ kPa}$ . Therefore

$$\Delta\sigma_1 = 100 \left( \frac{\sigma_1 - \sigma_3}{\sigma'_c} \right)$$

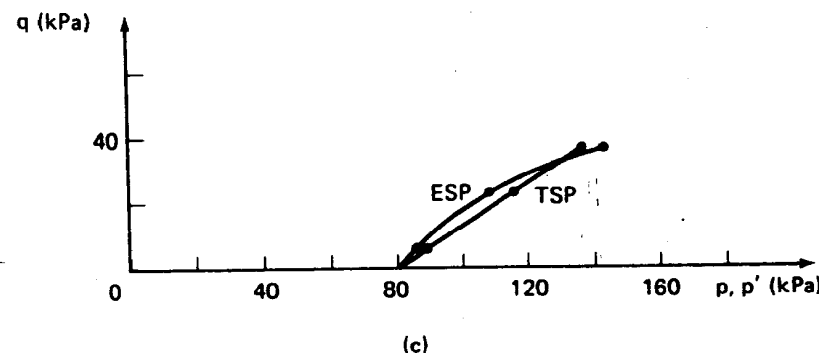


Fig. Ex. 11.18c

The quantity in parentheses is what is plotted in Fig. Ex. 11.18a. Now the values for  $\Delta\sigma_1$  and  $\Delta\sigma_3$  ( $= 0.2 \Delta\sigma_1$ ) can be determined from the figure and inserted appropriately in Table Ex. 11.18. Once the initial values are known,  $\sigma_1$  and  $\sigma_3$  at each strain are also readily obtained.

For calculation of  $\Delta u$ , use Eq. 11-14 (assume  $S = 100\%$  for a triaxial test with pore pressures measured) or

$$\begin{aligned}\Delta u &= \Delta\sigma_3 + A(\Delta\sigma_1 - \Delta\sigma_3) \\ &= 0.2 \Delta\sigma_1 + A(\Delta\sigma_1 - 0.2 \Delta\sigma_1) \\ &= (0.2 + 0.8A) \Delta\sigma_1\end{aligned}$$

Thus values of  $\Delta u$  in Table Ex. 11.18 are readily determined.

Stress paths are either calculated from Eqs. 10-18 and 10-19 or constructed graphically (Fig. Ex. 11.18c).

(After C. W. Lovell.)

Example 11.18 illustrates two important points. First, the ESP has the typical shape of an overconsolidated clay (compare with Figs. 10.25 and 11.34b). Second, you can use the principles developed previously for simple ordinary triaxial tests (constant cell pressure) to plot the results of more complex stress path tests.

#### 11.14 APPLICATIONS OF STRESS PATHS TO ENGINEERING PRACTICE

In this section, we offer some examples of how a knowledge of the stress paths helps to explain what is happening to the stresses in the ground during a given engineering loading or unloading situation. If you can draw the complete stress path for some critical elements in your engineering problem, then you will have a much better understanding of the entire problem. This knowledge will enable you to design an appropriate laboratory test program, to estimate the in situ load-deformation response of the soil and structure, and finally to plan a suitable observation and instrumentation program for monitoring the construction operations and final performance of the structure.

Let's look first at what happens when we take a sample of normally consolidated clay. We showed part of the stress path during sampling in Fig. 10.21. The more complete stress path during all the operations necessary before the specimen is ready for testing is shown in Fig. 11.81. No wonder then that the undrained shear strengths are often very much less than in situ strengths if the samples are poor.

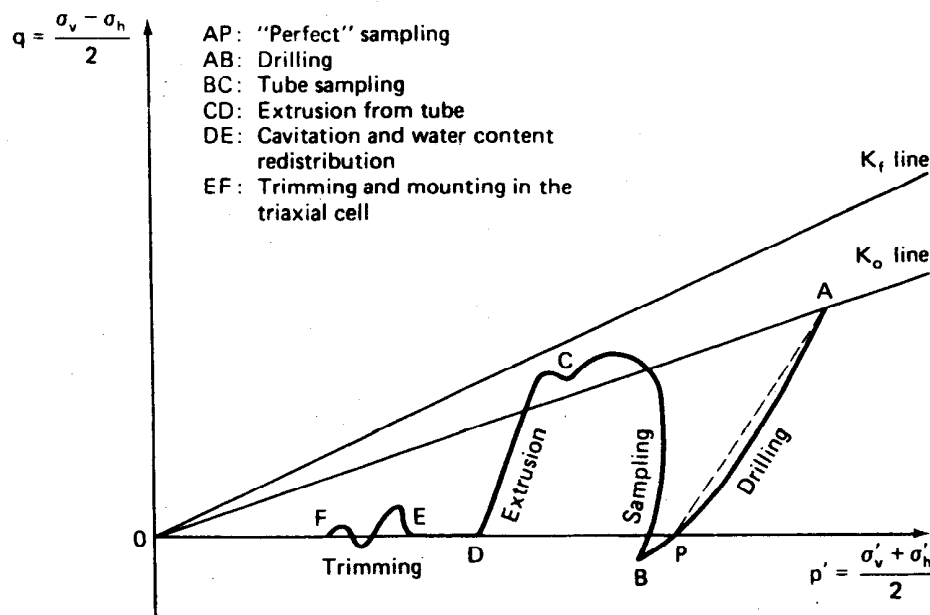
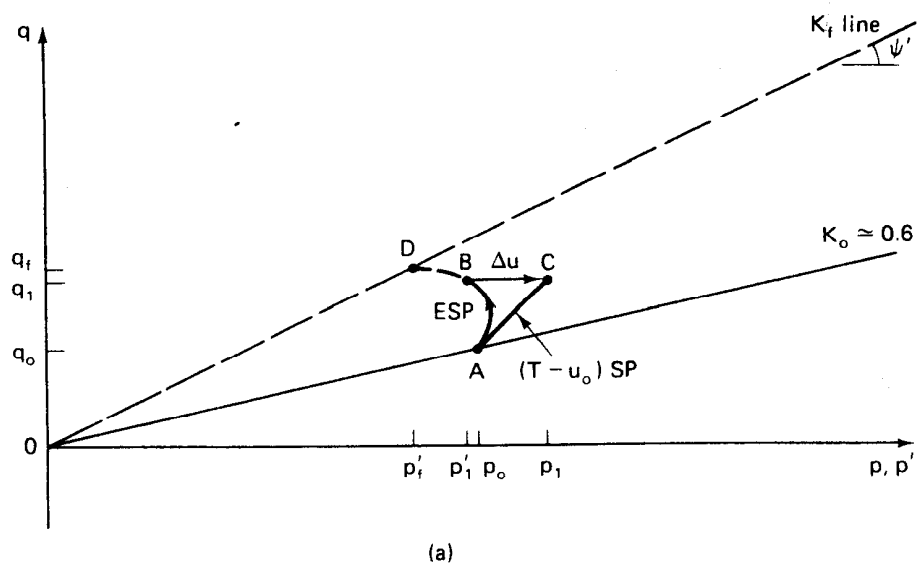


Fig. 11.81 Stress paths during sampling of a normally consolidated clay (after Ladd and Lambe, 1963).

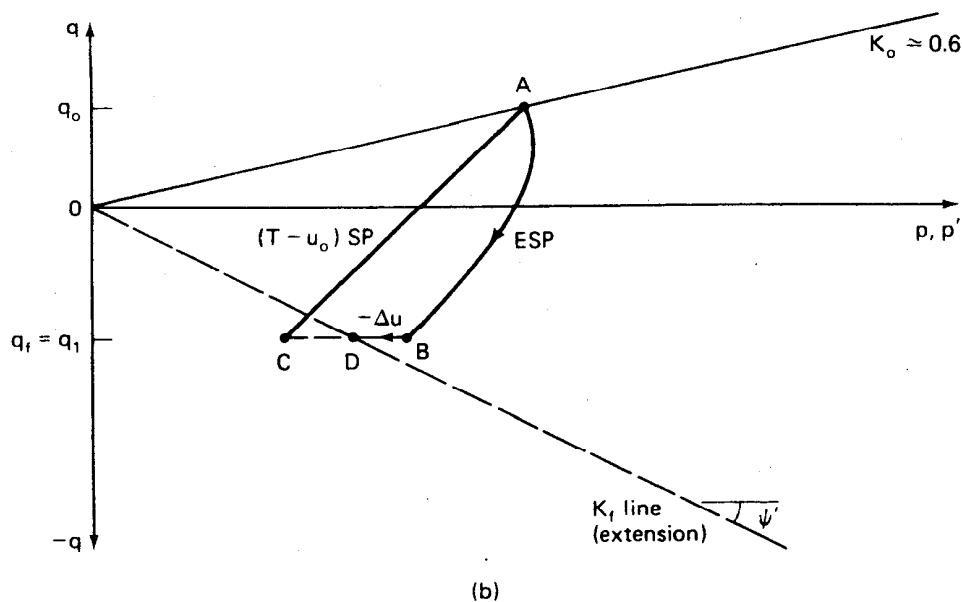
Procedures for evaluating sample disturbance and correcting the measured shear strength are suggested by Ladd and Lambe (1963) and Ladd, et al. (1977).

Next, we shall consider the case of foundation loading, for example, a highway embankment constructed on a soft clay foundation. Let us assume that the clay is very nearly 100% saturated and is normally consolidated. This case, as shown by Fig. 11.73a, may be modeled by axial compression stress conditions. Strictly speaking, as mentioned previously, the loading should be plane strain ( $\epsilon_2 = 0$ ) for a long embankment, but we shall use the common triaxial test, with which you are familiar, for illustrative purposes. The stress paths for this case are shown in Fig. 11.82 (compare with Fig. 10.26).

Let's look a little more closely at these stress paths and their engineering implications. For this normally consolidated clay, the  $K_o$  is less than 1 (about 0.6), so that the initial stress conditions in the ground are plotted as point A on the figure. In a foundation *loading*, the horizontal stresses probably increase slightly, as we assumed in Example 11.16, but for this case we will assume that they are essentially constant. Then, the  $(T - u_o)SP$  is the straight line AC. The total stresses represented by point C are applied at the end of construction. The induced pore pressures are positive, of course, for a normally consolidated clay, and so we will have



(a)



(b)

**Fig. 11.82 Stress paths for (a) foundation loading and (b) foundation excavation of normally consolidated clay.**

the typically shaped ESP hooking off to the left, as is illustrated by curve  $AB$ . The distance  $BC$ , then, is numerically equal to the excess pore pressure induced by the embankment loading. Note that the shear stress on a typical element under the embankment increases from its initial value of  $q_0$  to  $q_1$ . Had loading continued to the level of  $q_f$ , the ESP would have intersected the  $K_f$  line and failure would have occurred.

For this example, let's assume that we were good designers, that we correctly estimated the in situ shear strength of the soil, and that no failure occurred. Then we are at point  $B$  on the ESP at the *end of construction*, the most critical design condition for foundation loadings on normally consolidated clays. Why is this? Well, look at what happens after we reach point  $B$ . The applied loading is constant thereafter (assuming no additional construction occurs), the clay starts to consolidate, and the excess pore water pressure that was caused by the load dissipates. This excess pore pressure is represented by the distance  $BC$ . Thus the ESP proceeds along line  $BC$ . Ultimately at  $u = 100\%$ , all the excess pore pressure will be dissipated and our element will be at point  $C$  in equilibrium under the embankment load. It will still have a shear stress  $q_1$  acting on it, and  $p = p' = p_1$ . Since there is no excess pore water pressure remaining in the element, the total stresses will equal the effective stresses at point  $C$ . Now you can see why point  $B$  at the end of construction was the most critical for this case. Point  $B$  was the closest point to the failure line  $K_f$ . After that, because of consolidation, the foundation soil became stronger with time (safer) until at point  $C$  we were at the farthest point from the  $K_f$  line for this particular loading situation. That is why the end of construction is the most critical for foundation loading of normally consolidated clays. The engineering lesson here is that if you make it through the end of construction period for this type of loading, then conditions become *safer* with time.

For the foundation loading of an overconsolidated clay, the TSP and ESP would look something like the paths shown in Figs. 10.25 and 11.34b. As the negative excess pore pressure dissipates, the stresses on the element move closer to the  $K_f$  line, which means that the long-term conditions are actually the *least* safe after dissipation of the pore pressure has occurred. But in most cases, we are so far from the  $K_f$  line anyway that long term conditions are usually not critical.

---

### EXAMPLE 11.19

**Given:**

The embankment of Example 11.16. Triaxial compression tests indicate  $\phi' = 23^\circ$  and  $c' = 7 \text{ kPa}$ .

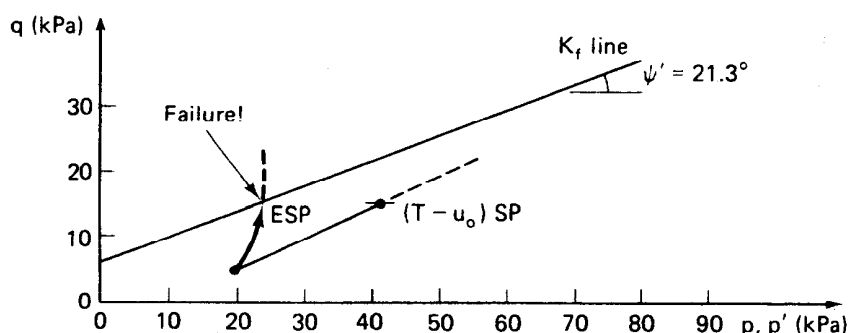


Fig. Ex. 11.19

**Required:**

Construct the  $K_f$  line and determine whether the embankment will be stable.

**Solution:**

From Eqs. 10-24 and 10-25,  $\psi' = 21.3^\circ$  and  $a' = 6.4 \text{ kPa}$ . Draw the  $K_f$  line on the  $p$ - $q$  diagram (Fig. Ex. 11.19). Since the ESP would intersect the  $K_f$  line before the final design loads could be applied, failure would occur. At that time,  $q$  would be approximately 15 kPa.

Another important engineering situation concerns an excavation for a foundation in normally consolidated clay. This situation is illustrated in Fig. 11.73 as an example of axial extension. We already know from Fig. 11.76 what the TSP and ESP look like for this case, they are also in Fig. 11.82b. Since the vertical stress decreases during an excavation, the total stress path goes from the initial conditions at point  $A$  to point  $C$ . As with the case of foundation loading, the horizontal stresses may also decrease slightly, but for illustration purposes, we shall assume that they remain essentially unchanged. Since negative pore pressures occur due to unloading the ESP must lie to the right of the  $(T - u_o)$ SP. For the case shown with unloading from  $q_0$  down to  $q_1$ , the ESP then follows curve  $AB$ , and point  $B$  represents conditions at the end of construction. For this case, failure did not occur, and we are safe at the end of construction. Now, the excess pore pressure starts to dissipate—it is negative in this case, and now it starts to become more and more positive, following line  $BDC$ . At point  $C$ , of course, all the excess negative pore pressure would be dissipated and the total stresses would equal the effective stresses. But, this would never

occur because when the ESP reached point *D*, it would intersect the  $K_f$  line in extension and failure would occur. Therefore the long-term conditions are the more critical for the case of an excavation in normally consolidated clays. In contrast to the case of foundation loading, just because you get through construction without a failure doesn't mean that you are free of a possible failure. No, the excavation will become less and less safe with time. Field measurements (for example, Lambe and Whitman, 1969) have shown that the rate of dissipation of this negative pore pressure occurs relatively fast, much faster than in the case of foundation loading. Therefore the engineering implication for this case is to get that excavation filled and the clay loaded as fast as possible. Otherwise you risk a failure occurring at some time, perhaps only a few weeks after completion of the excavation. This is another example of the long-term conditions being more critical than the end of construction conditions.

These examples illustrate the value of the stress path method. You can construct similar TSP and ESP diagrams for the other cases shown in Fig. 11.73, for both normally and overconsolidated clays, and see what the critical design situations are. Some of the critical conditions for stability are summarized in Table 11-10 (Ladd, 1971b).

TABLE 11-10 Critical Conditions for the Stability of Saturated Clays\*

Foundation Loading:		
Soil Type:	Soft (NC) clay	Stiff (highly OC) clay
Critical condition:	UU case (no drainage)	Probably UU case but check CD case (drainage with equilibrium pore pressures)
Remarks:	Use $\phi = 0$ , $c = \gamma$ , with appropriate corrections (Sec. 11.9).	Stability usually not a major problem
Excavation or Natural Slope:		
Soil type:	Soft (NC) clay	Stiff (highly OC) clay
Critical condition:	Could be either UU or CD case	CD case (complete drainage)
Remarks:	If soil is very sensitive, it may change from drained to undrained conditions.	Use effective stress analysis with equilibrium pore pressures. If clay is fissured, $c'$ and perhaps $\phi'$ may decrease with time.

\*After Ladd (1971b).

## PROBLEMS

- 11-1. A granular material is observed being dumped from a conveyor belt. It formed a conical pile with about the same slope angle, 1.8 horizontal to 1 vertical. What can you say about the material?
- 11-2. A battery filler is filled with a medium rounded sand in the densest state possible. Every effort is made to keep the sand saturated. A transparent tube allows observation of the water level in the battery filler. What will happen to the water level, if anything, as the bulb is squeezed very hard? Why? Would it matter if the sand were loose? Explain.
- 11-3. You are climbing up a large sand dune west of Yuma, Arizona. The slope angle is  $33^\circ$ . In what compass direction are you traveling? Don't forget the declination!
- 11-4. The principal stress ratio for a drained test at failure was 4.60. What was the probable relative density of the sand?
- 11-5. Derive Eq. 11-3.
- 11-6. A direct shear test is conducted on a fairly dense sample of Franklin Falls sand from New Hampshire. The initial void ratio was 0.668. The shear box was 76 mm square, and initially the height of the specimen was 11 mm. The following data were collected during shear. Compute the data needed and plot the usual curves for this type of test.

Time Elapsed (min)	Vertical Load (kN)	Horizontal Displacement (mm)	Thickness Change (mm)	Horizontal Load (N)
0	2.25	8.89	3.56	0
0.5	(constant)	8.82	3.54	356
1		8.63	3.52	721
2		8.44	3.51	1014
3		7.92	3.53	1428
4		7.18	3.59	1655
5		6.38	3.63	1770
6		5.49	3.65	1744

(After Taylor, 1948.)

- 11-7. A conventional triaxial compression test is conducted on a sample of dense sand from Ft. Peck Dam, Montana. The initial area of the test specimen was  $10 \text{ cm}^2$  and its initial height was 70 mm. Initial void ratio was 0.605. The following data were observed

during shear. First, calculate the average area of the specimen, assuming it is a right circular cylinder at all times during the test. Then make the calculations necessary to plot the axial stress versus axial strain and volumetric strain versus axial strain curves for this test. Assuming  $c' = 0$ , what is  $\phi'$ ?

Time Elapsed sec.	Chamber Pressure kPa (psi)	Strain Dial (giving $\Delta H$ )		Buret (giving $\Delta V$ )	Axial Load	
		mm	$(10^{-3}$ in)		N	(lbf)
0	206.8 (30)	5.08	(200)	2.00	0	(0)
		5.21	(205)	1.91	182	(41)
		5.33	(210)	1.86	374	(84)
45		5.69	(224)	1.92	641	(144)
		6.10	(240)	2.13	787	(177)
90		7.06	(278)	2.80	921	(207)
		8.10	(319)	3.66	970	(218)
		9.12	(359)	4.56	983	(221)
240		10.21	(402)	5.40	970	(218)
		12.90	(508)	7.30	898	(202)
460		15.32	(603)	8.09	814	(183)

(After Taylor, 1948.)

- 11-8. The results of two CD triaxial tests at different confining pressures on a medium dense, cohesionless sand are summarized in the table below. The void ratios of both specimens were approximately the

Test No. 1 ( $\sigma_c = 100$ kPa)			Test No. 2 ( $\sigma_c = 3000$ kPa)		
Axial Strain (%)	$(\sigma_1 - \sigma_3)$ (kPa)	Volumetric Strain (%)	Axial Strain (%)	$(\sigma_1 - \sigma_3)$ (kPa)	Volumetric Strain (%)
0	0	0	0	0	0
1.71	325	- 0.10	0.82	2090	- 0.68
3.22	414	+ 0.60	2.50	4290	- 1.80
4.76	441	+ 1.66	4.24	5810	- 2.71
6.51	439	+ 2.94	6.00	6950	- 3.36
8.44	405	+ 4.10	7.76	7760	- 3.88
10.4	370	+ 5.10	9.56	8350	- 4.27
12.3	344	+ 5.77	11.4	8710	- 4.53
14.3	333	+ 6.33	13.2	8980	- 4.71
16.3	319	+ 6.70	14.9	9120	- 4.84
18.3	318	+ 7.04	16.8	9140	- 4.92
20.4	308	+ 7.34	18.6	9100	- 4.96
			20.5	9090	- 5.01

(After A. Casagrande.)

- same at the start of the test. Plot on one set of axes the principal stress difference versus axial strain and volumetric strain (Eq. 11-4) versus axial strain for both tests. Estimate the initial tangent modulus of deformation, the "50%" secant modulus, and the strain at failure for each of these tests.
- 11-9. For the two tests of Problem 11-8, determine the angle of internal friction of the sand at (a) peak compressive strength, (b) at ultimate compressive strength, and (c) at 5% axial strain. Comments?
- 11-10. A sand is hydrostatically consolidated in a triaxial test apparatus to 420 kPa and then sheared with the drainage valves open. At failure,  $(\sigma_1 - \sigma_3)$  is 1046 kPa. Determine the major and minor principal stresses at failure and the angle of shearing resistance. Plot the Mohr diagram. (This problem should be followed by the next one.)
- 11-11. The same sand as in Problem 11-10 is tested in a direct shear apparatus under a normal pressure of 420 kPa. The sample fails when a shear stress of 280 kPa is reached. Determine the major and minor principal stresses at failure and the angle of shearing resistance. Plot the Mohr diagram. Explain the differences, if any, of these values with those obtained in the preceding problem.
- 11-12. Indicate the orientations of the major principal stress, the minor principal stress, and the failure plane of the tests in Problems 11-10 and 11-11.
- 11-13. A granular soil is tested in direct shear under a normal stress of 300 kPa. The size of the sample is 7.62 cm in diameter. If the soil to be tested is a dense sand with an angle of internal friction of  $42^\circ$ , determine the size of the load cell required to measure the shear force with a factor of safety of 2 (that is, the capacity of the load cell should be twice that required to shear the sand).
- 11-14. The stresses induced by a surface load on a *loose* horizontal sand layer were found to be  $\sigma_v = 4.62$  kPa,  $\tau_v = 1.32$  kPa,  $\sigma_h = 2.90$  kPa, and  $\tau_h = -1.32$  kPa. By means of Mohr circles, determine if such a state of stress is safe. Use Eq. 10-11 for the definition of factor of safety.
- 11-15. If the same stress conditions as in Problem 11-14 act on a *very dense* gravelly sand, is such a state safe against failure?
- 11-16. The effective normal stresses acting on the horizontal and vertical planes in a silty gravel soil are 1.91 MPa and 3.18 MPa, respec-

tively. The shear stress on these planes is  $\pm 0.64$  MPa. For these conditions, what are the magnitude and direction of the principal stresses? Is this a state of failure?

- 11-17. A sample of dense sand tested in a triaxial CD test failed along a well-defined failure plane at an angle of  $66^\circ$  with the horizontal. Find the effective confining pressure of the test if the principal stress difference at failure was 100 kPa.
- 11-18. A dry loose sand is tested in a vacuum triaxial test in which the pore air pressure of the sample is lowered below gage pressure to within about 95% of  $-1$  atm. Estimate the principal stress difference and the major principal stress ratio at failure.
- 11-19. For the data shown in Fig. 11.4a, what is (a) the principal stress difference and (b) the principal stress ratio at an axial strain of 10% for an effective confining pressure of 2 MPa?
- 11-20. For the conditions given in Problem 11-19, plot the Mohr circle.
- 11-21. Do Problems 11-19 and 11-20 for the data shown in Fig. 11.5a.
- 11-22. A sample of Sacramento River sand has a critical confining pressure of 1000 kPa. If the sample is tested at an effective confining pressure of 1500 kPa, describe its behavior in drained and undrained shear. Show results in the form of unscaled Mohr circles.
- 11-23. For the sand of Problem 11-22, describe the behavior in drained and undrained shear in a triaxial test if the effective confining pressure is 750 kPa.
- 11-24. A drained triaxial test is performed on a sand with  $\sigma'_{3c} = \sigma'_{3f} = 500$  kPa. At failure,  $\tau_{max} = 660$  kPa. Find  $\sigma'_{1f}$ ,  $(\sigma_1 - \sigma_3)_f$ , and  $\phi'$ .
- 11-25. If the test of Problem 11-24 had been conducted undrained, determine  $(\sigma_1 - \sigma_3)_f$ ,  $\phi'$ ,  $\phi_{total}$ , and the angle of the failure plane in the specimen.  $\Delta u_f = 100$  kPa.
- 11-26. If the test of Problem 11-25 were conducted at an initial confining pressure of 1000 kPa, estimate the principal stress difference and the induced pore water pressure at failure.
- 11-27. Assume the sand of Problem 11-24 is Sacramento River sand at a void ratio of 0.8. If the initial volume of the specimen was  $70$  cm $^3$ , what change in volume would you expect during shear?
- 11-28. What volume change would you expect during the test of Problem 11-25?

- 11-29. A silty sand is tested consolidated-drained in a triaxial cell where both principal stresses at the start of the test were 500 kPa. If the total axial stress at failure is 1.63 MPa while the horizontal pressure remains constant, compute the angle of shearing resistance and the theoretical orientation of the failure plane with respect to the horizontal.
- 11-30. The silty sand of Problem 11-29 was inadvertently tested consolidated-undrained, but the laboratory technician noticed that the pore pressure at failure was 290 kPa. What was the principal stress difference at failure?
- 11-31. If the consolidation pressure in the CU test of Problem 11-30 were 1000 kPa instead of 500 kPa, estimate the pore pressure at failure.
- 11-32. A sample of sand failed when  $(\sigma_1 - \sigma_3)$  was 900 kPa. If the hydrostatic consolidation stress were 300 kPa, compute the angle of shearing resistance of the sand. What else can you say about the sand?
- 11-33. If the sample of Problem 11-32 were sheared undrained and the induced pore pressure at failure were 200 kPa, estimate the principal stress difference at failure. What would be the angle of shearing resistance in terms of total stresses?
- 11-34. A sample of sand at the field density is known to have a  $(\sigma_1/\sigma_3)_{\max}$  of 4.0. If such a specimen is hydrostatically consolidated to 1210 kPa in a triaxial test apparatus, at what effective confining pressure  $\sigma'_3$ , will the sample fail if the vertical stress is held constant? (This is a lateral extension test.)
- 11-35. Two CD stress path triaxial tests are conducted on identical

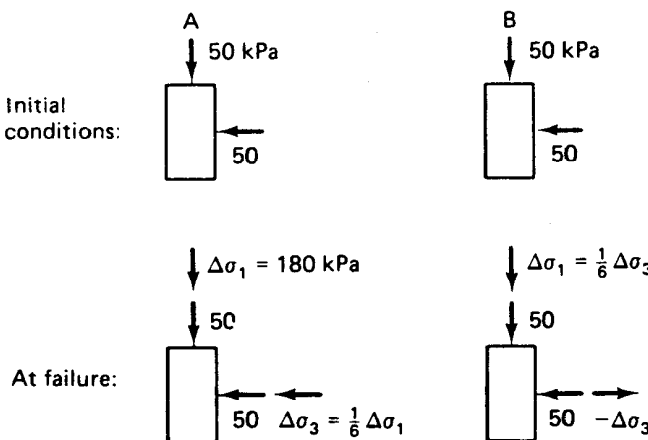


Fig. P11-35

## Problems

samples of the same sand. Both specimens are initially consolidated hydrostatically to 50 kPa; then each specimen is loaded as shown in Fig. P11-35. Specimen *A* failed when the applied  $\Delta\sigma_1$  was 180 kPa. Make the necessary calculations to plot (a) the Mohr circles at failure for both tests, and (b) the stress paths for both tests. (c) Determine  $\phi'$  for the sand. (After C. W. Lovell.)

- 11-36. Plot a graph of  $\sigma'_1/\sigma'_3$ , versus  $\phi'$ . (Aren't you sorry you didn't do this sooner? It would have been helpful for solving some of these problems.) What range of values of  $\phi'$  should be used?
- 11-37. Estimate the shear strength parameters of a fine (beach) sand (SP). Estimate the minimum and maximum void ratios.
- 11-38. A subrounded to subangular sand has a  $D_{10}$  of about 0.1 mm and a uniformity coefficient of 3. The angle of shearing resistance measured in the direct shear test was 47°. Is this reasonable? Why?
- 11-39. Estimate the  $\phi'$  values for (a) a well-graded sandy gravel (GW) at a density of 2.1 Mg/m<sup>3</sup>; (b) a poorly graded silty sand with a field density of 1.55 Mg/m<sup>3</sup>; (c) an SW material at 100% relative density; and (d) a poorly graded gravel with an in situ void ratio of 0.4.
- 11-40. The results of a series of CD triaxial tests on a medium dense, cohesionless sand are summarized in the table below. The void ratios for all the test specimens were approximately the same at the start of the test. Plot the strength circles and draw the Mohr failure envelope for this series of tests. What angle of internal friction should be used in solving stability problems in which the range of normal stresses is (a) 0–500 kPa; (b) 1000–1500 kPa; (c) 3–6 MPa; and (d) 0–6 MPa?

Test No.	Confining Pressure (kPa)	Compressive Strength (kPa)
1	100	480
2	400	1870
3	997	4080
4	1880	7050
5	2990	10200
6	3850	12690

(After A. Casagrande.)

- 11-41. Estimate the values of the coefficient of earth pressure at rest,  $K_o$ , for the four soils of Problem 11-39.

- 11-42. If the sands of Problem 11-41 had been preloaded, would your estimate of  $K_o$  be any different? If so, would it be higher or lower? Why?
- 11-43. Estimate  $K_o$  for sands 1, 4, 5, 6, 8, and 10 in Table 11-2 for relative densities of 40% and 85%.
- 11-44. For future reference, place a scale of  $K_o$  on the ordinate of Fig. 11.13. You should probably also indicate a range of values of  $K_o$ .
- 11-45. Explain the difference between liquefaction and cyclic mobility.
- 11-46. The Peacock diagram (Fig. 11.10) has been used to predict the pore pressure response of undrained tests on sands, based on the volume changes observed at failure in drained tests. At a given void ratio a sample consolidated at an effective confining pressure less than  $\sigma'_3$ <sub>crit</sub> would be expected to offer *more* resistance to liquefaction (since it should have a dilative tendency and therefore develop negative pore water pressure) than a sample consolidated at a confining pressure higher than  $\sigma'_3$ <sub>crit</sub> (as this one should tend to decrease in volume during shear). This is contrary to what has been found in the laboratory in cyclic triaxial tests. Explain the apparent contradiction.
- 11-47. Figure 11.18b shows that at the tenth cycle, the change in pore water pressure is about 66 kPa just at the beginning of the application of the principal stress difference. Yet, at a quarter of a cycle later (as well as slightly before) the pore water pressure is just about equal to the effective confining pressure. At this time the principal stress difference is zero! Explain this observation. (It will help if you understand the answer to Problem 11-46.)
- 11-48. A large power plant is to be constructed at a site immediately adjacent to the Ohio River. The soils at the site consist of 50 m of loose to medium dense granular materials, and the ground water table is near the ground surface. Since there are several potential earthquake source areas that could influence the site, list some measures that could be taken to protect the foundation of this important structure from liquefaction and/or cyclic mobility.
- 11-49. We stated in Secs. 10.5 and 11.9 that the unconsolidated-drained test was meaningless because it could not be properly interpreted. Why is this so? Discuss in terms of laboratory tests as well as possible practical applications.

- 11-50. A CD axial compression triaxial test on a normally consolidated clay failed along a clearly defined failure plane of  $57^\circ$ . The cell pressure during the test was 200 kPa. Estimate  $\phi'$ , the maximum  $\sigma'_1/\sigma'_3$ , and the principal stress difference at failure.
- 11-51. Suppose an identical specimen of the same clay as in Problem 11-50 was sheared undrained, and the induced pore pressure at failure was 85 kPa. Determine the principal stress difference, total and effective principal stress ratios,  $\phi'$ ,  $\phi_{\text{total}}$ ,  $A_f$  and  $\alpha_f$  for this test.
- 11-52. A series of *drained* direct shear tests were performed on a saturated clay. The results, when plotted on a Mohr diagram, gave  $c' = 10$  kPa and  $\tan \phi' = 0.5$ . Another sample of this clay was consolidated to an effective pressure of 100 kPa. An *undrained* direct shear test was performed, and the measured value of  $\tau_{ff}$  was 60 kPa. What was the pore water pressure at failure? Was the sample normally consolidated? Why?
- 11-53. The following information was obtained from laboratory tests on specimens from a completely saturated sample of clay:
- The sample had in the past been precompressed to at least 200 kPa.
  - A specimen tested in direct shear under a normal stress of 600 kPa, with complete drainage allowed, showed a shearing strength of 350 kPa.
  - A specimen which was first consolidated to 600 kPa, and then subjected to a direct shear test in which no drainage occurred, showed a shearing strength of 175 kPa.

Compute  $\phi'$  and  $\phi_T$  for the undrained case. Sketch the Mohr envelopes which you would expect to obtain from a series of undrained and drained tests on this clay. (After Taylor, 1948.)

- 11-54. Triaxial tests were performed on undisturbed samples from the same depth of organic clay whose preconsolidation load, determined from consolidation tests, was in the range 90 to 160 kPa. The principal stresses at failure of two CD tests were

$$\begin{array}{lll} \text{Test No. 1:} & \sigma_3 = 200 \text{ kPa}, & \sigma_1 = 704 \text{ kPa} \\ \text{Test No. 2:} & \sigma_3 = 278 \text{ kPa}, & \sigma_1 = 979 \text{ kPa} \end{array}$$

Data from one CU test on the same clay are shown below. The effective consolidation pressure was 330 kPa and the sample was loaded in axial compression.

Stress Difference (kPa)	Strain (%)	Pore Pressure (kPa)
0	0	0
30	0.06	15
60	0.15	32
90	0.30	49
120	0.53	73
150	0.90	105
180	1.68	144
210	4.40	187
240	15.50	238

- (a) Plot the Mohr circles at failure and determine  $\phi'$  from the CD tests for the normally consolidated portion of the failure envelope.
- (b) For the CU test, plot curves of principal stress difference and pore pressure versus strain.
- (c) On a  $p-q$  diagram, plot the stress paths for the CD and CU tests. What is the OCR of the normal stresses on the failure plane at failure?
- (d) Assuming that the single CU test for which data are given is representative for CU tests run at pressures well above the preconsolidation stress: (a) What is  $\phi$  in terms of total stresses above the effects of preconsolidation? (b) What is  $\phi'$  determined by the CU test above the effects of preconsolidation?

(After A. Casagrande.)

- 11-55. In Problem 11-54, failure in the CU test was assumed to have occurred when the maximum principal stress difference was reached. Calculate and plot the principal effective stress ratio versus strain for this test. What is the maximum  $\sigma'_1/\sigma'_3$ ? Is there any difference in  $\phi'$  for the two failure criteria? Hint: Study Fig. 11.35.
- 11-56. A CU triaxial test is performed on a cohesive soil. The effective consolidation stress was 750 kPa. At failure, the principal stress difference was 1250 kPa, and the major effective principal stress was 1800 kPa. Compute Skempton's pore pressure coefficient  $A$  at failure.
- 11-57. Suppose another specimen of the soil in the preceding problem developed a major effective principal stress of 2200 kPa at failure. What would Skempton's pore pressure coefficient  $A$  at failure be, if  $\sigma'_c = 900$  kPa?

- 11-58. Two samples of a slightly overconsolidated clay were tested in triaxial compression, and the following data at failure were obtained. The preconsolidation stress for the clay was estimated from oedometer tests to be about 400 kPa.

Specimen	X (kPa)	Y (kPa)
$\sigma'_c$	75	750
$(\sigma_1 - \sigma_3)_f$	265	620
$\Delta u_f$	- 5	+ 450

- (a) Determine the Skempton pore pressure parameter  $A$  at failure for both tests.
  - (b) Plot the Mohr circles at failure for both total and effective stresses.
  - (c) Estimate  $\phi'$  in the normally consolidated range, and  $c'$  and  $\phi'$  for the overconsolidated range of stresses.
- 11-59. Two identical specimens of soft saturated normally consolidated clay were consolidated to 150 kPa in a triaxial apparatus. One specimen was sheared drained, and the principal stress difference at failure was 300 kPa. The other specimen was sheared undrained, and the principal stress difference at failure was 200 kPa. Determine (a)  $\phi'$  and  $\phi_{total}$ ; (b)  $u_f$  in the undrained specimen; (c)  $A_f$  in the undrained specimen; and (d) the theoretical angle of failure planes for both specimens.
- 11-60. A clay sample is hydrostatically consolidated to 1.0 MPa and then sheared undrained. The  $(\sigma_1 - \sigma_3)$  at failure was also equal to 1 MPa. If drained tests on identical samples gave  $\phi' = 22^\circ$ , evaluate the pore pressure at failure in the undrained test and compute Skempton's  $A$  parameter.
- 11-61. An undrained triaxial compression test was performed on a saturated sample of normally consolidated clay. The consolidation pressure was 100 kPa. The specimen failed when the principal stress difference was 85 kPa and the induced pore water pressure was 67 kPa. A companion undrained test was performed on an identical sample of the same clay, but at a consolidation pressure of 250 kPa. What maximum principal stress difference would you expect at failure for this second test specimen? What are  $\phi'$  and

$\phi_{\text{total}}$ ? Predict the angle of the failure planes for the two undrained tests. Determine  $A_f$  for this clay.

- 11-62. The following data were obtained from a CU test with pore pressures measured on an undisturbed specimen of sandy silt. The consolidation pressure was 850 kPa and the specimen was sheared in axial compression.

Principal Stress Difference (kPa)	Strain (%)	Induced Pore Pressure (kPa)
0	0	0
226	0.11	81
415	0.25	187
697	0.54	323
968	0.99	400
1470	2.20	360
2060	3.74	219
2820	5.78	-009
3590	8.41	-281
4160	11.18	-530
4430	13.93	-703
4310	16.82	-767
4210	19.71	-789

- (a) Plot curves of principal stress difference and pore pressures versus strain. Plot on one sheet.
- (b) Plot the stress paths on a  $p-q$  diagram.
- (c) What is the maximum effective principal stress ratio developed in this test? Is it the same as the maximum obliquity for this specimen?
- (d) Is there any difference in  $\phi'$  as determined when the principal stress difference or the principal effective stress ratio is a maximum?

(After A. Casagrande.)

- 11-63. Typical consolidated-drained behavior of saturated normally consolidated samples of Ladd's (1964) simple clay are shown in Fig. P11-63. You are to conduct another axial compression CD triaxial test on the same clay with the effective consolidation stress equal to 100 kPa. For this test estimate (a) the water content and (b) the principal stress difference at an axial strain of 5%. (After C. W. Lovell.)

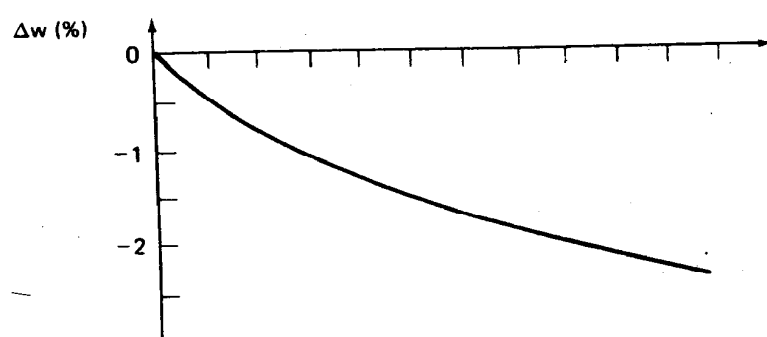
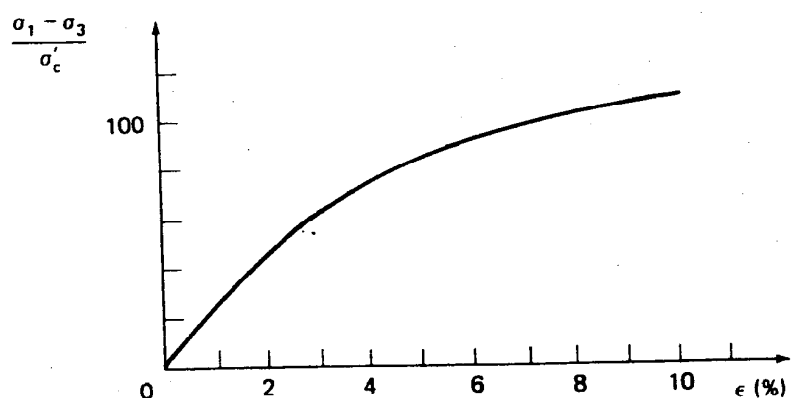
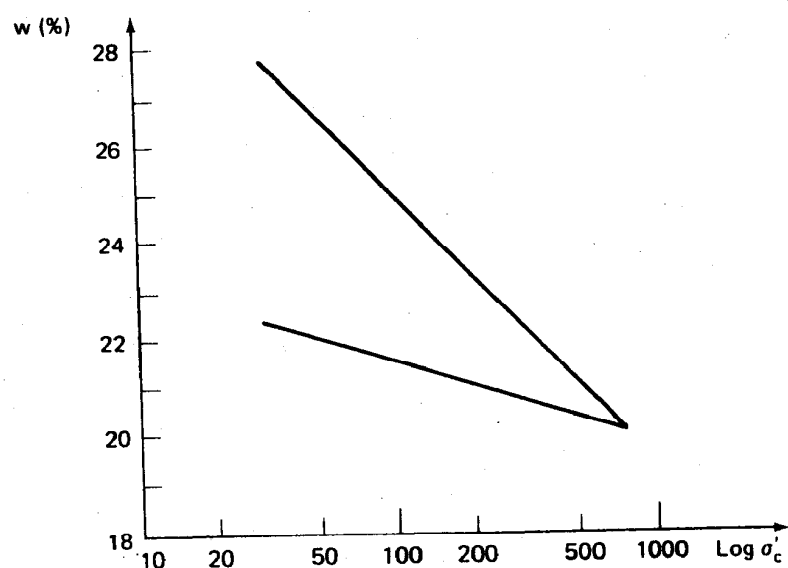


Fig. P11-63

- 11-64. The consolidation behavior of the simple clay of Problem 11-63 is shown in Fig. P11-63. Estimate the water content of a sample of this clay at an OCR of 10, if the maximum consolidation stress is 500 kPa instead of 800 kPa. (After C. W. Lovell.)
- 11-65. Triaxial compression tests were run on specimens from a large undisturbed block sample of clay. Data are given below. Tests 1 through 4 were run so slowly that complete drainage may be assumed. In tests 5 through 8, no drainage was permitted. Plot the Mohr failure envelopes for this soil. Determine the Mohr-Coulomb strength parameters in terms of both total and effective stresses. (After Taylor, 1948.)

Test No.:	1	2	3	4	5	6	7	8
$(\sigma_1 - \sigma_3)_f$ , kPa	447	167	95	37	331	155	133	119
$\sigma'_3 f$ , kPa	246	89	36	6				
$\sigma_c$ , kPa					481	231	131	53

What can you say about the probable in situ OCR and  $K_o$  of this clay? Is it possible to estimate the  $E_u$  and  $\tau_f$  of this soil?

- 11-66. Strength tests conducted on samples of a stiff overconsolidated clay gave lower strengths for CD tests than for CU tests. Is this reasonable? Why? (After Taylor, 1948.)
- 11-67. An undisturbed sample of clay has a preconsolidation load of 500 kPa. In which of the following triaxial tests would you expect the compressive strength to be larger? Why?
- A CD test performed at a chamber pressure of 10 kPa.
  - A CU test performed at a chamber pressure of 10 kPa.
- (After A. Casagrande.)
- 11-68. An unconfined compression test is performed on a dense silt. Previous drained triaxial tests on similar samples of the silt gave  $\phi' = 35^\circ$ . If the unconfined compressive strength was 475 kPa, estimate the height of capillary rise in this soil above the ground water table. Hint: Find the effective confining pressure acting on the specimen. Draw elements similar to Fig. 11.44.
- 11-69. Estimate the in situ value of  $K_o$  of the silt of Problem 11-68. Is this value reasonable in terms of the correlation shown in Fig. 11.69?
- 11-70. Another specimen of the dense silt of Problem 11-68 is tested in unconfined compression. Assume the average pore size of the silt is  $2 \mu\text{m}$ , and estimate the compressive strength of the sample.

- 11-71. What would happen if the specimen of Problem 11-68 was prepared in a loose state, then sheared? What would be its unconfined compressive strength?
- 11-72. The results of unconfined compression tests on a sample of clay in both the undisturbed and remolded states are summarized below. Determine the compressive strength, the initial tangent modulus of deformation, and the secant modulus of deformation at 50% of the compressive strength for both the undisturbed and remolded specimens. Determine the sensitivity of the clay. For the solution of a practical stability problem involving this clay in the undisturbed state, what shear strength would you use if no change in water content occurs during construction? (After A. Casagrande.)

Undisturbed State		Remolded State	
Axial Strain (%)	$\Delta\sigma$ (kPa)	Axial Strain (%)	$\Delta\sigma$ (kPa)
0	0	0	0
1	33	1	7
2	61	2	11
4	109	4	23
6	133	6	32
8	149	8	40
12	160	12	47
16	161	16	50
20	161	20	51

- 11-73. (a) Show that Eq. 11-8 (in Example 11.12) is correct for *undrained* triaxial or unconfined compression tests. (b) Derive a similar expression for the area of the specimen in a *drained* triaxial test.
- Hint:  $A_s = f(A_o, H_o, \epsilon, \Delta V)$ .

- 11-74. In each of the following cases state which test, *X* or *Y*, should show the greater shearing strength. Except for the difference stated below, the two tests are the same type in each case (triaxial, direct shear, etc.) and for identical clay samples.
- (a) The tests are run with no drainage allowed, and test *Y* is run much faster than test *X*.
  - (b) Sample *Y* is preconsolidated to a larger pressure than sample *X*; the pressures during the tests are alike for the two cases.
  - (c) Neither sample is preconsolidated; test *X* is allowed to drain during shear and test *Y* is not allowed to drain.
  - (d) Both samples are highly overconsolidated; test *X* is not allowed to drain and test *Y* is allowed to drain.

- (e) Test  $Y$  is on a sample that is essentially in the undisturbed state, and test  $X$  is on a specimen with appreciably disturbed structure but with the same void ratio as  $Y$ .  
 (After Taylor, 1948.)
- 11-75. List the advantages and disadvantages of each of the field tests listed in Table 11-6 for determining the undrained shear strength of cohesive soils.
- 11-76. Which of the tests in Table 11-6 are appropriate to measure the undrained shear strength for (a) a building foundation and (b) a cut slope for a highway in each of the following five cases:
- (i) Sensitive Scandinavian clay.
  - (ii) Organic marine clay from the U.S. Gulf Coast.
  - (iii) Stiff fissured clay till from the midwest United States.
  - (iv) Canadian fibrous peat.
  - (v) Heavily overconsolidated swelling clay from New Mexico.
- 11-77. Estimate the maximum expected value of the pore pressure parameter  $B$  for the following soils:
- (a) Compacted glacial till at  $S = 90\%$ .
  - (b) Soft saturated normally consolidated Boston blue clay.
  - (c) Soil (a) at  $S = 100\%$ .
  - (d) Stiff overconsolidated clay at  $S = 99\%$ .
  - (e) Loose Ottawa sand at  $S = 95\%$  and  $100\%$ .
  - (f) Compacted clayey silt at  $S = 90\%$  and subjected to high confining pressures.
  - (g) Dense Ottawa sand at  $S = 99\%$  and  $100\%$ .
- 11-78. A 2 m thick fill is constructed at the surface of the soil profile of Example 7.5. If the clay is slightly overconsolidated, estimate the change in pore pressure at point  $A$  of Fig. Ex. 7.5.
- 11-79. A soil sample is taken from the midpoint of the clay layer of Example 7.5, that is, from a depth of 6 m. If the pore pressure parameter  $A_u$  for unloading is 0.90, estimate the effective vertical and horizontal stresses acting on the sample just before testing in the laboratory. Assume  $\phi'$  for the clay is  $25^\circ$ . Hint: Draw elements with stresses similar to Fig. 11.38, and use the definition of stress increments in Appendix B-3. (After G. A. Leonards.)
- 11-80. What would your answer to Problem 11-79 be if you used Eq. 11-22 instead of 11-13?
- 11-81. A sample of normally consolidated clay is removed from  $-10\text{ m}$  below the ground surface. The effective vertical overburden stress

is 250 kPa, and  $K_o$  is 0.8. If the pore pressure parameter due to sampling is 0.7, estimate the change in pore pressure in the sample when it is removed from the clay layer. What effective stresses act on the specimen after extrusion from the sample tube? Assume the ground water table is at the surface.

- 11-82. Show that  $\Delta u$  in Example 11-16 is about 32 kPa, as predicted by Eqs. 11-22 and 11-25.
- 11-83. Prepare a listing of those relationships in Chapter 11 and elsewhere that can be used to predict a soil parameter or property (namely,  $\phi$ ,  $c$ ,  $K_o$ ) when some other property ( $w$ , PI, etc.) is known. List the page and figure number, ordinate, abscissa, and variables of the graph, if any. (This listing will be helpful for solving the next four problems.)
- 11-84. For the data shown in Fig. 8.5, estimate the unconfined compressive strength and the sensitivity of this soil. Typical values for the clay are LL = 88, PL = 43, and PI = 45.
- 11-85. The data presented in Fig. 8.15b are for a black fissured organic silty clay or clayey silt. At a depth of 6 m, estimate the expected value or range of values of the undrained modulus.
- 11-86. A cohesive soil with a liquidity index of 1 has a natural water content of 50%. Estimate as many soil parameters as you can. Include, if you can, compressibility and rate of compression parameters as well as those related to shear strength.
- 11-87. The medium gray silty clay of Fig. 8.18b at a depth of 20 m had an LL of 38 and a PL of 23. Estimate the following parameters for this soil: (a) coefficient of earth pressure at rest; (b) effective angle of internal friction; (c) ratio of  $\tau_f/\sigma'_{vo}$ ; (d) activity; (e) sensitivity; and (f) the undrained Young's modulus. Are there any inconsistencies in the values you obtained? If so, discuss the possible reasons.
- 11-88. A normally consolidated clay has a  $\phi'$  of 30°. Two identical specimens of this clay are consolidated to 200 kPa in a triaxial cell. Predict the maximum and minimum possible axial stresses in the specimens for a constant cell pressure. Hint: The first test is an axial compression test, the second test is an axial extension test. What assumptions are necessary to solve this problem?
- 11-89. The effective stresses at failure for three identical triaxial specimens of an overconsolidated clay are shown in Fig. P11-89. Plot the Mohr circles at failure and determine  $\phi'$  and  $c'$ . Determine the

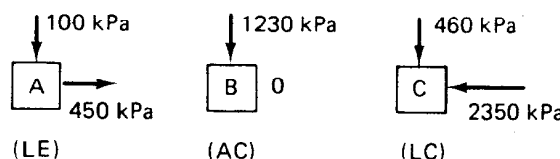


Fig. P11-89

theoretical angle of inclination of the failure planes in each test specimen, and show these on a small sketch. Also sketch the effective stress paths for the three tests. (After C. W. Lovell.)

- 11-90. Three identical specimens (same  $e, w$ ) of a clay are normally consolidated and sheared consolidated-drained (CD) in both compression and extension. The stresses at failure for the three specimens are as shown in Fig. P11-90.
- Plot the Mohr circles at failure, and determine  $\phi'$  and  $\phi_{\text{total}}$ .
  - Determine the inclination of the predicted failure planes (from the Mohr failure hypothesis). Sketch the failed specimens, showing their failure planes.
  - Sketch the three stress paths.
- (After C. W. Lovell.)

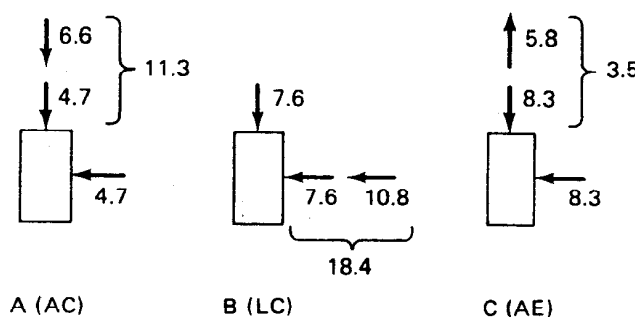


Fig. P11-90

- 11-91. A series of conventional triaxial compression tests were conducted on three identical specimens of a saturated clay soil. Test results are tabulated below.

Specimen	$\sigma_c$ (kPa)	$(\sigma_1 - \sigma_3)/(\text{kPa})$	$\Delta u_f$ (kPa)
A	100	170	40
B	200	260	95
C	300	360	135

- Sketch the total and effective stress paths for each test, and determine the Mohr-Coulomb strength parameters in terms of

both total and effective stresses. (b) Estimate the theoretical angle of the failure planes for each specimen. (c) Do you believe this clay is normally or overconsolidated? Why?

- 11-92. Assume that the induced pore pressures at failure for Problem 11-91 were: specimen *A*, -15 kPa; specimen *B*, -40 kPa; and specimen *C*, -80 kPa; and that everything else was the same. Now do parts (a) and (b) above, and then answer part (c).
- 11-93. An axial compression CU test has been performed on an undisturbed specimen of 100% saturated organic clay. The data for the test are given in Problem 11-54. A lateral extension test is to be performed on an identical specimen at the same consolidation pressure and with the same time of consolidation and time of loading as in the axial compression test.

- (a) Plot the total and effective stress paths. Determine the curve of pore pressure versus (1) principal stress difference and (2) axial strain that you would predict theoretically for the lateral extension test.
- (b) On the  $p$ - $q$  diagram, draw the line corresponding to zero induced pore pressure and the line along which the magnitude of the induced negative pore pressure is equal to the principal stress difference.
- (c) What is  $A_f$  for both the AC and LE test?  
(After A. Casagrande and R. C. Hirschfeld.)

- 11-94. The following data were obtained from a conventional triaxial compression test on a saturated ( $B = 1$ ), normally consolidated simple clay (Ladd, 1964). The cell pressure was held constant at 10 kPa, while the axial stress was increased to failure (axial compression test).

$\epsilon_{\text{axial}} (\%)$	$\Delta\sigma_{\text{axial}} (\text{kPa})$	$\Delta u (\text{kPa})$
0	0	0
1	3.5	1.9
2	4.5	2.8
4	5.2	3.5
6	5.4	3.9
8	5.6	4.1
10	5.7	4.3
12	5.8 failure	4.4

- (a) Plot the  $\Delta\sigma$  and  $\Delta u$  versus axial strain curves. Determine  $A_f$ .
- (b) Plot the total and effective stress paths for the AC test.
- (c) What is  $\phi'$ ? (Assume  $c' = 0$  for normally consolidated clay.)

A lateral extension (LE) test was conducted on an identical sample of the same clay (same  $e$ ,  $w$ ). In this test, the axial or vertical stress was held constant at 10 kPa, while the cell pressure was decreased to 4.2 kPa, at which time the specimen failed.

- (d) Plot both the total and effective stress paths for the LE test.
  - (e) Determine  $u_f$ ,  $\sigma'_{1f}$ ,  $\sigma'_{3f}$  and  $A_f$  for this test.
  - (f) Find  $\phi_{\text{total}}$  for both the AC and the LE tests.
  - (g) Find the theoretical inclinations (from the Mohr failure hypothesis) of the failure planes in each test. Sketch the specimen at failure, indicating the effective stresses at failure and the failure plane inclination.
- 11-95. A conventional triaxial compression (AC) test was conducted on a saturated sample of overconsolidated clay, and the following data, normalized with respect to the effective confining pressure, were obtained.

$\epsilon_{\text{axial}} (\%)$	$\Delta\sigma/\sigma'_c$	$\Delta u/\sigma'_c$
0	0	0
0.5	0.57	+ 0.07
1	0.92	+ 0.05
2	1.36	- 0.03
4	1.77	- 0.22
6	1.97	- 0.35
8	2.10	- 0.46
10	2.17	- 0.52
12	2.23	- 0.58
14	2.28	- 0.62
16	2.33 failure	- 0.67

A lateral extension (LE) test was conducted on an identical specimen of the same clay. While the vertical stress was maintained constant, the cell pressure was decreased until failure occurred at the same principal stress difference as the AC specimen ( $\Delta\sigma/\sigma'_c = 2.33$ ). From your knowledge of stress paths and soil behavior, determine (a) the effective and total stress paths for both tests and (b) the pore pressure versus strain response of the LE test. (c) Can the Mohr-Coulomb strength parameters be determined? Why? (After C. W. Lovell.)

- 11-96. A  $K_0$  consolidated-undrained triaxial compression ( $\sigma_{\text{cell}} = \text{constant}$ ) test was conducted on an undisturbed specimen of sensitive Swedish clay. The initial conditions were as shown in Fig. P11-96a. The stress-strain and pore pressure response of the specimen is shown in Fig. P11-96b.

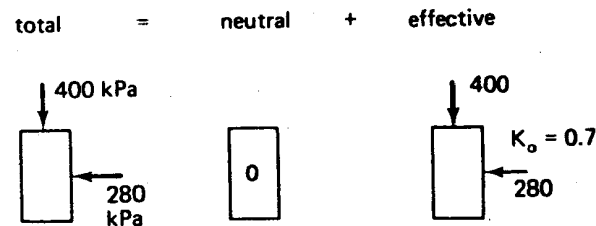


Fig. P11-96a

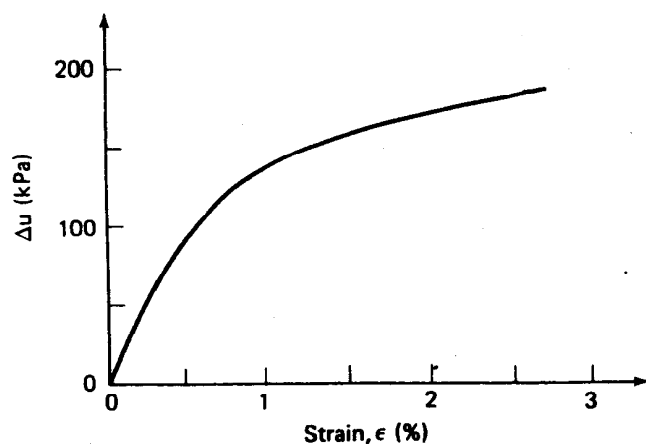
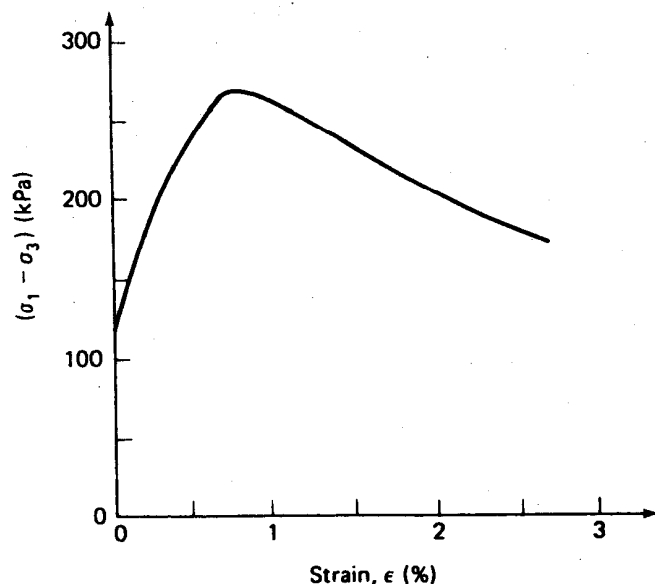


Fig. P11-96b

- (a) Find the stress conditions at failure and symbolically show the total, neutral, and effective stresses (like the "initial conditions" shown above).
- (b) Sketch the total and effective stress paths.
- (c) Plot  $A$  versus  $\epsilon$ . What is  $A_f$ ? What are  $\phi'$  and  $\phi_T$ ?
- 11-97. If an LE test were conducted on a sample of Swedish clay identical to that tested in Problem 11-96, predict the pore pressure versus strain response of the clay. What is  $u_f$  and  $A_f$ ? What is  $\phi_T$ ?
- 11-98. The data shown in Fig. P11-98 were obtained from several CU tests on a saturated clay which has an OCR of 10 and a precon-

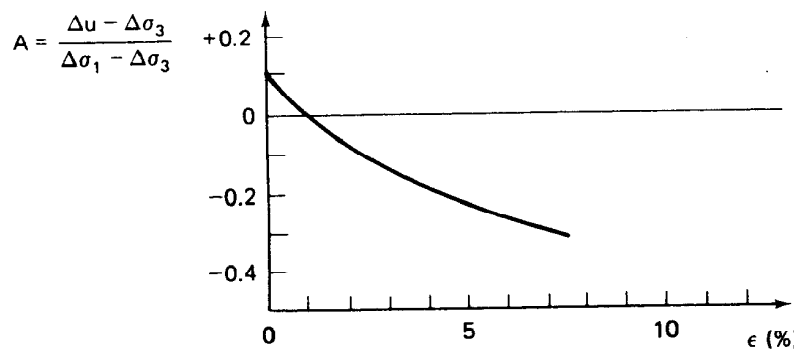
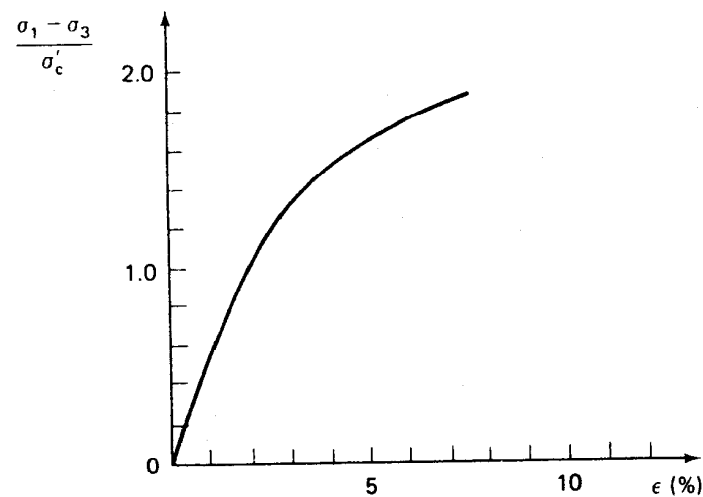


Fig. P11-98

**Problems**

solidation stress of 800 kPa. It is assumed that these results are valid for all compression stress paths on this clay. You are going to run a special stress path test on this clay. After consolidation at  $\sigma'_{vo}$ , the cell pressure will be increased in such a way that  $\Delta\sigma_3 = 0.2\Delta\sigma_1$  until failure occurs. For this special stress path test, fill in the table below and plot the total and effective stress paths. (After C. W. Lovell.)

$\epsilon$ (%)	$\Delta\sigma_1$ (kPa)	$\Delta\sigma_3$ (kPa)	$\sigma_1$ (kPa)	$\sigma_3$ (kPa)	$\Delta u$ (kPa)	$A$
0						
0.5						
2.5						
5.0						
7.5						

- 11-99. A series of CU compression tests on a simple clay (Ladd, 1964) provided the following test results:

$\epsilon_{axial}$ (%)	$2\tau_f/\sigma'_c$	$A$
0	0	—
1	0.35	0.53
2	0.45	0.64
3	0.50	0.72
4	0.52	0.76
6	0.54	0.88
8	0.56	0.92
10	0.57	0.93
12 failure	0.58	0.945

- (a) In an axial compression test, if  $\sigma'_c = 200$  kPa, determine  $q_f$ ,  $p_f$ , and  $p'_f$ . (b) Find  $\phi'$  and  $c'$ . A special lateral extension stress path test was conducted on this clay in which the decrease in lateral stress was exactly equal to the increase in axial stress; that is,  $-\Delta\sigma_3 = \Delta\sigma_1$ . For this case, if  $\sigma'_c = 400$  kPa, determine  $\Delta\sigma_1$ ,  $q$ ,  $p$ ,  $p'$ , and  $\Delta u$  when (c) the axial strain is 4% and (d) at failure. (After C. W. Lovell.)

- 11-100. Figure P11-100 shows normalized data from an axial compression (AC) triaxial test and a lateral compression (LC) triaxial test on saturated simple clay (Ladd, 1964). Make the appropriate calculations, and plot the complete total and effective stress paths for both tests. What are the Mohr-Coulomb strength parameters? Determine  $A_f$  for each test.

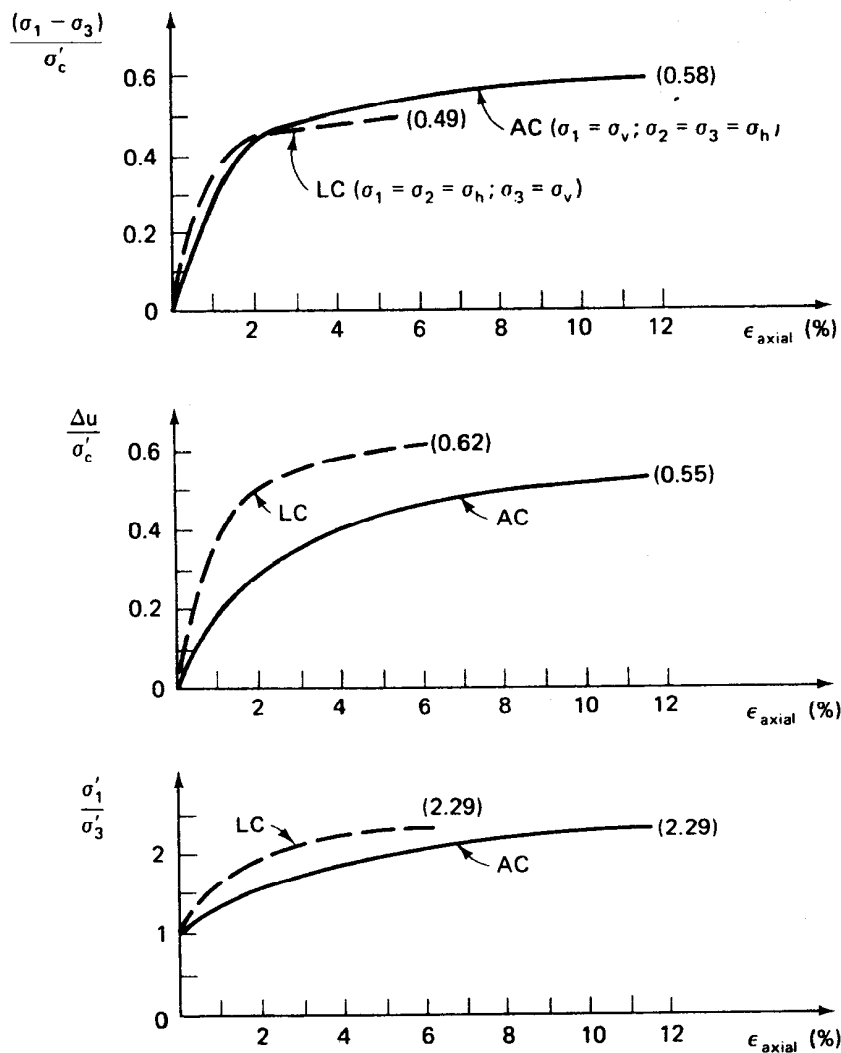
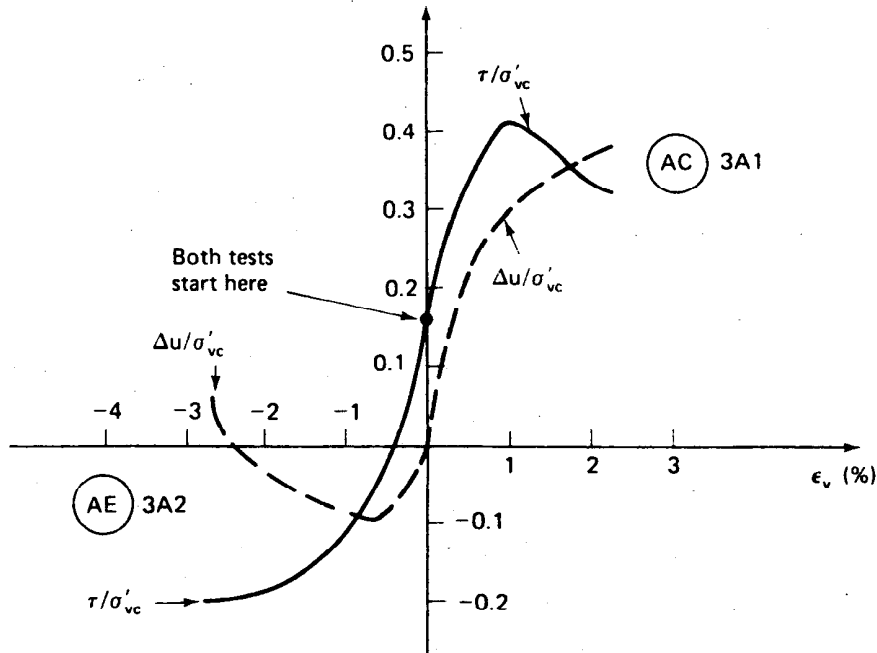


Fig. P11-100

11-101. Two specimens of a soft clay from the Skå-Edeby test field in Sweden were reconsolidated to their initial in situ effective stress conditions and then sheared to failure. One specimen was loaded in axial compression (AC), while the other was failed by axial extension (AE). The normalized stress-strain and pore pressure strain data for both tests are shown in Fig. P11-101 (after Zimmie, 1973). Pertinent specimen data is given in the accompanying table.  
 (a) On a  $p-q$  diagram, sketch the total, total  $- u_o$ , and effective stress paths for both tests. (b) Determine  $\phi'$  and  $\phi_{\text{total}}$  in both



Test	Type	Depth (m)	$\sigma'_{vo}$ (kPa)	LL	PL	$w_n$ (%)	$K_o^*$	OCR
3A1	AC	4.87	30.2	93	29	103.0	0.65	1.07
3A2	AE	5.02	31.0	87	29	84.2	0.65	1.07

\*Assumed.

Note: Tests were conducted with a back pressure of 20 kPa. In situ pore water pressure is approximately 40 kPa.

Fig. P11-101

compression and extension. (c) Calculate the Skempton pore pressure parameter  $A$  at failure for both tests. (d) Show in a sketch the predicted theoretical angles of the failure planes for the two specimens.

- 11-102. Are the values given and calculated for  $K_o$ ,  $\tau_f/\sigma'_{vo}$ ,  $\phi'$ , etc., for the Skå-Edeby clay of Problem 11-101 reasonable in terms of the simple correlations with PI, LI, etc., given in this chapter?
- 11-103. For the oil tank problem in Chapter 8 (Problem 8-46), plot the complete total, total  $- u_o$ , and effective stress paths due to construction and filling of the tank for an element under the centerline of the tank and at the midpoint of the clay layer. Assume that

$K_o$  at the site is 0.7 and that the average value of the  $A$  parameter before failure is 0.4; assume  $A_f = 0.5$ . Make reasonable estimates of the strength parameters, and estimate the factor of safety against failure.

- 11-104. What is the maximum safe height of the embankment for Examples 11.16 and 11.19? Plot a graph of factor of safety versus height of the embankment.
- 11-105. How would you recommend the shear strength be determined for the following design situations? Your answer can include both laboratory and field tests or, in some cases, no tests but some other design approach that may be appropriate. Be as specific as you can.
  - (a) Long-term stability of a compacted clay earth dam.
  - (b) Stability of a hydraulic fill sand dam under seismic loading.
  - (c) End of construction of a compacted clay earthfill dam.
  - (d) Foundation on a soft saturated normally consolidated clay.
  - (e) Shallow foundation on a loose dry sand.
  - (f) End of construction of an excavation in soft normally consolidated clay.
  - (g) Cut slope in an overconsolidated stiff fissured clay.
  - (h) Highway embankment on a stiff fissured clay.

## **appendix a**

---

# **Application of the SI System of Units to Geotechnical Engineering\***

---

### **A.1 INTRODUCTION**

Within the scientific and engineering community, there has always been some confusion as to the proper system of units for physical measurements and quantities. Many systems have been advanced during the last few centuries and some, such as the Imperial or British Engineering system, the so-called "metric system," and a few hybrids, have achieved popular usage. Recently, with the growth of international cooperation and trade, it has become increasingly apparent that one, single, commonly accepted system of units would be not only convenient but also of tremendous practical value.

Although the field of geotechnical engineering may not claim the greatest confusion in the use of units, it undoubtedly ranks near the top of all fields in the number of different systems in common usage. Laboratory engineers, following their counterparts in the physical sciences, have attempted to use some sort of metric system, usually the cgs (centimetre-gram-second) system, for the simple laboratory tests. They, with ease, apply the mks (metre-kilogram-second) system to measurements of pressure and stress in consolidation and triaxial tests, and, with some impunity, they use British Engineering units for compaction tests. As any teacher of soil mechanics can testify, the confusion to the uninitiated is tremendous. At least, practicing geotechnical engineers in North America have been somewhat consistent in the use of the British Engineering system for laboratory and field densities, stress measurements, etc., although they commonly alternate between pounds per square foot, kips per square foot,

\*This appendix has been adapted from an article written by R. D. Holtz at Northwestern University, November 1969. See also Holtz (1980).

tons per square foot, and pounds per square inch, depending on how they or their clients feel about the subject. Fortunately, 1 ton-force/ft<sup>2</sup> is within 2% of 1 kg-force/cm<sup>2</sup>, a common laboratory unit for stress and pressure, and the foundation engineer utilizing consolidation test data can convert directly with small error. Strictly speaking, using force as a basic unit is incorrect; mass should be the basic unit, with force derived according to Newton's second law of motion. Use of the kilogram as a unit of force is one of the difficulties with the so-called "metric system," a modified version of the mks system, which was common among continental European engineers. At least they tried to keep the distinction between mass and force by calling the kilogram-force a *kilopond* (kp).

A modernized version of the metric system has been developed over the past 30 years. The system is known as *SI*, which stands for "Le Système International d'Unités" ("The International System of Units"); it is described in detail in the ASTM (1966) *Metric Practice Guide* and in the *ASTM Standard for Metric Practice* (1980), Designation E 380-79, available in the back of every current ASTM Annual Book of Standards. The system may eventually become the common, and perhaps the only legal, system used in the United States, Canada and a few other countries still using the Imperial or British Engineering system. In fact, Great Britain itself converted completely to SI in 1972, and Australia and New Zealand followed suit shortly thereafter. Most European countries already have de facto conversion to SI, especially in engineering practice.

## A.2 THE SI METRIC SYSTEM

The SI metric system is a fully coherent and rationalized system. It is founded on seven basic units for *length* (metre or meter), *mass* (kilogram), *time* (second), *electric current* (ampere), *thermodynamic temperature* (kelvin), *luminous intensity* (candela), and *amount of substance* (mole). All these basic units have precise definitions, names, and symbols. Units for all other physical quantities can be derived in terms of these basic units. Sometimes the derived quantities are given specific names, such as the *newton* for force and the *watt* for power. The derived unit of force replaces the kilogram-force (kgf) of the mks system, so that the name of the unit indicates that it is a unit of force, not mass. A great advantage is that *one and only one unit exists for each physical quantity*, and all other mechanical quantities such as velocity, force, and work can be derived from the basic units. In addition, the SI units for force, energy, and power are *independent* of the nature of the physical process, whether mechanical, electrical, or chemical.

As previously mentioned, a major advantage of SI is that it is a fully coherent system, which means that a product or quotient of any two unit quantities is a unit of the resulting quantity. For example, unit length squared should be unit area, and unit force should be unit mass times unit acceleration. Obviously, many of the engineering units in common use (for example, acre, lb-force, kg-force) are not coherent units. Also, units which might be related to basic units by powers of 10 are *not* consistent within the SI system. A good example is the litre, or liter, which is a cubic decimetre. The equivalent volume of the litre has been defined as exactly  $10^{-3} \text{ m}^3$  ( $1000 \text{ cm}^3$ ). Additional advantages of SI include the use of unique and well-defined symbols and abbreviations and the convenient decimal relation between multiples and submultiples of the basic units.

In the next two sections of this appendix we describe in detail the SI units of particular interest in geotechnical engineering and present appropriate conversion factors for some of the common mks and British Engineering units. Since you are likely to encounter just about anything in your engineering practice, it is important that you know how to convert between these systems and SI, and that you have some feel for physical quantities in both sets of units.

### A.3 BASIC AND DERIVED SI METRIC UNITS

The three *base units* of interest to geotechnical engineers are *length*, *mass*, and *time*. The SI units for these quantities are the *metre*, m, the *kilogram*, kg, and the *second*, s. Temperature, which might also be of interest, is expressed in *kelvins* (K), although the system does allow for use of the degree Celsius ( $^{\circ}\text{C}$ ), which has the same interval. Electric current is expressed in *amperes* (A). Supplementary units include the *radian* and *steradian*, the units of plane and solid angles, respectively.

As mentioned, these basic SI units have precise physical definitions. For example, contrary to a popular misconception, the metre is *not* the distance between two bars in Paris, but rather it has been defined as exactly equal to a certain number of wavelengths of radiation corresponding to a specific transition level of krypton 86. The standard kilogram is equal to the mass of the international prototype kilogram, a cylinder of platinum-iridium alloy preserved in a vault at Le Bureau International des Poids et Mesures at Sèvres, France. Similar standard kilograms can also be found at the National Bureau of Standards near Washington, D.C. The second has been defined as the duration of a certain number of periods of the radiation corresponding to a specific transition state of cesium 133.

*Derived units* geotechnical engineers use include those listed in Table A-1.

*Prefixes* are used to indicate multiples and submultiples of the basic and derived units. SI prefixes are listed in Table A-2.

The prefixes should be applied to indicate orders of magnitude of the basic or derived units and to reduce redundant zeros so that numerical values lie between 0.1 and 1000. They should *not* be applied to the

**TABLE A-1**

Quantity	Unit	SI Symbol	Formula
acceleration	metre per second squared	$\text{m}/\text{s}^2$	—
area	square metre	$\text{m}^2$	—
area	hectare	ha	$\text{hm}^2 = 10^4 \text{ m}^2$
density	kilogram per cubic metre	$\text{kg}/\text{m}^3$	—
force	newton	N	$\text{kg} \cdot \text{m}/\text{s}^2$
frequency	hertz	Hz	$1/\text{s}$
moment or torque	newton metre	$\text{N} \cdot \text{m}$	$\text{kg} \cdot \text{m}^2/\text{s}^2$
power	watt	W	$\text{J}/\text{s}$
pressure	pascal	Pa	$\text{N}/\text{m}^2$
stress	pascal	Pa	$\text{N}/\text{m}^2$
unit weight	newton per cubic metre	$\text{N}/\text{m}^3$	$\text{kg}/\text{s}^2 \cdot \text{m}^2$
velocity	metre per second	$\text{m}/\text{s}$	—
voltage	volt	V	W/A
volume	cubic metre	$\text{m}^3$	—
volume	litre	L	$\text{dm}^3 = 10^{-3} \text{ m}^3$
work (energy)	joule	J	$\text{N} \cdot \text{m}$

**TABLE A-2**

Factor	Prefix	Symbol
$10^{18}$	exa	E
$10^{15}$	peta	P
$10^{12}$	tera	T
$10^9$	giga	G
$10^6$	mega	M
$10^3$	kilo	k
$10^2$	hecto	h
$10^1$	deka	da
$10^{-1}$	deci	d
$10^{-2}$	centi	c
$10^{-3}$	milli	m
$10^{-6}$	micro	$\mu$
$10^{-9}$	nano	n
$10^{-12}$	pico	p
$10^{-15}$	femto	f
$10^{-18}$	atto	a

*denominator* of compound units (kilogram is an exception since kg is a basic unit in the SI system). Note that *spaces*, not commas, should be used to separate groups of zeros (a concession to the Europeans to persuade them to stop using a comma as a decimal point!).

To maintain the coherence of the system, it is recommended that *only basic units be used to form derived units*. For example, the unit of force, the newton, is derived according to Newton's second law,  $F = Ma$ , where the mass  $M$  is in kilograms and the acceleration  $a$  is in  $\text{m/s}^2$ , all basic units. For derived combinational units such as pressure or stress (pascals or newtons per square metre), multiples and submultiples of the basic metric units (in this case metres) should be avoided. For example,  $\text{N/cm}^2$  and  $\text{N/mm}^2$  are wrong; the appropriate prefix should be used with the numerator to indicate larger or smaller quantities, for example,  $\text{kN/m}^2$  or  $\text{MN/m}^2$  (for kilonewtons per square metre or meganewtons per square metre).

#### A.4 SI UNITS OF INTEREST TO GEOTECHNICAL ENGINEERS AND THEIR CONVERSION FACTORS

**Length.** You should already be familiar with the SI unit for length (the metre, m). (By the way, this is the ASTM recommended spelling.) Useful SI length multiples and submultiples are the kilometre (km), millimetre (mm), micrometre ( $\mu\text{m}$ ), and nanometre (nm). Conversion factors for the common British Engineering and mks systems are:

1 inch, in.	= 25.4 mm = 0.0254 m
1 foot, ft	= 0.3048 m
1 yard, yd	= 0.9144 m
1 mile (U.S. statute)	= $1.609 \times 10^3$ m = 1.609 km
1 mile (nautical)	= $1.852 \times 10^3$ m = 1.852 km
1 angstrom, Å	= $1 \times 10^{-10}$ m = 0.1 nm
1 mil	= $2.54 \times 10^{-5}$ m = 0.0254 mm = 25.4 $\mu\text{m}$

Good SI practice suggests that multiple and submultiple metric units be used in increments of 1000, for example, mm, m, km. Use of the centimetre, especially for lengths under 300 mm, should be avoided.

**Mass.** You may recall from physics that the inertia or mass (SI unit: kilogram, kg) of a physical object is a measure of the property which controls the response of that object to an applied force. It is convenient to measure the mass in terms of the acceleration of an object produced by a unit force, as related by Newton's second law of motion. Thus a unit force causes 1 kg mass to accelerate  $1 \text{ m/s}^2$ . The mass then is an appropriate measure of the amount of matter an object contains. The mass remains the

same even if the object's temperature, shape, or other physical attributes change. Unlike weight, which is discussed later, the mass of an object does not depend on the local gravitational attraction, and thus it is also independent of the object's location in the universe.

Among all the SI units, the kilogram is the only one whose name, for historical reasons, contains a prefix. The names of multiples and submultiples of the kilogram are formed by attaching prefixes to the word *gram* rather than to *kilogram*. In other words,  $10^{-6}$  kg is not a micro-kilogram, but a milligram =  $10^{-3}$  g. Similarly, 1000 kg is not 1 kilo-kilogram but is equivalent to 1 megagram (Mg); 1000 kg is also the metric ton (t), sometimes spelled "tonne" to avoid confusion with the British ton = 2000 lb. ASTM recommends that the metric ton be restricted to commercial usage and that the term *tonne* be avoided altogether. Practical units of mass in engineering practice are the megagram (Mg), the kilogram (kg), and gram (g), the latter two units being primarily used in laboratory work.

Some useful relationships and conversion factors are:

1 pound mass, 1bm (avoirdupois)	= 0.4536 kg
1 British (short) ton = 2000 lbm	= 907.2 kg
1 gram, g	= $10^{-3}$ kg
1 metric ton, t	= $10^3$ kg = $10^6$ g = 1 Mg
1 slug (1 lb-force/ft/s <sup>2</sup> )	= 14.59 kg

**Time.** Although the second (s) is the basic SI time unit, minutes (min), hours (h), days (d), etc., may be used where convenient, even though they are not decimal related. (Maybe some day we will even have a decimal time system; see Carrigan, 1978.)

**Force.** As mentioned, the SI unit of force is derived from  $F = Ma$ , and it is termed the *newton* (N), which is equal to  $1 \text{ kg} \cdot \text{m/s}^2$ . Conversion factors for common engineering force units are:

1 lb-force	= 4.448 N
1 British short ton-force	= $8.896 \times 10^3$ N = 8.896 kN
1 kg-force = 1 kp	= 9.807 N
1 kip = 1000 lb-force	= $4.448 \times 10^3$ N = 4.448 kN
1 metric ton-force = 1000 kg-force	= $9.807 \times 10^3$ N = 9.807 kN
1 dyne (g · cm/s <sup>2</sup> )	= $10^{-5}$ N = 10 $\mu$ N

It is obvious that the numbers in newtons for such items as column loads would be very large indeed and consequently somewhat awkward. Therefore, consistent with the rules for application of prefixes, it is simple to adjust these rather large numbers to more manageable quantities for engineering work. The common prefixes would be kilo ( $10^3$ ), mega ( $10^6$ ), and giga ( $10^9$ ), so that engineering forces would be kilonewtons, kN, meganewtons, MN, and giganewtons, GN. (The symbol for mega is M, to avoid confusion with the symbol for milli, m.) Thus, since 1 ton-force is 8.9 kN, 1000 tons would be 8.9 MN.

Some useful relationships of these prefixes are:

1 kilonewton, kN	$= 10^3$ newton	$= 1000$ N
1 meganewton, MN	$= 10^6$ newton	$= 10^3$ kN $= 1000$ kN
1 giganewton, GN	$= 10^9$ newton	$= 10^5$ kN $= 10^2$ MN $= 100$ MN
3 giganewtons	$= 30$ giganewtons	$= 10^6$ kN $= 10^3$ MN $= 1000$ MN
14.4 giganewtons	$= 1$ grossafiganewtons*	1 boxafiganewtons*

\*This unit is only a constant prior to opening the box.

The correct unit to express the *weight* of an object is the newton since the weight is the gravitational force that causes a downward acceleration of the object. Or, weight  $W$  equals  $Mg$ , where  $M$  is the mass of the object and  $g$  is the acceleration due to gravity. You will recall that the acceleration due to gravity varies with latitude and elevation and, in fact, SI recommends that weight be avoided and that mass be used instead. If weight must be used, it is suggested that the location and gravitational acceleration also be stated. However, for most ordinary engineering purposes, the difference in acceleration (about 0.5%) can be neglected, and as long as we express the weight in newtons, the units will be consistent.

Another problem with weight is that it is commonly used when we really mean the mass of an object. For example, in the laboratory when we "weigh" an object on a laboratory balance, we really are comparing two masses, the mass of the unknown object with objects of known mass. Even scales or balances which displace linear springs are calibrated by using objects of known mass.

Further ambiguity occurs, of course, because common units of mass such as the pound or kilogram are often used in engineering practice as a unit of force. If pound is used as a unit of force, then depending on the resulting accelerations, different mass units are defined. For example, if a 1 lb-force causes an acceleration of  $1 \text{ ft/s}^2$ , then the mass is  $1 \text{ lb-force} \cdot \text{s}^2/\text{ft}$ , which is called a *slug*. In other words,  $1 \text{ lb-force} = 1 \text{ slug} \times 1 \text{ ft/s}^2$ . Using slugs as units of mass avoids the confusion with pounds-mass, and this unit has been commonly used in aerodynamics and fluid mechanics.

If we wanted to use instead a pound-mass system, we could define a unit of force called the *poundal*, where  $1 \text{ poundal} = 1 \text{ lbm} \times 1 \text{ ft/s}^2$ . Poundals are apparently used only in physics books.

### EXAMPLE A.1

Given:

A force of 1 lb acts on an object weighing 1 lb.

**Required:**

Find the resulting acceleration.

**Solution:**

From Newton's second law,

$$F = Ma = \left( \frac{W}{g} \right) a$$

or

$$a = \frac{Fg}{W} = \frac{(1 \text{ lbf})(32.17 \text{ ft/s}^2)}{1 \text{ lbf}} = 32.17 \text{ ft/s}^2$$

### EXAMPLE A.2

**Given:**

The object in Example A.1, which weighs 1 lbf.

**Required:**

Find its mass when a 1 lbf causes an acceleration of 1 ft/s<sup>2</sup>.

**Solution:**

$$F = Ma = \left( \frac{W}{g} \right) a$$

or

$$M = \frac{W}{g} = \frac{1 \text{ lbf}}{32.17 \text{ ft/s}^2} = 0.031 \frac{\text{lbf} \cdot \text{s}^2}{\text{ft}} = 0.031 \text{ slug}$$

### EXAMPLE A.3

**Given:**

Neil Armstrong weighs 150 lb on earth.

#### A.4 SI Units of Interest to Geotechnical Engineers and Their Conversion Factors 673

**Required:**

How much does he weigh on the surface of the moon?

**Solution:**

First, we have to calculate Mr. Armstrong's mass on earth. Unless he had health problems during the voyage, his mass will be the same on the moon.

$$M = \frac{W}{g} = \frac{150 \text{ lbf}}{32.17 \text{ ft/s}^2} = 4.66 \frac{\text{lbf} \cdot \text{s}^2}{\text{ft}}, \text{ or } 4.66 \text{ slugs}$$

Since 1 slug = 14.59 kg, his mass is 68.03 kg. Another way to calculate his mass is to convert his weight to newtons; then divide by  $g$ .

$$W = 150 \text{ lbf} \left( \frac{4.448 \text{ N}}{1 \text{ lbf}} \right) = 667.20 \text{ N or } 667.2 \frac{\text{kg} \cdot \text{m}}{\text{s}^2}$$

$$M = \frac{W}{g} = \frac{667.2 \text{ kg} \cdot \text{m/s}^2}{9.807 \text{ m/s}^2} = 68.03 \text{ kg}$$

Next, we have to either ask an astronomer or look up in the *Handbook of Chemistry and Physics* (1977) or some other reference the gravitational acceleration on the surface of the moon. We find that  $g_{\text{moon}} = 1.67 \text{ m/s}^2$ . Thus,

$$W_{\text{moon}} = Mg_{\text{moon}} = 68.03 \text{ kg} (1.67 \text{ m/s}^2) = 113.62 \text{ N}$$

Or, since 4.448 N = 1 lbf,

$$W_{\text{moon}} = 113.62 \text{ N} \left( \frac{1 \text{ lbf}}{4.448 \text{ N}} \right) = 25.54 \text{ lbf}$$

Check: On earth,  $667 \text{ N} \left( \frac{1.67}{9.81} \right) = 113.6 \text{ N}$  on the moon.

---

See how confusing the old British Engineering system can be? However, if you think this is bad, wait until you try to convert densities and unit weights!

**Stress and Pressure.** The SI unit for stress and pressure is the *pascal* (Pa), which is exactly equal to 1 newton per square metre ( $\text{N/m}^2$ ).

There has been some objection, especially in Europe, to the use of the pascal as the basic unit of stress and pressure because it is so small. The Germans and French, for example, often use the *bar*, which is exactly  $10^5$  Pa. However the pascal is more logical since it is a coherent unit; that is,

equations involving the pascal with other SI units can be written without coefficients of proportionality being required.

Conversion factors for some common engineering units are:

1 psi (lb-force/in. <sup>2</sup> )	= $6.895 \times 10^3$ Pa or 6.895 kPa
1 atm at STP*	= $1.013 \times 10^5$ Pa or 101.3 kPa
1 kg-force/cm <sup>2</sup>	= $9.807 \times 10^4$ Pa or 98.07 kPa
1 metric ton-force/m <sup>2</sup>	= $9.807 \times 10^3$ Pa or 9.807 kPa
1 bar	= $1 \times 10^5$ Pa or 100 kPa
1 ksi (kip/in. <sup>2</sup> )	= $6.895 \times 10^6$ Pa or 6.895 MPa
1 British ton-force/ft <sup>2</sup>	= $95.76 \times 10^3$ Pa or 95.76 kPa
1 lb-force/ft <sup>2</sup>	= 47.88 Pa

\*Standard temperature and pressure, not a motor oil additive or Soil Test Probe.

It is obvious that the pascal is a small unit, but as with SI force units, it is easy to add prefixes to make the large numbers more manageable. Thus, 1 psi in the above table is more conveniently expressed as 6.9 kPa ( $\text{kN}/\text{m}^2$ ) than as  $6.9 \times 10^3$  Pa. For ordinary triaxial testing of soils, for example, hydrostatic cell pressures rarely exceed 200 or 300 psi (1379 or 2068 kPa). Or, if all the pressures in a test series are in this range, it might be convenient to use 1.4 or 2.1 MPa. And, as with other systems of units, a rounded or even interval may be more convenient; for example, in this case, 1.5 and 2.0 MPa.

Similar examples could be given for engineering stresses. Either kilopascals or megapascals, kPa or MPa, or kilo- or meganewtons per square metre,  $\text{kN}/\text{m}^2$  or  $\text{MN}/\text{m}^2$ , will become commonly used for foundation stresses, lateral earth pressures, allowable bearing values, etc. In the laboratory, force is measured by a proving ring or load cell and then converted to stress (for example, in the unconfined compression or direct shear tests), so the computational process will be no more complicated than it is now. Similarly, with electrical pressure transducers, a calibration factor must be used to convert millivolts (mV) output to pressure in whatever units are used.

A convenient approximation, part of which is already in use in geotechnical engineering practice, is the following:

$$\begin{aligned} 1 \text{ British (short) ton-force/ft}^2 &\approx 1 \text{ kg-force/cm}^2 \approx 1 \text{ atmosphere} \\ &= 10 \text{ metric ton-force/m}^2 \approx 100 \text{ kPa} = 100 \text{ kN/m}^2 \end{aligned}$$

The error involved is between 2% and 4%, which is certainly less than ordinary engineering accuracy requirements.

#### EXAMPLE A.4

Given:

The pressure or stress is 100 kPa.

**A.4 SI Units of Interest to Geotechnical Engineers and Their Conversion Factors 675**

**Required:**

Convert this pressure or stress to (a) psi (lb-force/in<sup>2</sup>), (b) ksi (kips/in<sup>2</sup>), (c) tsf (British ton-force/ft<sup>2</sup>), (d) kg-force/cm<sup>2</sup>, (e) bar, (f) metric ton-force/m<sup>2</sup>, (g) mm of mercury, (h) ft of water, and (i) m of water.

**Solution:**

A simple way to convert from one set of units to another is to set up an equation with the equivalents in either the numerator or denominator of the equation so that the appropriate cancellations occur.

$$\begin{aligned} \text{a. } p &= 100 \text{ kPa} = 100 \frac{\text{kN}}{\text{m}^2} \left( \frac{1 \text{ lbf}}{4.448 \text{ N}} \right) \left( \frac{1000 \text{ N}}{\text{kN}} \right) \left( \frac{0.0254 \text{ m}}{1 \text{ in.}} \right)^2 \\ &= 14.5 \text{ psi} \end{aligned}$$

Note: The exact conversion value is 14.503 773 77 kN/m<sup>2</sup>, which comes about if you use the exact value for 1 lbf = 4.448 221 615 260 5 N. 1 in. is exactly equal to 0.0254 m.

$$\begin{aligned} \text{b. } p &= 100 \text{ kPa} \\ &= 100 \frac{\text{kN}}{\text{m}^2} \left( \frac{1 \text{ lbf}}{4.448 \text{ N}} \right) \left( \frac{1000 \text{ N}}{\text{kN}} \right) \left( \frac{1 \text{ kip}}{1000 \text{ lbf}} \right) \left( \frac{0.0254 \text{ m}}{1 \text{ in.}} \right)^2 \\ &= 0.0145 \text{ ksi} \end{aligned}$$

Again, as in part (a), the exact conversion value is slightly different.

$$\begin{aligned} \text{c. } p &= 100 \text{ kPa} \\ &= 100 \frac{\text{kN}}{\text{m}^2} \left( \frac{1 \text{ lbf}}{4.448 \text{ N}} \right) \left( \frac{1000 \text{ N}}{\text{kN}} \right) \left( \frac{1 \text{ tonf}}{2000 \text{ lbf}} \right) \left( \frac{0.3048 \text{ m}}{1 \text{ ft}} \right)^2 \\ &= 1.04 \text{ tonf / ft}^2 \end{aligned}$$

$$\begin{aligned} \text{d. } p &= 100 \text{ kPa} = 100 \frac{\text{kN}}{\text{m}^2} \left( \frac{1 \text{ lbf}}{9.807 \text{ N}} \right) \left( \frac{1000 \text{ N}}{\text{kN}} \right) \left( \frac{\text{m}}{100 \text{ cm}} \right)^2 \\ &= 1.02 \text{ kgf/cm}^2 \end{aligned}$$

Note: The exact conversion for kgf to N is 9.806 65.

$$\text{e. } p = 100 \text{ kPa} = 100 \text{ kPa} \left( \frac{1 \text{ bar}}{10^5 \text{ Pa}} \right) \left( \frac{10^3 \text{ Pa}}{1 \text{ kPa}} \right) = 1 \text{ bar}$$

$$\begin{aligned} \text{f. } p &= 100 \text{ kPa} = 100 \frac{\text{kN}}{\text{m}^2} \left( \frac{1 \text{ kgf}}{9.807 \text{ N}} \right) \left( \frac{1000 \text{ N}}{\text{kN}} \right) \left( \frac{1 \text{ tonf}}{1000 \text{ kgf}} \right) \\ &= 10.2 \text{ metric tonf/m}^2 \end{aligned}$$

g. For  $p$  in mm of mercury, we need to remember or look up the density of Hg. It is 13.6 g/cm<sup>3</sup>. Also recall from hydrostatics that  $p = \gamma z$

$= \rho g z$ , where  $z$  is the depth of the fluid. Thus for pressure in cm of mercury,  $z = p/\rho g$ . So

$$\begin{aligned} z &= 100 \frac{\text{kN}}{\text{m}^2} \left( \frac{1000 \text{ N}}{\text{kN}} \right) \left( \frac{\text{cm}^3}{13.6 \text{ g}} \right) \left( \frac{1000 \text{ g}}{\text{kg}} \right) \left( \frac{\text{m}}{100 \text{ cm}} \right)^3 \\ &\quad \cdot \left( \frac{\text{s}^2}{9.807 \text{ m}} \right) \left( \frac{1000 \text{ mm}}{\text{m}} \right) \\ &= 750 \text{ mm Hg} \end{aligned}$$

h. Again, use  $z = p/\rho g$

$$\begin{aligned} z &= 100 \frac{\text{kN}}{\text{m}^2} \left( \frac{1000 \text{ N}}{\text{kN}} \right) \left( \frac{\text{m}^3}{1000 \text{ kg}} \right) \left( \frac{\text{s}^2}{9.807 \text{ m}} \right) \left( \frac{1 \text{ ft}}{0.3048 \text{ m}} \right) \\ &= 33.5 \text{ ft of water} \end{aligned}$$

$$\begin{aligned} \text{i. } z &= 100 \frac{\text{kN}}{\text{m}^2} \left( \frac{1000 \text{ N}}{\text{kN}} \right) \left( \frac{\text{m}^3}{1000 \text{ kg}} \right) \left( \frac{\text{s}^2}{9.807 \text{ m}} \right) \\ &= 10.2 \text{ m of water} \end{aligned}$$

**Density and Unit Weight.** Density is defined as mass per unit volume. Its units in the SI metric system are kilograms per cubic metre,  $\text{kg}/\text{m}^3$ . In many cases, it may be more convenient to express density in megagrams per cubic metre,  $\text{Mg}/\text{m}^3$ . Conversions from the common laboratory and field densities are:

$$\begin{aligned} 1 \text{ lb-mass}/\text{ft}^3 &= 16.018 \text{ kg}/\text{m}^3 \\ 1 \text{ g}/\text{cm}^3 &= 10^3 \text{ kg}/\text{m}^3 = 1 \text{ Mg}/\text{m}^3 = 1 \text{ t}/\text{m}^3 \end{aligned}$$

You will recall that the density of water,  $\rho_w$ , is exactly  $1.000 \text{ g}/\text{cm}^3$  at  $4^\circ\text{C}$ , and the variation is relatively small over the range of temperatures encountered in ordinary engineering practice. Therefore it is usually sufficiently accurate to take  $\rho_w = 10^3 \text{ kg}/\text{m}^3 = 1 \text{ Mg}/\text{m}^3$ , which simplifies phase computations considerably. It is also useful to know that  $1000 \text{ kg}/\text{m}^3$  is equal to  $62.4 \text{ lb-mass}/\text{ft}^3$ .

Typical densities that might be encountered in geotechnical practice are  $1.2 \text{ Mg}/\text{m}^3$  ( $74.8 \text{ lb}/\text{ft}^3$ ),  $1.6 \text{ Mg}/\text{m}^3$  ( $100 \text{ lb}/\text{ft}^3$ ), and  $2.0 \text{ Mg}/\text{m}^3$  ( $125 \text{ lb}/\text{ft}^3$ ). Ranges of different densities are also listed in Table 2-1. The commonly used density for concrete,  $150 \text{ lb}/\text{ft}^3$ , is almost exactly  $2.4 \text{ Mg}/\text{m}^3$ .

You should note that all mass and volume ratios common in geotechnical engineering practice are not affected by the use of SI units. For example, void ratio or water content of any given soil still has the same numerical value.

#### A.4 SI Units of Interest to Geotechnical Engineers and Their Conversion Factors 677

Unit weight or weight per unit volume is still the common measurement in geotechnical engineering practice. However, since weight should be avoided in technical work for all the reasons discussed earlier, then unit weight also should be avoided. ASTM now recommends that density be used in place of unit weight. If you must convert from density to unit weight, then simply use  $\gamma = \rho g$ , which means you will have to consider the appropriate value for the acceleration due to gravity. The "standard" value of  $g$  is  $9.807 \text{ m/s}^2$  ( $32.17 \text{ ft/s}^2$ ), which as mentioned previously, can be used with sufficient accuracy for ordinary engineering work for most places on this earth. If you ever have a job on the moon or some other planet, then you must use the local value for  $g$ . Keep in mind, also, to be very careful which "pounds" you are working with, lbf or lbm, in these conversions.

---

#### EXAMPLE A.5

Given:

The density of water is  $1000 \text{ kg/m}^3$ .

Required:

The density of water in (a)  $\text{g/cm}^3$  and (b)  $\text{lb/ft}^3$ .

Solution:

Set up an equation as follows:

$$\text{a. } 1000 \frac{\text{kg}}{\text{m}^3} = 1000 \frac{\text{kg}}{\text{m}^3} \left( \frac{1000 \text{ g}}{1 \text{ kg}} \right) \left( \frac{1 \text{ m}}{100 \text{ cm}} \right)^3 = 1 \frac{\text{g}}{\text{cm}^3}$$

$$\begin{aligned} \text{b. } 1000 \frac{\text{kg}}{\text{m}^3} &= 1000 \frac{\text{kg}}{\text{m}^3} \left( \frac{1 \text{ lbm}}{0.4536 \text{ kg}} \right) \left( \frac{0.3048 \text{ m}}{1 \text{ ft}} \right) \\ &= 62.43 \frac{\text{lbm}}{\text{ft}^3} \end{aligned}$$

Another way to do part b is to recall that  $1 \text{ lbm/ft}^3 = 16.018 \text{ kg/m}^3$ ; so

$$\begin{aligned} 1000 \frac{\text{kg}}{\text{m}^3} &= 1000 \frac{\text{kg}}{\text{m}^3} \left( \frac{1 \text{ lbm/ft}^3}{16.018 \text{ kg/m}^3} \right) \\ &= 62.43 \frac{\text{lbm}}{\text{ft}^3} \end{aligned}$$

---

## EXAMPLE A.6

**Given:**

Density of water,  $\rho_w = 1000 \text{ kg/m}^3$ .

**Required:**

Convert this density to unit weight in (a) SI and (b) British Engineering units.

**Solution:**

a. *SI units:* We know that  $\gamma = \rho g$ ; so

$$\gamma = 1000 \frac{\text{kg}}{\text{m}^3} \left( 9.807 \frac{\text{m}}{\text{s}^2} \right) = 9807 \frac{\text{kg} \cdot \text{m}}{\text{m}^3 \cdot \text{s}^2}$$

Recall that  $1 \text{ N} = 1 \frac{\text{kg} \cdot \text{m}}{\text{s}^2}$

$$\therefore \gamma = 9807 \frac{\text{N}}{\text{m}^3} = 9.807 \frac{\text{kN}}{\text{m}^3}$$

b. *British Engineering units:* From Example A.5, we know that

$$1000 \frac{\text{kg}}{\text{m}^3} = 62.43 \frac{\text{lbf}}{\text{ft}^3}$$

$$\gamma = 62.43 \frac{\text{lbf}}{\text{ft}^3} \left( 32.17 \frac{\text{ft}}{\text{s}^2} \right) = 2008 \frac{\text{lbf} \cdot \text{ft}}{\text{s}^2 \cdot \text{ft}^3}$$

If lbf are used, from part a.,

$$\begin{aligned} \gamma &= 9.8 \frac{\text{kN}}{\text{m}^3} \left( \frac{1000 \text{ N}}{1 \text{ kN}} \right) \left( \frac{1 \text{ lbf}}{4.448 \text{ N}} \right) \left( \frac{0.3048 \text{ m}}{1 \text{ ft}} \right)^3 \\ &= 62.4 \frac{\text{lbf}}{\text{ft}^3} \end{aligned}$$

This is the commonly used value for the unit weight of water.

---

## EXAMPLE A.7

**Given:**

A soil has a dry density of  $1.7 \text{ Mg/m}^3$ .

**A.4 SI Units of Interest to Geotechnical Engineers and Their Conversion Factors 679**

**Required:**

Convert this density into unit weights, in terms of both (a) SI and (b) British Engineering units.

**Solution:**

a. *SI units:*

$$\rho_d = 1.7 \text{ Mg/m}^3 = 1700 \text{ kg/m}^3$$

$$\gamma = \rho g$$

$$\gamma = 1700 \frac{\text{kg}}{\text{m}^3} \left( 9.81 \frac{\text{m}}{\text{s}^2} \right) = 16677 \frac{\text{N}}{\text{m}^3} = 16.7 \frac{\text{kN}}{\text{m}^3}$$

b. *British Engineering units*, in terms of lbm:

$$\rho = 1700 \frac{\text{kg}}{\text{m}^3} \left( \frac{1 \text{ lbm}/\text{ft}^3}{16.018 \text{ kg/m}^3} \right) = 106.13 \frac{\text{lbm}}{\text{ft}^3}$$

$$\gamma = \rho g$$

$$\gamma = 106.13 \frac{\text{lbm}}{\text{ft}^3} \left( 32.17 \frac{\text{ft}}{\text{s}^2} \right) = 3414 \frac{\text{lbm} \cdot \text{ft}}{\text{s}^2 \cdot \text{ft}^3}$$

In terms of lbf: From part (a),

$$\begin{aligned} \gamma &= 16.7 \frac{\text{kN}}{\text{m}^3} \left( \frac{1000 \text{ N}}{1 \text{ kN}} \right) \left( \frac{1 \text{ lbf}}{4.448 \text{ N}} \right) \left( \frac{0.3048 \text{ m}}{1 \text{ ft}} \right)^3 \\ &= 106.3 \text{ lbf}/\text{ft}^3 \end{aligned}$$

The latter value in terms of lbf is, of course, the more familiar figure.

**Geostatic Stress.** For computations of geostatic stresses, the unit weights of the various soil layers can be easily replaced by the  $\rho g$  of the layers. The usual formula

$$\sigma_v = \sum_{i=1}^n \gamma_i z_i$$

then becomes

$$\sigma_v = \sum_{i=1}^n \rho_i g z_i \quad (7-14c)$$

where  $\sigma_v$  = total vertical stress at some depth,

$\rho_i$  = density of each layer,

$z_i$  = thickness of each layer, and

$g$  = acceleration of gravity.

If  $\rho g$  is a constant throughout the depth  $h$ , then

$$\sigma_v = \rho gh \quad (7-14b)$$

By analogy, computation of the static pore water pressure  $u_o$  at some depth  $h_w$  below the ground water table is

$$u_o = \rho_w g h_w \quad (7-15)$$

where  $\rho_w$  = the density of water ( $1 \text{ Mg/m}^3$ ).

Similarly, to obtain the effective vertical overburden stress, the effective or buoyant density  $\rho'$  for each layer below the ground water table can be used or, perhaps more simply,  $\sigma'_{vo} = \sigma_{vo} - u_o$ .

Dimensional analysis of these equations for stress shows that if the densities are expressed in  $\text{Mg/m}^3$ , then stresses automatically result in kPa, or

$$\left( \frac{\text{Mg}}{\text{m}^3} \right) \left( \frac{\text{m}}{\text{s}^2} \right) \text{m} = 1000 \frac{\text{kg} \cdot \text{m}}{\text{s}^2 \cdot \text{m}^2} = 1000 \frac{\text{N}}{\text{m}^2} = 1 \text{ kPa}$$

Several examples of geostatic stress computations using SI units can be found in Chapter 7.

## appendix b-1

### **Derivation of Laplace's Equation\***

As mentioned in Sec. 7.9, a flow net is actually a graphical solution of Laplace's equation, Eq. 7-24. The assumptions necessary for the derivation of this equation are:

$S = 100\%$

$e = \text{constant}$  [i.e., no consolidation (Chapter 8) or compression of the medium occurs]

$k$  is isotropic

Darcy's law (Eq. 7-5) is valid

Consider the flow of water into an element with dimensions  $dx$  and  $dy$  (Fig. B-1.1). Two-dimensional flow is assumed here for simplicity; you could do the exact same thing in three dimensions, but it would just be more complicated. The term  $(\partial v_x / \partial x) dx$  indicates the rate of change in velocity  $v_x$  in the  $x$ -direction; similarly,  $(\partial v_y / \partial y) dy$  is the rate of change in  $v_y$  in the  $y$ -direction. From continuity, we know that  $q = \text{constant} = VA_{\text{in}} = VA_{\text{out}}$ . So

$$VA_{\text{in}} = v_x dy + v_y dx$$

$$VA_{\text{out}} = \left( v_x + \frac{\partial v_x}{\partial x} dx \right) dy + \left( v_y + \frac{\partial v_y}{\partial y} dy \right) dx$$

If we set these two equations equal, we get

$$\frac{\partial v_x}{\partial x} dx dy + \frac{\partial v_y}{\partial y} dx dy = 0$$

\*Chapter 7.

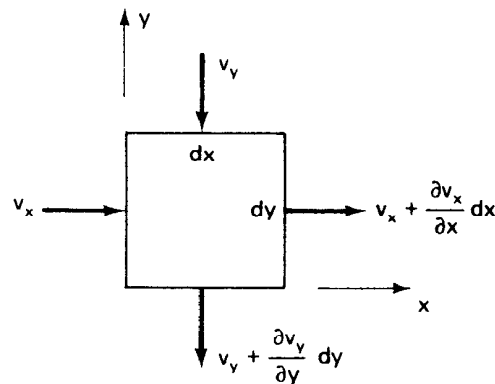


Fig. B-1.1 Flow into and out of an element  $dx$  by  $dy$ .

or

$$\frac{\partial v_x}{\partial x} + \frac{\partial v_y}{\partial y} = 0 \quad (\text{B-1-1})$$

since  $dx$  and  $dy$  cannot be zero.

From Darcy's law (Eqs. 7-2 and 7-5),  $v = ki = k\Delta h/L$ . Thus we can write for our element:

$$v_x = k_x \frac{\partial h}{\partial x}, \quad v_y = k_y \frac{\partial h}{\partial y}$$

Substituting these terms into Eq. B-1-1 we obtain

$$k_x \frac{\partial^2 h}{\partial x^2} + k_y \frac{\partial^2 h}{\partial y^2} = 0$$

Since  $k$  was assumed to be isotropic,  $k_x = k_y$ . So we have

$$\frac{\partial^2 h}{\partial x^2} + \frac{\partial^2 h}{\partial y^2} = 0 \quad (7-24)$$

which is *Laplace's equation in two dimensions*. For the equation in three dimensions, simply add the term  $\partial^2 h / \partial z^2$  to Eq. 7-24.

## **appendix b-2**

---

# **Derivation and Solution of Terzaghi's One-Dimensional Consolidation Theory\***

---

### **B-2.1 ASSUMPTIONS**

To develop the Terzaghi one-dimensional consolidation theory, we need to assume the following:

1. The clay is homogeneous and 100% saturated.
2. Drainage is provided at both the top and bottom of the compressible layer.
3. Darcy's law (Eq. 7-5) is valid.
4. The soil grains and water are incompressible.
5. Compression and flow are one dimensional.
6. The small load increment applied produces essentially no change in thickness (that is, small strains), and  $k$  and  $a_v$  remain constant.
7. There is a *unique* linear relationship between the volume change  $\Delta e$  and the effective stress  $\Delta \sigma'$ . In other words,  $de = -a_v d\sigma'$  and  $a_v$  is assumed constant over the increment of applied stress. This important assumption also implies that there is *no secondary compression*.

### **B-2.2 DERIVATION**

Now let us borrow a little element from Fig. 9.1 f and enlarge it in Fig. B-2.1. Our element exists at a depth  $z$  below the top of the compressible layer, has thickness  $dz$ , and has an area  $dx$  times  $dy$ . The volume change of the element is the difference between the amount of flow in and

\*Chapter 9.

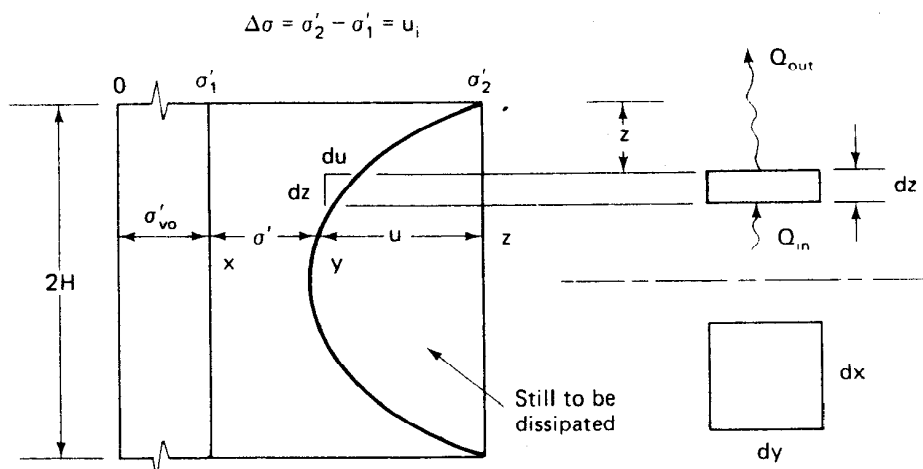


Fig. B-2.1 Soil layer undergoing compression, similar to Fig. 9.1f.

out of the element. Since consolidation under these conditions is directly dependent on the escape of pore water from the soil voids, we may develop the consolidation equation by considering the continuity of flow in our element. The hydraulic gradient  $i_z$  at the top of our element is given by

$$i_z = \frac{\text{head loss}}{\text{distance}} = \frac{\partial}{\partial z} \left( \frac{u}{\rho_w g} \right) = \frac{1}{\rho_w g} \frac{\partial u}{\partial z} \quad (\text{B-2-1})$$

The corresponding hydraulic gradient at the bottom of our element  $dz$  is given by

$$i_{z+dz} = \frac{1}{\rho_w g} \frac{\partial u}{\partial z} + \frac{1}{\rho_w g} \frac{\partial^2 u}{\partial z^2} dz \quad (\text{B-2-2})$$

From Darcy's law,  $dQ = k i_a dt$ , we may compute the quantity of flow  $dQ$  in time  $dt$  out of the top of our element by

$$dQ_{\text{out}} = k \frac{1}{\rho_w g} \frac{\partial u}{\partial z} dz dx dy dt \quad (\text{B-2-3})$$

Likewise we may compute the quantity of flow in time  $dt$  at the bottom into the element by

$$dQ_{\text{in}} = k \frac{1}{\rho_w g} \left( \frac{\partial u}{\partial z} + \frac{\partial^2 u}{\partial z^2} \right) dz dx dy dt \quad (\text{B-2-4})$$

We can now compute the volume change from the difference in rates of flow,  $Q_{\text{out}} - Q_{\text{in}}$ . Also we assume the area  $dx dy$  to be a unit area. Therefore

$$\text{volume change} = dQ_{\text{out}} - dQ_{\text{in}} = - \frac{k}{\rho_w g} \frac{\partial^2 u}{\partial z^2} dz dt \quad (\text{B-2-5})$$

The volume change may also be determined from the laboratory oedometer test. Remember, from Chapter 8, that we would obtain a laboratory curve similar to Fig. 8.4, which we again show as Fig. B-2.2. From Eqs. 8-5a and b, the coefficient of compressibility  $a_v$  is

$$a_v = -\frac{de}{d\sigma'} = \frac{e_1 - e_2}{\sigma'_2 - \sigma'_1} \quad (\text{B-2-6})$$

To be correct, we should write these equations in terms of effective stresses. From Fig. B-2.2, you can see that the slope of the  $e-\sigma'$  curve is negative, and you know that  $e_1$  is numerically larger than  $e_2$ .

From Eq. 8-4,  $s = \Delta e H_o / (1 + e_o)$ , or in terms of our element in Fig. B-2.1 and the  $e-\sigma'$  relationship in Fig. B-2.2, we obtain

$$s = \Delta dz = \frac{-de}{1 + e_1} dz \quad (\text{B-2-7})$$

where  $e_1$  corresponds to the initial void ratio  $e_o$ . From Eq. B-2-6,  $-de = a_v d\sigma'$ . Therefore

$$\Delta dz = \frac{a_v d\sigma'}{1 + e_1} dz \quad (\text{B-2-8})$$

Now, from our discussion in Chapter 9, we know that as the excess pore

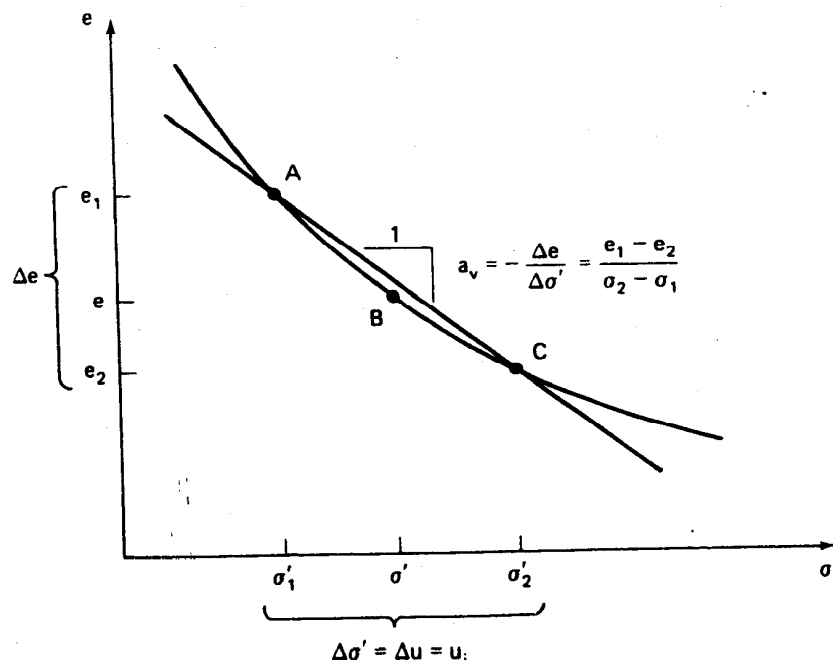


Fig. B-2.2 Laboratory compression curve (same as Fig. 9.2).

water pressure dissipates, the effective stress in the soil skeleton increases. This is shown schematically in Figs. 9.1c and f. Thus we can write that  $\Delta\sigma' = -\Delta u$ , because any *change* in effective stress is numerically equal to the negative of the change in excess pore water pressure. This relationship is true, of course, as long as the total stress does not change. Now, Eq. B-2-8 can be written as

$$\Delta dz = - \frac{a_v du}{1 + e_1} dz \quad (\text{B-2-9})$$

and since  $du = (\partial u / \partial t) dt$ , Eq. B-2-9 becomes

$$\Delta dz = - \frac{a_v}{1 + e_1} \frac{\partial u}{\partial t} dt dz \quad (\text{B-2-10})$$

By equating the volume change obtained in Eq. B-2-5 and the volume change in Eq. B-2-10, we have

$$-\frac{k}{\rho_w g} \frac{\partial^2 u}{\partial z^2} dz dt = - \frac{a_v}{1 + e_1} \frac{\partial u}{\partial t} dt dz \quad (\text{B-2-11})$$

We can collect the soil properties terms as in Eq. 9-3,

$$c_v = \frac{k}{\rho_w g} \frac{1 + e_1}{a_v} \quad (9-3)$$

where  $c_v$  is called the *coefficient of consolidation* since it governs the consolidation process. Note that it has units of  $L^2 T^{-1}$ . We thus obtain

$$c_v \frac{\partial^2 u}{\partial z^2} = \frac{\partial u}{\partial t} \quad (9-2)$$

Equation 9-2 is the Terzaghi *one-dimensional consolidation equation*. If we assume  $c_v$  is a constant with respect to time and position, then Eq. 9-2 is a second-order partial differential equation with constant coefficients. There are a variety of ways to solve such equations; some are mathematically exact, others are only approximate. For example, Harr (1966) presents an approximate solution using the method of finite differences. Taylor (1948), following Terzaghi (1925), provides a mathematically rigorous solution in terms of a Fourier series expansion. The development that follows is adapted from Taylor (1948) and Leonards (1962).

### B-2.3 MATHEMATICAL SOLUTION

The boundary and initial conditions for the case of one-dimensional consolidation are as follows:

1. There is complete drainage at the top and bottom of the compressible layer.

2. The initial *excess* hydrostatic pressure  $\Delta u = u_i$  is equal to the applied increment of stress at the boundary,  $\Delta\sigma$ .

These boundary and initial conditions can be written

when  $z = 0$  and when  $z = 2H$ ,  $u = 0$

when  $t = 0$ ,  $u = u_i = \Delta\sigma = (\sigma'_2 - \sigma'_1)$

The general solution of Eq. 9-2, when the initial excess pore pressure  $u_i$  is a function of the depth  $z$ , is

$$u = \sum_{n=1}^{n=\infty} \left( \frac{1}{H} \int_{z=0}^{z=2H} u_i \sin \frac{n\pi z}{2H} dz \right) \sin \frac{n\pi z}{2H} \exp \left( \frac{-c_v t n^2 \pi^2}{4H^2} \right) \quad (B-2-12)$$

When  $u_i$  is a constant or varies linearly with depth, the solution becomes

$$u = (\sigma'_2 - \sigma'_1) \sum_{n=0}^{\infty} \frac{4}{(2n+1)\pi} \sin \left( \frac{2n+1}{2} \pi \frac{z}{H} \right) \times \exp \left[ - \left( \frac{(2n+1)^2}{4} \pi^2 \frac{k(1+e_0)}{\underbrace{a_v \rho_w g}_{c_v}} \frac{t}{H^2} \right) \underbrace{T}_{Z} \right] \quad (B-2-13)$$

where  $\sigma'_1$  = initial effective stress,  $\sigma'_2 = \sigma'_1 + \Delta\sigma$ , and  $n = 0, 1, 2, 3, \dots$ . The solution provides the instantaneous value of the pore water pressure  $u$  at any specified time and point in the soil mass. The only part of Eq. B-2-13 that is a function of the soil properties is  $c_v$ .

You can see that the solution is in terms of two dimensionless quantities,  $Z$  and  $T$  or as we wrote in Eq. 9-4,

$$u = (\sigma'_2 - \sigma'_1) \sum_{n=0}^{\infty} f_1(Z) f_2(T) \quad (9-4)$$

You will recall that the dimensionless quantity  $T$  is called the *time factor*, and it is related to  $c_v$  (Eqs. 9-5 and 9-6) by

$$T = c_v \frac{t}{H_{dr}^2} = \frac{k(1+e_0)}{a_v \rho_w g} \frac{t}{H_{dr}^2} \quad (B-2-14)$$

In this equation  $H_{dr}$  is the longest drainage path a drop of water has to follow in a compressible soil deposit to get to a free draining boundary. In Fig. B-2.1 you can see that the height of a doubly drained layer is  $2H$ . Therefore the drainage path  $H_{dr}$  is equal to  $H$ . If we had only a singly drained layer, we would only consider the top half of Fig. B-2.1, and again the drainage path would be the height of  $H$ .

The *consolidation ratio*  $U_z$  relates the change in volume at depth  $z$  and time  $t$  to the ultimate volume change at depth  $z$ , or

$$U_z = \frac{\text{volume change at depth } z \text{ and time } t}{\text{ultimate volume change at depth } z} \quad (\text{B-2-15})$$

The change in volume, of course, means a change in void ratio, or as we wrote in Eq. 9-7,

$$U_z = \frac{e_1 - e}{e_1 - e_2} \quad (9-7)$$

The changes in void ratio can be related to the stress increment through the coefficient of consolidation  $a_v$ . These relationships are shown in Fig. B-2.2. Because in one-dimensional consolidation, the initial excess hydrostatic (pore) pressure is equal to the increment of applied stress, Eq. 9-7 becomes

$$U_z = \frac{\sigma' - \sigma'_1}{\sigma'_2 - \sigma'_1} = \frac{\sigma' - \sigma'_1}{\Delta\sigma'} = \frac{u_i - u}{u_i} = 1 - \frac{u}{u_i} \quad (9-8)$$

Now we can write our solution to the consolidation equation (Eq. 9-4) as in Eq. 9-9, or

$$U_z = 1 - \sum_{n=0}^{\infty} f_1(Z) f_2(T) \quad (9-9)$$

This equation is shown graphically in Fig. 9.3, and we explain in Chapter 9 how to use this figure to obtain the amount of consolidation at any depth and time in the consolidating layer (see Examples 9.1 and 9.2).

Generally in engineering practice we are interested in the volume change of the entire soil layer. So we want the *average degree or percent consolidation*  $U$ , which is defined as

$$U(\%) = \frac{\text{total volume change at time } t}{\text{ultimate total volume change}} \times 100(\%) \quad (\text{B-2-16})$$

For one-dimensional compression, the change in volume is, of course, equal to the change in height of the layer. To obtain the average degree of consolidation over the entire layer we have to find the area under the curve corresponding to a given time factor in Fig. 9.3; this is shown in Fig. 9.5. Mathematically,  $U(\%)$  = average value of  $U_z$ , or

$$U(\%) = \frac{\sum U_z dz}{2H} = \frac{1}{2H} \int_0^{2H} U_z dz \quad (\text{B-2-17})$$

or from Fig. B-2.1,

$$U(\%) = \frac{\int_0^{2H} xy}{\int_0^{2H} xz} = \frac{\int_0^{2H} [(\sigma'_2 - \sigma'_1) - u] dz}{(\sigma'_2 - \sigma'_1)2H} \times 100 \quad (\text{B-2-18})$$

## B-2.3 Mathematical Solution

Rewriting,

$$U(\%) = \frac{100}{2H(\sigma'_2 - \sigma'_1)} \int_0^{2H} [(\sigma'_2 - \sigma'_1) - u] dz \quad (B-2-19)$$

or

$$U(\%) = \frac{100}{2H(\sigma'_2 - \sigma'_1)} \left[ \int_0^{2H} (\sigma'_2 - \sigma'_1) dz - \int_0^{2H} u dz \right] \quad (B-2-20)$$

Substituting the value of  $u$  from Eq. B-2-13 into Eq. B-2-20 and integrating, we obtain:

$$\begin{aligned} U(\%) &= \frac{100}{2H(\sigma'_2 - \sigma'_1)} \left[ (\sigma'_2 - \sigma'_1)2H - (\sigma'_2 - \sigma'_1) \sum_{n=0}^{\infty} \frac{4}{(2n+1)\pi} \right. \\ &\quad \times (-1) \cos \frac{(2n+1)\pi}{2H} z \left. \left( \frac{2H}{(2n+1)\pi} \right) \right] \\ &\quad \times \exp \left. - \left( \frac{(2n+1)^2\pi^2}{4} T \right) \right|_0^{2H} \end{aligned} \quad (B-2-21)$$

Putting in the limits, we obtain

$$\begin{aligned} U(\%) &= 100 \left\{ 1 - \sum_{n=0}^{\infty} \frac{4}{(2n+1)^2\pi^2} (-1)(-1-1) \right. \\ &\quad \times \left. \exp \left[ - \left( \frac{(2n+1)^2\pi^2}{4} T \right) \right] \right\} \end{aligned} \quad (B-2-22)$$

or

$$U(\%) = 100 \left\{ 1 - \sum_{n=0}^{\infty} \frac{8}{(2n+1)^2\pi^2} \exp \left[ - \left( \frac{(2n+1)^2\pi^2}{4} T \right) \right] \right\} \quad (B-2-23)$$

This solution is for the special case of constant or linear initial hydrostatic excess pressure and is valid for all values of  $U$ . Solutions for other initial pore pressure distributions are provided by Taylor (1948) and Leonards (1962), but the differences are negligible for practical purposes. The summation indicated by Eq. B-2-23 can be carried out once and for all and tabulated (Table 9-1) or shown graphically (Fig. 9.5). Casagrande (1938) and Taylor (1948) give the following approximations for Eq. B-2-23, which are useful to know:

For  $U < 60\%$ ,

$$T = \frac{\pi}{4} U^2 \quad (9-10)$$

**690 Derivation and Solution of Terzaghi's One-Dimensional Consolidation Theory**

For  $U > 60\%$ ,

$$T = 1.781 - 0.933 \log(100 - U\%) \quad (9-11)$$

For values of  $U > 60\%$ , the series in Eq. B-2-23 converges extremely rapidly so that only the first term is significant. Therefore, letting  $n = 0$ , Eq. B-2-23 becomes

$$U(\%) = 100 \left[ 1 - \frac{8}{\pi^2} \exp\left(-\frac{\pi^2}{4} T\right) \right] \quad (B-2-24)$$

Rearranging, Eq. B-2-24 gives Eq. 9-11.

## **appendix b-3**

---

### **Pore Pressure Parameters\***

---

#### **B-3.1 DERIVATION OF SKEMPTON'S PORE PRESSURE EQUATION**

The pore pressure parameters (Sec. 11.10), first defined by Skempton (1954), relate the change in pore water pressure to the change in *total* stress during undrained loading.

First, let's derive Eq. 11-11. This can be done in several ways. One simple way is to assume for a start that we have a triaxial specimen in equilibrium with the cell pressure  $\sigma_c$  acting on it. Assume for the moment that the soil skeleton is elastic and isotropic, and that there are both air and water in the voids (that is,  $S < 100\%$ ). Now, when we apply a small change in the cell pressure  $\Delta\sigma_c$  to the sample, by Terzaghi's principle of effective stress (Eq. 7-13), the *change* in effective stress is

$$\Delta\sigma'_c = \Delta\sigma_c - \Delta u$$

The volume change  $\Delta V$  caused by this change in stress is

$$\Delta V = C_{sk}V_o(\Delta\sigma'_c) = -C_{sk}V_o(\Delta\sigma_c - \Delta u)$$

where  $C_{sk}$  is the compressibility of the soil skeleton and  $V_o$  is the original volume of the sample.

As mentioned in Chapter 8, the mineral grains themselves are relatively incompressible, so any decrease in the volume of the soil skeleton results in a decrease in volume of the voids, or

$$\Delta V = -V_oC_v\Delta u = -nV_oC_v\Delta u \quad (B-3-1)$$

where  $n$  is the porosity, and  $C_v$  is the compressibility of the pore fluid

\*Chapter 11.

(air + water). If  $S = 100\%$ , then  $C_v = C_w$ , the compressibility of water. If we allow no drainage to occur, then these two changes in volume must be equal, or

$$-nV_oC_v\Delta u = -C_{sk}V_o(\Delta\sigma_c - \Delta u)$$

Solving for the ratio  $\Delta u/\Delta\sigma_c$ , we obtain Eq. 11-11.

$$\frac{\Delta u}{\Delta\sigma_c} = \frac{1}{1 + \frac{nC_v}{C_{sk}}} = B \quad (11-11)$$

where  $\Delta\sigma_c = \Delta\sigma_3$ . We discussed in Sec. 11.10 the values of  $B$  for different soils and test conditions (see Table 11-8). A more general way to obtain Eq. 11-11 is shown later in this appendix.

We can follow a similar development for the change in pore pressure due to the change in the principal stress difference or shear stress in our triaxial test specimen in order to derive Eqs. 11-13 through 11-15. Assume that the soil skeleton still behaves elastically; then the volume change caused by the change in effective stresses is

$$\Delta V = -C_{sk}V_o \frac{1}{3}(\Delta\sigma'_1 + \Delta\sigma'_2 + \Delta\sigma'_3)$$

The symbols were previously defined. For the common triaxial compression test,  $\Delta\sigma_2 = \Delta\sigma_3$ , so

$$\Delta V = -C_{sk}V_o \frac{1}{3}(\Delta\sigma'_1 + 2\Delta\sigma'_3)$$

The coefficient  $1/3$  comes about because for elastic isotropic materials the volume change is due to the *average* of the changes in the three principal stresses. Now add and subtract  $3\Delta\sigma_3$  to the right-hand side of the equation, and invoke Terzaghi's principle of effective stress. We then obtain

$$\Delta V = -C_{sk}V_o \frac{1}{3}(\Delta\sigma_1 - \Delta\sigma_3 + 3\Delta\sigma_3 - 3\Delta u)$$

As before, the decrease in voids is

$$\Delta V = -nV_oC_v\Delta u \quad (B-3-1)$$

For undrained conditions, the two volumes must be equal. Solving for  $\Delta u$  and noting that

$$B = \frac{1}{1 + \frac{nC_v}{C_{sk}}} \quad (11-11)$$

we obtain

$$\Delta u = B \left[ \Delta\sigma_3 + \frac{1}{3}(\Delta\sigma_1 - \Delta\sigma_3) \right] \quad (B-3-2)$$

Note that the coefficient  $1/3$  for the stress difference term is for elastic

materials and triaxial compression conditions. If we make a similar derivation for *triaxial extension* conditions ( $\Delta\sigma_2 = \Delta\sigma_1$ ), we get

$$\Delta u = B \left[ \Delta\sigma_3 + \frac{2}{3} (\Delta\sigma_1 - \Delta\sigma_3) \right] \quad (B-3-3)$$

(Note that you have to add and subtract  $2\Delta\sigma_3$  in this case.) Thus for elastic soil skeletons, the pore pressure parameter in extension is twice that in compression.

Since soils in general are inelastic materials, Skempton (1954) replaced the two constants in Eqs. B-3-2 and B-3-3 by the coefficient  $A$ , so that

$$\Delta u = B [ \Delta\sigma_3 + A(\Delta\sigma_1 - \Delta\sigma_3) ] \quad (11-13)$$

Often it is convenient to write Eq. 11-13 as

$$\Delta u = B \Delta\sigma_3 + \bar{A} (\Delta\sigma_1 - \Delta\sigma_3) \quad (11-15)$$

where  $\bar{A} = BA$ . For saturated soils, we usually write Eq. 11-13 as

$$\Delta u = \Delta\sigma_3 + A(\Delta\sigma_1 - \Delta\sigma_3) \quad (11-14)$$

Other convenient ways to write the pore pressure equation (11-13) are given by Skempton (1954). For triaxial compression conditions,

$$\Delta u = B \left[ \frac{1}{3} (\Delta\sigma_1 + 2\Delta\sigma_3) + \frac{3A - 1}{3} (\Delta\sigma_1 - \Delta\sigma_3) \right] \quad (B-3-4)$$

And for triaxial extension conditions

$$\Delta u = B \left[ \frac{1}{3} (2\Delta\sigma_1 + \Delta\sigma_3) + \frac{3A - 2}{3} (\Delta\sigma_1 - \Delta\sigma_3) \right] \quad (B-3-5)$$

These equations show that if soils behaved as perfectly elastic materials (that is,  $A = 1/3$  in compression and  $A = 2/3$  in extension), then the pore pressure would depend only on the average change in principal stress, which is the first part of Eqs. B-3-4 and B-3-5.

### B-3.2 DEFINITION OF $\Delta\sigma_1$ AND $\Delta\sigma_3$ FOR ROTATION OF PRINCIPAL STRESSES

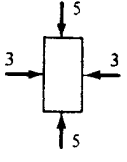
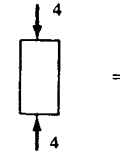
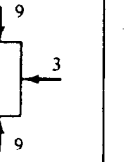
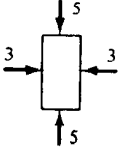
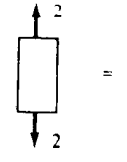
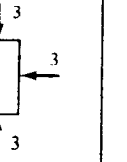
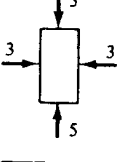
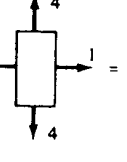
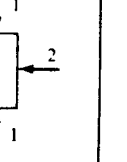
Law and Holtz (1978) showed that contradictory definitions of the pore pressure parameter  $A$  exist in the literature because of the lack of a consistent definition of principal stress increment for cases where the principal stresses rotate. They proposed the following system, to take care of any possible ambiguities when the principle stresses rotate  $90^\circ$ .

In this system,  $\Delta\sigma_1$  and  $\Delta\sigma_3$  are called the *major and minor principal stress increments*, respectively. A principal stress increment is defined as the maximum or minimum normal stress increment imposed on a given stress

system. The sign convention is positive for compression and negative for tension.  $\Delta\sigma_1$  is the *algebraically largest* normal component of a given system of stress increments, and  $\Delta\sigma_3$  is the *algebraically smallest* normal component of that system.

The advantage of this system is that the stress increment is not connected to the original stress. Thus the direction of  $\Delta\sigma_1$  is *independent* of the direction of the original or final  $\sigma_1$ , and so is  $\Delta\sigma_3$ . This point is illustrated in Table B-3-1, which shows some combinations of  $\Delta\sigma_1$  and  $\Delta\sigma_3$  being applied to typical existing stress systems represented by  $\sigma_1$  and  $\sigma_3$ .

**TABLE B-3-1** Examples Using the Proposed New Definition of Principal Stress Increments (units of stress are arbitrary, and axisymmetry in stress system is assumed)\*

Initial Stress System	Stress Increment	Final Stress State	$\Delta\sigma_1$		$\Delta\sigma_3$	
			Magnitude	Direction	Magnitude	Direction
			4	V†	0	H†
			0	H	-2	V
			-1	H	-4	V

\*V = Vertical; H = Horizontal.

After Law and Holtz (1978).

### B-3.3 FORMULAS FOR PORE PRESSURE PARAMETERS FOR DIFFERENT STRESS PATH TESTS

To aid in calculating the correct value of the parameter  $A$ , Law and Holtz (1978) derived the appropriate expressions for  $A$  for the four types of triaxial stress path tests, AC, AE, LC, and LE (Secs. 10.6 and 11.12). These

**TABLE B-3-2** Definition of Principal Stress Increments and Formulas for Pore Pressure Parameters for Various Types of Triaxial Tests\*

Test Type	$\Delta\sigma_1$	$\Delta\sigma_2$	$\Delta\sigma_3$	Formula for $A$	Equation
Compression test:					
Axial compression, AC	$\Delta\sigma_o$	0	0	$A_{ac} = \Delta u / \Delta\sigma_o$	11-16
Lateral extension, LE	0	$\Delta\sigma_h$	$\Delta\sigma_h$	$A_{le} = 1 - \Delta u / \Delta\sigma_h$	11-17
Extension test:					
Axial extension, AE	0	0	$\Delta\sigma_o$	$A_{ae} = 1 - \Delta u / \Delta\sigma_o$	11-18
Lateral compression, LC	$\Delta\sigma_h$	$\Delta\sigma_h$	0	$A_{lc} = \Delta u / \Delta\sigma_h$	11-19

\*After Law and Holtz (1978).

are shown in Table B-3-2. The derivation of these expressions is shown in the following example.

### EXAMPLE B-3.1

**Given:**

An axial extension (AE) triaxial test is conducted on a saturated clay.

**Required:**

Determine the correct formula for the pore pressure parameter  $A$ .

**Solution:**

In the AE test, the lateral (cell) pressure remains constant while the axial stress is decreased. Therefore

$$\Delta\sigma_1 = \Delta\sigma_2 = 0, \quad \Delta\sigma_3 = \Delta\sigma_o$$

According to the definition of principal stress increments proposed by Law and Holtz (1978),  $\Delta\sigma_o$  is negative since it decreases. Thus it is algebraically the smallest component of the stress increment. Substituting these definitions for  $\Delta\sigma_1$  and  $\Delta\sigma_3$  into Eq. 11-13 (assume  $B = 1$ ), we obtain

$$A_{ae} = 1 - \frac{\Delta u}{\Delta\sigma_o} \quad (11-18)$$

This formula is the same as shown for the AE test in Table B-3-2.

### B-3.4 PROOF THAT $A_{ac} = A_{le}$ AND $A_{ae} = A_{lc}$

It was shown by example in Sec. 11.12 that the pore pressure parameter  $A$  was the same in axial compression (AC) as in lateral extension (LE). It was inferred that  $A$  in axial extension (AE) was identical to  $A$  in lateral compression (LC). The statements are true even though these sets of tests have different total stress paths. The proof of this contention was given by Law and Holtz (1978).

We first define  $p' = (\sigma'_1 + \sigma'_3)/2$  as the average of the major and minor effective stresses and  $q = (\sigma_1 - \sigma_3)/2$  as half the principal stress difference (Sec. 10.6). We can express the slope at any point on the effective stress path in a  $p'-q$  diagram as

$$\left( \frac{dq}{dp'} \right) = \frac{d(\sigma_1 - \sigma_3)}{d(\sigma_1 + \sigma_3 - 2u)}$$

For the axial compression case  $d\sigma_1 = d\sigma_v$  and  $d\sigma_3 = 0$ . Hence

$$\left( \frac{dq}{dp'} \right)_{ac} = \frac{1}{1 - 2A_{ac}}$$

For the lateral extension case  $d\sigma_1 = 0$  and  $d\sigma_3 = d\sigma_l$ . Hence

$$\left( \frac{dq}{dp'} \right)_{le} = \frac{-1}{1 - 2(1 - A_{le})} = \frac{1}{1 - 2A_{le}}$$

Since both tests have the same effective stress paths (see, for example, Example 11.17) then

$$\left( \frac{dq}{dp'} \right)_{ac} = \left( \frac{dq}{dp'} \right)_{le}$$

Hence

$$A_{ac} = A_{le} \quad (11-20)$$

Similarly, we can show that

$$A_{ae} = A_{lc} \quad (11-21)$$

### B-3.5 DERIVATION OF THE HENKEL PORE PRESSURE EQUATION AND COEFFICIENTS\*

Assume an element of soil in equilibrium with stresses  $\sigma_1$ ,  $\sigma_2$ , and  $\sigma_3$  on it. When we apply stress increments  $\Delta\sigma_1$ ,  $\Delta\sigma_2$ , and  $\Delta\sigma_3$  to the element, an excess pore pressure  $\Delta u$  and a resulting change in effective stresses

\*After Scott (1963), and Perloff and Baron (1976).

occurs. So,

$$\Delta\sigma'_1 = \Delta\sigma_1 - \Delta u, \quad \Delta\sigma'_2 = \Delta\sigma_2 - \Delta u, \quad \Delta\sigma'_3 = \Delta\sigma_3 - \Delta u$$

Assume for now that the soil skeleton is elastic and isotropic. Thus it has a bulk modulus  $K_{sk} = E/3(1 - 2\nu)$ . Since the definition of bulk modulus is the volumetric effective stress  $\frac{1}{3}(\sigma'_1 + \sigma'_2 + \sigma'_3)$  divided by the volumetric strain  $\Delta V/V_o$ ,

$$K_{sk} = \frac{\frac{1}{3}(\sigma'_1 + \sigma'_2 + \sigma'_3)}{\Delta V/V_o} = \frac{E}{3(1 - 2\nu)}$$

Rearranging, the volumetric strain of the soil skeleton is

$$\frac{\Delta V}{V_o} = \epsilon_1 + \epsilon_2 + \epsilon_3 = C_{sk} \left( \frac{\sigma'_1 + \sigma'_2 + \sigma'_3}{3} \right)$$

where  $C_{sk} = 1/K_{sk}$  is called the *compressibility of soil skeleton*, and  $\epsilon_1$ ,  $\epsilon_2$ , and  $\epsilon_3$  are principal strains. Since  $E$  and  $\nu$  are difficult to determine for a real soil, the general coefficient  $C_{sk}$  is more practical (Scott, 1963). Now, if we state this equation in terms of total stress changes and pore pressure, then we have

$$\frac{\Delta V}{V_o} = C_{sk} \left( \frac{\Delta\sigma_1 + \Delta\sigma_2 + \Delta\sigma_3}{3} - \Delta u \right)$$

This equation states that the volumetric strain is a function only of the change in mean effective stress for a *linearly elastic* material (or, in fact, for any non-dilative, no-volume-change-during-shear material). However soils do change volume due to the change in shear stress, and this is accounted for by an empirical correction factor,  $D|\Delta\tau_{oct}|$ , where  $|\Delta\tau_{oct}|$  is the absolute value of the *increment* in  $\tau_{oct}$ . Thus we have

$$\frac{\Delta V}{V_o} = C_{sk}[\Delta\sigma_{oct} - u] + D|\Delta\tau_{oct}| \quad (B-3-6)$$

because, by definition from continuum mechanics,

$$\sigma_{oct} = \frac{\sigma_1 + \sigma_2 + \sigma_3}{3} \quad (11-23)$$

and

$$\tau_{oct} = \frac{1}{3} \sqrt{(\sigma_1 - \sigma_2)^2 + (\sigma_2 - \sigma_3)^2 + (\sigma_3 - \sigma_1)^2} \quad (11-24)$$

As Perloff and Baron (1976) point out, since  $\tau_{oct}$  is a nonlinear function of the principal stress differences, we cannot in general calculate it directly from the stress increments. Instead we must determine  $\Delta\tau_{oct}$  from the difference  $(\tau_{oct})_2 - (\tau_{oct})_1$ .

Now, as we did in Section B-3.1, let us look at what happens to the voids. The volumetric strain in the voids is

$$\frac{\Delta V_v}{V_v} = -C_v \Delta u \quad (B-3-1)$$

where  $C_v$  is the compressibility of the voids, and  $V_v$ , the volume of voids, is  $nV_o$ . If  $S = 100\%$ , then  $C_v = C_w$ , the compressibility of water. And if there is no change in volume permitted (that is, undrained conditions prevail), then setting Eq. B-3-1 equal to Eq. B-3-6 and solving for  $\Delta u$ , we have

$$\Delta u = \frac{1}{1 + n\left(\frac{C_v}{C_{sk}}\right)} \left[ (\Delta\sigma_{oct}) + \frac{D}{C_{sk}} |\Delta\tau_{oct}| \right] \quad (B-3-7)$$

Since soils are not linearly elastic materials, as before we use empirical coefficients which are to be determined by experiment,

$$B = \frac{1}{1 + \frac{nC_v}{C_{sk}}} \quad (11-11)$$

and

$$a = \frac{D}{C_{sk}} \quad (B-3-8)$$

So Eq. B-3-5 becomes

$$\Delta u = B(\Delta\sigma_{oct} + a\Delta\tau_{oct}) \quad (11-22)$$

The coefficient  $a$  is the *Henkel pore pressure parameter*.

Although this derivation for Eq. 11-22 is rather elegant mathematically, it may be easier to simply write the equation as

$$\begin{aligned} \Delta u = B & \frac{\Delta\sigma_1 + \Delta\sigma_2 + \Delta\sigma_3}{3} \\ & + \frac{a}{3} \sqrt{(\Delta\sigma_1 - \Delta\sigma_2)^2 + (\Delta\sigma_2 - \Delta\sigma_3)^2 + (\Delta\sigma_3 - \Delta\sigma_1)^2} \end{aligned} \quad (B-3-9)$$

This latter formulation is more consistent with the definition of principal stress increments presented in Sec. B-3.2. With this definition, a systematic separation of the stress increments from the initial and final stress states is possible.

Equations 11-13 and B-3-9 are useful since they allow the separation of pore pressure effects observed in soils into two components, that due to (1) the change in mean or average stress, and (2) the change in shear stress.

The Henkel parameter  $a$  is, like the Skempton parameter  $A$ , nonlinear and must be determined for each stress path. It is also very dependent

on strain, on the magnitude of  $\sigma_2$ , on the overconsolidation ratio, and on material properties such as anisotropy. The parameters  $a$  and  $B$  are for general changes in total stress. They enable the engineer to predict the pore pressure if the changes in the total stresses are known or can be estimated, therefore they can be very useful in engineering practice.

Sometimes in the geotechnical literature the Henkel parameters are denoted by the symbol  $\alpha$ , where  $\alpha = a/3$ . In this case, Eq. B-3-9 would be

$$\Delta u = B \frac{\Delta\sigma_1 + \Delta\sigma_2 + \Delta\sigma_3}{3} + \alpha \sqrt{(\Delta\sigma_1 - \Delta\sigma_2)^2 + (\Delta\sigma_2 - \Delta\sigma_3)^2 + (\Delta\sigma_3 - \Delta\sigma_1)^2} \quad (\text{B-3-10})$$

This is the way Henkel (1960) originally wrote his equation, but with the symbol  $a$  for  $\alpha$ . Thus Henkel's original  $a$  or  $\alpha$  was one-third our  $a$ . Later Henkel and Wade (1966) suggested the notation used herein, along with Eq. 11-22.

It is often useful to be able to convert between the Henkel parameter  $a$  and the Skempton parameter  $A$ . For the special case of triaxial compression (AC),  $\sigma_2 = \sigma_3$  and  $S = 100\%$  ( $B = 1$ ), we have

$$\Delta\sigma_{\text{oct}} = \frac{1}{3}(\Delta\sigma_1 + 2\Delta\sigma_3)$$

and

$$\Delta\tau_{\text{oct}} = \frac{\sqrt{2}}{3}(\Delta\sigma_1 - \Delta\sigma_3)$$

so (Eq. 11-22)

$$\Delta u = \frac{1}{3}(\Delta\sigma_1 + 2\Delta\sigma_3) + a \frac{\sqrt{2}}{3}(\Delta\sigma_1 - \Delta\sigma_3)$$

but since  $\Delta\sigma_2 = \Delta\sigma_3 = 0$  (constant cell pressure) and  $\Delta\sigma_1 = \Delta\sigma_v$ ,

$$\Delta u = \left( \frac{1}{3} + a \frac{\sqrt{2}}{3} \right) \Delta\sigma_v$$

From Eq. 11-13 and for triaxial compression conditions in Table B-3-2, we know that  $A_{ac} = \Delta u / \Delta\sigma_v$ . Therefore

$$A_{ac} = \frac{1}{3} + a \frac{\sqrt{2}}{3} \quad (11-25a)$$

For the lateral extension (LE) test,  $\sigma_2 = \sigma_3$ , and Eq. 11-22 becomes

$$\Delta u = \frac{1}{3}(\Delta\sigma_1 + 2\Delta\sigma_3) + a \frac{\sqrt{2}}{3}(\Delta\sigma_1 - \Delta\sigma_3)$$

But since  $\Delta\sigma_1 = 0$  and  $\Delta\sigma_2 = \Delta\sigma_3 = \Delta\sigma_h$ ,

$$\Delta u = \frac{2}{3} \Delta\sigma_h - a \frac{\sqrt{2}}{3} \Delta\sigma_h = \frac{2}{3} - a \frac{\sqrt{2}}{3} \Delta\sigma_h$$

From Eq. 11-13 and Table B-3-2, we know that  $A_{le} = 1 - \Delta u / \Delta\sigma_h$ . Therefore

$$A_{le} = 1 - \frac{2}{3} - a \frac{\sqrt{2}}{3} = \frac{1}{3} + a \frac{\sqrt{2}}{3} \quad (11-25b)$$

which is the same as Eq. 11-25a. This result should not be unexpected since we have already shown that  $A_{ac} = A_{le}$  (Eq. 11-20).

For the case of axial extension (AE),  $\sigma_2 = \sigma_1$ , and Eq. 11-22 becomes

$$\Delta u = \frac{1}{3} (2\Delta\sigma_1 + \Delta\sigma_3) + a \frac{\sqrt{2}}{3} (\Delta\sigma_1 - \Delta\sigma_3)$$

But since  $\Delta\sigma_1 = \Delta\sigma_2 = 0$  and  $\Delta\sigma_3 = \Delta\sigma_v$ ,

$$\Delta u = \frac{1}{3} \Delta\sigma_v - a \frac{\sqrt{2}}{3} \Delta\sigma_v = \frac{1}{3} - a \frac{\sqrt{2}}{3} \Delta\sigma_v$$

From Eq. 11-13 and Table B-3-2, we know that  $A_{ae} = 1 - \Delta u / \Delta\sigma_v$ . Therefore

$$A_{ae} = 1 - \frac{1}{3} - a \frac{\sqrt{2}}{3} = \frac{2}{3} + a \frac{\sqrt{2}}{3} \quad (11-26a)$$

For the lateral compression (LC) test,  $\sigma_2 = \sigma_1$ , so Eq. 11-22 becomes

$$\Delta u = \frac{1}{3} (2\Delta\sigma_1 + \Delta\sigma_3) + a \frac{\sqrt{2}}{3} (\Delta\sigma_1 - \Delta\sigma_3)$$

Since  $\Delta\sigma_1 = \Delta\sigma_2 = \Delta\sigma_h$  and  $\Delta\sigma_3 = 0$ , we have

$$\Delta u = \left( \frac{2}{3} + a \frac{\sqrt{2}}{3} \right) \Delta\sigma_h$$

From Eq. 11-13 and Table B-3-2, we know that  $A_{lc} = \Delta u / \Delta\sigma_h$ . Therefore

$$A_{lc} = \frac{2}{3} + a \frac{\sqrt{2}}{3} \quad (11-26b)$$

As expected (Eq. 11-21),  $A_{ae} = A_{lc}$ .

Note that for elastic materials,  $A_{ac} = A_{le} = 1/3$  and  $A_{ae} = A_{lc} = 2/3$ , and  $a = 0$ . In general, since  $A_{ac} \neq A_{lc}$ , then the  $a$  parameters are not necessarily the same for the two cases, primarily because the compressibility of the soil skeleton  $C_{sk}$  is not the same in compression as in extension.

---

## References

---

- ABDELHAMID, M.S., AND KRIZEK, R.J. (1976) "At Rest Lateral Earth Pressure of a Consolidating Clay," *Journal of the Geotechnical Engineering Division, ASCE*, Vol. 102, No. GT7, pp. 721-738.
- ABELEV, Y.M. (1957) "The Stabilization of Foundations of Structures on Loess Soils," *Proceedings of the Fourth International Conference on Soil Mechanics and Foundation Engineering*, London, Vol. I, pp. 259-263.
- ABOSHI, H. (1973) "An Experimental Investigation on the Similitude in the Consolidation of a Soft Clay, Including the Secondary Creep Settlement," *Proceedings of the Eighth International Conference on Soil Mechanics and Foundation Engineering*, Moscow, Vol. 4.3, p. 88.
- AL-HUSSAINI, M.M. (1977) "Contribution to the Engineering Soil Classifications of Cohesionless Soils," *Final Report*, Miscellaneous Paper S-77-21, U.S. Army Engineer Waterways Experiment Station, Vicksburg, Mississippi, 61 pp.
- AL-HUSSAINI, M.M., AND TOWNSEND, F.C. (1975) "Investigation of  $K_o$  Testing in Cohesionless Soils," *Technical Report S-75-11*, U.S. Army Engineer Waterways Experiment Station, Vicksburg, Mississippi, 70 pp.
- ALPAN, I. (1967) "The Empirical Evaluation of the Coefficient  $K_o$  and  $K_{oR}$ ," *Soil and Foundation*, Vol. VII, No. 1, pp. 31-40.
- AMERICAN ASSOCIATION FOR STATE HIGHWAY AND TRANSPORTATION OFFICIALS (1978) *Standard Specifications for Transportation Materials and Methods of Sampling and Testing*, 12th Ed., Washington, D.C. Part I, Specifications, 828 pp.; Part II, Tests, 998 pp.
- AMERICAN SOCIETY OF CIVIL ENGINEERS (1978) *Soil Improvement—History, Capabilities, and Outlook*, Committee on Placement and Improvement of Soils, Geotechnical Engineering Division, ASCE, 182 pp.
- AMERICAN SOCIETY FOR TESTING AND MATERIALS (1980) "Natural Building Stones; Soil and Rock," *Annual Book of ASTM Standards*, Part 19, Philadelphia, 634 pp.
- AMERICAN SOCIETY FOR TESTING AND MATERIALS (1966) *ASTM Metric Practice Guide*, 2nd Ed., 46 pp.

- ARAVIN, V.I., AND NUMEROV, S. (1955) "Seepage Computations for Hydraulic Structures," *Stpoitel'stu i Arkhitekture*, Moscow, (referenced in Harr, 1962).
- ATTERBERG, A. (1905) "Die Rationelle Klassifikation der Sande und Kiese," *Chemiker-Zeitung*, Vol. 29, pp. 195-198.
- ATTERBERG, A. (1911) "Lerornas Förhallande till Vatten, deras Plasticitetsgränser och Plasticitetsgrader," ("The Behavior of Clays with Water, their Limits of Plasticity and their Degrees of Plasticity,") *Kungliga Lantbruksakademiens Handlingar och Tidskrift*, Vol. 50, No. 2, pp. 132-158; also in *Internationale Mitteilungen für Bodenkunde*, Vol. 1, pp. 10-43 ("Über die Physikalische Bodenuntersuchung und über die Plastizität der Tone").
- AZZOUZ, A.S., KRIZEK, R.J. AND COROTIS, R.B. (1976) "Regression Analysis of Soil Compressibility," *Soils and Foundations*, Vol. 16, No. 2, pp. 19-29.
- BAGUELIN, F., JÉZÉQUEL, J.F., AND SHIELDS, D.H. (1978) *The Pressuremeter and Foundation Engineering*, Trans Tech Publications, Clausthal, Germany, and Aedermannsdorf, Switzerland, 617 pp.
- VON BANDAT, H.F. (1962) *Aerogeology*, Gulf Publishing Company, Houston, Texas, 350 pp.
- BARDEN, L., AND MCGOWN, A. (1973) "Microstructural Disturbance in Soft Clays Resulting from Site Investigation Sampling," *Proceedings of the International Symposium on Soil Structure*, Gothenburg, Sweden, p. 213.
- BARRETT, R.J. (1966) "Use of Plastic Filters in Coastal Construction," *Proceedings of the Tenth International Conference on Coastal Engineering*, Tokyo, pp. 1048-1067.
- BEGEMANN, H.K.S.PH. (1953) "Improved Methods of Determining Resistance to Adhesion by Sounding through a Loose Sleeve Placed Behind the Cone," *Proceedings of the Third International Conference on Soil Mechanics and Foundation Engineering*, Zurich, Vol. I, pp. 213-217.
- BESKOW, G. (1935) "Soil Freezing and Frost Heaving with Special Application to Roads and Railroads," *The Swedish Geological Society*, Series C, No. 375, 26th Year Book No. 3; translated by J.O. Osterberg, Northwestern University, 1947, 145 pp.
- BISHOP, A.W. (1958) "Test Requirements of Measuring the Coefficient of Earth Pressure at Rest," *Proceedings of the Conference on Earth Pressure Problems*, Brussels, Vol. I, pp. 2-14.
- BISHOP, A.W., AND HENKEL, D.J. (1962) *The Measurement of Soil Properties in the Triaxial Test*, Edward Arnold Ltd., London, 2nd Ed., 228 pp.
- BISHOP, A.W., AND WESLEY, L.D. (1975) "Triaxial Apparatus for Controlled Stress Path Testing," *Géotechnique*, Vol. XXV, No. 4, pp. 657-670.
- BJERRUM, L. (1954) "Geotechnical Properties of Norwegian Marine Clays," *Géotechnique*, Vol. IV, No. 2, pp. 49-69.
- BJERRUM, L. (1967) "Engineering Geology of Norwegian Normally Consolidated Marine Clays as Related to Settlements of Buildings," *Géotechnique*, Vol. XVII, No. 2, pp. 81-118.
- BJERRUM, L. (1972) "Embankments on Soft Ground," *Proceedings of the ASCE Specialty Conference on Performance of Earth and Earth-Supported Structures*, Purdue University, Vol. II, pp. 1-54.

## References

- BJERRUM, L., AND SIMONS, N.E. (1960) "Comparison of Shear Strength Characteristics of Normally Consolidated Clays," *Proceedings of the ASCE Research Conference on the Shear Strength of Cohesive Soils*, Boulder, pp. 711-726.
- BLACK, D.K., AND LEE, K.L. (1973) "Saturating Laboratory Samples by Back Pressure," *Journal of the Soil Mechanics and Foundations Division, ASCE*, Vol. 99, No. SM1, pp. 75-93.
- BOUSSINESQ, J. (1885) *Application des Potentiels à L'Étude de L'Équilibre et du Mouvement des Solides Élastiques*, Gauthier-Villars, Paris.
- BOZOZUK, M. (1963) "The Modulus of Elasticity of Leda Clay from Field Measurements," *Canadian Geotechnical Journal*, Vol. I, No. 1, pp. 43-51.
- BOZOZUK, M., AND LEONARDS, G.A. (1972) "The Gloucester Test Fill," *Proceedings of the ASCE Specialty Conference on Performance of Earth and Earth-Supported Structures*, Purdue University, Vol. I, Part 1, pp. 299-317.
- BROMS, B.B., AND FORSSBLAD, L. (1969) "Vibratory Compaction of Cohesionless Soils," *Proceedings of the Specialty Session No. 2 on Soil Dynamics*, Seventh International Conference on Soil Mechanics and Foundation Engineering, Mexico City, pp. 101-118.
- BROOKER, E.W., AND IRELAND, H.O. (1965) "Earth Pressures at Rest Related to Stress History," *Canadian Geotechnical Journal*, Vol. II, No. 1, pp. 1-15.
- BRUMUND, W.F., JONAS, E., AND LADD, C.C. (1976) "Estimating In Situ Maximum Past Preconsolidation Pressure of Saturated Clays from Results of Laboratory Consolidometer Tests," *Special Report 163*, Transportation Research Board, pp. 4-12.
- CADLING, L., AND ODENSTAD, S. (1950) "The Vane Borer," *Proceedings No. 2*, Royal Swedish Geotechnical Institute, pp. 1-88.
- CAMPANELLA, R.G., AND VAID, Y.P. (1972) "A Simple  $K_0$ -Triaxial Cell," *Canadian Geotechnical Journal*, Vol. 9, No. 3, pp. 249-260.
- CARRIGAN, R.A. (1978) "Decimal Time," *American Scientist*, Vol. 66, No. 3, pp. 305-313.
- CASAGRANDE, A. (1932a) Discussion of "A New Theory of Frost Heaving," by A.C. Benkelman and F.R. Ohlmeister, *Proceedings of the Highway Research Board*, Vol. 11, pp. 168-172.
- CASAGRANDE, A. (1932b) "Research on the Atterberg Limits of Soils," *Public Roads*, Vol. 13, No. 8, pp. 121-136.
- CASAGRANDE, A. (1932c) "The Structure of Clay and Its Importance in Foundation Engineering," *Journal of the Boston Society of Civil Engineers*, April; reprinted in *Contributions to Soil Mechanics 1925-1940*, BSCE, pp. 72-113.
- CASAGRANDE, A. (1936a) "Characteristics of Cohesionless Soils Affecting the Stability of Slopes and Earth Fills," *Journal of the Boston Society of Civil Engineers*, January; reprinted in *Contributions to Soil Mechanics 1925-1940*, BSCE, pp. 257-276.
- CASAGRANDE, A. (1936b) "The Determination of the Pre-Consolidation Load and Its Practical Significance," Discussion D-34, *Proceedings of the First International Conference on Soil Mechanics and Foundation Engineering*, Cambridge, Vol. III, pp. 60-64.
- CASAGRANDE, A. (1937) "Seepage Through Dams," *Journal of the New England*

- Water Works Association, Vol. LI, No. 2; reprinted in *Contributions to Soil Mechanics 1925-1940*, BSCE, pp. 295-336.
- CASAGRANDE, A. (1938) "Notes on Soil Mechanics—First Semester," Harvard University (unpublished), 129 pp.
- CASAGRANDE, A. (1948) "Classification and Identification of Soils," *Transactions, ASCE*, Vol. 113, pp. 901-930.
- CASAGRANDE, A. (1950) "Notes on the Design of Earth Dams," *Journal of the Boston Society of Civil Engineers*, October; reprinted in *Contributions to Soil Mechanics 1941-1953*, BSCE, pp. 231-255.
- CASAGRANDE, A. (1958) "Notes on the Design of the Liquid Limit Device," *Géotechnique*, Vol. VIII, No. 2, pp. 84-91.
- CASAGRANDE, A. (1975) "Liquefaction and Cyclic Deformation of Sands, a Critical Review," *Proceedings of the Fifth Panamerican Conference on Soil Mechanics and Foundation Engineering*, Buenos Aires; reprinted as Harvard Soil Mechanics Series, No. 88, 27 pp.
- CASAGRANDE, A., AND FADUM, R.E. (1944) Closure to "Application of Soil Mechanics in Designing Building Foundations," *Transactions, ASCE*, Vol. 109, p. 467.
- CASTRO, G. (1969) "Liquefaction of Sands," PhD Thesis, Harvard University; reprinted as Harvard Soil Mechanics Series, No. 81, 112 pp.
- CASTRO, G. (1975) "Liquefaction and Cyclic Mobility of Saturated Sands," *Journal of the Geotechnical Engineering Division, ASCE*, Vol. 101, No. GT6, June, pp. 551-569.
- CASTRO, G., AND POULOS, S.J. (1977) "Factors Affecting Liquefaction and Cyclic Mobility," *Journal of the Geotechnical Engineering Division, ASCE*, Vol. 103, No. GT6, pp. 501-516.
- CATERPILLAR TRACTOR Co. (1977) *Caterpillar Performance Handbook*, Form AEKQ 3313, 8th Ed., Chapter 14, Peoria, Illinois, p. 6.
- CEDERGREN, H.R. (1977) *Seepage, Drainage, and Flow Nets*, 2nd Ed., John Wiley & Sons, Inc., New York, 534 pp.
- CLEVENGER, W.A. (1958) "Experiences With Loess as a Foundation Material," *Transactions, ASCE*, Vol. 123, pp. 151-169.
- COLLINS, K., AND MCGOWN, A. (1974) "The Form and Function of Microfabric Features in a Variety of Natural Soils," *Géotechnique*, Vol. XXIV, No. 2, pp. 223-254.
- COULOMB, C.A. (1776) "Essai sur une application des règles de Maximus et Minimus à quelques Problèmes de Statique, relatifs à l'Architecture," *Mémoires de Mathématique et de Physique, Présentés à l'Académie Royale des Sciences, par divers Savans, et lus dans ses Assemblées*, Paris, Vol. 7, (volume for 1773 published in 1776), pp. 343-382.
- D'APPOLONIA, D.J., WHITMAN, R.V., AND D'APPOLONIA, E.D. (1969) "Sand Compaction with Vibratory Rollers," *Journal of the Soil Mechanics and Foundations Division, ASCE*, Vol. 95, No. SM1, pp. 263-284.
- D'APPOLONIA, D.J., LAMBE, T.W., AND POULOS, H.G. (1971) "Evaluation of Pore Pressures Beneath an Embankment," *Journal of the Soil Mechanics and Foundations Division, ASCE*, Vol. 97, No. SM6, pp. 881-897.

## References

- D'APPOLONIA, D.J., Poulos, H.G., AND LADD, C.C. (1971) "Initial Settlement of Structures on Clay," *Journal of the Soil Mechanics and Foundations Division*, ASCE, Vol. 97, No. SM10, pp. 1359-1377.
- DALLAIRE, G. (1976) "Filter Fabrics: Bright Future in Road and Highway Construction," *Civil Engineering*, ASCE, Vol. 46, No. 5, pp. 61-65.
- D'ARCY, H. (1856) "Les Fontaines Publiques de la Ville de Dijon," Dalmont, Paris.
- DAWSON, R.F. (1944) Discussion of "Relation of Undisturbed Sampling to Laboratory Testing," by P.C. Rutledge, *Transactions*, ASCE, Vol. 109, pp. 1190-1193.
- DE MELLO, V.F.B. (1971) "The Standard Penetration Test," State of the Art Paper, *Proceedings of the Fourth Panamerican Conference on Soil Mechanics and Foundation Engineering*, Vol. I, pp. 1-86.
- DiBERNARDO, A. (1979) "The Effect of Laboratory Compaction on the Compressibility of a Compacted Highly Plastic Clay," MSCE Thesis, Purdue University, 187 pp.
- DiBIAGIO, E., AND STENHAMAR, P. (1975) "Prøvefylling til Brudd på Bløt Leire," *Proceedings of the Seventh Scandinavian Geotechnical Meeting*, Copenhagen, Polyteknisk Forlag, pp. 173-185.
- DUNCAN, J.M., AND BUCHIGNANI, A.L. (1976) "An Engineering Manual for Settlement Studies," *Geotechnical Engineering Report*, University of California at Berkeley, 94 pp.
- EDEN, W.J. (1971) "Sampler Trials in Overconsolidated Sensitive Clay," *Sampling of Soil and Rock*, ASTM Special Technical Publication No. 483, pp. 132-142.
- EDEN, W.J., AND KUBOTA, J.K. (1962) "Some Observations on the Measurement of Sensitivity of Clays," *Proceedings of the American Society for Testing and Materials*, Vol. 61, pp. 1239-1249.
- EIDE, O., AND HOLMBERG, S. (1972) "Test Fills to Failure on the Soft Bangkok Clay," *Proceedings of the ASCE Specialty Conference on Performance of Earth and Earth-Supported Structures*, Purdue University, Vol. I, Part I, p. 163.
- ESOPT (1974) *Proceedings of the European Symposium on Penetration Testing*, Stockholm, Swedish Council for Building Research, Vols. 1, 2.1, 2.2, and 3.
- FINN, W.D.L., PICKERING, D.J., AND BRANSBY, P.L. (1971) "Sand Liquefaction in Triaxial and Simple Shear Tests," *Journal of the Soil Mechanics and Foundations Division*, ASCE, Vol. 97, No. SM4, pp. 639-659.
- FLAATE, K., AND PREBER, T. (1974) "Stability of Road Embankments," *Canadian Geotechnical Journal*, Vol. 11, No. 1, pp. 72-88.
- FOSTER, C.R., AND AHLVIN, R.G. (1954) "Stresses and Deflections Induced by a Uniform Circular Load," *Proceedings of the Highway Research Board*, Vol. 33, pp. 467-470.
- GARCIA-BENGOCHEA, I., LOVELL, C.W., AND ALTSCHAEFFL, A.G. (1979) "Pore Distribution and Permeability of Silty Clays," *Journal of the Geotechnical Engineering Division*, ASCE, Vol. 105, No. GT7, pp. 839-856.
- GIBBS, H.J. (1969) Discussion, *Proceedings of the Specialty Session No. 3 on Expansive Soils and Moisture Movement in Partly Saturated Soils*, Seventh International Conference on Soil Mechanics and Foundation Engineering, Mexico City.

- GRIM, R.E. (1959) "Physico-Chemical Properties of Soils: Clay Minerals," *Journal of the Soil Mechanics and Foundations Division, ASCE*, Vol. 85, No. SM2, pp. 1-17.
- GROMKO, G.J. (1974) "Review of Expansive Soils," *Journal of the Geotechnical Engineering Division, ASCE*, Vol. 100, No. GT6, pp. 667-687.
- Handbook of Chemistry and Physics* (1977) CRC Press, Cleveland, 58th Ed.
- HANSBO, S. (1957) "A New Approach to the Determination of the Shear Strength of Clay by the Fall-Cone Test," *Proceedings No. 14*, Swedish Geotechnical Institute, 47 pp.
- HANSBO, S. (1960) "Consolidation of Clay with Special Reference to Influence of Vertical Sand Drains," *Proceedings No. 18*, Swedish Geotechnical Institute, pp. 45-50.
- HANSBO, S. (1975) *Jordmateriallära*, Almqvist & Wiksell Förlag AB, Stockholm, 218 pp.
- HARR, M.E. (1962) *Groundwater and Seepage*, McGraw-Hill Book Company, New York, 315 pp.
- HARR, M.E. (1966) *Foundations of Theoretical Soil Mechanics*, McGraw-Hill Book Company, New York, 381 pp.
- HARR, M.E. (1977) *Mechanics of Particulate Media*, McGraw-Hill Book Company, New York, 543 pp.
- HAZEN, A. (1911) Discussion of "Dams on Sand Foundations," by A.C. Koenig, *Transactions, ASCE*, Vol. 73, pp. 199-203.
- HENKEL, D.J. (1960) "The Shear Strength of Saturated Remoulded Clays," *Proceedings of the ASCE Research Conference on Shear Strength of Cohesive Soils*, Boulder, pp. 533-554.
- HENKEL, D.J., AND WADE, N.H. (1966) "Plane Strain Tests on a Saturated Remolded Clay," *Journal of the Soil Mechanics and Foundations Division, ASCE*, Vol. 92, No. SM6, pp. 67-80.
- HILF, J.W. (1961) "A Rapid Method of Construction Control for Embankments of Cohesive Soils," *Engineering Monograph No. 26*, revised, U.S. Bureau of Reclamation, Denver, 29 pp.
- HIRSCHFELD, R.C. (1963) "Stress-Deformation and Strength Characteristics of Soils," Harvard University (unpublished), 87 pp.
- HÖEG, K., ANDERSLAND, O.B., AND ROLFSEN, E.N. (1969) "Undrained Behaviour of Quick Clay Under Load Tests at Åsrum," *Géotechnique*, Vol. XIX, No. 1, pp. 101-115.
- HOGETOGLER, C.A., AND TERZAGHI, C. (1929) "Interrelationship of Load, Road, and Subgrade," *Public Roads*, Vol. 10, No. 3, pp. 37-64.
- HOLDEN, J.C. (1974) "Penetration Testing in Australia," *Proceedings of the European Symposium on Penetration Testing (ESOPT)*, Vol. 1, pp. 155-162.
- HOLM, G., AND HOLTZ, R.D. (1977) "A Study of Large Diameter Piston Samplers," *Proceedings of the Specialty Session No. 2*, Ninth International Conference on Soil Mechanics and Foundation Engineering, Tokyo, p. 77; also in *Proceedings of the International Symposium on Soft Clay*, Bangkok, p. 381.
- HOLTZ, R.D. (1980) "SI Units in Geotechnical Engineering," *Geotechnical Testing Journal, ASTM*, Vol. 3, No. 2, pp. 75-88.

- HOLTZ, R.D., AND BROMS, B.B. (1972) "Long-Term Loading Tests at Skå-Edeby, Sweden," *Proceedings of the ASCE Specialty Conference on Performance of Earth and Earth-Supported Structures*, Purdue University, Vol. I, Part 1, pp. 435-464.
- HOLTZ, R.D., AND HOLM, G. (1979) "Test Embankment on an Organic Silty Clay," *Proceedings of the Seventh European Conference on Soil Mechanics and Foundation Engineering*, Brighton, England, Vol. 3, pp. 79-86.
- HOLTZ, W.G. (1959) "Expansive Clays—Properties and Problems," *Quarterly of the Colorado School of Mines*, Vol. 54, No. 4, pp. 89-125.
- HOLTZ, W.G., AND GIBBS, H.J. (1956) "Engineering Properties of Expansive Clays," *Transactions, ASCE*, Vol. 121, pp. 641-677.
- HOUGH, B.K. (1969) *Basic Soils Engineering*, 2nd Ed., The Ronald Press Company, New York, 634 pp.
- HOWARD, A.K. (1977) "Laboratory Classification of Soils—Unified Soil Classification System," *Earth Sciences Training Manual No. 4*, U.S. Bureau of Reclamation, Denver, 56 pp.
- HVORSLEV, M.J. (1949) *Subsurface Exploration and Sampling of Soils for Civil Engineering Purposes*, U.S. Army Engineer Waterways Experiment Station, Vicksburg, Mississippi, 521 pp; reprinted by the Engineering Foundation, 1962.
- HVORSLEV, M.J. (1960) "Physical Components of the Shear Strength of Saturated Clays," *Proceedings of the ASCE Research Conference on the Shear Strength of Cohesive Soils*, Boulder, pp. 169-173.
- INTERNATIONAL SOCIETY FOR SOIL MECHANICS AND FOUNDATION ENGINEERING (1977) "List of Symbols, Units, and Definitions," Subcommittee on Symbols, Units, and Definitions, *Proceedings of the Ninth International Conference on Soil Mechanics and Foundation Engineering*, Tokyo, Vol. 3, pp. 156-170.
- JÁKY, J. (1944) "The Coefficient of Earth Pressure at Rest," (in Hungarian), *Magyar Mérnök és Építész Egylet Közönye* (Journal of the Society of Hungarian Architects and Engineers), Vol. 78, No. 22, pp. 355-358.
- JÁKY, J. (1948) "Earth Pressure in Silos," *Proceedings of the Second International Conference on Soil Mechanics and Foundation Engineering*, Rotterdam, Vol. I, pp. 103-107.
- JANBU, N., AND SENNESET, K. (1973) "Field Compressometer—Principles and Applications," *Proceedings of the Eighth International Conference on Soil Mechanics and Foundation Engineering*, Moscow, Vol. 1.1, pp. 191-198.
- JOHNSON, A.W., AND SALLBERG, J.R. (1960) "Factors that Influence Field Compaction of Soils," *Bulletin 272*, Highway Research Board, 206 pp.
- JONES, D.E., AND HOLTZ, W.G. (1973) "Expansive Soils—the Hidden Disaster," *Civil Engineering, ASCE*, Vol. 43, No. 8, pp. 49-51.
- KARLSSON, R. (1977) "Consistency Limits," in cooperation with the Laboratory Committee of the Swedish Geotechnical Society, Swedish Council for Building Research, Document D6, 40 pp.
- KAUFMAN, R.I., AND SHERMAN, W.C., JR., (1964) "Engineering Measurements for Port Allen Lock," *Journal of the Soil Mechanics and Foundations Division, ASCE*, Vol. 90, No. SM5, pp. 221-247; also in *Design of Foundations for Control of Settlement, ASCE*, pp. 281-307.

## References

- KENNEY, T.C. (1959) Discussion of "Geotechnical Properties of Glacial Lake Clays," by T.H. Wu, *Journal of the Soil Mechanics and Foundations Division*, ASCE, Vol. 85, No. SM3, pp. 67-79.
- KENNEY, T.C. (1964) "Sea-Level Movements and the Geologic Histories of the Post-Glacial Marine Soils at Boston, Nicolet, Ottawa, and Oslo," *Géotechnique*, Vol. XIV, No. 3, pp. 203-230.
- KENNEY, T.C. (1976) "Formation and Geotechnical Characteristics of Glacial-Lake Varved Soils," *Laurits Bjerrum Memorial Volume—Contributions to Soil Mechanics*, Norwegian Geotechnical Institute, Oslo, pp. 15-39.
- KOVACS, W.D., EVANS, J.C., AND GRIFFITH, A.H. (1977) "Towards a More Standardized SPT," *Proceedings of the Ninth International Conference on Soil Mechanics and Foundation Engineering*, Tokyo, Vol. 2, pp. 269-276.
- LADD, C.C. (1964) "Stress-Strain Behavior of Saturated Clay and Basic Strength Principles," *Research Report R64-17*, Department of Civil Engineering, Massachusetts Institute of Technology, 67 pp.
- LADD, C.C. (1971a) "Settlement Analyses for Cohesive Soils," *Research Report R71-2*, Soils Publication 272, Department of Civil Engineering, Massachusetts Institute of Technology, 107 pp.
- LADD, C.C. (1971b) "Strength Parameters and Stress-Strain Behavior of Saturated Clays," *Research Report R71-23*, Soils Publication 278, Department of Civil Engineering, Massachusetts Institute of Technology, 280 pp.
- LADD, C.C. (1972) "Test Embankment on Sensitive Clay," *Proceedings of the ASCE Specialty Conference on Performance of Earth and Earth-Supported Structures*, ASCE, Purdue University, Vol. I, Part 1, pp. 103 and 107.
- LADD, C.C. (1975) "Foundation Design of Embankments Constructed on Connecticut Valley Varved Clays," *Research Report R75-7*, Geotechnical Publication 343, Department of Civil Engineering, Massachusetts Institute of Technology, 438 pp.
- LADD, C.C., AND LAMBE, T.W. (1963) "The Strength of Undisturbed Clay Determined from Undrained Tests," *Laboratory Shear Testing of Soils*, ASTM Special Technical Publication No. 361, pp. 342-371.
- LADD, C.C., AND LUSCHER, U. (1965) "Engineering Properties of the Soils Underlying the M.I.T. Campus," *Research Report R65-68*, Soils Publication 185, Department of Civil Engineering, Massachusetts Institute of Technology.
- LADD, C.C., AND EDGERS, L. (1972) "Consolidated-Undrained Direct-Simple Shear Tests on Saturated Clays," *Research Report R72-92*, Soils Publication 284, Department of Civil Engineering, Massachusetts Institute of Technology, 245 pp.
- LADD, C.C., AND FOOTE, R. (1974) "A New Design Procedure for Stability of Soft Clays," *Journal of the Geotechnical Engineering Division*, ASCE, Vol. 100, No. GT7, pp. 763-786.
- LADD, C.C., FOOTE, R., ISHIHARA, K., SCHLOSSER, F., AND POULOS, H.G. (1977) "Stress-Deformation and Strength Characteristics," State-of-the-Art Report, *Proceedings of the Ninth International Conference on Soil Mechanics and Foundation Engineering*, Tokyo, Vol. 2, pp. 421-494.
- LADD, R.S. (1965) "Use of Electrical Pressure Transducers to Measure Soil Pres-

- sure," *Research Report R65-48*, Soils Publication 180, Department of Civil Engineering, Massachusetts Institute of Technology, 79 pp.
- LADD, R.S. (1977) "Specimen Preparation and Cyclic Stability of Sands," *Journal of the Soil Mechanics and Foundations Division*, ASCE, Vol. 103, No. GT2, pp. 535-547.
- LADE, P.V., AND LEE, K.L. (1976) "Engineering Properties of Soils," *Report*, UCLA-ENG-7652, 145 pp.
- LAMBE, T.W. (1951) *Soil Testing for Engineers*, John Wiley & Sons, Inc., New York, 165 pp.
- LAMBE, T.W. (1953) "The Structure of Inorganic Soil," *Proceedings*, ASCE, Vol. 79, Separate No. 315, 49 pp.
- LAMBE, T.W. (1958a) "The Structure of Compacted Clay," *Journal of the Soil Mechanics and Foundations Division*, ASCE, Vol. 84, No. SM2, 1654-1 to 1654-34.
- LAMBE, T.W. (1958b) "The Engineering Behavior of Compacted Clay," *Journal of the Soil Mechanics and Foundations Division*, ASCE, Vol. 84, No. SM2, pp. 1655-1 to 1655-35.
- LAMBE, T.W. (1964) "Methods of Estimating Settlement," *Journal of the Soil Mechanics and Foundations Division*, ASCE, Vol. 90, No. SMS, pp. 43-67; also in *Design of Foundations for Control of Settlement*, ASCE, pp. 47-72.
- LAMBE, T.W. (1967) "Stress Path Method," *Journal of the Soil Mechanics and Foundations Division*, ASCE, Vol. 93, No. SM6, pp. 309-331.
- LAMBE, T.W., AND MARR, W.A. (1979) "Stress Path Method: Second Edition," *Journal of the Geotechnical Engineering Division*, ASCE, Vol. 105, No. GT6, pp. 727-738.
- LAMBE, T.W., AND WHITMAN, R.V. (1969) *Soil Mechanics*, John Wiley & Sons, Inc., New York, 553 pp.
- LAMBRECHTS, J.R., AND LEONARDS, G.A. (1978) "Effects of Stress History on Deformation of Sand," *Journal of the Geotechnical Engineering Division*, ASCE, Vol. 104, No. GT11, pp. 1371-1387.
- LAROCHELLE, P., AND LEFEBVRE, G. (1971) "Sampling Disturbance in Champlain Clays," *Sampling of Soil and Rock*, ASTM Special Technical Publication No. 483, pp. 143-163.
- LAROCHELLE, P., TRAK, B., TAVENAS, F., AND ROY, M. (1974) "Failure of a Test Embankment on a Sensitive Champlain Clay Deposit," *Canadian Geotechnical Journal*, Vol. 11, No. 1, pp. 142-164.
- LAW, K.T., AND HOLTZ, R.D. (1978) "A Note on Skempton's  $A$  Parameter with Rotation of Principle Stresses," *Géotechnique*, Vol. XXVIII, No. 1, pp. 57-64.
- LEE, K.L. (1965) "Triaxial Compressive Strength of Saturated Sands Under Seismic Loading Conditions," PhD Dissertation, University of California at Berkeley, 521 pp.
- LEE, K.L., AND SEED, H.B. (1967) "Drained Strength Characteristics of Sands," *Journal of the Soil Mechanics and Foundations Division*, ASCE, Vol. 93, No. SM6, pp. 117-141.

- LEE, K.L., AND SINGH, A. (1971) "Compaction of Granular Soils," *Proceedings of the Ninth Annual Symposium on Engineering Geology and Soils Engineering*, Boise, Idaho, pp. 161-174.
- LEONARDS, G.A., Ed. (1962) *Foundation Engineering*, McGraw-Hill Book Company, New York, 1136 pp.
- LEONARDS, G.A. (1973) Discussion of "The Empress Hotel, Victoria, British Columbia: Sixty-five Years of Foundation Settlements," *Canadian Geotechnical Journal*, Vol. 10, No. 1, pp. 120-122.
- LEONARDS, G.A. (1976) "Estimating Consolidation Settlements of Shallow Foundations on Overconsolidated Clays," *Special Report 163*, Transportation Research Board, pp. 13-16.
- LEONARDS, G.A. (1977) Discussion to Main Session 2, *Proceedings of the Ninth International Conference on Soil Mechanics and Foundation Engineering*, Tokyo, Vol. 3, pp. 384-386.
- LEONARDS, G.A., AND ALTSCHAEFFL, A.G. (1964) "Compressibility of Clay," *Journal of the Soil Mechanics and Foundations Division*, ASCE, Vol. 90, No. SMS, pp. 133-156; also in *Design of Foundations for Control of Settlement*, ASCE, pp. 163-185.
- LEONARDS, G.A., CUTTER, W.A., AND HOLTZ, R.D. (1980) "Dynamic Compaction of Granular Soils," *Journal of the Geotechnical Engineering Division*, ASCE, Vol. 106, No. 1, pp. 35-44.
- LEONARDS, G.A., AND GIRAUT, P. (1961) "A Study of the One-Dimensional Consolidation Test," *Proceedings of the Fifth International Conference on Soil Mechanics and Foundation Engineering*, Paris, Vol. I, pp. 116-130.
- LEONARDS, G.A., AND RAMIAH, B.K. (1959) "Time Effects in the Consolidation of Clay," *Papers on Soils—1959 Meeting*, American Society for Testing and Materials, Special Technical Publication No. 254, pp. 116-130.
- LEROUEIL, S., TAVENAS, F., TRAK, B., LAROCHELLE, P., AND ROY, M. (1978a) "Construction Pore Pressure in Clay Foundations Under Embankments. Part I: The Saint-Alban Test Fills," *Canadian Geotechnical Journal*, Vol. 15, No. 1, p. 56.
- LEROUEIL, S., TAVENAS, F., MIEUSSENS, C., AND PEIGNAUD, M. (1978b) "Construction Pore Pressures in Clay Foundations Under Embankments. Part II: Generalized Behaviour," *Canadian Geotechnical Journal*, Vol. 15, No. 1, pp. 66-82.
- LIU, T.K. (1970) "A Review of Engineering Soil Classification Systems," *Special Procedures for Testing Soil and Rock for Engineering Purposes*, 5th Ed., ASTM Special Technical Publication 479, pp. 361-382.
- LOOS, W. (1936) "Comparative Studies of the Effectiveness of Different Methods for Compacting Cohesionless Soils," *Proceedings of the First International Conference on Soil Mechanics and Foundation Engineering*, Cambridge, Vol. III, pp. 174-179.
- LOWE, J., III (1974) "New Concepts in Consolidation and Settlement Analysis," *Journal of the Geotechnical Engineering Division*, ASCE, Vol. 100, No. GT6, pp. 574-612.
- LOWE, J., III, ZACCHEO, P.F., AND FELDMAN, H.S. (1964) "Consolidation Testing with Back Pressure," *Journal of the Soil Mechanics and Foundations Division*.

- ASCE, Vol. 90, No. SM5, pp. 69-86; also in *Design of Foundations for Control of Settlement*, ASCE, pp. 73-90.
- LUKAS, R.G. (1980) "Densification of Loose Deposits by Pounding," *Journal of the Geotechnical Engineering Division*, ASCE, Vol. 106, No. GT4, pp. 435-446.
- MACDONALD, A.B., AND SAUER, E.K. (1970) "The Engineering Significance of Pleistocene Stratigraphy in the Saskatoon Area, Saskatchewan, Canada," *Canadian Geotechnical Journal*, Vol. 7, No. 2, pp. 116-126.
- MANNHEIM, B.R.S. (1979) "A New Conception of the Formation of the Kola Peninsula Apatite Deposit: The Coprogenic Impact Theory-CIT," *The Journal of Irreproducible Results*, Society for Basic Irreproducible Research, Vol. 25, No. 1, pp. 6-7.
- MASSARSCH, K.R. (1979) "Lateral Earth Pressure in Normally Consolidated Clay," *Proceedings of the Seventh European Conference on Soil Mechanics and Foundation Engineering*, Brighton, England, Vol. 2, pp. 245-250.
- MASSARSCH, K.R., HOLTZ, R.D., HOLM, B.G., AND FREDRICKSSON, A. (1975) "Measurement of Horizontal In Situ Stresses," *Proceedings of the ASCE Specialty Conference on In Situ Measurement of Soil Properties*, Raleigh, North Carolina, Vol. I, pp. 266-286.
- McGOWN, A. (1973) "The Nature of the Matrix in Glacial Ablation Tills," *Proceedings of the International Symposium on Soil Structure*, Gothenburg, Sweden, p. 95.
- MEEHAN, R.L. (1967) "The Uselessness of Elephants in Compacting Fill," *Canadian Geotechnical Journal*, Vol. IV, No. 3, pp. 358-360.
- MÉNARD, L. (1956) "An Apparatus for Measuring the Strength of Soils in Place," MSCE Thesis, University of Illinois.
- MÉNARD, L. (1975) "The Ménard Pressuremeter," *Les Éditions Sols-Soils*, No. 26, pp. 7-43.
- MÉNARD, L., AND BROISE, Y. (1975) "Theoretical and Practical Aspects of Dynamic Consolidation," *Géotechnique*, Vol. XXV, No. 1, pp. 3-18.
- MESRI, G. (1973) "Coefficient of Secondary Compression," *Journal of the Soil Mechanics and Foundations Division*, ASCE, Vol. 99, No. SM1, pp. 123-137.
- MESRI, G. (1975) Discussion of "New Design Procedures for Stability of Soft Clays," *Journal of the Geotechnical Engineering Division*, ASCE, Vol. 101, No. GT4, pp. 409-412.
- MESRI, G., AND GODLEWSKI, P.M. (1977) "Time- and Stress-Compressibility Interrelationship," *Journal of the Geotechnical Engineering Division*, ASCE, Vol. 103, No. GT5, pp. 417-430.
- MILLIGAN, V. (1972) Discussion of "Embankments on Soft Ground," *Proceedings of the ASCE Specialty Conference on Performance of Earth and Earth-Supported Structures*, Purdue University, Vol. III, pp. 41-48.
- MILLS, W.T., AND DESALVO, J.M. (1978) "Soil Compaction and Proofrolling," *Soils*, newsletter of Converse, Ward, Davis, and Dixon, Inc., Pasadena, California, and Caldwell, New Jersey, Autumn, pp. 6-7.
- MITCHELL, J.K. (1968) "In-Place Treatment of Foundation Soils," *Placement and Improvement of Soil to Support Structures*, ASCE, pp. 93-130; also in *Journal of the Soil Mechanics and Foundations Division*, ASCE, Vol. 96, No. SM1, (1970) pp. 73-110.

- MITCHELL, J.K. (1976) *Fundamentals of Soil Behavior*, John Wiley & Sons, Inc., New York, 422 pp.
- MITCHELL, J.K., AND GARDNER, W.S. (1975) "In Situ Measurement of Volume Change Characteristics," State-of-the-Art Report, *Proceedings of the ASCE Specialty Conference on In Situ Measurement of Soil Properties*, Raleigh, North Carolina, Vol. II, p. 333.
- MOH, Z.C., BRAND, E.W., AND NELSON, J.D. (1972) "Pore Pressures Under a Band on Soft Fissured Clay," *Proceedings of the ASCE Specialty Conference on Performance of Earth and Earth-Supported Structures*, Purdue University, Vol. I, Part 1, pp. 245-246.
- MOHR, O. (1887) "Über die Bestimmung und die graphische Darstellung von Trägheitsmomenten ebener Flächen," *Civilingenieur*, columns 43-68; also in *Abhandlungen aus dem Gebiete der technischen Mechanik*, 2nd Ed., W. Ernst u. Sohn, Berlin, pp. 90 and 109 (1914).
- MOHR, O. (1900) "Welche Umstände bedingen die Elastizitätsgrenze und den Bruch eines Materiale?" *Zeitschrift des Vereines Deutscher Ingenieure*, Vol. 44, pp. 1524-1530; 1572-1577.
- MORGENSTERN, N.R., AND EISENSTEIN, Z. (1970) "Methods of Estimating Lateral Loads and Deformation," *Proceedings of the ASCE Specialty Conference on Lateral Stresses in the Ground and Design of Earth-Retaining Structures*, Cornell University, pp. 51-102.
- MULILIS, J.P., SEED, H.B., AND CHAN, C.K. (1977) "Effects of Sample Preparation on Sand Liquefaction," *Journal of the Soil Mechanics and Foundations Division*, ASCE, Vol. 103, No. GT2, pp. 91-108.
- NEWMARK, N.M. (1935) "Simplified Computation of Vertical Pressures in Elastic Foundations," *University of Illinois Engineering Experiment Station Circular* 24, Urbana, Illinois, 19 pp.
- NEWMARK, N.M. (1942) "Influence Charts for Computation of Stresses in Elastic Foundations," *University of Illinois Engineering Experiment Station Bulletin*, Series No. 338, Vol. 61, No. 92, Urbana, Illinois, reprinted 1964, 28 pp.
- OSTERBERG, J.O. (1957) "Influence Values for Vertical Stresses in a Semi-infinite Mass Due to an Embankment Loading," *Proceedings of the Fourth International Conference on Soil Mechanics and Foundation Engineering*, London, Vol. I, pp. 393-394.
- OSTERBERG, J.O. (1963) "Current Practice in Foundation Design-II," *Chicago Soil Mechanics Lecture Series*, ASCE and Illinois Institute of Technology, pp. 6-22.
- OSTERMAN, J. (1960) "Notes on the Shearing Resistance of Soft Clays," *Acta Polytechnica Scandinavica*, Series Ci-2, (AP 263 1959), pp. 1-22.
- PARK, T.K., AND SILVER, M.L. (1975) "Dynamic Triaxial and Simple Shear Behavior of Sand," *Journal of the Geotechnical Engineering Division*, ASCE, Vol. 101, No. GT6, pp. 513-529.
- PARSONS, A.W., KRAWCZYK, J., AND CROSS, J.E. (1962) "An Investigation of the Performance on an 8 $\frac{1}{2}$ -Ton Vibrating Roller for the Compaction of Soil," Road Research Laboratory, Laboratory Note No. LN/64/AWP. JK. JEC.
- PAVLOVSKY, N.N. (1956) *Collected Works*, Akad. Nauk USSR, Leningrad.

- PECK, R.B., HANSON, W.E., AND THORNBURN, T.H. (1974) *Foundation Engineering*, 2nd Ed., John Wiley & Sons, Inc., New York, 514 pp.
- PENNER, E. (1963) "Sensitivity in Leda Clay," *Nature*, Vol. 197, No. 4865, pp. 347-348.
- PERLOFF, W.H., AND BARON, W. (1976) *Soil Mechanics—Principles and Applications*, The Ronald Press Company, New York, pp. 359-361.
- POULOS, H.G., AND DAVIS, E.H. (1974) *Elastic Solutions for Soil and Rock Mechanics*, John Wiley & Sons, Inc., New York, 411 pp.
- PROCTOR, R.R. (1933) "Fundamental Principles of Soil Compaction," *Engineering News-Record*, Vol. 111, Nos. 9, 10, 12, and 13.
- PUSCH, R. (1973) General Report on "Physico-Chemical Processes which Affect Soil Structure and Vice Versa," *Proceedings of the International Symposium on Soil Structure*, Gothenburg, Sweden, Appendix p. 33.
- QUIGLEY, R.M., AND THOMPSON, C.D. (1966) "The Fabric of Anisotropically Consolidated Sensitive Marine Clay," *Canadian Geotechnical Journal*, Vol. III, No. 2, pp. 61-73.
- RAJU, A.A. (1956) "The Preconsolidation Pressure in Clay Soils," MSCE Thesis, Purdue University, 41 pp.
- RAYMOND, G.P., TOWNSEND, D.L., AND LOJKACEK, M.J. (1971) "The Effects of Sampling on the Undrained Soil Properties of the Leda Soil," *Canadian Geotechnical Journal*, Vol. 8, No. 4, pp. 546-557.
- RAYMOND, G.P., AND WAHLS, H.E. (1976) "Estimating One-Dimensional Consolidation, Including Secondary Compression of Clay Loaded from Overconsolidated to Normally Consolidated State," *Special Report 163*, Transportation Research Board, pp. 17-23.
- REED, M.A., LOVELL, C.W., ALTSCHAFFL, A.G., AND WOOD, L.E. (1979) "Frost Heaving Rate Predicted from Pore Size Distribution," *Canadian Geotechnical Journal*, Vol. 16, No. 3, pp. 463-472.
- RUTLEDGE, P.C. (1944) "Relation of Undisturbed Sampling to Laboratory Testing," *Transactions*, ASCE, Vol. 109, pp. 1162-1163.
- SAADA, A.S., AND BIANCHINI, G.F. (1975) "Strength of One Dimensionally Consolidated Clays," *Journal of the Geotechnical Engineering Division*, ASCE, Vol. 101, No. GT11, pp. 1151-1164.
- SAGLERAT, G. (1972) *The Penetrometer and Soil Exploration*, Elsevier, Amsterdam, 464 pp.
- SCHMERTMANN, J.H. (1955) "The Undisturbed Consolidation Behavior of Clay," *Transactions*, ASCE, Vol. 120, pp. 1201-1233.
- SCHMERTMANN, J.H. (1970) "Suggested Method for Screw-Plate Load Test," *Special Procedures for Testing Soil and Rock for Engineering Purposes*, 5th Ed., ASTM Special Technical Publication 479, pp. 81-85.
- SCHMERTMANN, J.H. (1975) "Measurement of In Situ Shear Strength," State-of-the-Art Report, *Proceedings of the ASCE Specialty Conference on In Situ Measurement of Soil Properties*, Raleigh, North Carolina, Vol. II, pp. 57-138.
- SCHMIDT, B. (1966) Discussion of "Earth Pressures at Rest Related to Stress History," *Canadian Geotechnical Journal*, Vol. III, No. 4, pp. 239-242.

- SCHMIDT, B. (1967) "Lateral Stresses in Uniaxial Strain," *Bulletin No. 23*, Danish Geotechnical Institute, pp. 5-12.
- SCHWAB, E.F. (1976) "Bearing Capacity, Strength, and Deformation Behaviour of Soft Organic Sulphide Soils," PhD Thesis, Institutionen för Jord- och Bergmekanik, Kungliga Tekniska Högskolan, Stockholm, 368 pp.
- SCOTT, R.F. (1963) *Principles of Soil Mechanics*, Addison-Wesley Publishing Company, Inc., Reading, Massachusetts, pp. 267-275.
- SEED, H.B. (1959) "A Modern Approach to Soil Compaction," *Proceedings of the Eleventh California Street and Highway Conference*, reprint No. 69, The Institute of Transportation and Traffic Engineering, University of California at Berkeley, p. 93.
- SEED, H.B. (1964) Lecture Notes, CE 271, Seepage and Earth Dam Design, University of California at Berkeley (by W.D. Kovacs, April 13).
- SEED, H.B. (1979) "Soil Liquefaction and Cyclic Mobility Evaluation for Level Ground During Earthquakes," *Journal of the Geotechnical Engineering Division*, ASCE, Vol. 105, No. GT2, pp. 201-255.
- SEED, H.B., AND CHAN, C.K. (1959) "Structure and Strength Characteristics of Compacted Clays," *Journal of the Soil Mechanics and Foundations Division*, ASCE, Vol. 85, No. SM5, pp. 87-128.
- SEED, H.B., AND IDRISI, I.M. (1967) "Analysis of Soil Liquefaction: Niigata Earthquake," *Journal of the Soil Mechanics and Foundations Division*, ASCE, Vol. 93, No. SM3, pp. 83-108.
- SEED, H.B., AND LEE, K.L. (1966) "Liquefaction of Saturated Sands During Cyclic Loading," *Journal of the Soil Mechanics and Foundations Division*, ASCE, Vol. 92, No. SM6, pp. 105-134.
- SEED, H.B., AND LEE, K.L. (1967) "Undrained Strength Characteristics of Cohesionless Soils," *Journal of the Soil Mechanics and Foundations Division*, ASCE, Vol. 93, No. SM6, pp. 333-360.
- SEED, H.B., AND PEACOCK, W.H. (1971) "Test Procedures for Measuring Soil Liquefaction Characteristics," *Journal of the Soil Mechanics and Foundations Division*, ASCE, Vol. 97, No. SM8, pp. 1099-1119.
- SEED, H.B., AND WILSON, S.D. (1967) "The Turnagain Heights Landslide, Anchorage, Alaska," *Journal of the Soil Mechanics and Foundations Division*, ASCE, Vol. 93, No. SM4, pp. 325-353.
- SEED, H.B., WOODWARD, R.J., AND LUNDGREN, R. (1962) "Prediction of Swelling Potential for Compacted Clays," *Journal of the Soil Mechanics and Foundations Division*, ASCE, Vol. 88, No. SM4, pp. 107-131.
- SEEMEL, R.M. (1976) "Plastic Filter Fabrics Challenging the Conventional Granular Filter," *Civil Engineering*, ASCE, Vol. 46, No. 3, pp. 57-59.
- SELIG, E.T., AND YOO, T.-S. (1977) "Fundamentals of Vibratory Roller Behavior," *Proceedings of the Ninth International Conference on Soil Mechanics and Foundation Engineering*, Tokyo, Vol. 2, pp. 375-380.
- SIMONS, N.E. (1958) Discussion of "Test Requirements for Measuring the Coefficient of Earth Pressure at Rest," *Proceedings of the Conference on Earth Pressure Problems*, Brussels, Vol. III, pp. 50-53.
- SIMONS, N.E. (1974) "Normally Consolidated and Lightly Overconsolidated Cohe-

- sive Materials," General Report, *Proceedings of the Conference on Settlement of Structures*, Cambridge University, British Geotechnical Society, pp. 500-530.
- SKEMPTON, A.W. (1953) "The Colloidal Activity of Clays," *Proceedings of the Third International Conference on Soil Mechanics and Foundation Engineering*, Vol. I, pp. 57-61.
- SKEMPTON, A.W. (1954) "The Pore-Pressure Coefficients *A* and *B*," *Géotechnique*, Vol. IV, pp. 143-147.
- SKEMPTON, A.W. (1960) "Effective Stress in Soils, Concrete and Rocks," *Pore Pressure and Suction in Soils*, Butterworths, London, p. 5.
- SKEMPTON, A.W. (1964) "Long-Term Stability of Clay Slopes," *Géotechnique*, Vol. XIV, No. 2, pp. 77-101.
- SKEMPTON, A.W. (1977) "Slope Stability of Cuttings in Brown London Clay," *Proceedings of the Ninth International Conference on Soil Mechanics and Foundation Engineering*, Tokyo, Vol. 3, pp. 261-270.
- SKEMPTON, A.W., AND NORTHEY, R.D. (1952) "The Sensitivity of Clays," *Géotechnique*, Vol. III, No. 1, pp. 30-53.
- SKEMPTON, A.W., AND HENKEL, D.J. (1953) "The Post-Glacial Clays of the Thames Estuary at Tilbury and Shellhaven," *Proceedings of the Third International Conference on Soil Mechanics and Foundation Engineering*, Zurich, Vol. I, pp. 302-308.
- SODERMAN, L.G., AND KIM, Y.D. (1970) "Effect of Groundwater Levels on Stress History of the St. Clair Clay Till Deposit," *Canadian Geotechnical Journal*, Vol. 7, No. 2, pp. 173-187.
- STEWARD, J.E., WILLIAMSON, R., AND MOHNEY, J. (1977) "Guidelines for Use of Fabrics in Construction and Maintenance of Low-Volume Roads," *Internal Report*, U.S. Forest Service, Portland, Oregon; also published as *Report No. FHWA-TS-78-2-5* by the Federal Highway Administration, Washington, D.C., 171 pp.
- TAYLOR, D.W. (1948) *Fundamentals of Soil Mechanics*, John Wiley & Sons, Inc., New York, 700 pp.
- TAVENAS, F.A., CHAPEAU, C., LAROCHELLE, P., AND ROY, M. (1974) "Immediate Settlements of Three Test Embankments on Champlain Clay," *Canadian Geotechnical Journal*, Vol. 11, No. 1, pp. 109-141.
- TAVENAS, F.A., BLANCHETTE, G., LEROUEIL, S., ROY, M., AND LAROCHELLE, P. (1975) "Difficulties in the In Situ Determination of  $K_0$  in Soft Sensitive Clays," *Proceedings of the ASCE Specialty Conference on In Situ Measurement of Soil Properties*, Raleigh, North Carolina, Vol. I, pp. 450-476.
- TERZAGHI, K. (1922) "Der Grundbruch an Stauwerken und seine Verhütung," *Die Wasserkraft*, Vol. 17, No. 24, pp. 445-449; reprinted in *From Theory to Practice in Soil Mechanics*, John Wiley & Sons, Inc., New York, pp. 114-118.
- TERZAGHI, K. (1925) *Erdbaumechanik auf Bodenphysikalischer Grundlage*, Franz Deuticke, Leipzig und Wein, 399 pp.
- TERZAGHI, K. (1927) "Concrete Roads—A Problem in Foundation Engineering," *Journal of the Boston Society of Civil Engineers*, May; reprinted in *Contributions to Soil Mechanics 1925-1940*, BSCE, pp. 57-58.

## References

716

- TERZAGHI, K. (1943) *Theoretical Soil Mechanics*, John Wiley & Sons, Inc., New York, 510 pp.
- TERZAGHI, K., AND PECK, R.B. (1967) *Soil Mechanics in Engineering Practice*, 2nd Ed., John Wiley & Sons, Inc., New York, pp. 729.
- TURNBULL, W.J. (1950) "Compaction and Strength Tests on Soil," presented at Annual Meeting, ASCE, January, as cited by Lambe, T.W., and Whitman, R.V. (1969) *Soil Mechanics*, John Wiley & Sons, Inc., New York, p. 517.
- TURNBULL, W.J., AND FOSTER, C.R. (1956) "Stabilization of Materials by Compaction," *Journal of the Soil Mechanics and Foundations Division, ASCE*, Vol. 82, No. SM2, pp. 934-1 to 934-23; also in *Transactions, ASCE*, Vol. 123, (1958), pp. 1-26.
- U.S. ARMY CORPS OF ENGINEERS (1970) "Laboratory Soils Testing," *Engineer Manual, EM 1110-2-1906*.
- U.S. ARMY ENGINEER WATERWAYS EXPERIMENT STATION (1960) "The Unified Soil Classification System," *Technical Memorandum No. 3-357*. Appendix A, Characteristics of Soil Groups Pertaining to Embankments and Foundations, 1953; Appendix B, Characteristics of Soil Groups Pertaining to Roads and Airfields, 1957.
- U.S. BUREAU OF RECLAMATION (1974) *Earth Manual*, 2nd Ed., Denver, 810 pp.
- U.S. NAVY (1971) "Soil Mechanics, Foundations, and Earth Structures," *NAVFAC Design Manual DM-7*, Washington, D.C.
- WALLACE, G.B., AND OTTO, W.C. (1964) "Differential Settlement at Selfridge Air Force Base," *Journal of the Soil Mechanics and Foundations Division, ASCE*, Vol. 90, No. SM5, pp. 197-220; also in *Design of Foundations for Control of Settlement*, ASCE, pp. 249-272.
- WARSHAW, C.M., AND ROY, R. (1961) "Classification and a Scheme for the Identification of Layer Silicates," *Geological Society of America Bulletin*, Vol. 72, pp. 1455-1492.
- WESTERGAARD, H.M. (1938) "A Problem of Elasticity Suggested by a Problem in Soil Mechanics: A Soft Material Reinforced by Numerous Strong Horizontal Sheets," in *Contributions to the Mechanics of Solids, Stephen Timoshenko 60th Anniversary Volume*, Macmillan, New York, pp. 268-277.
- WILSON, S.D. (1970) "Suggested Method of Test for Moisture-Density Relations of Soils Using Harvard Compaction Apparatus," *Special Procedures for Testing Soil and Rock for Engineering Purposes*, 5th Ed., ASTM Special Technical Publication 479, pp. 101-103.
- WINELAND, J.D. (1975) "Borehole Shear Device," *Proceedings of the ASCE Specialty Conference on In Situ Measurement of Soil Properties*, Raleigh, North Carolina, Vol. I, pp. 511-522.
- WISSA, A.E.Z. (1969) "Pore Pressure Measurement in Saturated Stiff Soils," *Journal of the Soil Mechanics and Foundations Division, ASCE*, Vol. 95, No. SM4, pp. 1063-1073.
- WROTH, C.P. (1972) "General Theories of Earth Pressures and Deformations," General Report, *Proceedings of the Fifth European Conference on Soil Mechanics and Foundation Engineering*, Madrid, Vol. II, pp. 33-52.

- WROTH, C.P. (1975) "In Situ Measurement of Initial Stresses and Deformation Characteristics," *Proceedings of the ASCE Specialty Conference on In Situ Measurement of Soil Properties*, Raleigh, North Carolina, Vol. II, pp. 181-230.
- YODER, E.J., AND WITCZAK, M.W. (1975) *Principles of Pavement Design*, John Wiley & Sons, Inc., New York, 711 pp.
- YONG, R.N., AND SHEERAN, D.E. (1973) "Fabric Unit Interaction and Soil Behaviour," *Proceedings of the International Symposium on Soil Structure*, Gothenburg, Sweden, pp. 176-183.
- YONG, R.N., AND WARKENTIN, B.P. (1975) *Soil Properties and Behaviour*, Elsevier Scientific Publishing Co., New York, 449 pp.
- ZIMMIE, T.F. (1973) "Soil Tests on a Clay from Skå-Edeby, Sweden," Norwegian Geotechnical Institute, Internal Report No. 50306-3, 21 pp.



# Index

**AASHTO** (*see* Soil classification systems)  
**Activity:**  
defined, 41, 188  
typical values, 92  
**Allophane** (*see* Clay minerals)  
**Alumina (octahedral) sheet**, 78-80  
**Angle of internal friction**, 452 (*see also* Shear strength)  
correlation with e, 518  
effect of test type, 517  
with soil classification, 518  
summary of factors affecting, 517  
typical values, 516  
**Angle of repose**, 177  
definition, 492  
sand dune, 493  
**Anisotropy**, 597, 609  
**Anisotropic consolidation** (*see* Shear strength tests: triaxial test)  
**Apparent cohesion**, 176  
**Artesian pressure**, 242  
**ASCE**, 9  
**ASTM**, 9  
**Attapulgite** (*see* Clay minerals)  
**Atterberg limits**, 34-40  
cohesion limit, 34  
effect of air drying, 38  
engineering properties:  
relation to, 40  
flow index, 46  
liquid limit, LL, 34-39  
device, 37  
effect of grooving tool, 38-39  
flow curve, 38  
one point test, 38  
test description, 38  
plastic limit, 34-39  
test description, 38  
plasticity chart, 51, 54

**Atterberg limits (continued)**  
plasticity index, 39  
range, 39  
shrinkage limit, 34  
soil classification, use in, 40  
sticky limit, 34  
toughness index, 46  
**Bangkok clay**:  
compression index, 342  
consolidation behavior, 338  
**Bentonite**, 107, 189  
**Bernoulli energy equation**, 202, 227  
**Blasting** (*see* Compaction)  
**Body stress** (*see* Stress)  
**Boiling** (*see* Quicksand)  
**Borderline classification**, 53, 56-57  
**Boston blue clay**:  
coefficient of consolidation, 404  
compression index, 342  
profile, 336  
values of  $C_u/C_c$ , 408-9  
**Boulders**, 27, 49-50, 65  
used in classification, 50, 65  
**Boussinesq method** (*see also* Stress distribution)  
influence charts, 358  
integrated over areas, 346-54  
point load, 345-46  
**Brucite** (*see* Clay minerals)  
**Bulking**, 103, 174, 176  
**Bulldozer**, 126-27 (*see also* Compaction equipment)  
**Bull's liver**, 178  
**California Bearing Ratio, CBR, 125, 155-56**  
**CBR** (*see* California Bearing Ratio)  
**Capillarity**, 167-78  
adhesion forces, 167  
height of rise, 167-69

- Capillarity (continued)**
- typical values, 176
  - negative pressure, 172
  - in small tubes, 167-70
- Capillary pressures, 170-72**
- example, 185
  - in frost action, 192
- Capillary tubes, 167-73**
- Capillary water, 166**
- Cavitation, 170, 504**
- CD (see Shear strength: Shear strength tests)**
- CD tests, 438-45, 465, 493-503**
- Mohr failure envelopes:
    - normally consolidated clays, 541
    - overly consolidated clays, 542
    - sands, 505, 515  - shear strength parameters, 516-18, 543, 555
  - stress conditions, 539
  - stress paths, 481, 541
  - test details, 493-4, 538-9
  - typical behavior, 494-503
- Cell pressure, 465 (see also Confining pressure)**
- Chicago clay:**
- coefficient of consolidation, 404
  - compression index, 341-42
  - consolidation behavior, 305
  - soil profile, 340
  - value of  $C_a/C_c$ , 409
- Chlorite (see Clay minerals)**
- Classification systems (see Soil classification systems)**
- Clays, 6, 25-27**
- used in classification, 50, 65, 77
  - consistency, 61
  - consolidation behavior, 299-306
  - defined, 77
  - desiccated/or dry crust, 136, 186
  - frost susceptibility, 195
  - quick, 39
  - sensitive, 39
  - shrinkage, 178-90
  - stability, critical conditions, 639
  - structure, due to compaction, 117
  - swelling, 284, 306
- Clay minerals, 26, 78-88**
- absorbed water, 92-94
  - activity of, 92
  - alophane, 88
  - attapulgite, 85
  - SEM, 87
  - bonding agents:
    - co-valent, 108
    - hydrogen bond, 92
    - James, 108
    - brucite, 80  - chlorite, 85-87, 89, 91
  - crystal structure:
    - octahedral or alumina sheets, 78
    - tetrahedral or silica sheets, 78-82
- Clay minerals (continued)**
- toga party, 108
  - flocculation, factors causing, 95
  - gibbsite, 79
  - halloysite, 82-83, 89
  - SEM, 82
  - hydrous alumino silicates, 78
  - identification, 88-89
    - DTA, 88
    - electron microscopy, 88
    - x-ray diffraction, 88  - illite, 85-86, 89, 91
  - SEM, 86
  - ion concentration, 95
  - kaolinite, 81-82, 89, 91
    - atomic structure, 81
    - SEM, 82  - marine, 93
  - mixed layer minerals, 85, 88
  - montmorillonite (smectite), 83-85, 88-89, 91
    - atomic structure, 83-84
    - SEM, 85  - particle interaction, 95
  - use of Plasticity Chart, 88-89
  - stabilization, lime, 94
  - silica sheet, 94
  - soil structure:
    - dispersed, 95-96
    - flocculated, 95-96  - tetrahedral (silica) sheet, 78-79
- Clay soils, 25-26, 77 (see also Clays; Clay minerals; Shear strength)**
- van der Waal's forces, 83, 95
  - vermiculite, 85
- Clusters (see Soil fabric)**
- Coarse grained soils, 25-27, 49, 60**
- Cobbles, 27, 49-50**
- Coefficient of consolidation (see Consolidation)**
- Coefficient of curvature:**
- defined, 31, 50
  - typical values, 31
- Coefficient of lateral earth pressure (see  $K_o$ )**
- Coefficient of permeability:**
- determination by oedometer test, 402-3
- Coefficient of uniformity:**
- defined, 29, 50
  - effect on  $\phi$ , 516
  - typical values, 31, 104
- Coefficient of volume change, 311, 313**
- Cofferdam, 256**
- Cohesion, defined, 25**
- Cohesionless, 102**
- Cohesive soil, defined, 77**
- Collapsing soils, 188**
- Compacted clays:**
- performance of, 153-61
  - PH test results, 564
  - properties, 117-24
  - strength, 124
  - use in earth dams, 158-59

**Index**

- Compacted clays (continued)**  
     use in pavement design, 154-57
- Compaction:**  
     benefits of, 111  
     by blasting, 139  
     clays, properties of, 117-24  
     of cohesive soils, 117-24  
     control tests, 145-53  
     curve, 113  
         line of optimums, 115, 149  
         maximum dry density, 113  
         optimum water content, 113  
     definition, 110  
     dry densities, typical values, 113, 155-56  
     dynamic, 139-41  
     field versus laboratory, 116-17  
     impact, 111  
     kneading, 111-13, 116  
     lift thickness, 124, 127, 130, 133, 138-39  
     most efficient conditions, 143-44  
     objectives of, 111  
     percent, 142  
     proofrolling, 129-30, 144  
     rapid control (*see Compaction tests, rapid method*)  
     relative, 142  
     relative density, 142  
     saturation curve, 113-14  
     specifications, 141-45  
     static, 111, 113  
     theory, 111-16  
     types of, 111  
     vibratory:  
         effect of frequency, 133-34, 136  
         effect of lift thickness, 136-39  
         effect of number of passes, 136-37  
         effect of towing speed, 136-37  
         optimum frequency, 133-34  
         variables affecting, 133  
     vibratory insitu, vibrofloatation, 139  
     vibratory surface, plate compactors, 132-35
- Compaction control, 141-53**
- Compaction equipment, 124-40**  
     bovinas masculinus sonambulorum, 127  
     draglines, 124  
     dump trucks, 124, 127  
     4 X 4 and 5 X 5 rollers, 130  
     grid or mesh rollers, 130, 132  
     motor grader or "blade," 127  
     power shovels, 124  
     rollers, 127  
         rubber tire roller, 128, 130, 156-57  
         scrapers or "pans," 124, 126, 129  
         sheepsfoot rollers, 129-31, 156-57  
         smooth wheel rollers, 127-28, 156-57  
         tamping foot rollers, 130-31  
         vibratory compactors, 132-35  
             applications of, 135  
             types of, 134  
     vibrating drum, 132, 134-35
- Compaction equipment (continued)**  
     vibrating plates and rammers, 132, 134-35
- Compaction problems:**  
     overcompaction, 144  
     pumping or weaving, 144
- Compaction specifications, 141-45**  
     end product, 142-44  
     method specifications, 142, 145
- Compaction tests:**  
     curves, typical, 115  
     destructive, 145-53  
     equipment type, 146, 152  
     field check point test, 148-49  
     field density tests, 137, 145-53  
     use of field drying, 150  
     nondestructive, 145, 152-53  
     nuclear density meters, 153  
     one point Proctor test, 148-49  
     Proctor test, 111-15  
     Proctor test (modified), test details, 114-15  
     Proctor test (standard), test details, 111-12  
     rapid method, 150-51
- Compactive effort, 111-12, 143-44**
- Compressibility, 285-89**  
     causes of, 286  
     clays, 286  
     coefficient of, 310-13, 381-82, 685, 687  
     coefficient of volume change, 311  
     compacted clays, 118-20, 123  
     effect of LIR on, 326  
     one dimension, 285-86  
     sands, 286-87  
     soil skeleton, 691-92, 697-98
- Compression, 283**  
     elastic, in oedometer, 402, 405-10  
     index, 313, 341-42  
     modulus, 312  
     ratio, 314  
     secondary, 376, 380  
     triaxial, 693
- Compression index, 313, 341-42**  
     approximations, 341  
     equations for, 341  
     field, 330, 333  
     modified, 314  
     modified secondary, 406  
     secondary, 406  
     typical values of, 342
- Compression ratio, 314, (*see also Consolidation parameters; Modified compression index*)**
- Compressometer (*see Screw plate compressometer test*)**
- Confining pressure (*see Triaxial tests*)**
- Confining pressure:**  
     consolidation, 500  
     critical, 500  
         example, 509  
     effect on cyclic mobility, 530
- triaxial tests:**

- Confining pressure (continued)**
- hydrostatic, 538, 610
  - non-hydrostatic, 538, 610
- Conservation of mass, law of,** 202
- Consistency:**
- definition, 61
  - descriptors, 61
- Consistency limits,** 34, (*see also* Atterberg limits)
- Consolidation:**
- coefficient of, 381, 395, 686-87
  - correlations, 404
  - determination of, 395, 399, 401
  - relation to time factor, 383
  - typical values, 404
  - defined, 379
  - degree of, 383, 387, 688-90
  - effect of permeability, 286
  - natural soils behavior, 299-309
  - percent, 291, 383, 387, 688
  - phenomena explained, 286
  - primary, 376
    - prediction of, 418
  - process, 377-80
  - ratio, 383, 688
  - spring analogy, 288, 377-80
  - secondary, 376, 405-10
  - settlements, 376
  - stress, 291
- Terzaghi's 1-D Theory, 380
- assumptions, 380, 681
  - derivation, 381-82, 683-86
  - solution, 382-85, 686-90
- test, 289-94
- theory, 380-83, 683-86
- time rate of, 376-77
- underconsolidated, 294
- Consolidation parameters:**
- coefficient of
    - compressibility, 310-13
    - consolidation, 381
    - volume change, 311, 313
  - compression index, 313-14, 317
    - relation to modified compression index, 315
  - consolidation ratio, 383
  - degree of consolidation, 383
    - average degree of, 387-89, 391-92
    - relation with time factor, 388-90
  - modified compression index, 314, 317
    - relation to compression index, 315
  - modified recompression index, 320
    - relation to recompression index, 320
  - modified secondary compression index
    - (secondary compression ratio, rate of secondary compression), 406
  - percent of consolidation, 383
  - recompression index, 320
    - method to evaluate, 323-24
- Consolidation parameters (continued)**
- relation to modified recompression index, 320
    - secondary compression index, 406
    - time factor, 382-83, 399, 687
  - Consolidation ratio, 383-87, 688
  - Consolidation settlement, 285
    - calculation of, 309-26
    - time rate, 376-423
  - Consolidation testing, 289-293
    - data presentation:
      - percent consolidation vs. effective stress, 291-93
      - void ratio vs. effective stress, 291-93
    - fixed ring, 290-91
    - floating ring, 290-91
    - test details, 289-91
  - Consolidation tests:
    - effect of sample disturbance, 297-98
    - of typical soils, 299-309
      - Chicago and Indiana glacial clay, 305
      - Leda clay, 303
      - Loessial soils, 307
      - Mexico City clay, 304
      - NC clays and silts, 300
      - Newfoundland peat, 308
      - Newfoundland silt, 308
      - OC clay tills, 301-2
      - swelling clays, 306
  - Consolidation theory:
    - Terzaghi's theory
      - assumptions, 683
      - boundary conditions, 685-87
      - derivation, 683-86
      - solution, 686-90
      - time factor, 687, 689-90
  - Consolidometer, 289-91
  - Constrained modulus, 311-12
  - Continuity equation, 202
  - $c/p(\tau_f/\sigma_{v0})$  ratio:
    - effect of age, 591
    - defined, 587-88
    - effect of overconsolidation, 590-92
    - effect of stress path, 590
    - relation with L1, 590
    - relation with PI, 589
  - CU (*see also* Shear strength; shear strength tests)
  - CU tests, 545-58, 404-6, 465
    - Mohr failure envelopes:
      - normally consolidated clays, 550
      - over/consolidated clays, 551
      - preconsolidation stress, 551
      - sands, 505
      - sensitive clay, 554
    - shear strength parameters, 550
      - relation with CD tests, 555
      - typical values, 553-54
    - stress conditions, 547

**Index**

- CU test (continued)**  
 stress paths, 552-53, 583-84  
 ESP, 552-53  
 TSP, 552-53  
 $(T-U_0)SP$ , 552-53  
 test details, 545  
 typical behavior, 549  
**Curve fitting methods**, 395-402  
 Casagrande's, 396-400  
 Taylor's, 397, 400-402  
**Cyclic mobility**:  
 definition, 522, 524  
 differences between liquefaction, 534  
 factors affecting, 530  
 use of Peacock diagram, 527  
**Cyclic strain history**:  
 effect on cyclic mobility, 530  
**Cyclic stress**, definition, 530
- Darcy's law**, 202-4, 681  
 application to sands, 203-4  
 definition, 203-4  
 deviation from, 205  
 in theory of consolidation, 380, 683-84  
 validity for other soils, 205  
**Datum plane**, 227  
**Daytona Beach, Florida**, 176, 196  
**Defects**, 4, 256  
**Deformations**:  
 in oedometer, 402  
 types of, 283  
 distortion, 283  
 compression, 283  
**Degree of saturation**, definition, 13  
**Densification (see Compaction)**  
**Density**:  
 buoyant or submerged, definition, 15  
 chunk, 43  
 descriptors, 60  
 dry:  
   definition, 15  
   typical values, 105  
 field, 142  
 index, 103, 142  
 nuclear, 153  
 relative:  
   defined, 103  
   typical values, 104  
 saturated, definition, 15  
 solids, definition, 14  
 submerged, typical values, 105  
 total, (wet) definition, 14  
 typical values, 15, 105  
 water, 15  
**Density index (see Relative density)**  
**Desiccation**:  
 causing preconsolidation, 295  
 dry crust, 136, 186
- Differential thermal analysis**, 88  
**Dilatancy (see Soil characteristics)**  
**Distortion settlement**, 283  
**Drainage path**, 379, 382  
 double drainage, 379, 383, 385, 393, 399  
 single drainage, 379, 383, 393  
**DS (see Shear strength tests, direct shear)**  
**DSS (see Shear strength tests, special tests)**  
**Domains (see Soil fabric)**  
**Double angle equations**, 436  
**Dry strength (see Soil characteristics)**  
**DTA (see Differential thermal analysis)**  
**Dutch cone test**, 572-73, 579-81
- Earth pressure (see  $K_0$ )**  
**Earth pressure, coefficient of**, 225  
**Earth structures, examples**, 110  
**Effective consolidation stress**, 291  
**Effective grain size**, 211  
 typical values, 516  
**Effective pore diameter**, 174  
**Effective size**:  
 definition, 29  
 in filter design, 271  
 typical values, 104  
**Effective stress**, 175  
 change in, 691  
 defined, 213  
 effect of ground water lowering/raising, 217-18, 222-25  
 physical meaning, 214-16  
 principle of, 215, 691  
 profiles, 270-75  
 in consolidation testing, 291  
**Effective stress analysis**, 537-38  
 definition, 538  
**Elastic**:  
 compression in oedometer, 402  
 materials, 283  
 secant modulus, 592  
 settlement, 285  
 stress distribution, 344-67  
 tangent modulus, 592  
 theory, 285, 344  
**Elasticity**:  
 linear elastic material, 697  
 theory, 344  
**Elastic material**:  
 pore pressure coefficients for, 692-93, 697  
 stress-strain-time relationships, 283  
**End-product specifications (see Compaction specifications)**  
**Equipotential drops**, 252  
**Erosion, liquefaction cause**, 521  
**Excess hydrostatic pressure**, 289, 291, 377-80, 382, 687  
**Excess pore water pressure**, 377

- Exchangable cations, 83, 93-94  
valence of, 94
- Exit gradient, 256  
by method of fragments, 263
- FAA (see Soil classification systems)**
- Fabric (see also Soil fabric; Soil structure; Structure)  
Fabrics as filters, 272
- Failure criteria:  
maximum shear stress, 454  
Mohr, 449  
Mohr-Coulomb criterion, 449-58  
Mohr failure hypothesis, 454
- Failure plane, angle of inclination of, 563
- Field density tests (see Compaction tests)
- Field identification procedures, 55
- Figanewtons, 671
- Filters:  
criteria, 271-72  
fabrics, 272  
protective, 270-72  
used to control see page, 270-72  
criteria, 272
- Fine grained soils, 25-26, 49, 60
- Fines, 49
- Flow:  
Bernoulli energy equation, 202-3  
channels, 251-52  
confined, 251  
discharge velocity, 204  
energy, 201  
head loss, 201  
heads, illustration, 228  
index, 46  
Laplace's equation, 251, 681-82  
piezometric head, 227, 246-47  
potential (position) head, 202, 227  
pressure head, 202, 227  
seepage velocity, 204  
tortuosity, 205  
total, example calculations, 248-49  
total head (piezometric), 202, 227  
types, defined, 200-201  
unconfined, 253  
velocity head, 202, 227
- Flow lines (see Flow nets)
- Flow nets (see Fragments, method of)
- Flow nets:  
defined, 249  
drawing rules, 251-52  
equation of, 251  
equipotential drops, 252  
equipotential (flow) lines, 249-51  
exit gradients, 255-57  
flow channels, 251-52  
flow lines, 249-51  
flow quantity calculation, 252-53  
uplift calculations, 253-55
- Flow slides (see Liquefaction)  
Flow slides, 245
- Form factor (see Fragments, method of)
- Foundation engineering, definition, 2
- Fragments, method of, 253, 258-70  
detailed example, 261-68  
exit gradient calculation, 261, 264  
form factor, 259, 262, 264, 267  
fragment types, 259-60
- Free swell test, 188-89
- Free water surface, 169
- Friction angle (see also Shear strength; Angle of internal friction)
- Frost action, 190-95  
defined, 190  
effect of pore size, 192  
frost susceptible soils, identification of, 192-95  
ice lenses, 190-92  
necessary conditions, 191-92  
solutions to, 193-95
- Frost heave (see Frost action)
- Frozen soils (see Frost action)
- Gap-or skip-graded soil, 29-30**
- Genus bovinas masculinas sonambulorum, 127
- Geotechnical engineering, definition, 1
- Gibbsite (see Clay minerals)
- Glaciation, causing preconsolidation, 295
- Gradation (see also Grain size distribution)  
Gradation:  
poorly-graded, 50  
skip-or gap-graded, 50  
well-graded, 50
- Grain size, effective use in capillarity, 174
- Grain shape:  
effect on  $\phi$ , 516  
types:  
angular, 33  
bulky, 33  
flakey, 33  
rounded, 33  
subangular, 33  
subrounded, 33
- Grain size distribution, 26-32  
effect on shear strength, 514, 517  
gap-graded, 29  
gradation test, 28  
hydrometer analysis, 28  
mechanical analysis, 28  
poorly graded, 29  
sieve analysis, 28  
skip graded, 29  
uniformly graded, 29-30  
well-graded, 29-31
- Gravel, 6, 27, 50, 65  
characteristics, 26  
used in classification, 50, 65

**Index**

- Ground water table, 166  
 Group index, 65-66, 68
- Halloysite (see Clay minerals)**  
 Hazen's equation, 211  
**Heads (see Flow)**  
**Head loss, 201**  
 examples of, 246-48  
**Heave (see Swelling)**  
**Henkle pore pressure coefficients, 696-700**  
**Hydraulic gradient, 205**  
 critical:  
 defined, 234-35  
 typical values, 235  
 defined, 201  
 in permeability tests, 206  
**Hydrometer analysis, 28**  
**Hydrostatic consolidation (see also Shear strength tests; cyclic triaxial; Triaxial tests; confining pressure)**  
**Harvard miniature compactor, 116**
- Ice lenses (see Frost action)**  
**Illite (see Clay minerals)**  
**Immediate settlement, 285**  
**Impact theory, Coprogenic, 711**  
**Influence charts (see Stress distribution)**  
**Intergranular stress (see Effective stress)**  
**Intermediate principal stress, effect on shear strength, 514**  
**Immediately after construction (see Shear strength, clays)**  
**Iowa borehole shear test, 572-73, 585**  
**Isobars, 379**  
**Isochrones, 379, 384, 420**  
**Isomorphous substitution, 79, 85, 93**  
**Isopachs, 379**  
**Isotropic consolidation (see Shear strength tests, triaxial test)**  
**ISRM, 9**  
**ISSMFE, 9**
- Kaolinite (see Clay minerals)**  
**Kapectate, 82**  
**K<sub>f</sub>, 479, 637**  
 Mohr-Coulomb, relationship with, 482  
 parameters, pf, qf, 482
- K<sub>o</sub>, 225-26, 479**  
 clays, 605-10  
 effect of OCR, 608-10  
 effect of stress path, 607  
 relation to  $\phi'$ , 605  
 relation to PI, 607  
 defined, 225  
 effect on cyclic mobility, 530  
 theoretical relationship:  
 normally consolidated sands, 519  
 overconsolidated sands, 520
- K<sub>o</sub> (continued)**  
 typical values, 226, 480  
 sands, 519
- Laminar flow, 201**  
**Laplace's equations, 251**  
 derivation, 681-82  
**Lateral earth pressure at rest, coefficient of, K<sub>o</sub>, 225-26**  
**Leda clay:**  
 compression index, 342  
 consolidation behavior, 303  
 profile, 339  
 values of C<sub>a</sub>/C<sub>c</sub>, 408-9  
**Lifts (see Compaction)**  
**Line of optimum's (see Compaction curve)**  
**Liquefaction:**  
 defined, 245, 521  
 differences between cyclic mobility, T 11-5, 534  
 flow slides, 245  
 classification, 523  
 how to avoid, 533  
 relation to quicksand, 242, 245  
 steady state line, 532-33  
 use of Peacock diagram, 527  
**Liquid limit, LL (see Atterberg limits)**  
**Liquidity index, 39, 586-87, 590**  
**Linear materials, 283**  
**LIR (see Load increment ratio)**  
**LL (see Atterberg limits)**  
 defined, 326  
 effect on c<sub>v</sub>, 395  
**Load increment ratio, 395**  
 defined, 326  
 effect on c<sub>v</sub>, 395  
**Loess, 306-7**
- Materials:**  
 anisotropic, 3  
 brittle, 447-48  
 density, typical values, 15  
 elastic, 283, 446  
 heterogeneous, 3  
 homogeneous, 3  
 isotropic, 3  
 linear, 283, 446-47  
 nonconservative, 3, 283  
 nonlinear, 3, 283, 446-47  
 plastic, 447-48  
 visco-elastic, 283, 446  
 work hardening and softening, 447-48
- Meniscus:**  
 below ground water table, 177-78  
 defined, 167-68  
 geometry, 167-70  
 Giacomo, 167  
 Shape, 170

- Method specifications (*see* Compaction specifications)  
 Metric system, 666-69  
 Metric units, 665-80  
 Mexico City clay:  
    $C_\alpha/C_c$ , values of, 408-9  
   coefficient of consolidation, 404  
   compression index, 342  
   consolidation behavior, 303-4  
 Mica, 85  
 Mjälö, 51  
 Mo, 51  
 Modified compression index, 314  
   approximations, 341  
   secondary, 406  
 Modified Proctor test (*see* Compaction tests)  
 Modified recompression index, 320  
 Modulus (*see also* Elastic)  
   constrained, 312  
   oedometric, 312  
   secant, 592  
   tangent, 592  
   undrained, 592-95  
 Mohr circle:  
   failure plane,  $\alpha_f$ , 451  
   obliquity, maximum, 467, 554  
   obliquity relationships, 457  
   pole method, 436  
   origin of planes (pole method):  
     definition, 436  
     examples of, 436, 438, 440, 442, 444  
   property of, 436, 450  
 Mohr-Colomb strength criteria, 453-58  
 Mohr-Colomb strength parameters, 453  
 Mohr failure envelopes, 449-51 (*see also* Shear strength)  
   curved, 516  
   effect of preconsolidation pressure, 543, 551  
   normally consolidated clays, 541-550  
   overconsolidated clays, 541-42, 551  
   sands, 505, 515  
   sensitive clay, 554  
 Mohr failure hypothesis:  
   definition, 451  
   Mohr failure theory, difference between, 451  
   use in direct shear, 460  
 Monotonic loading, 521, (*see also* Liquefaction)  
 Montmorillonite (*see* Clay minerals)
- N.C. (*see* Normally consolidated soils)  
 Neutral stress (*see* Pore water pressure)  
 Newmark's charts, 258-59  
 Nonconservative materials, 283  
 Normal stress, 453  
   octahedral, 697-9  
 Normally consolidated soils, defined, 294  
 Nuclear density meters (*see* Compaction tests)
- OC (*see* Overconsolidated soils)  
 Octahedral (alumina) sheet, 78-80  
 Octahedral:  
   normal stress, 697-99  
   shear stress, 697-99  
 Oedometer (*see* Consolidometer)  
 Oedometric modulus (*see* Constrained modulus)  
 One-dimensional:  
   compressibility, 285-86  
   consolidation theory, 380-85, 683-86  
   loading, 342  
 Optimum water content, 113  
 Organic soils, 50  
 Origin of planes (*see* Mohr circle)  
 Overburden pressure, 288 (*see also* Stress)  
 Overconsolidated soils:  
   defined, 186, 294  
   reasons for, 294-95  
   settlement calculations, 320-26  
 Overconsolidation:  
   causes, 295  
   effect on pore pressure parameters, 600-603  
   effect on shear strength, 514, 541-43, 550-52, 593-95  
 Overconsolidation ratio, OCR:  
   defined, 294  
   effect on cyclic mobility, 530  
   effect on  $K_o$ , 520, 608-10  
   effect on undrained shear strength, 593-95  
   effect on undrained modulus, 595-97
- p (*see* Stress path)  
 Particle shape (*see also* Grain shape)  
 Particle shape, effect on shear strength, 514-17  
 Particle size, effect on shear strength, 514  
 Particle surface roughness, effect on shear strength, 514, 517  
 Pavement:  
   flexible, 154  
   rigid, 154  
 Peacock diagram, 503-04  
 Peat, 6, 49-50  
   compression index, 342  
   consolidation behavior, 308-9  
   values of  $C_\alpha/C_c$ , 408-9  
 Pedology, 1  
 Peds (*see* Soil fabric)  
 Penetrometer, 60  
   Dutch cone, 473, 572-74, 579-81 pocket, 572-74  
   Standard penetration test, 473, 572-74, 578  
 Permeability:  
   coefficient of, 204, 382  
   Casagrande's bench mark values, 209  
   empirical formulas, 209-12  
   factors affecting, 205, 209  
   measurement of, 206-8

- Permeability (continued)**
- relation to pore size, 211-12
  - relation with effective grain size, 211
  - typical values, chart, 210
  - units, 204
  - compacted clays, 118-19, 123
  - determination by oedometer test, 402-3
- Permeability tests:**
- constant head, 206-7
  - factors affecting, 209
  - falling head, 206-9
  - laboratory measurements, 206-9
- PH test, 563**
- Phase diagram defined, 11-12**
- Phase problems, solution of, 16-25**
- Phase relations, 11-25**
- $\phi = \text{zero}$  analysis, 563, 586-88
- PI (see also Atterberg limits; Plasticity index)**
- Piezometer, 227, 230**
- Piping, 116**
- critical location, 255
  - defined, 211, 255
- Plain strain, 468-9, 517, 610, 637**
- Plasticity chart (see Atterberg limits)**
- Plasticity chart, with SL, 182-84**
- Plasticity index, 34, 39 (see also Atterberg limits)**
- Plastic limit, PL (see Atterberg limits)**
- correlation with  $K_o$ , 607
  - correlation with  $\phi$ , 543-45
  - correlation with undrained modulus, 593-94
  - correlation with undrained shear strength, 588-92
- Pocket penetrometer, 572-74**
- Poisson's ratio, 362**
- Pole (see Mohr circle)**
- Poorly-graded soil, 29-30**
- Pore pressure coefficients (see Pore pressure parameters)**
- Pore pressure parameters, 599-605, 691-700**
- $A$  parameter, 693
  - defined, 602, 693
  - variables that affect, 602
  - $\bar{A}$  parameter, 602, 693
  - $A$  parameter at failure, 603-04, 624
  - $B$  parameter, 599-602, 692-93
  - defined, 599
  - PH test, 564
  - defined by principal stress increments, 604, 693-96
  - for different stress paths, 604, 625, 694-95
  - effect of saturation on  $B$ , 600-601
  - Henkel's parameters (coefficients), 604-5
  - derivation, 696-700
  - with rotation of principal stresses 625, 693-94
  - Skempton's parameters (coefficients), 599-605
- Pore pressure parameters: (continued)**
- derivation, 691-93
  - theoretical  $B$  values, 600
  - use in engineering practice, 602-3
- Pore size, effective, 174-75**
- frost action, 192
  - permeability, 211-12
- Pore water pressure:**
- back pressure, 548, 556
  - calculation of, 213
  - definition, 213
  - in CU test, 512, 548, 550, 556, 616
  - residual pore pressures, 561
- Porosity:**
- defined, 12
  - typical values, 104
- Preconsolidated soils (see Overconsolidated soils)**
- Preconsolidation, causes, 294-95**
- Preconsolidation pressure, 291, 294-97**
- Casagrande construction, 296
  - determination of, 295-97
  - effect of sample disturbance, 297-98
  - factors affecting determination of, 326-28
  - graphical procedure for, 296
  - methods to evaluate, 296-97
- Preloading, 420**
- Pressure, relation between atmospheric and vapor, 171**
- Pressuremeter test, 572-73, 582**
- Prestress, effect on shear strength, 514**
- Primary consolidation, 376 (see also Consolidation)**
- Principal planes (see Stress)**
- Principal stress (see Stress)**
- Principal stress:**
- at failure, 456-57
  - increments, 693-94
  - rotation of, 461, 471, 625, 693
- Principal stress ratio, definition, 497**
- Proctor test (see Compaction tests)**
- Profiles (see Soil profiles)**
- Proof rolling, 129, 144**
- 
- q (see Stress path)**
- Q test, 500, (see also UU tests)**
- Quartz, density of, 15**
- Quick clays, 39**
- Quick condition, 233-34, 236**
- examples of, 242-45
  - blow up, 244
- Quick tests (see UU tests)**
- Quicksand, 103, 233**
- drowning in, 242
- Quicksand tank, 240-43**

- R test (see CU tests)**
- Rankine, 8**
- Reaction to shaking (see Soil characteristics, dilatancy)**
- Recompression index, 320**  
procedure for determining, 323-24
- Reconsolidation curve, 294**
- Reference elevation, 227**
- Relative compaction, 142**  
relation to relative density, 142
- Relative density, 78, 103-07**  
effect on cyclic mobility, 530  
relation to relative compaction, 142
- Rock engineering, definition, 3**
- Rock flour, 77**
- Rock mechanics, 2**
- Rollers (see Compaction equipment)**
- Rubber tire rollers (see Compaction equipment)**
- Sample preparation, effect on cyclic mobility, 530**
- Sampling, effect on consolidation test, 297-98**
- Sand, 6, 27, 50, 65**  
used in classification, 50, 65
- Sand boil (see Quick condition)**
- Sands (see Shear strength)**  
characteristics, 26  
frost susceptibility, 195
- San Francisco Bay mud:**  
coefficient of consolidation, 404  
compression index, 342  
consolidation behavior, 292-93  
value of  $C_a/C_c$ , 408
- Scanning electron microscope (see also Clay minerals; SEM)**
- Schmertmann procedure:**  
for normally consolidated soils, 328-32  
for overconsolidated soils, 329, 332-33
- Scrapers (see Compaction equipment)**
- Screw plate compressometer, 572-73, 583-84**
- Secant modulus (see Elastic theory)**
- Secondary compression, 376, 380, 405**  
evaluation of, 405-13  
index, 406  
ratio, 406  
rates of, 405-10  
in derivation of theory consolidation, 380, 683
- Secondary compression ratio (see Consolidation parameters)**
- Secondary settlement, 285, 405-9 (see also Consolidation parameters, evaluation of)**
- Seepage (see Flow)**
- Seepage, 166**  
control of, 270-72  
flow quantity calculations:  
with flow nets, 252-53, 257
- Seepage (continued)**  
with method of fragments, 261-63
- Seepage analyses (see Flow)**  
flow nets, 246-58  
method of fragments, 258-70
- Seepage forces:**  
defined, 232  
evaluation of, 236-40  
in filters, 271  
per unit volume, j, 237
- Seepage velocity, 204**
- Sensitive clays, 39, 554, 603**
- Sensitivity:**  
defined, 585-86  
example of, 390  
relation with LI, 587  
typical values of, 586
- Settlement:**  
calculations, 309-26  
components of, 284-86  
comprehensive example, 414-23  
consolidation, 285, 317  
distortion (immediate), 285, 592  
as a function of time, 391, 418  
of multiple layers, 320  
overconsolidated soils, 320-26  
prediction accuracy, 418  
rate of, 380  
secondary compression, 376  
total, 284, 387
- Shear box (see also Shear strength tests: Direct shear)**
- Shear strength:**  
angle of internal friction,  $\phi$ , 452, 497  
clays:  
critical conditions for stability, 639  
drained strength parameters, 543-45  
effective stress approach, 537  
effect of time, 587  
factors affecting, 597-98  
immediately after construction, 587  
saturated, 536-98  
total stress approach, 537  
unconfined compression, 566  
use of CD strength, 545  
use of CU strength, 556-57  
use of UU strength, 586-88  
cohesion, c, 453  
definition, 449  
envelope, Mohr failure, 449  
stable condition, 450  
factor of safety, 454  
failure angle,  $\alpha_f$ , 454  
failure criteria, 446, 448-49, 453-54, 457, 494, 535, 554-56  
compressive strength, 494  
maximum principal effective stress ratio, 494, 535, 554  
maximum principal stress difference, 494, 535, 554

**Index**

- Shear strength(*continued*)**
- r* at a prescribed strain, 494
  - failure definitions, 554, 556
  - maximum shear stress, 454
  - mobilized, 454
  - parameters, c.  $\phi$ , 453, 556
  - principal stress difference, definition, 465
  - problem soils, 595-98
  - residual, 468, 597
  - sands:
    - behavior during shear, 496
    - cavitation, 504
    - CD triaxial test, example, 507
    - drained shear, 493-503
    - effects of confining pressure, 496
    - factors that affect, 514
    - Mohr circle, undrained shear, 505
    - Mohr circle concepts, 506
    - negative pore water, 504
    - undrained shear, 504-14
    - ultimate, 468
  - Shear strength behavior:
    - clays:
      - CD, consolidated-drained, S test, 538-39
      - CU, consolidated-undrained, R tests, 545, 547
      - effect of loading rate, 537, 557-58
      - similarity to sands, 536-38
      - UU, unconsolidated-undrained, Q tests, 562
      - compacted clays, 124
      - CD tests, 540
      - effect of sensitivity, 561
      - partially saturated clays, PH test, 563-64
    - Shear strength testing:
      - area correction with strain, 568
      - strain controlled loading, definition, 539
      - stress controlled loading, definition, 539
  - Shear strength tests, 458-73
    - CD, 465, 493-94, 538-39
    - CU, 465, 504, 545-50
    - cyclic stress, definition, 530-31
    - cyclic triaxial, 527-30
      - dense sands, 527, 529
      - hydrostatically consolidated, 527
      - loose sands, 527-28
    - direct shear, 458-63
      - advantages and disadvantages, 461
      - Mohr circle, 462
      - Mohr diagram, 459
      - principal stress rotation, 460-61
      - typical results, 459
      - direct simple shear DSS, 470-71
    - Dutch cone penetrometer, 473, 572-74, 579-81
    - hollow cylinder test, 468
    - Iowa borehole shear, 473, 572, 585
    - plain strain test, 468-69
    - pressuremeter test, 473, 572, 582
  - Shear strength test (*continued*)
    - screw plate compressometer test, 473, 572, 583-84
    - torsional or ring shear, 468
    - true triaxial or cuboidal test, 468
    - Standard Penetration Test, 473, 572-74, 578
    - test conditions, drainage, 465
    - triaxial test, 463-68, 494, 539, 546-47
      - advantages and disadvantages, 463
      - anisotropic (non-hydrostatic) consolidation, 538
      - cyclic, 527-30
      - isotropic (hydrostatic) consolidation, 538
      - principles of, 464, 469, 494
    - unconfined compression, why it works, 566-70
      - assumptions, 566
      - UD, unconsolidated-drained, 465, 538
      - UU, defined, 465
    - Shear stress, octahedral, 697-99
    - Sheepsfoot rollers (*see* Compaction equipment)
  - Shrinkage:
    - causing overconsolidation, 186
    - compacted clays, 121, 124
    - engineering significance, 186-90
    - tube analogy, 178-80, 185
  - Shrinkage limit (*see also* Atterberg limits)
    - defined, 180
    - quick and dirty solution, 182-84
    - of sensitive clays, 182
    - test details, 180-84
  - SI units, 9, 665-80
    - basic units, 667
    - conversion factors, 669-71, 674
    - density and unit weight, 676-79
    - derived units, 668
    - figanewtons, 671
    - force, 670-73
    - geostatic stress, 679-80
    - used in geotechnical engineering, 668-80
    - length, 669
    - mass, 669-70
    - prefixes, 668
    - stress and pressure, 673-76
    - time, 670
  - Sieve analysis (*see* Grain size distribution)
  - Sieve sizes, U. S. Standard sizes, 28
  - Silica (tetrahedral) sheet, 78-79
  - Silts, 6, 25-27, 77
    - bull's liver, 178
    - characteristics, 26
    - coefficient of consolidation, 404
    - compression indices, 341-42
    - consolidation behavior, 306-9
    - frost susceptibility, 195
    - used in classification, 50, 65
    - values of  $C_a/C_c$ , 408-9
  - Skempton's pore pressure equation, derivation of, 691-93

- Skempton's pore pressure parameters,** 599-605, 691-700  
**SL (see Shrinkage limit)**  
**Slaking:**  
 defined, 185  
 tube analogy, 185  
**Slow test (see CD tests)**  
**Smectite (see Clay minerals)**  
**Soil behavior:**  
 stress history, 107  
 use of plasticity chart, 51  
**Soil characteristics:**  
 compressibility, 51  
 dilatancy, 55  
 dry strength, 51, 55  
 permeability, 204  
 role of volume change, 51  
 toughness, 55, 77  
 near PL, 51  
**Soil classification:**  
 field identification procedures, 55  
 USCS and AASHTO compared, 70-72  
 visual description, 61  
**Soil classification systems, 47**  
 AASHTO, 48, 64-72  
 comparison of, 72  
 FAA, 48-49  
 purpose, 47-48  
 Unified soil classification system, 48-64  
 Unified, 49-61  
 procedures, 57-61  
 use of Atterberg limits, 49  
**Soil deposits, 6-7, 99-102, 521-23, 586, 595-96**  
 (*see also Soil profiles*)  
 Kola Peninsula, 711  
**Soil formation, 6-7**  
 Kola Peninsula, 711  
**Soil fabric:**  
 cohesionless soils, 102-7  
 cohesive soils, 96-102  
 clusters, 97-98  
 domains, 97-98  
 granular, 102-7  
 honeycombed, 102  
 peds, 97-98, 101  
 single grained, 102  
**Soil mechanics:**  
 definition, 2  
 father of, 8, 215  
 historical development, 7-9  
**Soil profiles, typical, 335-40**  
 glacial clays, 340  
 marine clays, 336, 338  
 quick clays, 339  
 Swedish clays, 337  
**Soils:**  
 residual, 6  
 transported, 6  
**Soil structure, 96**  
 dense, 102-3  
 effect on cyclic mobility, 530  
 loose, 102-3  
 macrostructure, 97  
 microstructure, 97-102  
 at same relative density, 106  
 single grained, 102  
**Specific surface, defined, 89-91**  
**Spring "breakup," 190**  
**Stability, critical conditions, 639**  
**Stabilization:**  
 chemical, 109  
 dewatering, 109  
 mechanical, 109  
 preloading, 109  
**Standard Penetration test, 473, 572-73, 578**  
**Standard Proctor test (see Compaction tests)**  
**Standpipe (see Piezometer)**  
**Steady state line (see Liquefaction)**  
**Stress:**  
 body, 213  
 due to surface loads, 342-67  
 effective, 213  
 physical meaning, 214-16  
 Mohr circle, derivation, 434  
 neutral (pore water), pressure defined, 213  
 overburden, 294  
 plane (two dimensional), 436  
 at a point, 432  
 preconsolidation, 291, 294-97  
 principal planes, 434-36  
 principal stresses, 434-36  
 intermediate, 435-36, 457  
 principal:  
 intermediate, 436  
 major, 436  
 minor, 436  
**in soil masses:**  
 effect of density changes, 220-21  
 effect of ground water changes, 217-18,  
 222-25  
 example calculations, 216-25  
 relation between horizontal and vertical,  
 225-26  
**Stress distribution:**  
 Boussinesq theory, 345-48, 362, 364-67  
 circular load, 352-54  
 influence charts:  
 Newmark's 358-61  
 Westergaard, 360, 362  
 line load, 346-48  
 long embankment, 354-55  
 point load, 345-46, 360-66  
 rectangular load, 348, 362-63  
 square load, 362, 364, 366  
 strip load, 365  
 theory of elasticity, 344

- Stress distribution (*continued*)**
- triangular load, 356-58
  - 2 to 1 (2:1) method, 342-44
  - Westergaard theory, 347, 363-67
  - uniform load, 348-52
- Stress paths:**
- for AE and LC tests, 627
  - applications:
    - engineering practice, 634-39
    - foundation excavation, 638-39
    - foundation loading, 635-37
    - sampling process, 635
    - axial compression, 483
    - normally consolidated clay, 483
    - examples, 484
    - heavily overconsolidated clay, 484
  - clays, normally consolidated:
    - during drained loading, 481, 541
    - during undrained loading, 483-84, 552-53, 565, 610, 636
  - clays, overconsolidated:
    - AE and LC tests, 631
    - during undrained loading, 483-84, 630-31
  - definitions, 474
  - differences between AC-LE, 625
  - differences between AE-LC, 625
  - effective (ESP), 483, 614, 617-18, 621-22, 624-26, 630, 632, 637-38
  - example computations, 612-14, 631-34
  - failure line ( $K_f$ -line):
    - parameter  $a$ ,  $\psi$ , 482
    - parameters  $K$ ,  $\beta$ ,  $\psi$ , 480
  - foundation unloading, 636
  - hydrostatic, 476
  - non hydrostatic, 476
  - overconsolidated clay, 483
  - p-q diagram, 474-76
  - plane strain condition, 610
  - pore pressure parameters, formula for, 694-95
  - pore water, effect of, 483
  - stress point representation, 473-74
  - total (TSP), 483, 614-15, 617-18, 621-22, 624-26, 632, 637-39
  - total minus pore pressure ( $T - U_0$ ), 483, 614, 635
  - for triaxial tests, 475
  - TSP, ( $T - U_0$ )SP, ESP examples, 614-30
  - typical loading conditions, 610-11
  - UU test, 565
- Stress ratio (*see*  $K_f$ )**
- Stress strain behavior:**
- brittle, 448
  - during deposition, sampling and reloading, 297-98
  - elasto-plastic, 448
  - examples, 447
- Stress strain (*continued*)**
- linear elastic, 446
  - nonlinear, 446
  - plastic, 448
  - rigid-plastic, 448
  - visco-elastic, 446
- Stress-strain relationships:**
- elastic, 283, 446
  - non-conservative, 283
  - non-linear, 283, 446
  - plastic, 448
  - visco-elastic, 293, 446
  - work hardening, 448
  - work softening, 448
- Structure:**
- compacted clays, 117-18
  - comparison of properties, 123
- Superficial velocity, 204**
- Surface tension, 167, 169**
- Swedish clays:**
- $C_a/C_c$  values of, 408
  - coefficient of consolidation, 404
  - compression index, 342
  - profiles, 337
- Swedish fall cone test, 572-73, 575**
- Swelling:**
- clays, 284, 306
  - compacted clays, 118, 124
  - correlation with Atterberg limits, 187
  - correlation with colloidal content, 187
  - engineering significance, 186-90
  - laboratory tests, 188-89
  - physio-chemical aspects, 186-87
  - how to predict, 187-90
  - pressures developed, 187
  - prevention of damage, 190
  - related to activity, 188
- Tamping foot rollers (*see* Compaction equipment)**
- Tangent modulus (*see also* Elastic theory; Modulus)**
- Terzaghi, Karl, 8, 215**
- consolidation theory (*see also* Consolidation)**
- Tests (*see* specific type of)**
- Texture:**
- clays, 25-26
  - coarse grained, 25
  - fine, 25-26
  - fine-grained, 25
  - gravels, 25-26
  - sands, 25-26
  - silts, 25-26
- Theory:**
- consolidation, 380-83, 683-86
  - coprogenic impact, 711

- Time factor, 382, 687  
 approximate formula, 399, 689-90  
 relation to coefficient of consolidation, 383
- Toe drain, 253
- Toga party, 108
- Tortuosity, 205
- Total settlement, 284-85, 387
- Total stress, change in, 691
- Total stress analysis, definition, 537
- Torvane test, 571-73
- Toughness index, 46, 55
- Triaxial extension, 693, 695, 699-700
- Triaxial tests, 463-65, 494, 539, 546-47  
 cyclic stress:  
 definition, 530-31  
 hydrostatic, 610  
 non-hydrostatic, 610  
 undrained modulus, 592-95
- Turbulent flow, 201
- 2:1 method, 342-44
- Typical values of:  
 angle of internal friction, 516  
 CD strength parameters, 543  
 coefficient of consolidation, 404  
 compression index, 342  
 CU strength parameters, 553-54  
 density, 15, 105  
 effective grain size, 516  
 height of capillary rise, 176  
 $K_o$  and  $\phi'$ , 606  
 $\phi'$  and PI for clays, 543  
 pore pressure parameter A at failure, 603  
 ratio of  $C_a/C_c$ , 408  
 sensitivity of clays, 586  
 undrained modulus, 593-95  
 UU strengths, 566
- Unconfined compression tests:**  
 comparison of  $\tau_{ff}$  with  $\tau_f$ , 568-70  
 test assumptions, 566  
 why it works, 570
- Unconfined compressive strength, difference between undrained shear strength, 566-67
- Underconsolidated soils, defined, 294
- Undrained modulus, 592-95  
 typical values of, 593-95
- Undrained shear strength (*see Shear strength*)
- Undrained shear strength.  
 clays, 537  
 difference between unconfined compressive strength, 566-67  
 effect of stress history, 593, 595-96  
 from field tests, 570-85  
 Dutch cone penetrometer, 572-73, 579-81  
 Iowa borehole shear test, 572-73, 585  
 pocket penetrometer, 572-74  
 pressuremeter test, 572-73, 582
- Undrained shear strength (*continued*)  
 screw plate compressometer, 572-73, 583-84  
 standard penetration test, 572-73, 578  
 vane shear test, 572-73, 576-77, 591  
 laboratory tests:  
 pocket penetrometer, 572-74  
 Swedish fall cone test, 572-73, 575  
 torvane test, 571-73  
 vane shear test, 572-73, 576-77  
 Unified soil classification system, 49-61  
 Uniformity coefficient, 29  
 Uplift pressures, 253, 258  
 by method of fragments, 266-68  
 USCS (*see also Soil classification systems; Unified soil classification system*)  
 UU (*see also Shear strength; Shear strength tests; UU tests*)  
 UU tests, 465, 559-66 (*see also Shear strength, shear strength tests*)  
 Mohr failure envelopes  
 in terms of effective stress, 564  
 partially saturated clays, 562-64  
 saturated clays, 561-62  
 stress conditions, 560  
 stress paths, 565  
 test details, 559-61
- Van der Waal's forces (*see Clay minerals; Bonding agents*)**
- Vane shear test, 572-73, 576-77, 591  
 Bjerrum's correction factor, 591
- Vapor pressure, 170-71
- Varved clays, 360  
 values of  $C_a/C_c$  for, 408
- Vermiculite (*see Clay minerals*)
- Vertical strain, 309-10, 312  
 area correction, 568  
 use in consolidation tests, 318-19  
 use in settlement calculations, 318-19
- Vibroflotation (*see Compaction*)
- Vibratory compactors, 132-35
- Virgin compression curve, 294, 296-97  
 evaluation of field curves for:  
 normally consolidated soil, 328-32  
 overconsolidated soil, 329, 332-33  
 field, 328, 330  
 slope of, 313-14
- Visco-elastic materials, 283
- Visual classification and visual description, 61
- Void ratio, 12, 362  
 critical:  
 definition, 494  
 example, 508  
 effect on cyclic mobility, 530  
 effect on shear strength, 514, 516  
 maximum, typical values, 104  
 minimum, typical values, 104

**Index**

- Void ratio (*continued*)  
typical values, sands, 516
- Volume change (*see also* Swelling; Shrinkage)
- Volume change:  
coefficient of, 311, 313  
related to settlement, 283
- Volume change tendencies, 504, 505, 510
- Volumetric strain:  
definition, 497  
dilation, 498  
Peacock diagram, 503
- Volumetric strain at failure, 500
- Water:**  
density, 11, 14-15  
dipolar molecule, 92-93  
effect on shear strength, 514  
free water, 93
- Water, absorbed (*see Clay minerals*)
- Water content:  
definition, 13
- Water contents (*continued*)  
natural, 39  
optimum, 113
- Water flow (*see Flow*)
- Water pressure (*see Pore water pressure*)
- Water table, changes in causing  
preconsolidation, 295
- Weathering:  
physical, mechanical, 6  
chemical, 6
- Well graded (*see also* Gradation; Grain size distribution)
- Well-graded soil, 29-30
- Westergaard theory, 360-66  
point load, 360-62  
rectangular area, 364  
square area, 364-66  
strip load, 365
- X-ray diffraction, 88
- Zero air voids curve, 114